THÈSE

En vue de l'obtention du

DOCTORAT DE L'UNIVERSITÉ DE TOULOUSE

Délivré par : *l'Institut Supérieur de l'Aéronautique et de l'Espace (ISAE)*

Présentée et soutenue le *09/10/2018* **par :**

Nabil KBAYER

Advanced Signal Processing Methods for GNSS Positioning with NLOS/Multipath Signals

---

JURY

Joseph Tabrikian	Professor	Rapporteur de thèse
Paul D. Groves	Associate Professor	Rapporteur de thèse
Jean-yves Tourneret	Professeur	Président du jury
Juliette Marais	Chargé de Recherche	Examinateur
Jerome Galy	Maître de Conférences	Examinateur
Sylvie Marcos	Directeur de Recherche	Examinateur
Eric Chaumette	Enseignant-Chercheur	Directeur de thèse

École doctorale et spécialité :

MITT : Domaine STIC : Réseaux, Télécoms, Systèmes et Architecture

Unité de Recherche :

Equipe d'Accueil ISAE-SCAN, Laboratoire TéSA

Directeur(s) de Thèse :

M. Eric CHAUMETTE et *M. Mohamed SAHMOUDI*

Rapporteurs :

M. Joseph TABRIKIAN et *M. Paul D. GROVES*

Acknowledgements

I would like to express my sincere gratitude to those who have helped me in whatever ways along my journey to complete my thesis. I especially wish to acknowledge my two supervisors, Dr. Eric Chaumette and Dr. Mohamed Sahmoudi, whom I am forever indebted, for making this research possible. I really appreciate the way I have been guided through this thesis. Thank you both for the supervision and guidance throughout this thesis and also for the encouragement and providing insightful comments. I would like also to thank Dr. Jerome Galy for his kind support with problems related to lower bounds and deterministic estimation.

I would like to extend my thanks also to the jury members who have taken their time to review the thesis and shared their vast knowledge and experience in providing their comments and recommendations.

On the whole, this thesis has been an excellent and rewarding experience. The past three years at ISAE-SUPAERO and TéSA Lab was an interesting opportunity for me to gain some hands on experience in the scientific research field. I acquired many new skills and improved many already existing skills that I am sure will be useful for me in the near future. In conclusion, I would like to thank all members and colleagues of DEOS department at ISAE-SUPAERO and TéSA Lab for their help. My particular gratitude goes to my colleagues at DEOS (Marie, Vincent, Antoine, Francesco, Pierrick, Laurent, Michèle, Benoit, Gael, Khairol, Quintin, Syed, Cheng, Azeddine and others) who in one way and another give me the sense of companionship during this long experience.

And last but not least, a particular gratitude go to my beloved family who supported me and accompanied me till the end.

Table des matières

Table des figures

Liste des tableaux

Abbreviations and Nomenclature

A-GNSS	Assisted GNSS
AL	Alert Limit
C/N_0	Carrier-to-noise ratio
CDF	Cumulative Distribution Function
DOP	Dilution Of Precision
DLL	Delay Lock Loop
ECEF	Earth-Centered, Earth-Fixed
EKF	Extended Kalman Filter
ENU	East-North-Up
FDE	Fault Detection and Exclusion
GBAS	Ground Based Augmentation System
GIS	Geographic Information System
GLONASS	GLObal'naya Navigasionnay Sputnikovaya Sistema (GNSS of Russia)
GNSS	Global Navigation Satellite Systems
GPS	Global Positioning System
HAL	Horizontal Alert Limit
HDOP	Horizontal Dilution of Precision
HPE	Horizontal Position Error
HPL	Horizontal Protection Level
ICAO	International Civil Aviation Organization
IMU	Inertial Measurement Unit
INS	Inertial Navigation System
ITS	Intelligent Transport System
KF	Kalman Filter
LBS	Location-Based-Service
LHCP	Left-Handed Circular Polarization
LOS	Line-Of-Sight
LSR	Least Square Residual
MEMS	Micro Electro-Mechanical Systems
MM	Map Matching
MP	Multipath
NLOS	Non-Line-Of-Sight

PAYD	Pay-As-You-Drive
PF	Particle Filter
PL	Protection Level
PLL	Phase Lock Loop
PR	Pseudorange
PRN	Pseudorandom noise
PVT	Position, Velocity and Timing
RAIM	Receiver Autonomous Integrity Monitoring
RF	Radio-Frequency
RHCP	Right-Handed Circular Polarization
RUC	Road-User-Charging
SBAS	Satellite Based Augmentation System
SNR	Signal-to-Noise Ratio
TOW	Time of Week
UERE	User Range Equivalent Error
UKF	Unscented Kalman Filter
UTC	Coordinated universal time
VDOP	Vertical Dilution of Precision
VPL	Vertical Protection Level
WLS	Weighted Least-Squares

List of Symbols and Notations

In this thesis, the notational convention adopted is as follows : italic indicates a scalar quantity, as in a ; lower case boldface indicates a column vector quantity, as in $\mathbf{a}$; upper case boldface indicates a matrix quantity, as in $\mathbf{A}$. The n-th row and m-th column element of the matrix $\mathbf{A}$ will be denoted by $\mathbf{A}_{n,m}$ or $(\mathbf{A})_{n,m}$. The n-th coordinate of the column vector $\mathbf{a}$ will be denoted by $\mathbf{a}_n$ or $(\mathbf{a})_n$. The scalar/matrix/vector transpose is indicated by the superscript ^{T}. $[\mathbf{A}, \mathbf{B}]$ denotes the matrix resulting from the horizontal concatenation of matrices $\mathbf{A}$ and $\mathbf{B}$. $(\mathbf{a}^T, \mathbf{b}^T)$ denotes the row vector resulting from the horizontal concatenation of row vectors $\mathbf{a}^T$ and $\mathbf{b}^T$. $\mathbf{I}_M$ is the identity matrix of order M. $\mathbf{1}_M$ is a M- dimensional vector with all components equal to one. If $\mathbf{A}$ is a square matrix, $|\mathbf{A}|$ denotes its determinant.

Qualifiers

$E()$	Expectation operator
$\subset$	is a proper subset of
$\sim$	is following a distribution
$\mathbf{z}$	Code pseudorange measurements
$\mathbf{x}_0$	Reference position
$\mathbf{x}$	State Vector or Unknowns to be estimated : an incremental deviation from $\mathbf{x}_0$
$\mathbf{y}$	Measurements Innovation
$\mathbf{H}$	Measurements Matrix
$\mathbf{v}$	Observation or Measurements nuisance signals
$\mathbf{n}$	Receiver measurements noise
$\mathbf{b}$	MP/NLOS bias
N	Number of received GNSS signals
M	Number of unknowns to be estimated
$s(t)$	Complex GNSS baseband signal at timestamp t
$\mathcal{CN}$	Complex Gaussian distribution

Introduction

Systèmes GNSS

Bien que le système de positionnement global (GPS) fût initialement destiné à l'usage militaire en 1994, la décision de donner libre accès aux utilisateurs civils a motivé son usage dans une large gamme d'applications allant des plus pointilleuses, à l'instar de l'aviation civile, aux applications « grand public ». Ainsi, ces systèmes de navigation par satellites (GNSS) sont considérés comme la solution préférée pour la localisation et la navigation dans diverses applications.

GNSS est une technologie de radionavigation par satellites qui permet aux utilisateurs du monde entier, équipés d'un récepteur dédié, de se localiser, de naviguer et d'avoir un moyen de synchronisation par rapport à une référence temporelle commune. Une constellation de satellites transmet des signaux spécifiques dont les temps de propagation peuvent être estimés précisément. Ces derniers sont appelés les mesures pseudo-distances (PR). Elles sont entachées par diverses sources d'erreurs telles que des retards supplémentaires sur la propagation à la traversé des couches ionosphérique et troposphérique.

La position de l'utilisateur peut être estimée par le principe de triangulation à partir d'au minimum trois mesures pseudo-distances. Cependant, une mesure satellitaire supplémentaire s'avère nécessaire pour résoudre le problème de synchronisation entre l'horloge du récepteur GNSS et les horloges satellitaires.

Un système GNSS est généralement séparé en 3 segments principaux, à savoir le segment spatial, le segment de contrôle au sol et le segment utilisateur. Le segment spatial consiste en une constellation de satellites gravitant autour de la Terre tout en transmettant des signaux radio aux utilisateurs. Le segment de contrôle au sol dispose d'un réseau de stations de surveillance sur terre. En général, ce segment de contrôle surveille et maintient les opérations des satellites, telles que la génération des messages de navigation. Enfin, le segment utilisateur est simplement constitué des récepteurs GNSS, dont la fonction est de recevoir et de traiter les signaux GNSS pour obtenir la solution position, vitesse, temps (PVT).

Les systèmes GNSS englobent de nombreux systèmes opérationnels tels que le GPS américain, le GLONASS russe et le GALILEO européen, et prévoient des améliorations considérables des performances et des services à l'horizon de 2020. En effet, a ce jour, plusieurs systèmes GNSS existent et sont en cours de développement. Le système américain NAVSTAR (couramment appelé GPS - Global Positioning System) et le système russe GLONASS font partie des systèmes établis. L'Europe a déjà mis en place sa propre constellation GNSS connue sous le nom de Galileo et le système BeiDou chinois est déjà mondialisé. Outre ces systèmes, il existe également des systèmes régionaux tels que le système japonais de satellites Quasi-Zenith (QZSS) et le système régional indien de navigation par satellite (IRNSS).

Les systèmes de navigation par satellites (GNSS) sont considérés comme la solution préférée pour la localisation et la navigation dans de nombreuses applications. Considérée comme la solution la plus accessible pour le positionnement en environnement urbain, le nombre de services à base de géolocalisation par GNSS est en forte croissance. Cependant, même avec cette augmentation de la disponibilité des satellites, ces services souffrent d'un manque de robustesse du service final de géolocalisation dans de tels environnements en raison d'un certain nombre de problèmes techniques persistants. De l'autre côté, avec l'augmentation exponentielle des applications basées sur la géolocalisation, les attentes et les exigences des utilisateurs, en terme de précision et de fiabilité, sont de plus en plus difficiles à satisfaire par les technologies de géolocalisation existantes.

Challenges GNSS en zones urbaines

Bien qu'il y ait une augmentation exponentielle des applications des systèmes de navigation par satellites (GNSS) en milieux urbains, ces services souffrent de manque de robustesse dans la géolocalisation dans des tels environnements. La principale raison de cet écart entre les attentes et les exigences des utilisateurs d'un côté, et les technologies de géolocalisation existantes de l'autre côté, c'est que ces milieux présentent des défis importants pour le positionnement par satellites. Pour satisfaire l'accroissement des exigences des utilisateurs en termes de disponibilité, de précision et d'intégrité de la solution de navigation, les services GNSS doivent offrir des performances minimales à l'aide des nouveaux algorithmes plus robustes aux phénomènes physiques qui apparaissent dans ces environnements.

Plusieurs défis présents dans les environnements urbains constituent un frein au développement de certaines applications modernes du GNSS. La forte densité des immeubles de grande hauteur, la présence de nombreux obstacles et le blocage des signaux transmis par les satellites posent des problèmes techniques très difficiles pour l'acquisition, la poursuite et la modélisation des signaux GNSS. En outre, l'interaction avec l'environnement se traduit généralement par une superposition de divers signaux qui ont suivi des chemins différents appelés signaux Multitrajets (*Multi-Path* en anglais (MP)). Ces interactions peuvent aboutir à trois grands types de phénomènes physiques, chacun répondant à des lois physiques différentes et qui peuvent se combiner entre elles :

- La réflexion spéculaire.
- La diffraction sur des arêtes.
- La diffusion sur des surfaces rugueuses.

Aussi, les hauts bâtiments ainsi que les autres objets entourant l'antenne réceptrice peuvent bloquer le signal direct dit signal *Line-Of-Sight* (LOS) de nombreux satellites. Ceci engendre la réception d'un signal après réflexion sans la réception du signal direct. Cette situation est appelé situation *Non-Line-Of-Sight* (NLOS).

Tous ces phénomènes réduisent la visibilité des satellites, ce qui engendrent un problème de disponibilité du service ou bien des valeurs élevés de DOP (*Dilution of Precision*) affectant ainsi la précision de la solution de navigation malgré l'exploitation de plusieurs constellations pour le calcul de la position dans ces environnements. Les signaux MP et NLOS produisent un retard additionnel sur les mesures Pseudo-distance (PR), ce qui impacte la précision des algorithmes de positionnement. Dans ces conditions, le récepteur GNSS peut se trouver en situation d'incapacité de calculer sa position ou de délivrer une position biaisée par plusieurs mètres voire dizaine de mètres d'erreur. Dans tous ces cas, le récepteur se trouve dans une situation d'incapacité de produire une solution fiable de positionnement à transmettre à la couche application du système basé sur la géolocalisation.

Motivation de la thèse

Cette thèse est une synthèse des travaux de recherche menés depuis 2014 sur les méthodes de positionnement robuste utilisant des mesures GNSS en présence de réflexions MP et NLOS, dans le but d'améliorer les performances GNSS dans des environnements contraints (canyons urbains, urbains ou périurbains, forêts et zones montagneuses...). Les motivations de ces travaux de recherche sont énumérées ci-dessous :

1. **Demandes accrues en zones urbaines :** L'application des systèmes GNSS pour la navigation terrestre a gagné en popularité dans les zones urbaines pour son accessibilité libre et sa précision appropriée. Motivé par les développements importants des techniques basées sur les GNSS, le positionnement par satellite devrait avoir un large éventail d'applications dans les domaines de la navigation terrestre, des systèmes de transport intelligents (ITS), des robots/drones, des services basés sur la localisation (LBS) et des réseaux de capteurs sans fil (WSN). Aussi, pour les applications de marché de masse, l'utilisation des systèmes GNSS par le grand public, en particulier par les téléphones intelligents équipés de chipsets GNSS, devient de plus en plus fréquents dans les zones urbaines. Avec cette demande accrue, les utilisateurs en milieu urbain attendent une précision de positionnement supérieure à celle obtenue en zones rurales, ce qui constitue une des motivations de ces travaux de recherche.
2. **Valeur ajoutée d'un positionnement fiable :** Les exigences des utilisateurs dans les zones urbaines peuvent être très strictes et dépendent des applications spécifiques. Par exemple, la fiabilité GNSS est obligatoire, en particulier pour les applications ayant des incidences sur les aspects financiers, la légalité ou la sécurité de la vie, telles que le repérage spécifique d'une voiture ou la tarification des usagers de la route. Certaines de ces applications sont critiques, car, par exemple, les usagers de la route devraient être facturés de manière juste, précise et sécurisée dans les applications *road user charging* (RUC). En cas de positionnement non fiable du GNSS, les opérateurs sont responsables de tout acte répréhensible tel que surtaxe ou surcharge. Ainsi, parallèlement à l'apparition et à l'innovation de nouvelles applications terrestres, de nombreuses demandes proviennent des environnements urbains, où les besoins en localisation précise et fiable sont beaucoup plus complexes que dans les environnements à ciel ouvert. Ce facteur a motivé nos recherches scientifiques visant à améliorer les performances GNSS dans ces domaines afin de répondre aux exigences et aux attentes des utilisateurs.
3. **Performances GNSS dégradées dans les zones urbaines :** les progrès continus des

applications GNSS en navigation terrestre ne sont pas sans obstacles majeurs dans leur développement. En effet, même avec l'augmentation de la disponibilité des satellites et l'amélioration de la géométrie de la constellation, le positionnement du GNSS dans les zones urbaines souffre de performances dégradées en raison de plusieurs problèmes qui persistent. Fondamentalement, le processus d'urbanisation rapide dans de nombreuses villes entrave les performances des technologies de positionnement basées sur le GNSS pour trois raisons principales : masquage et atténuation du signal des satellites, réflexions des signaux GNSS et géométrie dégradée des satellites. Face à de tels défis techniques, il est urgent de remédier aux dégradations des performances GNSS : c'est l'une des principales motivations de ce travail de recherche.

Objectifs et réalisation de la thèse

L'objectif principal de cette thèse de recherche est de développer des méthodes de positionnement robuste utilisant des mesures GNSS en présence de réflexions MP et NLOS, en intégrant des informations assistées sur l'environnement du récepteur. Par conséquent, les questions suivantes sont posées et ont été traitées dans ces travaux :

1. Quel est le niveau de précision de positionnement maximum atteignable par le positionnement GNSS en présence des erreurs MP/NLOS, en cas de non utilisation d'informations externes ? Pour répondre à cette question, nous avons proposé une famille de bornes inférieures sur les performances de localization GNSS dans les conditions MP/NLOS, permettant de calculer les meilleures performances d'estimation GNSS en présence d'un environnement non gaussien, sans utilisation d'informations externes pour aider les systèmes GNSS.
2. Un simulateur GNSS 3D, c'est-à-dire des informations externes sur l'environnement de réception du récepteur, peut-il être utilisé de manière constructive pour aider le GNSS dans les situations MP/NLOS ? Ces informations supplémentaires sont essentielles dans le cas d'une très faible disponibilité du signal GNSS. Les points suivants ont été abordés dans cette recherche :
   — Quel est le niveau de réalisme requis des informations fournies par la simulation 3D pour être utilisé de manière constructive pour le positionnement GNSS ? Quel est l'intérêt d'utiliser un simulateur GNSS 3D ?
   — Comment les informations du simulateur GNSS 3D pourraient-elles être utilisées pour améliorer les performances de positionnement ? A quel niveau de l'architecture du récepteur faut-il utiliser ces informations ?

Les principales contributions de cette thèse sont :

1. Le mérite d'utiliser des informations provenant d'un simulateur de propagation des signaux GNSS pour aider le GNSS dans les conditions MP/NLOS :
   Nous avons étudié le niveau de réalisme minimum requis et souhaité pour un simulateur GNSS. Le simulateur, ou tout outil fournissant des informations sur le biais MP/NLOS, doit être intégré pour aider le positionnement GNSS. C'est l'objet du chapitre 3.

2. Utilisation d'informations externes provenant d'un simulateur de propagation de signaux GNSS 3D pour améliorer le positionnement GNSS dans des conditions MP/NLOS :
   Différentes méthodes ont été proposées pour l'intégration de ces informations 3D au récepteur GNSS, au niveau du module PVT en se positionnant sur une grille de positions candidates ou sur le bloc de navigation en corrigeant les mesures de pseudorange dégradées. C'est l'objet du chapitre 3.
3. Dérivation des limites inférieures des performances GNSS en présence d'un environnement non-gaussien :
   Evaluation des performances de positionnement GNSS maximales pouvant être atteintes en présence de signaux MP/NLOS utilisant uniquement des techniques d'estimation avancées, sans informations externes. La présence de réflexions MP et NLOS ne permet plus d'obtenir une forme analytique de la fonction de densité de probabilité marginale des observations GNSS, ce qui empêche d'utiliser les bornes inférieures déterministes standard connues sur l'erreur quadratique moyenne (MSE). Nous avons donc introduit une famille générale de bornes inférieures modifiées (MLB) dans le cadre d'une estimation déterministe non standard, bornes moins précises (au sens de plus opimistes, "less tight") que les bornes standard, mais qui ont le mérite d'être calculables. C'est l'objet du chapitre 4.

Chapitre 1

Introduction

Contents

1.1 General Introduction : Development of Navigation and Positioning

Since the Middle Ages, man's desire to be able to locate itself and to master time and space have always been a necessity and a great scientific challenge. To do that, from the early astronomical surveyors to the present satellite geodesists, men moved from a rough navigation based on stars observation to suitable accurate navigation by means of electromagnetic-wave-broadcasting satellites. Despite this huge technological advance, the role of these surveyors or navigators in society has remained unchanged since the dawn of civilization ; that is to determine land boundaries, provide maps of his environments and use the scientific advancement to foster everyday life.

Until the 20^{th} century, the term "navigation" have been laid for mariners and referred mainly to sailing directions determination to guide ships across the seas. Indeed, the word "navigate" comes from the Latin navis (meaning "ship") and agere (meaning "to move or direct"). Hence, the basis of localisation using scientific instruments such as the mariner's astrolabe, first occurred in the Mediterranean during the Middle Ages. Modern navigation reap the rewards of this chain of technical developments from the early celestial observation to the current satellite-based positioning. Therefore, today, the term “navigation” encompasses the determination of positions of observing sites on land or at sea, in the air, and in inner and outer space.

Among all major navigation breakthroughs along the whole history, we have decided in this introduction to devote few lines to a huge human discovery, which has revolutionized the navigation field : the first clock sufficiently accurate to be used to determine longitude for navigation. This precise clock was created by John Harrison, which was a historical introduction of time in the navigation problem. Indeed, for navigating at sea, observing the landmarks and coast's phares visible from the coast has long been the only repository for maritime navigation. Because of this cumbersome and limited method, thousands of maritime shipwrecks have occurred during the 16^{th} and 17^{th} Century, including goods loss and sailors death.

Determining latitude was relatively easy in that it could be found from the altitude of the sun at noon with the aid of a table giving the sun's declination for the day. For longitude, early ocean navigators had to rely on dead reckoning. This was inaccurate on long voyages out of sight of land, which sometimes ended in tragedy as a result. The longitude of a location is directly related to the difference between the local time and the time at another place of known longitude at that very same moment (longitude ambiguity). The local time can conveniently be fixed by a noon sighting of the Sun, but the time at any other location requires a reliable clock, or some other way of distant time synchronization. Thus, there was necessary to build precise clocks. Hence, the British government formed in 1714 to administer a scheme of prizes intended to encourage innovators to solve this problem, popularly called Board of Longitude. A practical solution came from a gifted carpenter, John Harrison, who solved one of the most difficult problems of his time by creating an accurate chronometer [4].

After four decades of perfecting, the humble carpenter John Harrison invented four versions of mechanical clocks that helped navigators to find an accurate way of determining longitude. The final solution, called clock H4, won the prize established by the British government, and beyond the recognition and appreciation of all scientists of all time (Fig. 1.1).

Inspired by Harrisson's invention, current satellite-based navigation is based on a more modernized version of these chronometers setting at the heart of satellites moving in the sky (called atomic clocks)...

FIGURE 1.1 – John Harrisson's final maritime chronometer : H4 (1755-1759)

1.2 Thesis Background : GNSS System Overview

Over time, the use of electromagnetic waves has allowed the development of radio-navigation to revolutionize the means of navigation and time measurement. Widely developed during the second world war to localize aircrafts, systems using these waves are limited in particular by their range, which imposes a relatively high cost when it comes to implementing a system with significant coverage. However, systems like DECCA, LORAN C, OMEGA have been used for aviation and maritime navigation. The major breakthrough toward the use of artificial satellites for navigation has occurred after the discovery of the ability to exploit the Doppler shift in a broadcast signal for positioning [5].

First conceived and developed for military purposes, the immediate predecessors of the present positioning systems are the American Navy Navigation Satellite System, commonly called Transit [6], and the Russian Tsikada. These early systems share nearly the same principle, which is the use of satellites and spacecraft for ranging, and suffer both from the same shortcomings, namely low navigation accuracy (about 25 meters of navigator's error at a fixed site [7] and about 400 meters for moving ships [8] for the TRANSIT system) and poor system continuity (six used satellites : three for positioning and three as spares [9]).

To follow this concept of using a constellation of satellites and to overcome the limitations of the TRANSIT system, the American military have developed the Global Positioning System (GPS) for both military and civil use [10]. Popularized first through receivers for road navigation, and over the last few years by the integration of affordable receiver chipsets in smartphones, these systems have experienced huge evolutions making the possibility of knowing his position anywhere and anytime as an essential part of the daily life of the general public [11]. For their free accessibility and suitable accuracy, these GNSSs are nowadays considered as the preferred solution for location and timing in a very wide and growing range of applications.

Free availability and considerable progress of GNSS during recent years have paved the way for providing more and more reliable geolocation solutions essential for a broad range of technologies. Nowadays, the use of satellite-based positioning systems is becoming more widespread all over the world in a plethora of fields that have been grouped into three broad categories cited in [12] : navigation, surveying and scientific applications.

Navigation applications encompass basically transportation, defense, aviation, maritime and rail. As an illustration, a high precision use of GNSS within aviation is Localiser Performance with Vertical guidance (LPV) runway approaches. Besides, GNSS provides guidance to aircraft above the runway, which allows them to safely approach and land. Road navigation is the most widespread GNSS application, providing turn-by-turn indications to drivers through portable navigation devices. Enabled by the uptake of modern automotive connectivity solutions, connected vehicles represent the evolution towards integrated platforms capable of supporting, thanks to GNSS, smart mobility services and a range of safety applications. GNSS, together with other technologies, is a key answer to autonomous vehicles, which need precise sub-meter positioning combined with guaranteed reliability of localisation. In summary, applications in the Road and LBS segments dominate all other market segments in terms of cumulative revenue for GNSS related industry, according to the European GNSS Agency (GSA) latest report [11].

1.2.1 GNSS Operational Systems

Nowadays, the GNSS implies two fully operational systems, the American GPS and the Russian GLObal'naya Navigasionnay Sputnikovaya Sistema (GLONASS), and several under development systems or regional systems mainly like the European Galileo, the Chinese Beidou, the Japanese Quasi-Zenith Satellite System (QZSS) and the Indian Indian Regional Navigational Satellite System (IRNSS). In addition, these systems are supplemented by Space-Based Augmentation Systems (SBAS) or Ground-Based Augmentation Systems (GBAS). SBAS encompass various systems such as the American Wide-Area Augmentation System (WAAS), the European Geostationary Navigation Overlay Service (EGNOS) and the Indian GPS Aided Geo Augmented Navigation system (GAGAN). Fig. 1.2 gives an exhaustive overview to the current development plans for each satellite navigation system over the next five years by detailing the signal sets, status and number of satellites.

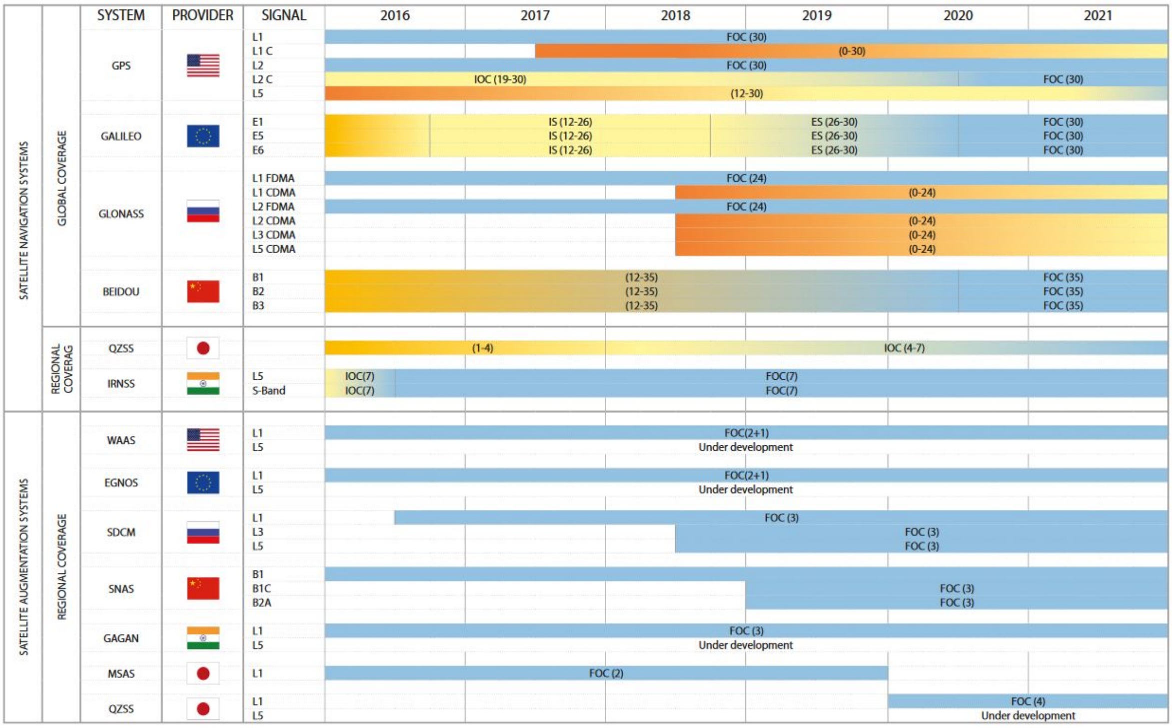

FIGURE 1.2 – GNSS Operational Systems Overview [1]

Despite the difference between different GNSS systems in terms of signal structure, control and space segments, they contain the same three main segments namely, the Space Segment, the Ground Control Segment and the User Segment. The Space Segment is composed of a satellite constellation, with a sufficient number for full earth coverage. Equipped with atomic clocks among others, the satellite follows a precise orbit around the earth and broadcasts radio signals to users necessary for ranging. Using a network of monitoring stations on earth, the Control Segment is responsible for steering and monitoring of the whole system. In particular, it is responsible for producing the navigation messages transmitted via uplink then broadcast to users. Finally, the User Segment is the GNSS receivers, able to receive and process the emitted GNSS signals from the Space Segment to determine the user position by means of range differences measured to satellites.

Some brief descriptions of the principal GNSS systems are as follows :

1. **Global Positioning System (GPS) :** Considered as the oldest and most widely used GNSS system, GPS was first conceived by the United States Department of Defence (U S DoD) as a space-based navigation system for the American military forces to accurately navigate during missions. Promoted next for civil use, GPS became fully operational in 1995 and is always under continuous enhancement and modernization. The present Space segment consist of 30 operational Medium Earth Orbit (MEO) satellites deployed in six orbital spaced planes with 55° degrees inclination at an altitude of about 20200 km. This configuration provides a global coverage of more than four satellites simultaneously observable above 15° elevation at any time of day, except in the polar regions.

   With a fleet of various types of satellite, the GPS Space Segment transmit two BPSK navigation signals on two carrier frequencies of the L band : L1 (1575.42 MHz) and L2 (1227.6 MHz). The modernization of GPS encompasses an additional carrier frequency L5 (1176.45 MHz). The L1 signal consists of two pseudo-random navigation (PRN) codes with a phase quadrature modulation : unencrypted C/A (Coarse Acquisition) code conceived for the civil use, encrypted P(Y) code dedicated to military applications. The encrypted P(Y) code is transmitted on both the L1 and L2 frequencies and requires a decoding key to be able to be used. Finally, these two signals are modulated by the navigation massage, with a bit rate of 50 bits/sec, and carries the satellite ephemeris data, which are information about GPS satellites location plus timing and "health" data.

   The GPS ground control segment consists of a calculation center located in a base in Colorado Springs, and composed of 11 command and control antennas and 16 monitoring stations. The role of control stations is to facilitate the track of GPS satellites, monitor their transmissions, perform analyses, and send commands and data to the constellation. After having been processed at the computing center, this information makes it possible to update the ephemeris of the satellites so that their orbits can be calculated exactly. The new ephemeris are then transmitted to each satellite via transmitting antennas so that they can update their navigation message.

   Additional information on GPS history, services, segments and it signal structure may be obtained in the following references [12, 10, 13, 14, 15].

2. **GLObal'naya Navigasionnay Sputnikovaya Sistema (GLONASS) :** Considered as the Russian counterpart to GPS, GLONASS is operated by the Ministry of Defense of the Russian Federation. Based on the experiences with it immediate predecessor Tsikada, GLONASS was developed by the former Union of Soviet Socialist Republics (ex-Soviet Union) in 1982 and reaches it full operational capability (FOC) in 1996. Like GPS, the Russian GLONASS was operated by the Russian army for military purposes

before being opened to others civil users in 1995.

Due to lack of funding, GLONASS had experienced a continuously declining number of available satellites until the year 2001. While the complete constellation must consist of 24 satellites, only six to eight satellites were operational in 2001. Since then, Russia has made a huge restoration of the system and launched new generation of GLONASS satellites allowed to bring the constellation back to an operational level. The 24 MEO satellites of this constellation are placed in three circular orbits at an altitude of about 19100 km. Each orbital plane is inclined by 64.8° to the equator. GLONASS satellites have a rotation period of about 11h15min. This distribution of the satellites allows a good coverage of the polar zones by GLONASS, which is not the case of the GPS system. Besides, GLONASS constellation assures a global coverage of more than five satellites simultaneously visible on 99% of the sites on the earth at any time of day.

Unlike GPS which is based on Code Division Multiple Access (CDMA) technique, GLONASS implements a Frequency Division Multiple Access (FDMA) technique to distinguish between the signals of various satellites. All satellites in the constellation use the same PRN code that allows the receiver to measure the time of flight of the signals. Fifteen different frequencies distributed around two carrier frequencies : L1 (1602 MHz), commonly called G1, and L2 (1246 MHz), commonly denoted as G2. This FDMA technique is more robust against interference, allows low cross-correlation between signals but have a short ranging code. After discussions between the American and the Russian government, a GPS/GLONASS interoperability and compatibility had became possible since GLONASS satellites will broadcast signals in the L3/L5 bands using CDMA principles. Further information on the Russian GLONASS system may be found in [12, 16, 17, 18].

3. **European Navigation System Galileo :** Recognized the strategic and economic impact of satellite-based navigation and the need to guarantee its own autonomy and competitiveness, the European Union (EU) has embarked to develop an independent GNSS system, called Galileo, without any intention to compete with the other existing GNSS systems but in a vision of interoperability and compatibility with them. Unlike non-civilian American GPS or Russian GLONASS, Galileo provides an alternative that remains under civilian control. The complete Galileo constellation will comprise 27 operational and 3 spare MEO satellites spread evenly around three orbital planes with 56° of inclination with reference to the equatorial plane. Each satellite will take about 14 hours to orbit the Earth and will be at an altitude of 23222 km. This distribution guarantees six to eight satellites to be in view above 10° elevation mask at any location.

   Conceived in a service-oriented approach in the design phase, Galileo provides four different services :

   — Open Service (OS) : Intended for the mass market, this service is accessible to all users free of charge but without any service guarantee or liability. It can be ensured by means of six unencrypted signals modulated onto three different carrier frequencies : E1 (1575.42 MHz), E5a (1176.45 MHz) and E5b (1207.14 MHz).

   — Commercial Service (CS) : Intended to generate a revenue stream for the Galileo Operation Company (GOC), this service offers higher performance than the

OS with added guaranty and liability of service. CS broadcast encrypted signals modulated onto the Galileo frequency band E6 (1278.75 MHz).

— Public Regulated Service (PRS) : Intended to provide a continuous and encrypted signal even if other services are disabled in situations of crisis, this service is allocated to government-authorized users. The bands allotted for this service are the E1 and E6.

— Search and Rescue Service (SAR) : Intended to provide a continuous global service for humanitarian search and rescue activities under Cosmicheskaya Sistyema Poiska Avariynich Sudov-Search and Rescue Satellite-Aided Tracking (COSPAS-SARSAT) organisation, Galileo satellites will be able to pick up emergency signals from distress emitting beacons carried on ships, planes or persons and ultimately forward these back to national rescue centres (SAR ground segment) in the SAR down-link frequency band.

The ground segment of Galileo comprises two control centers, thirty monitoring stations around the world and five satellite link stations. Further information on the European Galileo system may be obtained, for instance, in [12, 19].

4. **BeiDou Navigation Satellite System (BDS) :** Started as an experimental regional navigation system, called Beidou 1, with four experiment satellites from 2000 providing Radio Determination Service System (RDSS), China announce the third step of development of it own satellite positioning system BeiDou with a fully operational regional covarage in 2012 and with a clear plan to provide a global coverage around the year 2020. Initially this system, called Beidou, allows a satellite-based location on all China an on the outskirts of China. Under ongoing modernization, BDS consists in 2016 of 23 satellites in orbit that will be extended to a constellation of 35 satellites in 2020, which include 5 geostationary orbit (GEO) satellites, 3 IGSO (Inclined Geosynchronous Orbit), and 27 MEO (Medium Earth Orbit) satellites [20]. MEO satellites are placed in tilt orbits of 55° and at an altitude of about 21528 km [21]. Like GPS, BDS provides civilian service and military service (or authorized service). These official documents published by the China Satellite Navigation Office [20, 22] describe the frequency bands used by BDS which are : B1I (1561.098 MHz) and B2I (1207.140 MHz).

5. **Quasi-Zenith Satellite System (QZSS) :** Considered more as an augmentation system and complementary to GPS, the Japanese regional satellite navigation system QZSS is intended to provide an enhanced satellite availability in the East Asia and Oceania region. With a current constellation of four satellites in orbit, Japanese Space Policy have decided in January 2015, to begin operating QZSS as a total of 7-satellite for GPS augmentation that allows sustainable positioning around by 2023.

   The orbits of QZSS geosynchronous satellites oscillate in the north-south direction with a constant longitude. They are shaped like a figure eight with north-south asymmetry. With the intention of total compatibility with the American GPS, QZSS is conceived to broadcast signals similar to GPSs L1 C/A, L1C, L2C and L5. Additional information about the Japanese GNSS may be found in this official website [23].

6. **Indian Regional Navigational Satellite System (IRNSS) :** Conceived to provide an autonomous regional navigation system for the Indian sub-continent, the Indian

IRNSS project was approved by Indian government in May 2006 and developed by the Indian Space Research Operation (ISRO) since then.

For the time being, the space segment of IRNSS consist of a constellation of seven satellites : 3 satellites in GEO and 4 satellites in Geosynchronous orbit (GSO) at approximately 36000 km of altitude above earth surface. IRNSS provides two types of services, namely, Standard Positioning Service (SPS) for common civilian users and Restricted Service (RS), which is an encrypted service provided only to the authorised users. The Indian IRNSS uses dual-frequency service in L-band in coallocation with GPS L5 and Galileo E5a and in S-band. [24] gives additional information on IRNSS.

1.2.2 GNSS Working Principle

By means of emitted navigation signals from the GNSS Space Segment, i.e. operational satellites, the user is capable to determine his position, expressed for example by latitude, longitude and height coordinates. The task of processing the broadcast satellite signals in the user segment is accomplished by a simple resection process using an essential information which is the range measured to satellites, this process is called multilateration.

First of all, the range measured to satellites is proportional to the amount of time taken by the GNSS signal to travel from the satellite to the receiver, i.e., the travel time. This time can be determined based on a comparison or a correlation between received coded signals and receiver-generated signals, i.e. local coded signals. To do this, the receiver has to know the time the signal left the satellite as well as the time the signal arrived at the receiver. Hence, two clocks are involved : one in the satellite side and the other in the receiver side. The accurate satellite clock gives the navigation signal time-tag, when transmitting it. The receiver clock is used to measure the time of arrival of the signal. For economical reasons, usually a very cheap clock is used inside the receiver. The receiver has then to compute the clock offset of its own cheap clock. Thus, measured range to satellites are biased by satellite and receiver clocks errors and consequently they are denoted as pseudoranges.

To solve for the four principal unknowns, namely the three coordinates of user position and the receiver clock bias, at least four simultaneously and independent measured pseudoranges are needed. Using, the ephemeris broadcast by the satellite, its position can be computed. Knowing the position of at least four satellites and the corresponding pseudoranges, user position is estimated using a multilateration process : each pseudorange defines a sphere centred at the satellite location, then these four spheres overlap in two locations. The first one corresponds to the receiver location while the second point is distinct in space. This allows to compute the user position. This process is presented in Fig. 1.3.

For this pseudoranges (PRs) measurement to be carried out, the GNSS signals have been designed with particular properties allowing the receiver to estimate their flight time, i.e. the time they have spent travelling the satellite/receiver distance. The receiver itself can be broken down into several "stages" with specific missions for each that allow the calculation of the final user position. The conventional architecture of a GNSS receiver is shown in Fig 1.4.

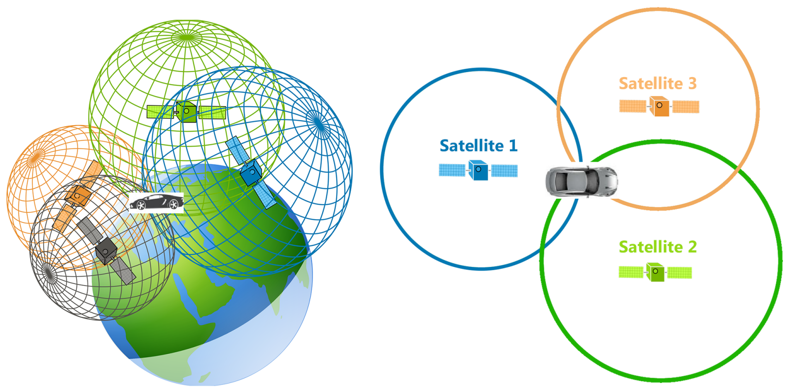

FIGURE 1.3 – Trilateration concept for Positioning using GNSS

It must be recalled that a general GNSS receiver contains several reception channels running in parallel for PRs estimation, but are not shown in Fig 1.4 for a matter of simplicity.

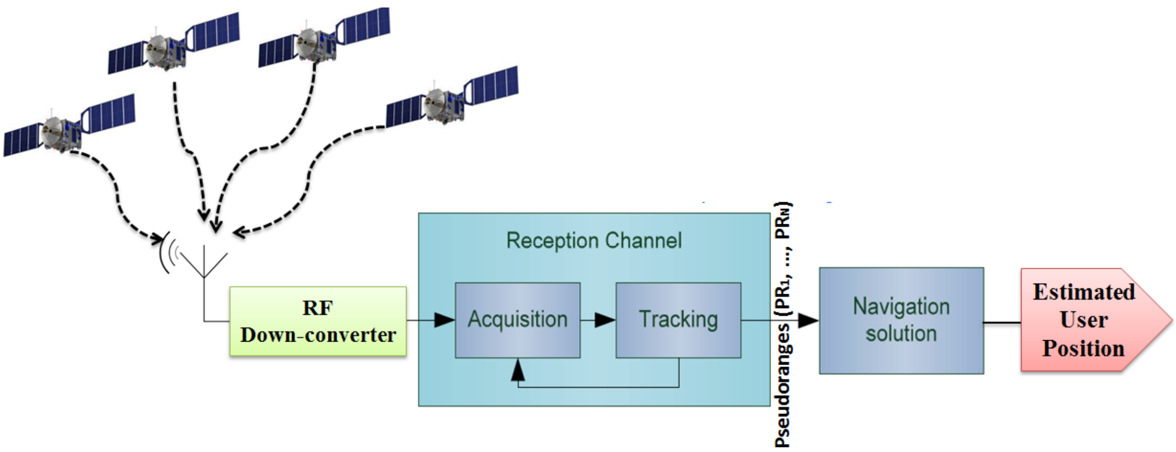

FIGURE 1.4 – Architecture of a GNSS receiver - NB : several reception channels are generally running in parallel but not shown in this figure.

The navigation message and the PRN code are both modulated onto the same carrier frequency. Pseudo-random (PRN) codes are used because of their excellent characteristics for correlation. Indeed, the correlation of two different PRN codes will give an almost zero result. On the other hand, the autocorrelation of a PRN code will give a strong triangular peak when the two replicas are in phase, and will be almost zero elsewhere. This specific property allows on one hand to separate the different GNSS signals from one another and on the other hand to initiate the estimation of the delay between the received signal and the replica that the receiver generated locally, i.e. pseudoranges. This process is performed in the acquisition stage (as in the tracking stage as well), in which a coarse estimation of the Doppler frequency and the time delay is performed.

After performing the acquisition step, the receiver starts the process of tracking the navigation signal. The tracking step makes it possible to follow the evolution of the delay on the code, the frequency and the carrier phase generated by the relative movements between the satellite and the user and thus update the calculation of the point. Indeed, because of the movement of satellites at high speed, the frequency and delay characteristics of each signal evolve very quickly. If they were not re-estimated regularly, the receiver would lose the signal. Further details may be obtained in [13, 14, 25, 26].

The final stage in the receiver architecture is the navigation block which permits to compute the final user position using the estimated pseudoranges. The code pseudorange (PR) is equal to the difference between the receiver and satellite clock readings multiplied by the speed of light c, and can be expressed as :

$$z_i = c(T_{Rec-Rx} - T^i_{Emit-Sat}) \tag{1.1}$$

Here, z_i refers to the measured code pseudorange between the observing receiver site and the satellite i, the term T_{Rec-Rx} is the time at which the GNSS signal is received by the receiver and $T^i_{Emit-Sat}$ refers to the time at which the same GNSS signal is transmitted from the satellite i. In practice, the navigation signals are affected by systematic errors or biases and random noise as well. Broadly speaking, these error sources could be classified into three main groups : satellite-related errors namely orbital errors or satellite clock bias, propagation-related errors including ionospheric, tropospheric delays and multipath and non-line-of-sight (NLOS) reception and receiver-related errors including receiver random noise. We note that the clock bias is a parameter to be estimated in the state vector of position and time, because it is very difficult to compensate for. Taking into account these errors, measured PR from an emitted satellite i can be represented by [13, 26] :

$$z_i = h_i(\mathbf{x}_u) - c.dT^i_{Sat} + I_i + T_i + v_i \tag{1.2}$$

Where :

— $h_i(\mathbf{x}_u)$ is the line-of-sight (LOS) distance between the receiver at user location $\mathbf{x}_u = (x_u, y_u, z_u)^T$ and the satellite i. Note x^i_{Sat}, y^i_{Sat}, z^i_{Sat} the three components of the position vector of the satellite i in the Earth-Centred-Earth-Fixed (ECEF) frame [1] at epoch t, this last LOS distance can be expressed as :

$$h_i(\mathbf{x}_u) = \sqrt{(x_u - x^i_{Sat})^2 + (y_u - y^i_{Sat})^2 + (z_u - z^i_{Sat})^2} + c.dT_{Rx}$$

— dT_{Rx} is the receiver clock bias. This term represents the offset between the cheap receiver clock time and the true system time and has to be considered as an unknown to be estimated.

— dT^i_{Sat} is the satellite clock offset. Since the atomic satellite clocks are very stable, this term can be predicted using a second order polynomial model based on parameters sent

1. In this thesis, we consider that all needed frame changes have been done before computing the satellites positions in the ECEF frame. Hence, the Sagnac effect has been compensated for in the used software.

in the ephemeris messages.

— I_i represents the ionospheric delay caused by the signal propagation in the ionosphere layer. This ionospheric refraction can be corrected by an adequate combination of dual-frequency data or using some known models such as Klobuchar model [27].

— T_i refers to tropospheric delay due to GNSS signal propagation in the troposphere layer. Many models have been used to correct for this delay such as the Minimum Operational Performance Standards (MOPS) adopted by the SBAS (WAAS, EGNOS,...) [28].

— v_i denotes all undesired errors, including the receiver noise n_i, Multipath (MP) and non-line-of-sight (NLOS) errors. Receiver noise refers to the pseudorange error caused by the GNSS receiver hardware and software. This noise is generally assumed to be a white noise. MP and NLOS biases are very difficult to be predicted and indeed become one of the focused subjects in this thesis. These two terms will be further explained.

After Model-based compensation of ionospheric delay, I_i, tropospheric delay, T_i, and the satellite clock offset, dT^i_{Sat}, the measurement model for all received satellite could be simplified as :

$$\mathbf{z} = h(\mathbf{x}_u) + \mathbf{v} \tag{1.3}$$

Equation (1.3) contains a nonlinear function on the three unknown user position $\mathbf{x}_u = (x_u, y_u, z_u)^T$. Since this function is nonlinear, problem (1.2) cannot be resolved analytically in general. This function is then linearised using a first order of Taylor expansion around a known location $\mathbf{x_0} = (x_0, y_0, z_0)^T$, which is usually taken as the previous estimated user position. Then, considering N emitting GNSS satellites, the following linearised equation formulates the satellite positioning problem, called the navigation equation [13, 10] :

$$\delta\mathbf{z} = \mathbf{H}\delta\mathbf{x} + \mathbf{v}$$

The term $\delta\mathbf{x}$ is the offset in the user's position and time bias relative to the linearisation point. The term $\delta\mathbf{z}$ is the PR measurements innovation (i.e. measured minus predicted pseudorange). The linearisation is valid in the case of GNSS, because the displacement in the user's position is within close proximity of the linearisation location.

For the sake of simplicity of application of estimation methods in this thesis, we denote the input vector as $\mathbf{y} = \delta\mathbf{z}$ and the state vector to be estimated as $\mathbf{x} = \delta\mathbf{x}$ to obtain the following observations model :

$$\delta\mathbf{z} = \mathbf{H}\delta\mathbf{x} + \mathbf{v} \;\rightarrow\; \mathbf{y} = \mathbf{H}\mathbf{x} + \mathbf{v}; \qquad \mathbf{y} = \delta\mathbf{z}, \mathbf{x} = \delta\mathbf{x} \tag{1.4}$$

Throughout this dissertation, we adopt the following notations :

— **State Vector or Unknowns** : $\mathbf{x} = (x_u - x_0, y_u - y_0, z_u - z_0, b_{Rx})^T$ is the $[4, 1]$ state vector containing the parameters of primary interest, i.e. the three coordinates of the user position $(x, y, z)^T$ and the receiver clock bias b_{Rx}. $\mathbf{x}$ represents an incremental deviation from the known reference point $\mathbf{x_0}$.

— **Measurement Innovation vector** : $\mathbf{y} = (y_1, \cdots, y_N)^T$ is the $[N, 1]$ linearised pseudorange (PR) measurements vector. For each satellite i, this term is related to the PR measurements from the same satellite with the following relation : $y_i = z_i - z_i^{Pre}(\mathbf{x_0})$, where $z_i^{Pre}(\mathbf{x_0}) = h_i(\mathbf{x_0}) - c.dT_{Sat}^i + I_i + T_i$ is the predicted PR measurement from satellite i at reference point $\mathbf{x_0} = (x_0, y_0, z_0)^T$.

— **Measurement Matrix** : $\mathbf{H} = (\frac{\partial h_1(\mathbf{x_0})}{\partial \mathbf{x}}, \cdots, \frac{\partial h_N(\mathbf{x_0})}{\partial \mathbf{x}})^T$ contains the unit line-of-sight (LOS) vectors between satellites and reference point $\mathbf{x_0} = (x_0, y_0, z_0)^T$. This matrix describes the linear connection between measurements innovation $\mathbf{y}$ and unknowns $\mathbf{x}$, obtained as the Jacobian matrix of h function in (1.3) by 1^{st} order Taylor expansion.

— **Observation or Measurements error signals** : $\mathbf{v} = (v_1, \cdots, v_N)^T = \mathbf{n} + \mathbf{b_{MP-NLOS}}$ refers to pseudorange measurements error signals. $\mathbf{b_{MP-NLOS}}$ refers to the additional measurement bias caused by MP/NLOS receptions and the remaining satellite-related and propagation-related errors after the application of the corrections, commonly called as PR bias. $\mathbf{n}$ is the receiver measurements noise. Traditionally, this latest term is supposed to be a white Gaussian noise characterized by a known covariance matrix $\mathbf{R} = E[\mathbf{n}\mathbf{n}^T]$.

It is important to note that the first three parameters in the new unknown $\mathbf{x}$ to be estimated represent an incremental deviation from the known reference point $\mathbf{x_0} = (x_0, y_0, z_0)^T$ about which the linearization took place. This position is calculated in WGS84 (World Geodetic System 1984) ECEF coordinate system [29] and then transformed to the geodetic coordinates system composed of longitude, latitude and ellipsoidal height.

1.2.3 GNSS Basic Estimation Techniques

Using PR measurements, the navigation block has as its mission to estimate the unknown state vector in the classical equation (1.4) to predict the user position. A plethora of estimation algorithms had been proposed in the literature to solve for the user location in the GNSS navigation equation (1.4). In particular, the well-known standard Least-Squares (LS) and Extended Kalman Filter (EKF) are ones of the most widely used algorithms in science and particularly in GNSS localization with GNSS measurements. Some brief descriptions of these algorithms are as follows :

1.2.3.1 Standard Weighted Least-Squares Estimation

According to (1.2) and (1.3), the GNSS measurement model is non linear. Thus, we have to linearize this model as it have been shown in (1.4) to apply the standard Least-Squares. The conventional Least-Squares (LS) estimate of (1.4) is given by the following :

$$\hat{\mathbf{x}}_{LS} = (\mathbf{H}^T\mathbf{H})^{-1}\mathbf{H}^T\mathbf{y} = \mathbf{H}^+\mathbf{y} \tag{1.5}$$

The Weighted Least-Squares (WLS) estimate of (1.4) is given by the following [10] :

$$\hat{\mathbf{x}}_{WLS} = (\mathbf{H}^T\mathbf{W}\mathbf{H})^{-1}\mathbf{H}^T\mathbf{W}\mathbf{y} = \mathbf{H}_\mathbf{W}^+\mathbf{y} \tag{1.6}$$

Where $\mathbf{H}_{\mathbf{W}}^{+} = (\mathbf{H}^T\mathbf{W}\mathbf{H})^{-1}\mathbf{H}^T\mathbf{W}$, and $\mathbf{W}$ is a weighting matrix. To achieve optimal performance, the weighting matrix should be proportionnal to the inverse of the measurement error covariance [30] that is $\mathbf{W} = \mathbf{C}_p^{-1}$, where $\mathbf{C}_p$ is the covariance matrix of the observation noise $\mathbf{v}$. So, we denote $\mathbf{H}_{\mathbf{C}_p}^{+} = \mathbf{H}_{\mathbf{W}}^{+}$. It is important to note that the final user position is estimated using the following update rule : $\mathbf{x}_u = \mathbf{x}_0 + \delta\hat{\mathbf{x}}$, where $\delta\hat{\mathbf{x}}$ is given by (1.5) or (1.6).

By omitting the MP/NLOS bias from PR measurements in (1.4) at the outset, i.e. considering firstly that $\mathbf{b_{MP-NLOS}} = 0$ (neglicting also the remaining satellite-related and propagation-related errors after the application of the corrections), observation noise are assumed to be Gaussian distributed with zero mean and covariance matrix $\mathbf{C}_p = \mathbf{R}$. A used metric to qualify the efficiency/accuracy of an estimation is the covariance matrix of the estimation error. In the case of the WLS estimation, it can be shown that this metric is given by [10] :

$$\begin{aligned} Cov(\mathbf{\Delta\hat{x}}_{WLS}) &= E[\mathbf{\Delta\hat{x}}_{WLS}\mathbf{\Delta\hat{x}}_{WLS}^T] = E[\mathbf{H}_{\mathbf{R}}^{+}\mathbf{n}(\mathbf{H}_{\mathbf{R}}^{+}\mathbf{n})^T] \\ &= \mathbf{H}_{\mathbf{R}}^{+}E[\mathbf{n}\mathbf{n}^T](\mathbf{H}_{\mathbf{R}}^{+})^T = \mathbf{H}_{\mathbf{R}}^{+}\mathbf{R}(\mathbf{H}_{\mathbf{R}}^{+})^T = (\mathbf{H}^T\mathbf{R}^{-1}\mathbf{H})^{-1} \end{aligned} \tag{1.7}$$

Where $\mathbf{\Delta\hat{x}}_{WLS} = (\hat{\mathbf{x}}_{WLS} - \mathbf{x})$ denotes the WLS estimation error and E represents the expectation operator. To illustrate the effect of the quality of measurements and the geometrical configuration of the satellites visibility, we assume that the PR measurements from different GNSS satellites are identically distributed and independent. However in practice the PRs maybe correlated and specific processing techniques are available as well as filter tuning to deal with this fact. Hence the noise covariance matrix $\mathbf{R}$ can be simplified to $\mathbf{R} = \sigma_{UERE}^2\mathbf{I_N}$, where $\mathbf{I_N}$ is the $N \times N$ identity matrix and σ_{UERE}^2 represents the User-Equivalent Range Error (UERE) variance. Under this assumption, substitution into the covariance matrix of the estimation error expression (1.7) yields :

$$Cov(\mathbf{\Delta\hat{x}}_{WLS}) = (\mathbf{H}^T\mathbf{H})^{-1}\sigma_{UERE}^2 \tag{1.8}$$

Hence the covariance of the WLS errors are proportional to the matrix $(\mathbf{H}^T\mathbf{H})^{-1}$, called the Dilution of Precision (DOP) matrix. The accuracy of the position/time WLS estimation is determined as a product of a geometry factor, known as the DOP, and a pseudorange errors factor, i.e. pseudorange measurements quality [31]. In other words, the satellite-user geometry dilute the range domain accuracy by the DOP factor. The lower the DOP value, the more favorable is the satellite-user geometry (satellites well spread on azimuth), the more accurate is the WLS estimation. The DOP can be seen as a projection of the errors from the measurement domain onto the errors in the position domain.

DOP value become lower in case of GNSS satellites equally spaced and well distributed in the horizon. To characterize the accuracy of various components of the postion/time solution, different DOP parameters can be defined, namely the geometric dilution of precision (GDOP), the position dilution of precision (PDOP), the horizontal dilution of precision (HDOP), the vertical dilution of precision (VDOP) and the time dilution of precision (TDOP). If the satellite and user positions are expressed in East-North-Up (ENU) or North-East-Down (NED) coordinates, then these DOP parameters are linked to the trace of the

$\mathbf{G} = [\mathbf{G}]_{i,j} = (\mathbf{H}_{ENU}^T \mathbf{H}_{ENU})^{-1}$, DOP matrix, as follows :

$$\begin{cases} GDOP = \sqrt{\mathbf{G}_{1,1} + \mathbf{G}_{2,2} + \mathbf{G}_{3,3} + \mathbf{G}_{4,4}}; \qquad PDOP = \sqrt{\mathbf{G}_{1,1} + \mathbf{G}_{2,2} + \mathbf{G}_{3,3}} \\ HDOP = \sqrt{\mathbf{G}_{1,1} + \mathbf{G}_{2,2}}; \qquad VDOP = \sqrt{\mathbf{G}_{3,3}}; \qquad TDOP = \sqrt{\mathbf{G}_{4,4}} \end{cases} \tag{1.9}$$

Finally, the attractiveness of this WLS estimation stems from it ease of implementation, but it requires a minimum of four satellites in visibility so that a solution can be calculated.

1.2.3.2 Extended Kalman Filtering

The linear Kalman filler (KF) is an advanced estimator that uses a dynamic model of motion and requires a prior knowledge of certain parameters, mainly the covariance matrices of measurements and dynamic models [32]. It is capable of operating with less than four GNSS measurements for short time periods. The main theoretical strength of KF is the relaxation of the stationarity of the state vector being estimated, as opposite to Wiener filtering and LS [33]. This filter also has the advantage of smoothing the navigation solution taking into account motion model. The ability of the Kalman filter to operate in the presence of few signals and its simplicity of real-time implementation have promoted the use of this solution as the most common navigation filter in most standard GNSS receivers.

The state vector to be estimated in (1.4) is obviously a function of time. Hence, current user position estimation will benefit from previous sequence of measurements, user positions and clock errors over time. Kalman Filter is based on incorporating past pseudorange measurements into position estimation by means of motion model of the user over time and model of the progression of the Rx clock bias over time. The considered state vector in the Kalman filter assembles also the user velocity and the receiver clock bias drift. At each discrete time increment, these unknown parameters may be modeled by the following system [34, 35] :

$$\begin{cases} \mathbf{y}_n = \mathbf{H}_n \mathbf{x}_n + \mathbf{v}_n & : \textbf{Measurement Model} \\ \mathbf{x}_n = \mathbf{\Phi}_n \mathbf{x}_{n-1} + \mathbf{w}_{n-1} & : \textbf{Motion Model} \end{cases} \tag{1.10}$$

Analogously for other quantities, the notation $\mathbf{x}_n = \mathbf{x}(t_n)$ is introduced to indicate that following formulations are considered at discrete time epoch t_n. $\mathbf{\Phi}_n$ refers to the discrete dynamic or transition matrix and $\mathbf{w}_{n-1}$ is the dynamic distribution, supposed to be white Gaussian noise with a known covariance matrix $\mathbf{Q}_n$. The motion model describes the predicted state vector motion based on some assumed model for how the state vector changes/evolves in time. The KF process is accomplished using a recursive computation of four steps :

— **Step 0 : Initialisation :** Give a prior estimate and error covariance matrix.

— **Step 1 : Prediction Step :** The state prediction and the prior covariance matrix of the estimation uncertainty $\mathbf{P}_n^-$ can be propagated as :

$$\begin{cases} \hat{\mathbf{x}}_n^- = \mathbf{\Phi_n}\hat{\mathbf{x}}_{n-1} \\ \mathbf{P}_n^- = \mathbf{\Phi}_n\mathbf{P}_{n-1}\mathbf{\Phi}_n^T + \mathbf{Q}_n \end{cases} \tag{1.11}$$

This step is based on prior knowledges of the dynamic, without any use of measurements.

— **Step 2 : Kalman Gain Computation Step :** The Kalman gain or weight matrix $\mathbf{K}_n$ is obtained in order to optimize, under the assumption of white Gaussian noise and linear model, the estimation accuracy and is given by :

$$\mathbf{K}_n = \mathbf{P}_n^-\mathbf{H}_n^T(\mathbf{H}_n\mathbf{P}_n^-\mathbf{H}_n^T + \mathbf{R}_n)^{-1} \tag{1.12}$$

— **Step 3 : Update Step :** The final solution of the system (1.10) and the covariance matrix of the estimation uncertainty $\mathbf{P}_n$ are update as :

$$\begin{cases} \hat{\mathbf{x}}_n = \hat{\mathbf{x}}_n^- + \mathbf{K}_n(\mathbf{y}_n - \mathbf{H}_n\hat{\mathbf{x}}_n^-) \\ \mathbf{P}_n = \mathbf{P}_n^- - \mathbf{K}_n\mathbf{H}_n\mathbf{P}_n^- \end{cases} \tag{1.13}$$

Other equivalent formulas of $\mathbf{K}_n$ and $\mathbf{P}_n$ could be found in the literature. Here, $\hat{\mathbf{x}}_n$ and $\hat{\mathbf{x}}_{n-1}$ are EKF solutions at discrete time epochs t_n and t_{n-1}. Using a motion model, EKF improves current user estimate by means of previous estimates and new measurements, this process is called smoothing. However, EKF performance relies on Gaussian measurements and motion noise assumptions and on prior knowledge of the receiver dynamics. When these assumptions are incorrect, problems can arise quickly and the estimation is degraded.

Since the GNSS measurement model is non linear, we need to linearize the state and measurement equations in order to resort to the Extended Kalman Filter (EKF) [33].

1.2.4 GNSS Quality Metrics

The performance of any system can be characterized by a number of different features or quality parameters. In the case of a navigation system, a number of statisticals features or metrics have been defined in the literature [10, 31]. Brief descriptions of some of these features are as follows :

— **Accuracy :** The accuracy of a navigation system is a statistical measure of the degree of conformance between estimated and true positions and/or velocities. Usually, this metric is build from the statistical distribution of the estimation errors. Accuracy requirements are generally expressed as a statistical measure of the position error together with a fixed confidence level, e.g. 95%. In the case of GNSS, the accuracy of the PVT depends on :

  — The measurement accuracy : This factor represents the quality of pseudorange measurements used for PVT estimation. The quality of PR measurements may be degraded because of several factors such as ionospheric delays, multipath and non-line-of-sight errors, navigation signal attenuation...

— The estimation mode : This factor represents the estimation framework or algorithm used for PVT computation. It reflects also the presence or not of aided measurements from others sensors. Typically, SBAS, Differential-GNSS (DGNSS) and Real Time Kinematic (RTK) are some used modes for increasing the estimation accuracy.

— The satellite-user geometry : This factor reflects the satellite geometrical distribution in the sky and is expressed in the DOP matrix. It indicates the ratio of positional errors to range errors. If the DOP is high in case of bad satellite-user geometry, the estimation accuracy will be degraded. This factor includes also the measurement redundancy, since the more satellites are available, the lower the DOP.

— The choice of the dynamics model : This factor is considered only in the case of using a motion model in the estimation of the PVT. If the dynamics parameters are set to erroneous values that does not correspond to the actual receiver dynamics, the position estimation will be degraded.

— **Integrity :** The integrity is a measure of the trust that can be placed in the correctness of the information supplied by a navigation system. It includes the ability of this system to provide timely and valid warning or alerts to users in the case when the system should not be used. Conceptually, integrity monitoring in navigation can be defined as the capacity of providing positioning confidence which is able to detect blunder in the measurements and unacceptably large position errors. Integrity monitoring was first developed in the aim of maintaining safety and efficiency of GNSS positioning for air navigation. Integrity requirements involves different parameters, namely Integrity Risk (IR), Protection Levels (PL), Alert Limit (AL) and Time to Alert (TTA).

High accuracy does not mean high integrity : is is not enough that position errors are small in average (accuracy), they must remain small all the time to avoid any risk of unacceptable large errors. Fig. 1.5 illustrates the interest of integrity monitoring and it difference with accuracy.

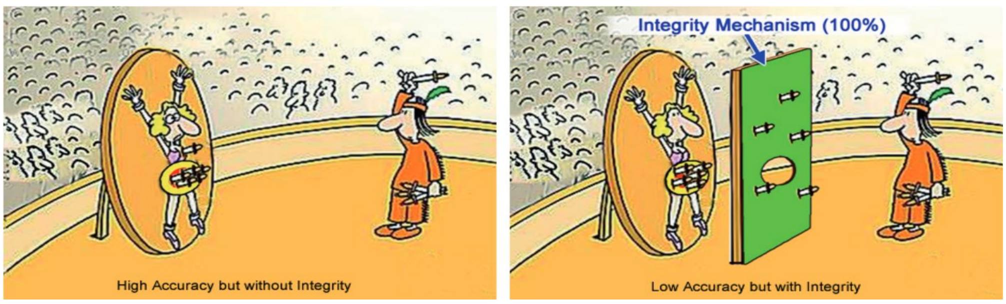

FIGURE 1.5 – An illustration of the difference between Integrity and Accuracy [2]

— **Continuity :** The continuity of a navigation system is the ability to perform its function without interruptions during an intended operation. This feature is expressed in a statistical quantity that quantifies the probability that the specified system performance will be maintained for the duration of a phase of operation, presuming that the system was available at the beginning of that phase of operation.

— **Availability :** The availability of a navigation system is the percentage of time that the services of the system are usable. Availability is an indication of the ability of the system to provide usable service within the specified coverage area under specified conditions of providing required levels of accuracy, integrity and continuity. It is a function of both the physical characteristics of the environment and the technical capabilities of the transmitter facilities.

1.3 Thesis Motivation : GNSS Challenges in Harsh Areas

This dissertation is a synthesis of the research work carried out since 2014 on methods for robust positioning using GNSS measurements in presence of MP and NLOS reflections in the order to enhance GNSS performances in harsh environments, e.g. canyons urban, urban or peri-urban areas, forest and mountainous areas. The motivations of this research works are listed in below :

1.3.1 Increased Demands and Added Value of Reliable Positioning

The Global Navigation Satellites Systems application for land navigation has grown in popularity in urban areas for their free accessibility and suitable accuracy. Motivated by the significant developments of GNSS-based techniques, satellite positioning are poised to have a wide spectrum of applications in land navigation, intelligent transportation systems (ITS), robots/Drones, Location-Based Services (LBS) and Wireless Sensors Networks (WSN) [11].

User requirements in these environments can be specified from numerous perspectives, including accuracy, integrity, reliability, continuity. These requirements can be very stringent and depends on the specific applications. For instance, GNSS reliability is mandatory especially for applications having impacts on financial, legal or safety-of-life repercussions such as specific car tracking or road user charging (RUC) [36]. Some of these application are mission-critical, since, for instance, road users should be charged fairly, accurately and securely in RUC applications. In case of unreliable GNSS positioning, operators have the liability for any wrong doing such as overcharge or undercharge. Moreover, the availability of navigation-based services in urban areas depends directly on the great extent on the positioning performance that that navigation system can provide.

For mass market applications, the use of GNSS systems by the general public, especially through smartphones equipped with GNSS chipsets, is becoming more and more frequent in urban areas. Unlike in the countryside, the different points of interest for users in towns are very close to each other. A few meters away, GNSS users can take the wrong street, take the wrong motorway exit ramp or not even get to find the restaurant they are looking for. Urban users therefore expect a very good positioning precision using GNSS systems. Besides, they ask for a very important service availability, since in a short time they are likely to pass by a large number of points of interest and a position estimation using GNSS unavailable for only one minute may cause them to miss the crossover where they should turn.

As a conclusion, users in urban environments are expecting for a positioning accuracy greater than that obtained in open sky areas, because of the proximity of the various points of interest and intersections in these areas. Hence, along with the appearance and innovation of new land applications, many of the demands come from urban environments where the processing needs of the received signals are extensively more complex than in open sky environments. This factor have motivated our scientific research aiming to enhance GNSS performances in these areas to meet user requirements and expectations.

1.3.2 Degraded GNSS Performances in Urban Areas

Nowadays, GNSS encompass many operational systems such as the American GPS, the Russian GLONASS and the European GALILEO, which forecast on a large increase of performance and services. However, the exponential progress of GNSS applications in land navigation is not without major hurdles in it course of development. Indeed, even with this increase in the satellite availability and the improvement of the constellation geometry, GNSS positioning in urban areas suffer from degraded performance because of several problems that persist. Basically, the rapid urbanizing process in many cities hinders existing GNSS-based positioning technologies performances to achieve the technical and regulation requirements for three main reasons, namely satellites masking and signal attenuation, GNSS signal reflections and degraded satellite-user geometry.

1.3.2.1 Satellite Masking and Signal Attenuation

One of the main problems incurred in the receiver measurements process in urban areas is the masking and the attenuation of the satellite signals. Tall buildings, foliage and surrounding objects present in urban environments tend to obstruct the direct line-of-sight (LOS) signal from many satellites which reduce satellite visibility and degrade the position availability. Purely from geometry it is clear that signals received from low to medium elevation satellites are susceptible to be masked by the densely-built areas and high buildings. Hence, the continuity of position estimation cannot be guaranteed if tunnels, tall building and foliage disrupt the GNSS navigation completely.

Besides, satellite signal could be only partially blocked when propagating though dense foliage which will attenuate the signal strength. This factor engender very challenging technical issues for acquiring and tracking the attenuated GNSS signals.

1.3.2.2 Signal Reflections

Urban environment, on the whole, consists of narrow streets and high buildings with smooth surfaces that may reflect the transmitted signals. Thus, it is very common that GNSS signals reach the receiver via multiple, direct and/or indirect, paths. Similarly, the satellite signal gets bent at the building edges and reaches the GNSS receiver after diffraction, where LOS signal is blocked. Signals received in indirect paths can be classified into two separate types, that generally occur together : Multipath (MP) signal if the signal is received through both direct and alternative paths and Non-Line-Of-Sight (NLOS) signal if the signal is received only through reflections. These combined NLOS and multipath (MP) biases degrade the pseudorange measurements quality and hence degrade the position estimation. In the next paragraphs, we illustrate the adverse effect of these reflections on user position estimation, from a physical point of view. A theoretical demonstration of the effects of MP/NLOS errors on final position estimation is provided in appendix A.

Multipath and NLOS Reception : Physical Consideration : Even though both the NLOS reception and multipath interference are often grouped together as "multipath", they are actually separate phenomena that cause very different ranging errors and different caracteristics [37]. In GNSS, for optimal positioning, it is assumed that the received signals propagate through a LOS path. However, infringement of this assumption can result in inaccurate positioning data. The pseudorange (PR) error is defined as the extra distance travelled by the received signal with respect to the LOS path. This extra distance can occurs in case of reflection of the LOS signal : if both reflected and LOS signals are received, this situation is called multipath interference ; otherwise, if only reflected signals are received, we are in Non-Line-of-Sight (NLOS) situation. Figure 1.6 illustrates the different GNSS signals propagations scenarios in urban environments.

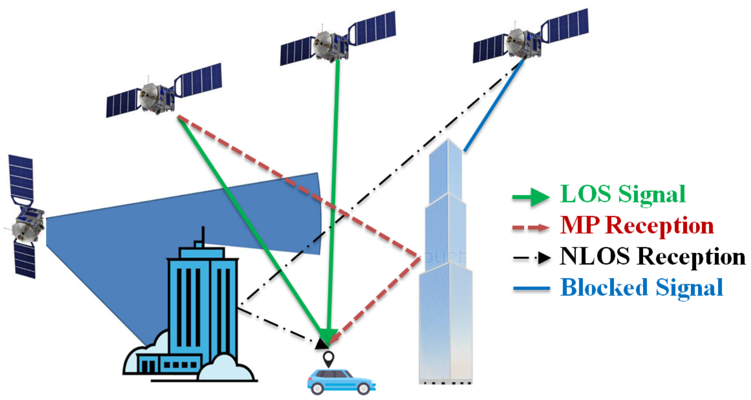

FIGURE 1.6 – An illustration of different GNSS signals propagation possibilities in urban areas

Multipath interference occurs when the transmitted satellite signals are received through multiple replicas which follows different paths than the original satellite-user direct link. These different path are caused by the reflection or diffraction of the direct signals. Such multipaths distort the correlation function between the received composite (direct path plus multipaths) signal and the locally generated reference in the receiver. Theoretically, the magnitudes of multipath error can reach about 0.5 of a code chip depending on the receiver correlation technology [14, 37].

Non-Line-of-Sight (NLOS) is a term to describe a link where there is no visual line-of-sight (LOS) between the transmitting antenna and the receiving antenna. If the line of sight (LOS) is blocked and the satellite signal is received through a reflected NLOS path, the related pseudo-range (PR) measurement will be affected by an additional, always positive, potentially unlimited in range and with an magnitude dependent on the propagation environment.

Improvements due to GNSS augmentations and GNSS modernization are reducing many sources of error, leaving multipath and shadowing as significant and sometimes dominant contributors to error. As they usually arise together in urban settings, these two phenomena distort the composite phase of the received signal, introducing errors in pseudorange measurements, and thus produce errors in position, velocity, and time.

1.3.2.3 Degraded Geometrical Satellite Distribution

The masking of the satellite signals, in urban environments, induces a poor constellation geometry that may affect the Dilution Of Precision (DOP) unfavourably and hence degrade the positioning accuracy. The remaining non-masked received signals are often contaminated with large ranging errors and have all together a poor geometrical distribution which corrupts the position accuracy by several tens of meters of error.

In view of such technical challenges, there is a pressing need to counteract the disadvantages of GNSS degradations, namely MP/NLOS reception : This is one of the principal motivations of this research work.

1.4 Thesis Objectives

The main objective of this research is to develop methods for robust positioning using GNSS measurements in presence of MP and NLOS reflections, by integrating aided information on the receiver environment. Therefore, the following questions are set and have been dealt with in this research :

1. **What is the maximum achievable positioning accuracy level reached by GNSS positioning in MP/NLOS setting, in case of no use of external information ?** To answer this question, we have characterized Lower Bounds (LB) on GNSS positioning performance in MP/NLOS conditions, i.e. the best GNSS estimation performance in the presence of a non-Gaussian environment, without use of external information to assist GNSS systems.

2. **Can a 3D GNSS Simulator, i.e., external information about the receiver environment of reception, be used constructively in real-time to assist GNSS in MP/NLOS situations ?** These additional information are essential in the case of very low GNSS signal availability. The following points have been addressed in this research :
   (a) *What is the required level of realism of the information provided by 3D simulation to be constructively used for GNSS positioning ? What is the merit of using a 3D GNSS simulator ?*
   (b) *How information from the 3D GNSS Simulator could be used to enhance positioning performance ? At what level of processing should this information be used ?*

1.5 Thesis Contributions

The main contributions of this thesis are :

1. **The merit of using aiding information from a 3D GNSS signal propagation simulator to assist GNSS in MP/NLOS setting :**
   We have studied the required and desired minimum level of realism that a 3D GNSS Simulator, or any tool providing information about the MP/NLOS bias, must achieve to be integrated with GNSS for positioning. This is the subject of chapter 3.
2. **Use of external information from a 3D GNSS signal propagation simulator to assist GNSS positioning in MP/NLOS conditions** :
   Different proposed methods for integration of this 3D information to assist the GNSS receiver, at the PVT module by positioning over a grid of candidate positions or the navigation block by correcting degraded pseudorange measurements. This is the subject of chapter 3.
3. **Derivation of Lower Bounds of GNSS performance in presence of a non-Gaussian environment :**
   Evaluation of the maximum achievable GNSS positioning performance in presence of MP/NLOS signals using only "stand-alone" advanced estimation techniques, without external information. The presence of MP and NLOS reflections make the marginal probability density function of the GNSS observations without an analytical form and mathematically intractable, which prevents from using the known standard deterministic lower bounds (LBs) on the mean-squared-error (MSE). Therefore, we derived modified Lower bounds (MLBs) in the framework of non-standard deterministic estimation, at the expense of tightness however.This is the subject of chapter 4.

The methodology followed in this research work is shown in Fig. 1.7.

In this thesis, GNSS positioning methods performed at the position level are methods based on scoring of candidate positions, while GNSS positioning methods performed at the measurements level are methods based on PR measurements correction to enhance positioning performance.

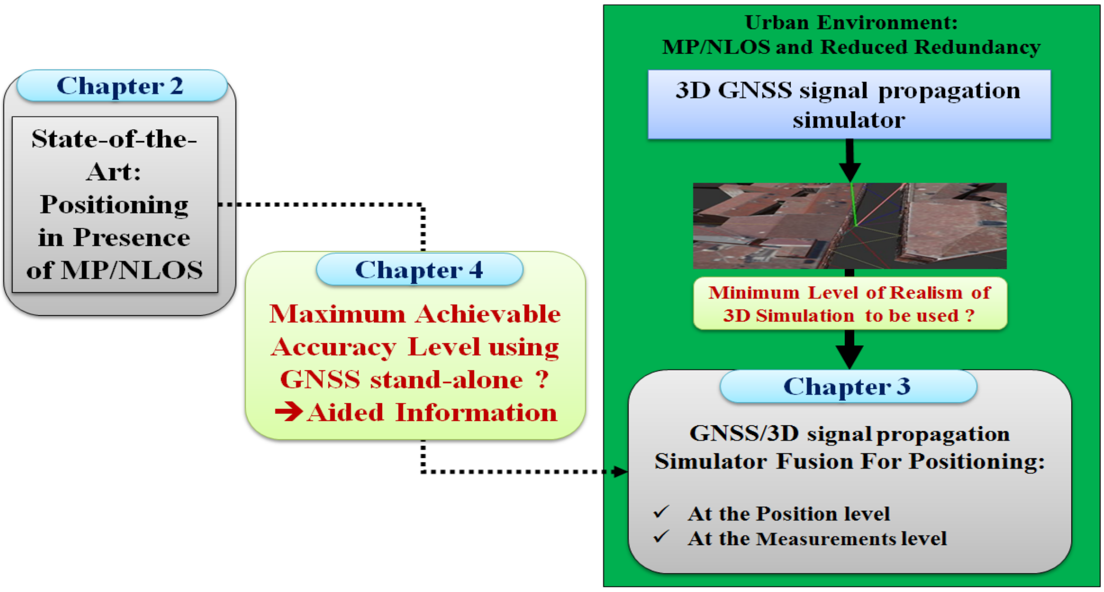

FIGURE 1.7 – Methodology followed in this research work

1.6 Thesis Structure

This dissertation is organized as follows :

Chapter 1 presents the motivations and objectives of this research work, as well as the contributions and the structure of this dissertation. This chapter introduces also the principle of GNSS positioning and its different applications for land navigation. The challenges faced for GNSS positioning in urban environments are also highlighted.

Chapter 2 presents an extensive overview about the most known and used state of the art approaches to tackle the GNSS positioning challenges in urban setting. This chapter gives a detailed summary and a review of these published works in the field of Multi-Path (MP)/Non-Line-Of-Sight (NLOS) mitigation for GNSS-based positioning applications. Broadly speaking, recent published studies on this field fall under three headings : LOS/NLOS classification techniques, i.e. MP/NLOS detection and identification techniques, MP/NLOS modeling and mitigation techniques and constructive use of MP/NLOS degraded measurements for positioning. A special description will be given to techniques based on the use of 3D models/3D GNSS simulators for MP/NLOS constructive use.

Chapter 3 presents our contributions on 3D-Mapping Aided GNSS positioning. In this chapter, we include prior information about the reception environment, provided by a 3D GNSS simulator, to reduce positioning errors. We use information on PR bias provided by a 3D GNSS simulator to assist GNSS positioning in harsh environments. The first section details the used 3D GNSS simulator in this study and discusses it level of reliability. The proposed technique for positioning based on pseudorange errors bounding will be presented in section 2. Two different methods based on using the 3D information, provided by the

3D GNSS simulator, for scoring an array of candidate positions are presented in the third section. Finally, original research about the minimum requirements to be achieved by 3D GNSS simulator, or any others PR-errors-prediction tools, to be constructively used with GNSS will be presented in the fourth section.

Chapter 4 presents our contributions on asymptotic positioning accuracy in the presence of a non-Gaussian environment. Indeed, this practical GNSS problem of MP/NLOS biases falls into a wider one form a theoretical point of view, that is deterministic parameter estimation in the situation where the probability density function (p.d.f) is parametrized by unknown deterministic parameters results from the marginalization of a joint p.d.f. depending on random variables as well. Indeed, when one wants to incorporate a Multipath fluctuation p.d.f different from the Gaussian distribution in presence of Gaussian noise, in most cases, none of the existing estimation performance characterization methods (for instance lower bounds) can be used since the marginal p.d.f of the observations has not an analytical form.

Chapter 5 summarizes the main objectives and challenges addressed in this research. It gives also an overview about the developed techniques and solutions to circumvent the limitations of conventional GNSS algorithms. Resulting from the work of this thesis, several perspectives are noticeable and need a special interest.

1.7 Main Thesis Outputs : List of Publications

1. **Journal Papers**

   [1] N. Kbayer, J. Galy, E. Chaumette, F. Vincent, A. Renaux and P. Larzabal, «On Lower Bounds for Nonstandard Deterministic Estimation,» in IEEE Transactions on Signal Processing, vol. 65, no. 6, pp. 1538-1553, 15 March 2017.

   [2] N. Kbayer, M. Sahmoudi, «Performances Analysis of GNSS NLOS Bias Correction in Urban Environment Using a 3D City Model and GNSS Simulator,» in IEEE Transactions on Aerospace and Electronic Systems, 2018.

2. **International Conferences**

   [1] N. Kbayer, M. Sahmoudi, E. Chaumette, «Robust GNSS Navigation in Urban Environments by Bounding NLOS Bias of GNSS Pseudoranges Using 3D City Model,» Proceedings of ION GNSS+ conference, September 2015.

   [2] N. Kbayer, M. Sahmoudi, «Constructive Use of MP/NLOS Bias of GNSS Pseudoranges : Performance Analysis by Type of Environment,» Proceedings of ION ITM conference, January 2017.

   [3] N.Kbayer, J.Galy, E.Chaumette, F.Vincent, A.Renaux, P.Larzabal, «Estimation Accuracy Of Non-Standard Maximum Likelihood Estimators,» On International Conference on Acoustics, Speech, and Signal Processing (ICASSP), March 2017.

   [4] N. Kbayer, M. Sahmoudi, H. Ortega-Gonzàlez, C. Rouch, «Approximate Maximum Likelihood Estimation Using a 3D GNSS Simulator for Positioning in MP/NLOS Conditions,» Proceedings of ION GNSS+ conference, September 2017.

[5] N. Kbayer, M. Sahmoudi, H. Ortega-Gonzàlez, C. Rouch, «Position Matching Estimation Using 3D Simulator for GNSS Positioning in Multipath/Non-Line-Of-Sight Environments,» Proceedings of ITNST conference, November 2017.

Etat-de-l'art

Vue d'ensemble

Bien qu'ils soient utilisés régulièrement par des millions d'utilisateurs aujourd'hui pour la localisation, les technologies de positionnement par satellites souffrent des effets néfastes de réceptions MP et NLOS. En effet, la réception des signaux par MP et NLOS sont considérés comme les principaux contributeurs d'erreur de positionnement GNSS dans les zones urbaines. Par conséquent, des nombreux travaux de recherches ont été menés et sont toujours activement en cours afin de développer des méthodes pour surmonter ces difficultés et améliorer la qualité de la localisation, même en présence de conditions MP/NLOS. De manière générale, la littérature sur le problème des MP/NLOS se répartit dans les thématiques principales suivantes :

- Détection MP/NLOS : méthodes abordant l'identification des signaux degradés et la détection des réceptions MP et/ou NLOS.
- Elimination des MP/NLOS : méthodes abordant l'élimination des signaux MP/NLOS.
- Modélisation de MP/NLOS : méthodes abordant la modélisation des signaux MP/NLOS.
- Pondération MP/NLOS : méthodes abordant la réduction et l'atténuation des effets des signaux MP/NLOS.
- Estimation des MP/NLOS : méthodes abordant l'estimation des biais MP et NLOS.
- Utilisation constructive des MP/NLOS : méthodes abordant l'utilisation constructive de ces signaux MP/NLOS pour le positionnement au lieu de les éliminer, car les signaux LOS peuvent être trop rares dans certaines situations.

Bien que la littérature sur le problème MP/NLOS soit très riche, très peu sont efficaces pour la cas de GNSS en raison de la structure spécifique des signaux GNSS. Une des principales raisons est que pour le positionnement GNSS, nous visons à estimer avec précision le retard réel des signaux transmis par satellite et pas la puissance du signal lui-même comme dans les communications sans fil. Une combinaison entre plusieurs techniques de traitement des signaux MP/NLOS est souvent utilisée pour le positionnement.

Detection/identification des erreurs MP/NLOS

Ce premier type de techniques appliquées au problème MP/NLOS tend à faire la distinction entre les signaux LOS et les signaux MP/NLOS. Ces techniques peuvent être décomposées en techniques utilisant un hardware additionnel et d'autres ne nécessitant pas de hardware additionnel. Les techniques de distinction basées sur l'utilisation d'un hardware additionnel incluent l'utilisation d'une antenne double polarisation, un réseau d'antennes, un modèle 3D de l'environment et/ou un simulateur GNSS, une fusion du GNSS avec des capteurs inertiels (INS) et un laser-scanner, ou une caméra pour une navigation basée sur la vision.

Sans utiliser de capteurs supplémentaires ni d'informations externes, de nombreux méthodes publiées proposent des indicateurs basés sur la qualite du signal réçu pour l'identification de la réception NLOS.

Elimination des erreurs MP/NLOS

Considérées comme la source dominante d'erreurs dans les applications basées sur le positionnement GNSS dans les environnements urbains, les erreurs MP et NLOS constituent un obstacle majeur au positionnement haute précision. Il est donc primordial de caractériser et d'éliminer ces erreurs. Pour ces raisons, plusieurs recherches ont été menées et sont toujours en cours pour éliminer l'influence des biais MP/NLOS. La plupart des travaux principaux peuvent être en grande partie classés dans trois classes : méthodes utilisant du matériel ou des antennes spéciales éliminant les signaux MP, techniques de corrélation interne au récepteur dans les boucles du module récepteur et techniques de post-traitement appliquées sur les mesures pseudo-distances.

Modélisation des erreurs MP/NLOS

Classiquement, les algorithmes de positionnement GNSS supposent que le bruit d'observation est distribué selon une distribution gaussienne. Cette hypothèse simplifiée n'est plus valide dans les environnements urbains car les signaux GNSS sont contaminés par de grandes erreurs MP et NLOS. Les distributions d'erreurs MP et NLOS sont loin d'être gaussiennes et présentent des "queues" de distribution statistique plus lourdes que celles représentées par le modèle idéaliste gaussien.

Sur une fenêtre temporelle glissante, certaines méthodes se concentrent sur la caractérisation des erreurs PR sous forme de distribution gaussienne avec une moyenne et une variance variables dans le temps. Les erreurs MP/NLOS sont caractérisées aussi avec un modèle de mélange gaussien (GMM) avec un nombre variable de Gaussiens ou de modes en fonction de la taille de la fenêtre d'observation. D'autres modèles statistiques sont utilisés, tels qu'un mélange de processus de Dirichlet infini, des distributions de Rayleigh et exponentielles.

Pondération des erreurs MP/NLOS

L'idée de base des techniques de pondération MP/NLOS est d'attribuer un poids faible aux mesures "contaminées" aberrantes, c'est-à-dire une faible contribution à l'estimation de la position, tout en donnant une pondération nominale ou une contribution totale aux "mesures propres" dans le calcul de la position. Le principal défi consiste à définir cette procédure de pondération afin d'optimiser les performances de positionnement et de réduire autant que possible les effets néfastes des signaux MP et NLOS. Dans cette optique, il existe deux approches principales, l'une basée sur les tests de vérification de la cohérence de l'information d'innovation et l'autre sur le concept des techniques d'estimation robsute (M-estimation par exemple).

Estimation des erreurs MP/NLOS

Les erreurs MP et NLOS entraînent des altérations majeures sur la navigation avec les mesures GNSS, principalement par l'introduction de biais sur l'estimation des PR. Il est donc essentiel d'estimer ces biais pour surmonter cette limitation. Des méthodologies récentes ont été étudiées afin d'estimer simultanément la position de l'utilisateur et les biais sur les mesures. Les méthodes d'estimation des signaux MP/NLOS peuvent être classées en deux catégories : les méthodes tendant à estimer les signaux MP/NLOS dans les boucles de corrélation internes du récepteur et les méthodes d'estimation des erreurs MP/NLOS dans le bloc de navigation.

Utilisation constructive des erreurs MP/NLOS

Afin d'améliorer les performances des systèmes GNSS dans les environnements urbains, beaucoup de travaux existants visent à modéliser ces dégradations MP/NLOS et de les supprimer au niveau des boucles de poursuite ou dans le filtre de navigation. Toutefois, ces méthodes d'élimination des mesures dégradées ne sont pas adaptées aux environnements contraints puisqu'ils induisent généralement une mauvaise constellation géométrique DOP et une visibilité réduite des signaux. La plupart des satellites en environnement urbain sont affectés par des réceptions en MP ou NLOS. Il est donc nécessaire dans ces environnements, d'utiliser tous les signaux disponibles (les signaux corrects et les signaux dégradées) tout en veillant à réduire l'effet des biais dans l'estimation finale. Ces techniques récentes essaient d'utiliser les signaux MP/NLOS d'une manière constructive pour améliorer les performances de la solution de navigation en environnement urbain.

Etant riche en informations, un simulateur 3D de la propagation GNSS permet une prédiction des biais des signaux MP/NLOS. Cependant, cette bonne prédiction des biais est conditionnée par des bonnes performances du simulateur GNSS et une bonne estimation de la position "input" introduite au simulateur. Cette position "input", fournie au simulateur, est utilisée par le simulateur GNSS pour la prédiction du biais. Cette position doit être proche de la vraie position du récepteur (inconnue). Ce problème, similaire à celui de l'œuf et de la poule, pose une difficulté naturelle à l'exploitation du simulateur 3D pour les applications GNSS.

Plusieurs approches de l'état de l'art choisissent de traiter ce problème en considérant un nombre de points fournis au simulateur GNSS sous forme d'une grille de points candidats aux alentours d'une position calculée par le récepteur GNSS autonome en environnement dégradé. La comparaison ensuite entre la prédiction du modèle 3D et les observations au niveau du récepteur permet de trouver la position candidate la plus proche de la vraie position du récepteur parmi toutes les positions candidates de la grille. Le critère de sélection de cette position parmi les différentes positions candidates a été l'objet de plusieurs travaux de recherche. De façon générale, la sélection de cette position se base sur la comparaison entre des observations reçues au niveau du récepteur et des informations fournies par le modèle 3D (ou le simulateur GNSS). Ces observables comprennent la visibilité des satellites, les mesures pseudo-distances pondérés par des valeurs de DOP, les rapports signal sur bruit C/N0, et les biais PR. En supposant que la structure des bâtiments est symétrique en zone urbaine, un modèle 3D simplifié de l'environnement proposé par le laboratoire IFFSTAR, appelé tranchée urbaine, permet d'améliorer les performances de positionnement en villes.

Chapitre 2

State-of-the-Art : Positioning in Presence of MP/NLOS

Contents

Multipath and NLOS reception are considered as the major potential error contributors to GNSS positioning applications in urban areas. However, this problem in GNSS signals falls into a wider one. MP/NLOS reception is a general problem in various applications of wireless telecommunications, including positioning using GNSS signals, targets detection using radar processing, communication using digital radio communication such as Global System for Mobile Communications (GSM) and localization using Ultra-wideband (UWB), Bleutooth, wireless Local Area Network (LAN)/Wi-Fi technologies.

While they are being used regularly by millions of users today for localization, these signal-based positioning technologies suffer all from the adverse effects of these time-varying MP and NLOS ranging errors. Hence, since the early years of the use of wireless telecommunications, a huge amount of researches have been conducted and still actively ongoing in order to develop methods to overcome these challenges and improve the quality of localization, even in presence of MP/NLOS conditions. Broadly speaking, the literature on the MP/NLOS problem fall in these main categories :

— **MP/NLOS Detection :** Methods focusing on identifying the contaminated signals and detecting MP and/or NLOS receptions.

— **MP/NLOS Mitigation :** Methods focusing on mitigating the contaminated MP/NLOS signals.

— **MP/NLOS Modeling :** Methods focusing on modeling the contaminated MP/NLOS signals.

— **MP/NLOS Weighting :** Methods focusing on reducing and down-weighting the unwanted effects of MP/NLOS signals.

— **MP/NLOS Estimation :** Methods focusing on estimating the time-varying MP and NLOS ranging bias.

— **MP/NLOS Constructive Use :** Methods focusing on using constructively these degraded MP/NLOS signals for positioning instead of their elimination, since LOS signals may be too scarce in some situations.

Although the literature of MP/NLOS problem is very rich, very few are efficient for the case of GNSS because of the specific structure of GNSS signals. A key reason is that for GNSS positioning we aim to estimate precisely the true delay of satellite transmitted signals and not the signal itself as in wireless communications. Let us mention also that a combination of several multipath mitigation techniques is often used for positioning.

2.1 MP/NLOS Identification/Detection Techniques

This former type of techniques applied to MP/NLOS problem tends to distinguish between “clean” Line-of-Sight (LOS) signals and "deteriorated" MP/NLOS signals. These distinction methods can be largely grouped into those using an additional hardware or information sources with the principal positioning system and those focusing on detecting MP/NLOS signals without using any external information.

2.1.1 MP/NLOS Detection Using Additional Hardware

Hardware-based distinction techniques include the use of a dual polarization antenna, an antenna array, 3D city models and/or 3D GNSS simulators, a fusion of GNSS/INS and a laser-scanner, or a camera for vision-based navigation.

1. **Dual polarization antenna** : GNSS signals are transmitted with a right-handed circular polarization (RHCP). Specular Reflection of these signals will mostly change their polarization to left-handed circular polarization (LHCP). Hence, exploiting the polarization information may be a simple indicator on the signal reception status. For this purpose, a dual-polarized antenna, containing a single antenna with two receivers sensitive to each polarization, have been used to identify NLOS reception using both the polarization and the C/N0 level [38]. It have been proven that this method detect most but not all of the NLOS signals. Following the same methodology, a method for

NLOS signal detection using single orthogonal dual-polarized antenna is proposed in [39]. These two techniques have also some other limitations : Signals reflected twice or four times will be mostly RHCP and without specific antenna it is difficult to predict the polarization of the received signals.

2. **Antenna array** : Following the concept of interferometric attitude determination, angle of arrival (AOA) of GNSS signals can be measured using an antenna array [40]. This angle information can be used as an LOS/NLOS distinction criteria by comparing azimuth of the received signals (measured using estimated AOA) and the determined lines of sight to the satellite position computed using ephemeris data.
3. 3D **city models and/or 3D GNSS simulators** : 3D city models are digital representations of buildings and other objects present in cities. As these models are becoming more precise and widely available for most big cities around the world, there are growing interest in their exploitation to predict GNSS satellites reception status. Knowing objects surrounding the user location using a 3D city model [41], it is possible to detect blocked signals. Besides, by using a ray-tracing algorithm applied to a 3D city model, commonly called 3D GNSS simulator, reflected and direct signals can be easily identified for simulated signals. However, for real signals the gap between simulation and real propagation is a big challenge for applying this approach. Assuming a prior user location, [42] and [43] use a 3D digital map, jointly with a ray tracing algorithm, to detect multipath interference. Using a 3D GNSS Simulator, called SE-NAV, [44] predict the LOS/NLOS reception state based on a prior user location. The work in [45] propose a simplified 3D model, called urban trench model, based on a geometrical street model with constant width and height and a highly symmetrical building layout, which is mainly the case in the down-towns of some French cities. This simplified 3D model, light in terms of information contents and computation throughput, is then used to identify NLOS and LOS signals based on a prior knowledge of the user true location.

   As the input point used in 3D model is crucial for LOS/NLOS reception state determination and as the true user location is unknown, the work in [46] consider GNSS signal shadowing at multiple location in real time. The building boundary at each candidate position is then computed using ray tracing method to determine the azimuth and elevation angles of the building boundary [47]. To differentiate between LOS and blocked signals, the elevation of each satellite is compared with that of the building boundary at the corresponding azimuth of the satellite at each candidate position over a search grid. As the exact user position is unknown to determine the true satellite visibility, this paper proposes different ways of tackling this problem : a search by position based on founding for a position and signal selection that are mutually consistent or a search by signal combination based on combining the satellite visibility provided by the 3D model with another NLOS detection method, such as consistency checking.
4. **GNSS/INS with a laser scanner** : By exploiting an integration of a GPS receiver, a laser scanner and an inertial navigation system (INS), the work in [48] propose a method for Multipath identification in the reception channel block based on the Doppler shift information. Detecting multipath interference is made by matching between measured frequencies if local energy maxima observed in the tracking process of the GPS receiver and predicted frequencies computed using laser scanner and inertial measurements.

These predicted frequencies are estimated based on parameters of reflecting surfaces that are extracted from laser scan images and inertial measurements of the receiver velocity.

5. **Vision-based navigation** : Generating an image of the entire fields of view above the receiver's masking angle can be a considerable source of information for LOS/NLOS reception state determination. A sky-pointing camera can be used to observe surrounding obstacles. If the orientation of the camera is known, blocked and direct signals can be easily separated from the image based on satellite position obtained using ephemeris message [49, 50]. A research project, called CAPLOC, is developed in the French institute of science and technology for transport, development and networks IFSTTAR in the aim of using image processing techniques to detect visible sky in fish-eye acquired images [51]. The aim consists in separating LOS satellites and blocked/reflected satellites [52]. A sky-facing series of 360° × 180° fish-eye cameras have been used in [53] exploit extracted planes to build a visibility mask for NLOS detection. Finally, virtual camera images can be combined with information from a 3D city model to detect NLOS measurements based on the comparison between actual satellite elevation angle and the critical elevation angle obtained from the 3D model at the position estimated a priori by the navigation process [54].

2.1.2 MP/NLOS Detection Without Additional Hardware

Without using additional sensors or any external information, various published literature proposes many indicators for NLOS reception identification. This type of indicators have been extensively studied in UWB-based positioning algorithms, especially for indoor applications. Indeed, indoor areas contain, on the whole the same features as urban environments, and hence localization applications are often unable to cater continuous navigation accuracy.

— **LOS/NLOS distinction methods in non-GNSS applications** : [55] and [56] give a survey on NLOS identification techniques for wireless signals and classify them into three main categories : Range estimation-based methods, easy to implement and applicable to GNSS but highly depend on fixed thresholds, compares variance of range estimates with a LOS threshold to distingush NLOS reception [57] or to detect transition between LOS and NLOS. The second category of methods are channel statistics-based methods, which are applicable to GNSS but not efficient since they need very high bandwidth [58, 59, 60, 61]. The latest class of methods, which are applicable to GNSS, is applied in the measurements domain to detect NLOS receptions, by exploiting the redundancy of the range estimate using Mini-max or least-median-of-squares techniques [62] or by making use of the dynamics of the system to track NLOS situations and/or LOS/NLOS transitions in the Kalman or particle filters [63, 64].

— **Satellite elevation angle-based LOS/NLOS distinction methods** : In the GNSS field, several studies have attempted to distinguish MP/NLOS reception from LOS reception. Reference [65] presents a brief assessment of various techniques for mitigating and detecting MP/NLOS signals. These techniques include some classic distinction approaches through basic indicators such as satellite elevation angle and signal Carrier-to-noise ratio (C/N0). Purely from geometry, it is obvious that signals received from low satellite elevations are more susceptible to be blocked or reflected by obstacles than signals from high satellite elevations. As a consequence, the elevation of the satellite can be used as a simple indicator of the quality of received pseudorange measurements, by assuming as LOS signals those received from high satellite elevations. However, in dense urban areas, this assumption is not always valid. High buildings may obstruct signal from high elevation satellites, while low elevation satellites could be received in direct path because not all directions are hindered by buildings. Elevation-angle-based distinction criteria may cause a drastic unfavourable effect on satellite-user geometry which degrades the final position estimation.

— **C/N0-based LOS/NLOS distinction methods** : As reflected signals are generally attenuated, signal-to-noise ratio (SNR) or Carrier-to-noise ratio (C/N0) can be indicative of NLOS reception or multipath interference. However, the configuration of the surrounding reflecting objects in urban areas may cause drastic exceptions to this distinction criteria. Low SNR can be caused by propagation through foliage, object masking or a null in the antenna gain pattern. On the other hand, smooth surfaces such as wet surfaces could produce reflected signals almost as strong as LOS signals. Furthermore, constructive multipath may increase C/N0 which make it difficult to distinguish between LOS and NLOS using only C/N0. Tests in a urban environment presented in [66] show that down-weighting low C/N0 measurements may lessen but not totally nullify the impact of MP/NLOS signals. This C/N0-based weighting provides more accurate positioning than weighting based on satellite elevation angle, indicating that C/N0 is probably a more reliable indicator of LOS/NLOS reception than satellite elevation angle.

  Another NLOS/LOS selection criteria based on signal C/N0 levels is presented in [65, 67]. This criteria is based on comparing the difference in C/N0 between different frequencies of the same GNSS satellite with the value expected for the satellite type and elevation angle to indicate MP/NLOS or LOS reception. [65] argues that using a three-frequency comparisons give more reliable distinction criteria that using dual-frequency comparisons. Tests of this distinction technique in urban areas using GPS and GLONASS data show that this multipath detection method is more suitable for static applications and less reliable for dynamic applications, despite its ease of implementation.

— **Residual/Innovation-based NLOS/LOS distinction methods** : Another basic in-receiver indicator of MP/NLOS reception is the measurements residual or innovation. Residual metric consists of the difference between the actual measured PR and the predicted PR based on the time-propagated navigation solution from current epoch solution, while innovation metric is computed using the difference between the actual measured PR and the predicted PR based on the time-propagated navigation solution from previous epoch solution. Modeled as a variance changes in the case of multipath interference and a mean value jumps in case of NLOS reception, [68] studies a series of innovations from previous epochs to detect MP and/or NLOS signals. By introducing a prior and update information about the PR bias magnitude, [69] propose an approximated marginalized likelihood ratio (MLR) stitstic test based on Monte Carlo integration and Jensen's inequality to detect MP/NLOS signals. Following the same methodology and to handle the non-linearities in GNSS measurements, [70] investigates the use of an Unscented Kalman Filter (UKF) based marginalized likelihood ratio (MLR) to identify the biased PR measurements. Using a similar mean value jumps model for multipath NLOS situation, [71] studied a Rao Blackwellized particle filter based on a jump Markov system for joint MP/NLOS detection and positioning. Other prior distributions for the MP/NLOS errors are considered such as the Gaussian mixtures model used in [72] to explore a two-hypothesis Bayesian approach for MP/NLOS detection.

While previous techniques are using a filtred solution, other techniques are working with a single epoch solution. A conventional "top down" sequential testing approach to consistency checking have been implemented in [73] to detect MP/NLOS measurements, with the conclusion that this type of approach is unreliable in case of large number of degraded measurements such as in dense urban areas. Another "bottom up" consistency checking method based on subset comparison is proposed in [74] and [66] based on identifying the most self-consistent set of signals. On the whole, these measurements residual/innovation-based NLOS/LOS distinction methods suffer from several limitations : they generally cannot handle several NLOS errors at a time, they require enough multipath-free LOS signals to generate a reliable LOS/NLOS distinction. Thus, the measurements residuals or innovation is not reliable and robust information to reflect the quality of PR measurements in urban environments.

— **Consistency checking** : Post-receiver techniques for MP/NLOS detection encompass inter-satellite consistency checking. Consistency checking is based on the same principle as the fault detection process in the Receiver Autonomous Integrity Monitoring (RAIM) method, designed to detect faulty satellite signals. By adapting this method to harsh environments, consistency checking operates on the principle that contaminated signals will produce a less consistent navigation solution than "healthy" multipath-free direct-LOS signals. Another consistency checking based technique inspired from RANdom SAmple Consensus (RANSAC) approach is considered in [74] by comparing multiple position solutions in the position-domain, using different combinations of PR measurements, and select the most consistent position set.

— **Receiver-Based LOS/NLOS distinction methods** : Extensive research has been carried out on MP/NLOS detection inside the GNSS receiver itself. As reflected signals from objects presents in urban areas have different range rates from direct signals, it is possible to use the Doppler shift as an indicator of the signal reception status when tracking different signals in both code-phase and Doppler shift domains. Early-Late Phase correlator comparison could be also used as an indicator of MP reception [75]. The amplitude variation of the early and late correlator outputs are compared in [76] to identify multipath interferences. In [77], authors assess vector tracking in a dense urban environment to detect multipath interference and NLOS reception.

2.2 MP/NLOS Mitigation Techniques

Considered as the dominant source of ranging errors in GNSS-based applications in harsh environments, Multipath and NLOS errors are undesirable and present a major hurdle to high-precision positioning. Therefore, it is of utmost importance to characterize and remove these measurement errors. For these reasons, several researches have been conducted and are still ongoing to mitigate the influence of MP/NLOS biases. Most principal works can be largely classified into these three classes : methods using special multipath limiting antennas or hardware, receiver-internal correlation techniques in the signal domain and post processing techniques in the measurements domain.

2.2.1 Hardware-based Methods

High-end receivers are able to suppress multipath to a certain extent, but it is good engineering practice to suppress multipath in the antenna as much as possible. The concept of hardware-based MP/NLOS mitigation approaches is to discard or eliminate multipath and NLOS signals by means of adding new hardware such as a bank of correlators or multiple antennas or modifying the receiver antennas. Discarding these unhealthy measurements will introduce then "clean" pseudorange measurements to the signal processing stage for position computation. These techniques falls under two main headings : methods based on antenna configuration and method based on adding new hardware.

1. **Antenna Configuration :** One of the antenna-based reflections mitigation methods is to enhance the antenna design. If the GNSS antenna is well-designed to receive RHCP signals, the amplitude of reflected LHCP signals will be reduced and hence reduce the effect of multipath interference [39]. However, there is very little polarization discrimination for low-elevation signals which are more prone to reflections than high elevation signals. To reduce the size and cost of these antennas, new technologies are proposing a small polarization-discriminating GNSS antenna [78]. Other classical approaches consist of improving the antenna gain pattern, by means of hardware design or with signal processing techniques, to counter multipaths and reflections [79]. A choke ring antenna is specially designed to reject the reception of reflected signals from the ground surface [80]. This solution based on applying a sharp cut-off below a certain elevation angle, is giving a considerable elimination of signals reflected from the ground. Some new and innovative methods argue for an installation of a small wave-absorbing shield around the GNSS antenna to reduce reflections reception [81].

   Different configurations of antennas have been studied in the literature in order to mitigate the multipath and NLOS adverse effects. Among these methods, antenna array-based GNSS receivers have been widely proposed in the aim of applying beamforming techniques to GNSS signals [82, 83]. The basic idea is to maximize the antenna gain pattern in the direction of direct signals while minimising it in the direction of reflected signals. A beam-forming Controlled Reception Pattern Antenna (CRPA) has been proven to considerably reduce PR errors [84], despite some cost and size limitations. Antenna arrays are also combined with output from the receiver-internal tracking loops in order to mitigate MP. Examples encompass the integration of the beamforming process into the tracking module in [85], the use of carrier phase differences along with multiple closely-spaced antennas in [86] and the integration of the Space-Alternating Generalized Expectation-Maximisation (SAGE) algorithm with a classical GNSS tracking loop in [87].

2. **Additional Hardware :** Using an additional hardware to counteract the disadvantages of GNSS basic architecture in presence of MP/NLOS conditions have been widely studied in the literature. Matching GNSS outputs with panoramic lens camera or an array of cameras is of growing interest [50, 51, 53, 54]. This matching is generally based on superimposing satellite positions obtained using ephemeris data on the image of the sky given by cameras. This class of method suffer from some inherent limitations such as the additional image processing, the additional physical equipment, the cost, the weight and the limited visibility requirement of the camera. A rotating antenna-based processing seems to be efficient against some kind of multipaths [88].

2.2.2 Signal domain Methods

The reception of multipath creates a bias into the time delay estimate of the Delay Lock Loop (DLL) of a conventional navigation receiver, which potentially jeopardizes GNSS positioning accuracy. To mitigate this effect, working in the receiver loops is another well-known approach. Some in-receiver MP/NLOS mitigation techniques are mature and represent standard features of professional grade GNSS receivers, in particularly those based on narrow and double-delta correlators [89]. References [90, 91, 92] provide a comprehensive survey of basic in-receiver signal processing methods for multipath mitigation.

In-receiver MP mitigation methods can be classified into two classes : methods aligning the more or less traditional receiver components (e.g. the early/late correlator) in order to reduce the effect of reflected signals and methods of multipath estimation techniques within the receiver, which treat multipath as an unknown to be estimated before removing it. The second type of in-receiver multipath estimation techniques will be detailed in section 2.5. The former class is based on varying the early-late correlator spacing in the implementation of delay lock loops (DLLs) or aligning the discriminator/timing error detector (TED) of the DLL to the signal received. Examples encompass narrow correlator spacing, double-delta discriminator, the strobe and edge correlator [93], Multipath Elimination Technology (MET) [94] and Multipath Mitigation Technology (MMT) [95].

In-receiver MP mitigation techniques are very well-known, standard and mature methods that approaches the theoretical performance limits. These techniques presents several limitations such as the complex and expensive implementation, the increased power consumption compared to conventional GNSS architecture. These limitations hinder their use for consumer-grade receivers, which are the main used receivers in urban areas. Most of these methods have been patented by leader industrial in the GNSS market which constrains their adoption. Moreover, details of real-time implementation are never provided in open publications. Furthermore, the main limitation of these methods is that they have no improvement in the case of NLOS reception because of the absence of the direct LOS signal.

2.2.3 Measurements domain Methods

Mitigation of the MP/NLOS effect in the navigation block has been extensively studied in the literature. A plethora of algorithms have been reported with different positioning performances, different levels of robustness against MP/NLOS errors, a-priori knowledge requirements and computational complexities. A comprehensive survey of different time-of-arrival (TOA)-based localization algorithms is provided in [96].

Adjustment of the optimal Maximum-likelihood solution in the case of Multipath and NLOS reception has been largely studied. Based on prior knowledge regarding the MP/NLOS distribution and assuming that NLOS scenarios are detected, [97] proposes an improvement of the classical ML position estimation technique to mitigate MP/NLOS errors. Assuming an exponential distribution to NLOS bias, [98] derives a new ML solution more adapted to large measurement errors. Another ML-based solution is also proposed in [99], assuming a Rayleigh distribution for the NLOS error. Different positioning solutions have been proposed in [100] depending on three main level of how much a priori knowledge of NLOS bias is available : with known NLOS statistics, case of limited a priori information and the worst case of no knowledge of the NLOS error.

By supposing some constraints associated with MP/NLOS errors, a new class of constrained localization solutions have been widely studied. A new constrained LS (CLS) formulation have been introduced in [101] and have been solved using quadratic programming techniques. By bounding NLOS errors and assuming a random walk for PR bias modeling, a modified Extended Kalman Filter (EKF) with bound constraints have been studied in [102], with a new enhanced variant constrained Unscented Kalman Filter (UKF) in [103]. Assuming perfect identification of LOS and NLOS measurements, [104] proposes to integrate constraints in user location in the form of a linear feasible region and the final estimation is obtained using linear programming within this region.

Mitigating MP and NLOS signals by Identify and Discard based method is based on indicators on measurements quality. Traditionally, innovation filtering in the Extended Kalman Filter (EKF) is used as an MP/NLOS identification indicator. Measurements having inconsistent innovation values, compared to predicted values, are discarded. Residual test algorithms have been used for joint identification and rejection of MP/NLOS measurements, by selecting the most consistent set of measurements [66, 73]. These methods are using innovation information to first detect and then mitigate MP/NLOS signals. An innovation test algorithm is proposed in [105], based on the assumption that normalized LOS innovations have a central Chi-Square distribution, while normalized NLOS innovations have a non-central Chi-Square distribution. This test is not specific to the physical meaning of NLOS but only to the non-Gaussianity of remaining errors.

Other decomposition based techniques have been also proposed in order to mitigate MP ans NLOS errors. The work in [106] is based on expression of MP/NLOS biases in a new basis to obtain a sparse representation of measurement errors that can be introduced to a classical EKF algorithm or fast convex optimization solvers. Assuming a repetition of multipath pattern between consecutive days for a static receiver with GPS measurements, wavelet decomposition technique have been used to extract multipath from GPS observations and correcting them [107]. Wavelet decomposition and sidereal filtering have also been used to denoise and mitigate multipath effects [108, 109].

2.3 MP/NLOS Statistical Modeling Methods

Classical positioning algorithms in GNSS assume that the observation noise is white-Gaussian distributed. This simplified assumption does not hold in urban environments since GNSS signals are contaminated with large Multipath and NLOS errors [110]. Besides, high-sensitivity receivers can acquire much weaker signals [46]. This may significantly increase the number of acquired reflected signals and therefore their corresponding additional path which results in more large PR bias values. Due to these circumstances, the strong environmental dependency of these errors jointly with the variable features of obstacles in urban areas make it challenging to model mathematically. This erroneous PR errors modeling can lessen the accuracy of the position estimation. In view of such need, better modeling of the MP and NLOS errors is very much sought after.

MP and NLOS errors distributions are far from being Gaussian and exhibit heavier tails than represented by the idealistic Gaussian model [111]. Over a sliding time window, [68] focuses on characterizing the PR errors as Gaussian distribution with variable time-varying mean and variance : the mean jump refers to NLOS reception and the variance represents multipath interference. This assumption have been validated for short observation periods. Since the measurements errors distributions slightly depends on the observation window length, [112] proposes a Gaussian distribution with adapted C/N0 dependent variance model (SIGMA-ϵ), judged as reliable in 80%–90% of MP/NLOS environments. Following the same methodology of adapting the Gaussian model, MP/NLOS errors are charactarized with a Gaussian mixture model (GMM) with a variable number of Gaussians or modes depending on the observation window size [**?**, 113]. However, these non-Gaussian or like-Gaussian error distributions are attributed depending on the reception state of satellites : direct LOS reception, reflected MP reception and blocked NLOS reception. Erroneous LOS/NLOS reception state estimation may affect this result since this will lead to attributing a wrong errors distribution to the estimation stage. The GMM distribution of a set of NLOS corrupted range estimations has been also considered for positioning using range estimation based on Radio Signal Strength (RSS) in indoor applications [114].

Other non-Gaussian models have been proposed in the literature. To overcome the limitation of the dependence on the sliding window size, the non-stationariness of pseudorange errors and the finite aspect of GMM, [115, 116] examine an infinite Dirichlet Process Mixture (DPM) to track the PR errors distribution in real-time. Despite it better fitting to unknown GNSS pseudorange measurements errors distributions compared to GMM, infinite DPM are more complex. Finally, for indoor positioning and for the sake of convenience and simplification, MP/NLOS bias have been assumed to be uniformly distributed between two bias bounds in [117], Rayleigh distributed in [99] or exponential in [118, 98].

Some other works tried to characterize the degradation at the position level and not in the measurements domain. These works tend to characterize the horizontal position errors (HPE). Reference [119] proposes a heavy-tailed generalized Pareto distribution (GPD) to model the unknown position in urban environments, with tuning parameters fixed off-line. Moreover, in the aim to model the horizontal position error for integrity monitoring, a large number of overbounding distributions have been proposed in the literature including a Gaussian sigma inflation distribution [120], a model of Gaussian core and Laplacian tails [121] and a model with a Gaussian core and Gaussian sidelobes [122].

It is worthwhile to note that assuming different models for measurements errors characterization may leads to different strategies of position estimation with different derivations. For instance, Unscented Kalman Filter (UKF) and Extended Kalman Filter (EKF) are known to be optimal solutions in case of white Gaussian noise and other assumptions [26] but are not suitable when assuming non-Gaussian errors distributions. As a conclusion, despite the considerable work attempting to model MP/NLOS errors, accurate characterization of these errors is still far to be achieved because of the underlying and sometimes arbitrary arrangement of obstacles in urban areas making these errors hard to model accurately. Modeling MP/NLOS in harsh environments is still an open research topic that needs to be tackled especially with the pressing need for a minimum level of reliability on the safety critical applications in these areas.

2.4 MP/NLOS Weighting Techniques

The basic idea of MP/NLOS weighting techniques is to assign a low weight to outlier "contaminated" measurements, i.e., a low contribution in the position estimation, while giving a nominal weight or total contribution to "clean measurements" in the PVT computation. The main challenge is how to define this weighting procedure to ensure a maximisation of the positioning performances and to reduce as much as possible the adverse effects of MP and NLOS signals. To design the measurements weights, there are two main approaches, one is based on the consistency checking or innovation tests [66] and the second is based on the concept of M-estimation [123].

Basic weighting-based techniques encompass weighted least squares approaches in equation (1.6) as well as the residual weighting algorithm [66]. The conventional weighted least squares (WLS) solution is modified to reduce the effects of MP/NLOS by giving less emphasis to MP/NLOS measurements in the LS solution. Using some statistics of MP/NLOS errors, such as the kurtosis and the root-mean-square (RMS) delay spread, works in [118, 58] compute the likelihood value of each received signal to be LOS and use them to define according weighting parameters introduced to the WLS solution. Residual Weighting Algorithm in [124] is a weighting solution expressed on the position domain based on scoring or weighting different positions estimated based on different subsets of measurements. Sometimes, these approaches are named consistency checking in the literature [26]. As the computational load of such method may be high in case of large number of received measurements, the work in [125] proposes a lighter and less computational complex solution to compute the residual weighting solution. This issue is related to the detection of MP/NLOS signals to be down-weighted.

One of the main techniques used for measurement weighting is the M-estimator. The general idea behind robust M-estimation technique is making a weighting of measurements based on a new modified cost function, i.e. different from the L_2 norm used in the conventional LS estimation expressed in equation (1.6), that ensure good model fitting : this cost function should ensure high weights to be assigned to good measurements and low weights to degraded ones. First proposed by Huber in 1964 in [123], M-estimation technique is a very well-known class of robust estimators introduced to overcome the limitation of LS regression. All M-estimators share the following proprieties : employ a modified convex cost function for state estimation to capture the effects of outlying data, which are the MP and NLOS errors in the case of GNSS. The convexity of the cost function (to ensure that the cost function is minimized in an unique point) is an essential condition since it ensures the uniqueness of the estimated solution. A function is called convex if the line segment between any two points on the graph of the function lies above or on the graph. Convex functions are especially important in the study of optimization problems where they are distinguished by a number of convenient properties. It can be shown that M-estimation can be simply seen as a weighting technique applied to residuals of the position solution via a convex cost function, usually called the influence function. The choice of the suitable influence function adapted to measurement errors is the main interest of many previous works [126, 127, 128, 129, 130, 131, 132].

Different approaches use weight matrix obtained from different influence functions and weighting strategies. But each influence function gives solutions with different accuracy properties which make the choice of the appropriate function for each application a challenging issue. The choice of the appropriate function is based on a priori statistical analysis of the environment but the need of tuning threshold parameters for optimal performance makes the M-estimators difficult to use in real-time applications. Besides, the risk of ending up with deteriorated performance renders these estimators inappropriate to high-variable environments with multiple sources of outliers. A detailed introduction of robust estimation, including the M-estimation method, may be obtained in the first section "Robust Estimation Principle" of the next chapter "Stand-Alone GNSS Positioning in MP/NLOS Conditions".

Other robust estimators are applied to GNSS measurements such as the S-estimator in [133]. From a general point of view, S-estimator is an estimator minimizing a scale function of the residual of measurements.

Simple and effective Weighting techniques have been mainly proposed in the GNSS literature. As a big correlation exists between PR measurement quality and signal SNR, a basic pseudorange measurement noise variance model based on C/N0 of satellites, called the SIGMA-ϵ, is proposed to weight received phase measurements [134, 135] and code measurements [136]. This previous model was enhanced by taking into account the satellite elevation factor [137, ?] to leverage the relationship between the pseudorange measurements quality and satellite elevation angles.

2.5 MP/NLOS Estimation Techniques

Multipath and non-line-of-sight (NLOS) errors cause major impairments to navigation with GNSS measurements. It is essential then to estimate these biases to overcome this limitation. Recent methodologies have been studied in order to estimate simultaneously the user position and the measurements biases all along the observation interval. MP/NLOS estimation methods may be classified into two categories : methods tending to estimate MP/NLOS in the receiver-internal correlation loops and methods estimating the MP/NLOS errors in the navigation block.

The major method used in the signal domain is the vision correlator [138]. On the whole, receiver-internal MP/NLOS estimation techniques are considering basically two major scenarios : static applications and dynamic applications. Examples of static multipath estimation are those belonging to the family of maximum likelihood (ML) estimators, where the probably best-known technique is the multipath estimating delay lock loop (MEDLL) [139]. MEDLL technique is based on estimating code delays and carrier phases of LOS and MP signals within the receiver. Although MEDLL requires a large number of correlators and large algorithmic computations, it eliminates any multipath biases for delays larger than 0.1 chip and has better performance than standard wide and narrow correlators [140]. In order to reduce computational complexity, [141] suggested a non-coherent implementation of MEDLL. The non-coherent integration is a technique used to increase the acquisition performance, i.e. the correlation between the received and reference signals by applying a discrete Fourier transformation (DFT). It consists in simply summing instances of the output of the basic acquisition block. Further information on the non-coherent integration may be found in the chapter 5 of [142].

Dynamic algorithms for estimation of time-varying multipath have been suggested in the field of communications using the extended Kalman filter as well as the sequential Monte Carlo approach [143]. For navigation systems, various multipath estimators have been considered based on sequential importance sampling (SIS) methods (particle filtering), bayesian estimation or alernating projection algorithms for static and dynamic scenarios [144, 145, 146]. Finally, using a deep fusion of GNSS/INS and laser scanners have been exploited to jointly detect and estimate multipath reflections in [48].

Aside from the aforementioned mitigation techniques in the signal domain, various other techniques have been proposed in order to estimate MP/NLOS errors. A Rao-Blackwellized particle filtering algorithm have been proposed to jointly detect and estimate MP errors [71, 147]. Tracking multipath bias using a Kalman filter solution using time-of-arrival (TOA), time-difference-of-arrival (TDOA) and angle of arrival (AOA) measurements is considered in [148]. Based on a Gaussian Mixture Model (GMM) for MP/NLOS errors, a jump markov system is proposed in [149] to estimate the satellite reception state and not the MP/NLOS errors. Others works propose joint particle filter (PF) and unscented kalman filter (UKF)

[150] and a marginalized likelihood ratio test (MLRT) [69] to track the reception LOS/NLOS state and estimate additional MP/NLOS bias.

2.6 MP/NLOS Constructive Use Techniques

Since direct LOS signals may be too scarce in urban environment, a new trend of techniques has recently received some attention in the literature. These methods aim to detect degraded measurements and use them constructively instead of eliminating them. In fact, under the poor conditions of satellites visibility, it is more interesting to use constructively these NLOS observables. MP/NLOS Constructive use based techniques totally differ from MP/NLOS mitigation based techniques and MP/NLOS weighting based techniques : using constructively MP/NLOS errors signifies using all available pseudorange measurements without down-weighting any measurements, unlike MP/NLOS weighting based methods, and without discarding any measurement, contrary to MP/NLOS mitigation based methods.

2.6.1 PR Measurements Correction-based Methods

The first class of MP/NLOS Constructive use based techniques investigates information on the additional MP/NLOS path in order to correct the degraded PR measurements. Thus, the new corrected measurements could be used in a positioning estimator to enhance positioning accuracy.

Once MP/NLOS measurement is detect using any of the proposed MP/NLOS Identification-based techniques, MP and/or NLOS bias of this measurement can be estimated and corrected. Hence, MP/NLOS Detection-based techniques can be combined with MP/NLOS estimation based techniques to correct PR measurements and use them constructively. Modeled as geometry-based components, multipath delays or parameters can be estimated by considering a series of specular reflections off planar surfaces if the positioning accuracy is sufficiently high [151]. Positioning accuracy can be maintained sufficiently high using NLOS measurements even if some of the direct paths became undetectable.

Once identified and estimated using a fusion of GNSS/INS and laser scanner information for reflecting surfaces detection, multipath reflections are used constructively for navigation using the predict multipath Doppler shifts at the receiver tracking level [48, 152]. However, this technique requires the receiver to be moving in a direction that is not parallel to the reflection surface. The works in [69, 68] use measurement innovation filtering combined with a prior modeling of PR errors to jointly detect, estimate and correct additional multipath and NLOS biases. Based on an autoregressive (AR) process model for GNSS errors, PR bias are detected based on the Mahalanobis distance between the predicted and the observed GNSS PR data, estimated and inserted in the Kalman filter, by adding a detection step in the Kalman filter process in order to detect GNSS data disturbances and by augmenting the state vector using only detected PR bias from the AR process, to correct PR measurements

[153, 154].

This constructive use of degraded measurements by PR correction is a sensitive task : poor PR biases prediction may engender an erroneous ranging correction and then may sensitively reduce the position estimation instead of enhancing it if the compensation term is not accurate enough.

2.6.2 Use of 3D Models and 3D GNSS Simulators

Among the scientific studies in this field, the idea of using aiding information about the geometric environment of reception from 3D city models have received considerable interest. 3D city models are digital representations of buildings with other objects in urban areas. Broadly speaking, we may distinguish between two kinds of 3D models : ones providing pure geometrical information on the buildings and street sizes [155] and others merging ray-tracing algorithms to provide also simulated GNSS signals at any input position and time, called 3D GNSS simulator [156]. 3D models are used to predict blockage and reflection of GNSS signals, and if used jointly with ray-tracing algorithms 3.1.2.2 (3D GNSS simulator) tend to characterize the measurements errors in urban environments.

1. **3D Model based Positioning**

   This type of method is based on simple use of 3D models for positioning without GNSS simulation. As 3D models becoming more and more advanced, they have been used recently for identifying satellite blockage and hence LOS/NLOS state reception in urban areas [157]. These methods are based on predicting the reception status of the GNSS signals across an array of candidate positions, i.e. considering signal reception at multiple candidate positions. The positioning technique is then based on scoring position hypotheses by comparison between the received observations at the receiver navigation block level and prediction using the information provided by 3D models such as the sky visibility [158] provided using bulding boundary information, the SNR measurements combined with a bayesian formulation [159], the position consistency [46] and the superposition of satellite shadow maps based on particle filtering for candidate positions propagation [160]. The final user location is generally estimated by weighting of candidate positions with the highest matching scores.

   Considered among the most mature 3D model based positioning approaches, Shadow Matching solution [157] uses 3D building models to improve cross-track positioning accuracy in harsh environments by predicting which satellites are visible from different candidate locations and comparing this with the measured satellite visibility to determine the final user position solution. By achieving good accuracy improvements for cross-street positioning in urban canyons, this positioning approach based on GNSS and 3D model fusion for satellite shadows scoring of candidate positions, was implemented for smartphone applications [161, 162]. An improved version of this approach is proposed in [158] by combing Shadow-Matching based visibility approach with a 3D based ranging approach for accurate cross-street and along-street positioning in urban canyons.

Other proposed methods are using 3D models for visual positioning without use of GNSS signals. These approaches proposes to use 3D models information jointly with information provided from cameras for positioning without GNSS measurements. As aforementioned techniques, these methods are based on scoring of a grid of candidate positions, but the main difference lies in the scoring function itself. For instance, work in [163] investigates a scoring function based on matching skylines extracted from upward facing omnidirectional images and skyline segments from coarse 3D models of cities. Another similar technique [164] proposes the use of 3D map, camera, accelerometer, and magnetic sensor on a smartphone. The likelihood of candidate positions are computed using the same image-matching technique proposed in [163], with two main differences : virtual photos are generated using Google Earth and the camera attitude is determined using accelerometer and magnetic sensors. GNSS measurements are only used for candidate positions generation in the initialisation step.

2. **3D GNSS simulator based Positioning**

   With an initial position input, 3D GNSS simulators simulate the GNSS propagation in representative type of environments (e.g. open sky, urban and deep urban) and provide the user with several types of information such as the number and the characteristics of reflections, additional PR biases, etc. These simulators output originaly developed for performance nalysis, are recently used in techniques that aim to improve the measurements model for degraded measurements characterization. Like 3D model based positioning approaches, the information provided by 3D GNSS simulation are used to score multiple candidate positions by predicting the path delay of the NLOS signals across an array of candidate positions, i.e., considering signal reception at multiple candidate positions. The positioning technique is then based on likelihood scoring of these candidate location by comparison between the received observations at the receiver and ones of the information provided by 3D simulator such as the the NLOS signal delay at the receiver level [165], the PR measurements matching with a particle filter for candidate position generation [166], the PR measurements matching based on some models on PR errors [158], position error correction based on PR bias predicted by 3D simulation [167] and PR measurements matching weighted with HDOP values [168]. The final solution is then determined by weighting of candidate positions with the highest likelihood scores.

   To reduce the computational complexity, other works are not supposing multiple candidate positions imputed in 3D GNSS simulator but use a-priori input position taken generally as the previous estimated solution or location near the unknown user position. For instance, the previous estimated solution is introduced in a high realistic 3D simulator of the GNSS propagation to predict the geometric path of NLOS signals [169]. This information is then used constructively in a new version of EKF augmented with 3D simulated PR errors. Other approach combines a simplified 3D model of the environment with a multi-hypothesis of state reception with different probabilities to enhance performance [170, 171]. This urban trench technique supposes that the building layout is highly symmetric, which is mainly the case in the down-towns of some French cities. Using this simplified 3D model, called urban trench, path delays of NLOS signals may be computed according to some assumed probabilities of reception. This assumption has been relaxed in a recent paper of the same author [172]. Finally, by constructively using NLOS measurements from virtual satellites at mirror-image locations, [173] developed a Maximum Likelihood Estimate (MLE) solution based on modified Direct Position Estimation (DPE) taken into account NLOS signal information at different candidate positions using 3D maps. However, this method, applied at the receiver level, does not make any update of the used 3D model.

The work of this thesis falls in the class of techniques based on 3D simulation in which we propose several original contributions.

3D models represntation of the environment surrounding the receiver is merely an approximation. Besides, although the 3D GNSS simulator are becoming more and more accurate, they contain a certain level of inaccuracy due to not modeling of the moving objects in the environment (buses, cars, pedestrians. . .) and some immovable objects such as trees. In addition, it is obvious that the predicted biases from the 3D propagation model cannot be instantaneous and highly accurate especially with the sensitivity of the phase lag of the reflected signal. Hence, there is a need to ensure the quality of the 3D model or 3D GNSS simulator to be suitable for positioning performance enhancement. Reference [174] gives an exhaustive list of challenges encountered by shadow matching approach and that can be generalized to most of approaches based on 3D modeling.

2.6.3 Simultaneous Localization and Mapping (SLAM) with GNSS Signals

Simultaneous Localization and Mapping (SLAM) is a well-known technique developed in the robotic community. In radio localization (Wi-Fi, LTE, GNSS), it consists of constructing (building) or updating a map of an unknown environment while at the same time keeping track of transmitters within it and navigating within this map [175]. SLAM methods have been adapted to GNSS applications in order to constructively use NLOS paths. The basic idea is to suppose that NLOS paths can be seen also as LOS paths from satellites to virtual receivers located at receiver mirror-image positions. Reciprocally, NLOS signals can be considered as signals transmitted from virtual transmitters, i.e. virtual GNSS satellites, synchronized in time with the receiver and located at mirror-image positions.

Other approaches are using Long Term Evolution (LTE) signals with fixed transmitters to deal with the problem of positioning in challenging scenarios. For instance, by estimating the multipath components (MPCs) at the receiver level using a Kalman enhanced super resolution tracking (KEST) approach, works in [176, 177] exploit heading information from an inertial measurement unit (IMU) to estimate angle of arrival (AoA) that will be integrated in a particle filter process in order to estimate virtual transmitter location to jointly enhance position estimation and update the map of the unknown environment surrounding the receiver.

Based on GNSS signal strength and 3D maps, the user region of interest (ROI) is divided in "can-be" and "cannot-be" partial regions using satellite shadows to end-up with a LOS maps for all satellites in the ROI [178]. This information is then exploited to how to increase the accuracy of GNSS positioning using 2.5D models of the urban canyon and simultaneously reconstruct the 2.5-dimensional maps using GNSS signal data and user location [179]. 2.5D city models are simplified models built from extruding building footprints or roof edge polygons and that can be converted to 3D city models using aerial oblique photography.

By considering signal propagation at multiple potential navigation candidate positions as usually done in 3D-Mapping aided positioning approaches, other works tend to exploit 3D models to enhance user location in urban areas while at the same time detect potential modelling errors in these considered models. The proposed technique in [180] use information fusion from Control Area Network (CAN) bus providing speedometer data, Inertial Measurement Unit (IMU) providing heading direction, an onboard camera for lane detection and a 3D model of the city combined with a 3D tracing algorithm. These information are hybridized using a Kalman filter or a particle filter to obtain an optimized estimated location that can be used to detect anomalies in 3D modeling and rectify/update the initial 3D building model. A similar approach is proposed in [159] where SNR measurements are used for SLAM via a particle filter map matching algorithm.

2.7 Summary

With an ongoing modernization of services and various constellation of satellites orbiting around the earth, GNSS systems are envisaged to provide enhanced positioning accuracy around the globe. While millions of users are expecting more and more reliable GNSS performance, there are still multiple limitations making GNSS localization degraded in constrained environments, namely multipath and non-line-of-sight reception. In view of such need to overcome these challenges, several positioning techniques have been proposed in order to solve the MP/NLOS problem. Principal proposed methods for localization under MP/NLOS conditions are highlighted in Table 2.1.

1. [ ] : no reference found

TABLE 2.1 – Positioning-based Approaches in presence of MP/NLOS [1]

MP/NLOS Problem : Positioning-based Approaches			
	MP/NLOS Mitigation	**MP/NLOS Weighting**	**MP/NLOS Constructive Use**
Hardware	Choke ring Antenna [80]	[ ]	[ ]
	Polarization-discriminating Antenna [78]	[ ]	[ ]
	Antenna Array [40]	[ ]	[ ]
	Space-Alternating Generalized Expectation-Maximisation (SAGE) [87]	[ ]	[ ]
	Panoramic Cameras [50, 51, 53, 54]	[ ]	[ ]
	Wave-absorbing Shield [81]	[ ]	[ ]
Signal Domain	Narrow Correlator [93]	[ ]	[ ]
	Double-delta Discriminator [93]	[ ]	[ ]
	Strobe Correlator [93]	[ ]	[ ]
	Vision Correlator [138]	[ ]	[ ]
	Fast Iterative Maximum-Likelihood Algorithm (FILMA) [92]	[ ]	[ ]
Meas. Domain	ML-adapted Solutions [97, 98, 99, 100]	weighted least squares (WLS) Solution	PR Correction
	Constrained Localization Solutions [101, 102, 103, 104]	Consistency Cheicking, Residual Weighting Algorithm [66, 118, 58, 124, 125]	3D GNSS Simulator & 3D Model : Scoring of candidate positions [?, 46, 160, 159, 161, 162, 164, 165, 166, 168, 181, 182, 183, 184]
	"Identify and Discard" Solutions [66, 73, 105]	Robust estimation, M-estimator [123, 126, 127, 128, 129, 130, 131, 132], RAIM [26, 185, 186]	3D GNSS Simulator : PR Correction [169, 170, 171, 187]
	"Basis Decomposition" Solutions [106, 107, 108, 109]	C/N0-based Variance [26]	SLAM [159, 178, 179, 180]

TABLE 2.2 – Identification, Estimation and Modelling in presence of MP/NLOS [2]

MP/NLOS Problem : Identification, Estimation and Modeling			
	MP/NLOS Identification	**MP/NLOS Estimation**	**MP/NLOS Modeling**
Hardware	Dual Polarization Antenna [38, 39]	[ ]	[ ]
	Antenna Array [40]	[ ]	[ ]
Signal Domain	GNSS/INS/Laser Scanner [48]	Bayesian Multipath Estimators [95, 138, 92, 144, 145, 146]	[ ]
	Vector tracking [77]	Non-coherent integration MEDLL [141]	[ ]
		Multipath Estimating Delay Lock Loop (MEDLL) [139]	
Meas. Domain	3D GNSS Simulator & 3D Model [?, 46, 160, 159, 161, 162, 164, 165, 166, 168, 181, 182, 183, 184]	Unscented Kalman Filter (UKF) [150]	Gaussian distribution with Heavy-tails [111]
	Cameras [49, 50, 51, 52, 53, 54]	Rao-Blackwellized Particle Filter [71, 147]	Gaussian with Time-Varying Variance and Mean [68]
	Residuals, RAIM and Consistency Checking [68, 74, 66, 26, 185, 186]	Marginalized Likelihood Ratio Test (MLRT) [69]	Direchlet Model and Mixture Gaussian Model (GMM) [?, 113]
	Satellite Elevation and C/N0 [65, 66, 67]		SIGMA-ϵ Variances [112]

Other works have tried to identified, estimate or model degraded MP/NLOS signals, with or without worrying about user positioning itself. Table 2.2 gives an overview about the most relevant works.

2. [ ] : no reference found

Finally, the references used in this survey about MP/NLOS problem can be classified according to their objective in Fig. 2.1. Last, for a broader perspective, let us mention that other taxonomies of research studies dealing with the MP/NLOS problem could be found for instance in [188].

	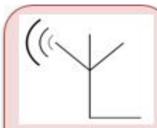 Hardware	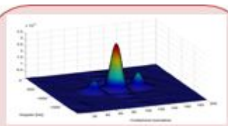 Signal Domain	 Meas. Domain
MP/NLOS Identification	[37, 38, 39]	[46, 75]	[47-52, 63-66, 183-188, 166-170]
MP/NLOS Statistical Modeling	[ ]	[ ]	[66, 96, 97] [109-121]
MP/NLOS Mitigation	[39, 51-52, 78, 79, 85]	[90, 91, 138]	[93-105] [64, 71]
MP/NLOS Down-Weighting	[ ]	[ ]	[25, 64, 115, 56, 120-129, 187-188]
MP/NLOS Estimation	[ ]	[90, 141, 137-139, 144-146]	[67, 69] [147-150]
MP/NLOS Constructive Use	[ ]	[ ]	[159-160, 166-168, 170-173, 180-186]

Figure 2.1 – Representative references of the State-of-the-Art of MP/NLOS problem

Utilisation d'un simulateur GNSS pour la localization

Simulateur SPRING

Le simulateur SPRING est un logiciel de simulation capable de modéliser la propagation des signaux GNSS envoyés depuis les satellites de différentes constellations vers le récepteur GNSS tout en prenant en compte la modélisation géométrique de l'environnement entourant l'antenne de réception (Niveau 2). Un modèle de canal de réception et un modèle de récepteur permettent ainsi l'acquisition et la poursuite des signaux propagés dans l'environnement afin de calculer les mesures de Pseudo-distance, phase et Doppler des satellites acquis. Des algorithmes de calcul de PVT ont été aussi implémentés pour la détermination de la solution position, vitesse et temps récepteur.

SPRING supporte les constellations GPS, GLONASS, Galileo, BEIDOU en configuration mono-fréquence ou bi-fréquence. Les corrections des systèmes SBAS (EGNOS, WAAS, MSAS, GAGAN) sont également prises en compte. Différents modèles de correction ionosphériques et troposphériques ont été également intégrés. SPRING supporte la plupart des formats de données en mode analyse des données GNSS permettant ainsi d'afficher une multitude de sorties graphiques et des fichiers de données avec plusieurs formats possibles (csv, kml, RINEX...). Cet outil d'ingénierie a été développé par Thales Services dans le cadre d'un contrat avec le CNES (Centre National d'Etudes Spatiales).

Pour répondre aux besoins des utilisateurs, le logiciel SPRING possède cinq niveaux de service :

- Niveau 0 : permettant l'analyse en mode temps réel ou post-traitement de mesures d'un récepteur GNSS en supportant la plupart des formats de fichiers GNSS conventionnels.
- Niveau 1 : permettant l'analyse en détail des performances simulées en un point géographique donné, sur une trajectoire ou une région géographique.
- Niveau 2 : offrant la possibilité d'étudier en détail les problèmes causés par la réception indirecte des signaux GNSS dans des environnements contraints. Ce niveau implémente des modèles de propagation couvrant les trois phénomènes physiques définis dans la section précédente. SPRING fournit donc à partir d'une position définie la solution PVT et les différents caractéristiques des signaux reçus et masqués.
- Niveau 3 : permettant l'hybridation des données GNSS réelles avec d'autres senseurs additionnels.
- Niveau 4 : permettant l'analyse des performances en mode simulation pour des données GNSS et des capteurs additionnels dont le comportement est modélisé.

En ce qui concerne le mode général de fonctionnement de SPRING-3D (niveau 2 de SPRING), le simulateur SPRING est compatible avec des modèles 3D au format Kmz. Le logiciel ScenixTM permet d'afficher l'environnement 3D entourant le récepteur selon une taille modifiable, les positions des satellites et de visualiser aussi les différents interactions et propagations des signaux GNSS à travers le milieu géométrique au voisinage de l'antenne (ou de la position input donnée). Le lancer de rayons s'effectue à partir d'une position « input », qui représente la position de l'antenne du récepteur, à travers l'environnement géométrique jusqu'aux émetteurs à l'aide du logiciel OptixTM en utilisant des modèles de propagation en fonction des types d'interactions activées (réflexion simple avec prise en compte de la diffusion, réflexion double spéculaire ou diffraction sur les arêtes des bâtiments).

La figure suivante résume l'architecture globale de SPRING Niveau 2 ou SPRING-3D :

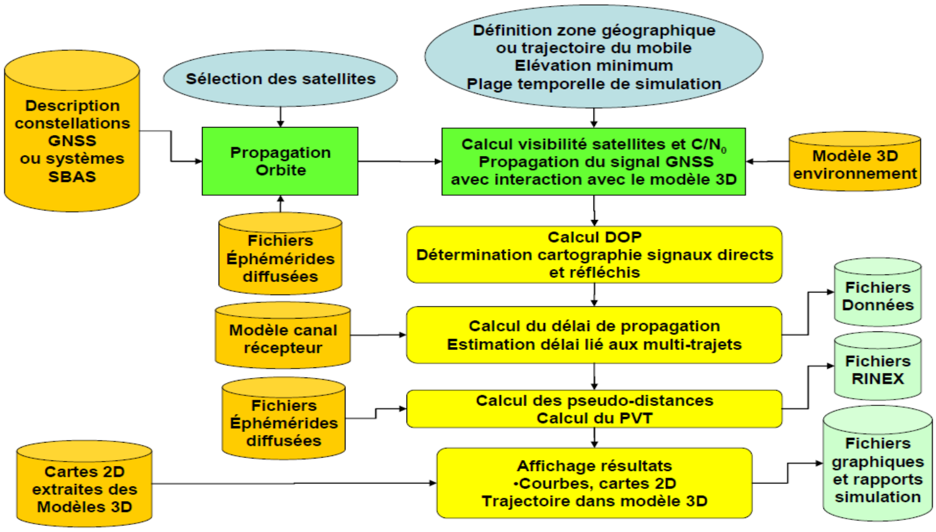

FIGURE 2.2 – Architecture générale de SPRING-3D - Crédits : Formation ISAE 2015

Notre utilisation de SPRING

Dans cette thèse, le simulateur SPRING a été fourni par le CNES afin d'étudier, caractériser la performance et proposer des améliorations à cet outil. La première partie de la thèse consistait à étudier la fiabilité de SPRING. Comme nous n'avions pas accès au logiciel, cette première partie était basée sur la configuration des paramètres du logiciel pour donner l'approximation la plus fiable de la propagation des signaux GNSS dans l'environnement étudié.

Les paramètres de configuration de base de la simulation SPRING sont associés à la configuration de la constellation GNSS, la propagation des signaux GNSS et la configuration de la modélisation 3D (par exemple configuration des matériaux de la scène 3D en modifiant les caractéristiques électromagnétiques des matériaux sélectionnés, la configuration du nombre de rayons par satellite, la configuration du nombre des réflexions du signal et l'activation ou non de réflexions et diffractions multiples) et la configuration de l'acquisition du signal (configuration du modèle d'antenne (gain, diagramme d'antenne) en fonction de la polarisation et de l'angle d'élévation, la configuration du module récepteur en simulant les canaux du réception GNSS, la configuration du modèle de bruit et la configuration du type et des paramètres des boucles récepteur). Le but de cette partie est de configurer tout ces paramètres pour améliorer la fiabilité de la simulation. Idéalement, le paramétrage du récepteur SPRING doit être identique aux paramètres du récepteur utilisé lors de la collecte des données. Comme beaucoup de ces paramètres de configuration sont inconnus, l'incertitude dans la simulation GNSS à travers SPRING est inévitable. La propagation du signal GNSS à l'aide du simulateur SPRING n'est qu'une approximation et ne peut pas être identique à la propagation du signal dans le monde réel. Cependant, nous avons configuré le modèle de récepteur SPRING pour donner une bonne approximation du récepteur utilisé lors de la collecte des données. Cette étape de configuration est essentielle avant toute utilisation du logiciel pour une bonne estimation des biais PR.

Limitations de SPRING

Comme les simulations GNSS à l'aide du simulateur SPRING visent à approximer les erreurs PR en utilisant la propagation du signal GNSS, nous discutons ici la manière dont une interférence MP est généré dans un récepteur GNSS. Le mesures pseudo-distances sont générées dans le récepteur GNSS à l'aide des mesures de code. Les signaux MP réfléchis déforment le pic de corrélation de code dans le récepteur, ce qui dégrade l'estimation des mesures PR. L'amplitude de cette dégradation dépend des retards MP du message réfléchi par rapport au signal LOS, de l'amplitude de ces signaux, du décalage de phase entre le signal LOS et différents signaux réfléchis et de la conception du récepteur GNSS. Par conséquent, la prédiction des erreurs MP, à l'aide des simulations de propagation de signaux GNSS, nécessite un modèle d'environnement précis au cm près et une position du récepteur connue au cm près pour obtenir une bonne approximation des mesures. Cependant, la cartographie 3D utilisée dans SPRING n'est pas précise au niveau centimétrique. En outre, les trajectoires de réference introduites dans le simulateur sont de précision décimétrique. Par conséquent, l'incertitude sur la prédiction des erreurs MP par simulation SPRING est inévitable.

Une conséquence de ces problèmes est que les erreurs de pseudo-distance dues aux interférences par trajets multiples prédites par le simulateur SPRING n'auront aucune correspondance avec les valeurs expérimentées par le récepteur utilisé. Seul l'écart-type de ces erreurs peut être estimé, et pas l'erreur elle-même. Ces problèmes ne concernent que les interférences MP et non les signaux NLOS. Pour la réception NLOS, l'erreur de pseudo-distance est simplement égal au délai supplémentaire par rapport au signal LOS.

Pour améliorer les performances des algorithmes de positionnement basés sur la prédiction des biais PR à l'aide de SPRING, les prédictions de signaux MP doivent être supprimées des erreurs PR et seules les prédiction des signaux NLOS doivent être conservées. Mais, puisque la réception NLOS et les interférences MP sont fusionnés dans les simulations SPRING, éliminer les corrections MP prédite par SPRING n'était pas possibles.

Méthodes proposées

Correction des mesures PR à l'aide des bornes sur les biais MP/NLOS

Une utilisation fiable des informations obtenues par le simulateur 3D repose sur plusieurs hypothèses, en particulier une bonne qualité de la scène 3D, une bonne estimation de la position des satellites, une bonne identification des satellites en visibilité directe et des échos en un point donné via des calculs représentatifs de la propagation. Donc cette modélisation reste toujours source de petites imprécisions, quel que soit le niveau de réalisme du simulateur et du modèle 3D. Dans cette logique, nous essayons d'exploiter des bornes sur les biais estimés par modélisation 3D au lieu de chercher à exploiter directement les valeurs temporelles données par le simulateur. Dans cette sous-section, deux manières d'utiliser ces bornes sur les biais PR pour l'amélioration du positionnement en milieu urbain sont introduites.

Cette approche de correction des mesures dégradées par simulation GNSS est basée sur l'utilisation d'une grille des positions candidates dans l'environnement étudié. Le simulateur SPRING-3D est ensuite utilisé pour prédire des bornes sur le biais PR de chaque satellite. Dans cette approche, nous ne cherchons pas à estimer la position finale comme une position parmi les points de la grille des positions candidates comme classiquement fait par les autres approches existantes dans la littérature. Les bornes du biais, prédites par simulation GNSS, sont utilisées dans le domaine des mesures pour corriger les mesures PR en utilisant des métriques sur la moyenne et la variance. La position finale sera obtenue par application d'un estimateur conventionnel (LS ou EKF) sur les mesures corrigées.

Positionnement par correspondance sur une grille des positions candidates

A cause des différentes sources d'erreurs présentes dans les environnements urbains, obtenir des bonnes performances de positionnement, afin de répondre aux besoins des utilisateurs dans ces milieux, est un vrai challenge. Il est nécessaire d'avoir des sources d'informations supplémentaires pour traiter cette problématique. Etant riche en informations, un simulateur 3D de la propagation GNSS dans l'environnement de l'utilisateur permet une prédiction des biais des signaux MP/NLOS, ce qui engendrera une nette amélioration des performances. Cependant, cette bonne prédiction est conditionnée par des bonnes performances du simulateur GNSS utilisé et une bonne estimation de la position input utilisée dans le modèle lui-même. La bonne estimation de la position "input", fournie au simulateur, signifie que la position utilisée par le simulateur GNSS pour la prédiction du biais doit être assez proche de la vraie position du récepteur (inconnue). Ce problème, similaire à celui de l'œuf et de la poule, pose une difficulté naturelle à l'utilisation du simulateur 3D pour les applications GNSS.

Plusieurs approches de l'état de l'art choisissent de traiter ce problème en considérant un nombre de points input fourni au simulateur sous forme d'une grille des points inputs candidats aux alentours d'une position conventionnelle calculée par le récepteur GNSS autonome en environnement dégradé. La comparaison ensuite entre la prédiction du modèle 3D et les observations au niveau du récepteur permet de trouver la position la plus proche de la vraie position du récepteur parmi toutes ces positions candidates.

Dans cette thèse, nous proposons deux contributions pour la sélection de la position finale parmi une grille des positions candidates à l'aide des métriques calculées par le simulateur SPRING-3D :

— Approximate Maximum Likelihood-3D : une métrique qui évalue la correspondance entre les mesures PR obtenues au niveau récepteur est les mesures PR obtenues par simulation SPRING-3D sur plusieurs points candidats.

— Position Matching-3D : une métrique qui évalue, sur l'ensemble des points candidats, la correspondance entre l'ensemble des positions candidates et un ensemble des positions calculées après correction des mesures PR par les biais prédits via simulation SPRING-3D. Elle évalue également la correspondance entre la solution conventionnelle LS et l'ensemble des solutions obtenues par application d'une projection de type Least-Squares « LS » aux mesures PR prédites par simulation SPRING-3D. Si le simulateur GNSS est précis, la projection de type « LS » appliqué aux mesures PR, prédites par le simulateur SPRING-3D, à une position égale ou proche de la vraie position devra donner la solution LS obtenue par application de l'algorithme LS sur les vraies mesures PR reçus au niveau récepteur.

Résultats expérimentaux et conclusions

Pour analyser les performances des méthodes proposées, une trajectoire de 4 minutes le long d'un environnement urbain autour de la place « Capitole » à Toulouse a été sélectionnée. Une grille de positions candidates de 1600 points a été selectionnée. Les algorithmes proposés permettent une amélioration significative de la précision de 52% par rapport à la solution conventionelle de LS dans environnements urbains profonds. Les résultats de méthodes basées sur la sélection de la position finale parmi une grille des positions candidates donnent des performances similaires à la méthode de l'état de l'art (*Shadow-Matching*).

En milieux urbains denses avec une visibilité réduite des satellites, l'utilisation d'une information de l'environnement pour l'amélioration des performances de positionnement GNSS est nécessaire. Les algorithmes proposés dans cette thèse se basent sur l'utilisation d'une grille de positions introduites au simulateur SPRING. Ces algorithmes donnent une amélioration des performances de positionnement comparable à celles de la solution de l'état de l'art (*Shadow-Matching*), sur ce scénario. Cette amélioration de la précision de la solution est obtenue au détriment d'une augmentation exponentielle du temps du calcul des algorithmes proposés, en fonction de la grille des positions candidates utilisée pour la prédiction des biais PR par simulation GNSS. Néanmoins, cet inconvénient peut être atténué, voire supprimé, en utilisant une implémentation de ces techniques en mode déporté à un serveur de calcul.

Chapitre 3

3D-Mapping Aided GNSS Positioning in MP/NLOS Conditions

Contents

As shown in the previous chapter, achieving reliable positioning in an urban environment using only GNSS pseudorange measurements is a very challenging task. As GNSS technology is based on the reception of signals via direct paths from satellites, any infringement of this basic assumption, caused by NLOS reception, may cause large positioning errors compromising, the user's required performance. Therefore, fusing the GNSS with other sensors or information is essential in these areas.

Becoming more and more available, 3D information about the geometric environment of reception is valuable for properly and constructively using degraded GNSS measurements to improve the positioning accuracy in harsh environments. Hence, we present in this chapter our original investigations on the use of a 3D GNSS signal propagation simulator as a source of 3D aiding information to assist a conventional GNSS receiver. The 3D GNSS signal propagation simulators provide GNSS with some prior information on pseudorange errors that should be wisely integrated in order to optimally enhance the final obtained positioning accuracy. Therefore, we present in this chapter our contributions to this 3D-Mapping Aided GNSS positioning.

This chapter is divided into 6 main sections :

— **Section 3.1 :** The motivations behind the use of 3D GNSS signal propagation simulators in this study will be detailed. A detailed analysis of the used 3D GNSS signal propagation simulators in the context of this research study will be provided.

— **Section 3.2 :** A description of the proposed approach for the fusion of GNSS and 3D GNSS signal propagation simulators aiding information at the PR measuremants level.

— **Section 3.3 :** A description of the proposed approaches for the fusion of GNSS and 3D GNSS signal propagation simulators aiding information at the position level.

— **Section 3.4 :** An experimental validation of the proposed GNSS/3D GNSS signal propagation simulators fusion methods. The proposed integration methods in the position domain will be compared with a Shadow-Matching algorithm.

— **Section 3.5 :** A study aiming to define the minimum required level of 3D simulation accuracy for constructive use of this information for navigation with GNSS PR measurements. This determines how accurate the 3D information, provided by the 3D GNSS signal propagation simulators, should be in order to obtain a better positioning accuracy when integrating this information with GNSS measurements.

— **Section 3.6 :** A summary of the principal conclusions of this chapter is provided.

3.1 3D GNSS Signal Propagation Simulators

3D city models are 3-dimensional digital representations of terrain surfaces, sites, buildings, vegetation, infrastructure and landscape elements as well as related objects present in cities. Buildings in 3D models are represented by collection of points in 3D space, connected by various geometric entities such as triangles, lines, curved surfaces, etc. It is now possible to incorporate detailed highly representative 3D maps of real environments, such as buildings or infrastructure of cities to some 3D GNSS signal propagation simulators. Throughout this dissertation, this integration will be termed as 3D GNSS signal propagation simulator.

Thanks to advances in computing, 3D GNSS signal propagation simulators for the propagation of GNSS signals have been developed in order to offer various signal models complex enough (in terms of the numbers of contributors) to be representative of GNSS signal propagation in complex and dense population centers such as urban canyons [169, 182, 168]. It is worth noting that the complexity and the representativeness of such simulators has increased with the actual computing power of computers.

3.1.1 Motivation of the use of 3D GNSS signal propagation simulators

Today, 3D models are used in a wide variety of fields including navigation. Several factors make the use of this 3D information attractive and useful for positioning with GNSS signals, including :

1) **A natural way for the constructive use of degraded signals :** As simply discarding degraded pseudoranges in an urban setting may deteriorate GNSS positioning, using them constructively is the best alternative in these environments. However, to do that, information about the reception environment is essential. Offering highly representative 3D maps of these environments, 3D building models represent a very valuable source of aiding information to properly use multipath and NLOS signals. This is the main driver of adapting 3D maps for positioning.

2) **3D maps availability :** We have witnessed, these recent years, an increased availability of digital 3D maps. These data are available now for most cities worldwide. 3D maps are also provided from national mapping agencies and private commercial companies such as Google (Google Maps 3D), Apple (Apple 3D Maps), Microsoft (Bing Maps 3D). Besides, some 3D mapping data, such as OpenStreetMap, are available free of charge, but without any guaranty of reliability. Generally, these model cover most dense urban areas where it is most needed for positioning.

3) **Possibility of wireless implementation :** To cope with different positioning limitations in harsh areas, the GNSS receiver can be assisted by various sources of information, such as inertial sensors, cameras and laser scanners. But solutions offering reduced size, price, data storage, processing load and power consumption are more sought after especially for smartphone applications. 3D maps may be used as a wireless solution (data base type solution) : 3D information is stored on a remote server, uploaded to the mobile server and used to enhance positioning accuracy.

4) **Advancements in 3D modeling and simulation power :** The trend of growing interest in 3D models is driven by the continuous advancements made in environment modeling. 3D city models tend to be available for most big cities worldwide. The variety of research in this field indicates the growing interest that make the use of the 3D information a promising and fruitful area of study.

5) **Efficient solution :** As Dr. Groves argues : "3D city mapping has the potential to revolutionize positioning in challenging urban areas" [189]. 3D models have been proved to improve positioning performance in harsh environment [158].

3.1.2 SPRING : Working Principle

SPRING (*Simulateur de Performances d'un Récepteur Intégrant la Navigation par GNSS*) [156, 190] is a 3D GNSS signal propagation simulator developed by the French Space Agency (CNES) that has the capability of simulating, via ray-launching techniques, all paths (from satellites to receiver) to be received in a certain input position at a certain time. SPRING aims to predict PR errors in urban areas. It allows the simulation of the propagation of the GNSS signals inside a 3D scene for an analysis of the multipath interference. A reception channel model and a receiver model enable the acquisition and tracking of the signals propagated in the environment. It allows to calculate pseudoranges, phase and Doppler measurements of the acquired satellites. This simulator is provided by CNES and used in this thesis to assist the GNSS receiver in order to enhance positioning performance. Next, the details of the SPRING simulator is presented.

3.1.2.1 Used 3D City Model

SPRING simulations have been conducted with the use of several 3D models. The used 3D model in this research work is a Toulouse 3D model. This 3D city model was developed by the French National Geographic Institute (IGN). It is based on high resolution images with level 2 of detail (LoD2). The LoD of a 3D model describes how thoroughly the 3D objects representation adheres to the real-world representation. A building in LoD2 city model has differentiated roof structures and thematically differentiated boundary surfaces. More information about these different levels of detail is available in the following documentation [191]. The modelling of 3D scene is achieved via Trimble SketchUp Pro [192] and imported in SPRING from KMZ files. SketchUp allows also the importation of numerous existing 3D models in various formats. The conversion to the KMZ format is supported by SPRING. In order to optimize the simulation performances, these 3D models are converted into an internal SPRING format which ensures the classification of the imported buildings into geographic tiles.

3.1.2.2 Ray-launching Algorithm

In order to simulate the propagation of GNSS signals in the SPRING simulator, a ray launching algorithm has been chosen. Ray launching [193] is a method of ray propagation that requires an accurate model of the 3D scene. This technique is based on optical physics and models all effects that can occur during the propagation of rays : free-space propagation (direct path), reflection, refraction, diffraction, shadowing etc. It is assumed that the GNSS satellites are considered as far field electro magnetic sources, and that the GNSS receiver antenna receives either far field or near-field EM waves according to the distance of the contributor to the antenna. Rays are launched in each possible sampled direction inside a propagation cone. The smaller the directional sampling interval is, the more accurate the propagation model is. Each ray is propagated until it intersects an object in the 3D modelled scene.

Depending on the intersected object type, interactions such as reflections, refractions, diffractions are processed and secondary rays are emitted at the intersection point. Again, these rays are propagated until they hit an object on their path. Reflection coefficients are set by the user depending on the chosen building materials and are uniform for all the considered 3D scene.

3.1.2.3 Software Receiver

Once the characteristics of the different simulated rays have been computed, SPRING uses a specific aggregation algorithm to compute the main echoes of each satellite signal. The echoes are also used by an internal software receiver module to compute the final pseudo-range, phase, Doppler and signal strength measurements (details are in [156]). Different software receiver models can be considered in the SPRING software, with modified and adaptable parameters. Finally, an internal PVT module can be used to compute a position solution. As SPRING don't use any model for ionospheric and tropospheric errors, the MP/NLOS bias is simply equal to the difference between the predicted pseudoranges at the level of the software receiver and the LOS path between the input user position and the satellite position.

3.1.2.4 GPU Resources

The SPRING simulator uses Graphics Processing Unit (GPU) graphical cards to parallelize and accelerate the propagation and visualization algorithms. To implement the ray launching method in the SPRING simulator, the NVIDIA® OptiX™ Ray Tracing Engine [194] has been chosen. It is a programmable system designed for highly parallel architectures such as the Nvidia (graphics card maker) GPU. OptiX is a simple but powerful model of a ray tracer. This ray tracer employs user-provided programs to control the initiation of rays, intersection of rays with surfaces, shading of materials, and creation of new rays. As for the visualization of 3D scene, it is performed by NVIDIA SceniX [195] that is an effective scene management tool, compatible with the NVIDIA GPU. Furthermore, NVIDIA OptiX is used for simulation of the propagation of signals parallelized on GPU.

3.1.2.5 Simulator Outputs

During a simulation, SPRING is able to display in real-time different graphical outputs, including satellite PR measurements errors, satellite reception status, signal strength. At the end of the simulation, these outputs could be easily exported through print-outs or image data. Besides, numerous other statistical and textual outputs regarding the propagation and the interaction of GNSS with the environment are displayed and can be exported.

Simulated PR measurements are computed using GNSS signal propagation within the 3D city model and after signal acquisition and tracking using the receiver model implemented in SPRING. The LOS distance between the satellite and the input position of the receiver antenna introduced in the software is defined as the direct path between these two points. As all the other ranging errors (ionospheric, tropospheric, thermal noise...) are not modelled, the PR bias, which is the parameter of main interest in this dissertation, is predicted as the difference between simulated PR measurements and the LOS distance.

In summary, SPRING is a 3D GNSS signal propagation simulators developed by the French Space Agency (CNES) that has the capability of simulating, via ray-launching techniques, numerous paths from GNSS satellites to receiver antenna to be received in a certain input position at a certain time.

Fig. 3.1 gives a screen-shot of an example of SPRING simulation in an urban environment. Continuous lines refer to signals received in direct line-of-sight while dotted lines represent signals received through indirect paths after multiple reflections. Dashed lines represent signals received after diffractions.

3.1.2.6 Our use of SPRING

Different modeling techniques have been used to develop GNSS simulators for the sake of GNSS performance analysis [196, 197, 198, 199]. However, for a constructive use of PR errors and errors prediction, these simulators suffer from a lack of enough precision as it will be shown in section 3.1.3.1. This is the case of SPRING simulator for example. But, information delivered by these simulators are valuable to approximate different errors affecting the GNSS signals. In this thesis, we focus on the approximation and prediction of PR errors using SPRING simulations in order to mitigate their effect in the processing of the measurements to improve the positioning accuracy.

In this thesis, the simulator SPRING has been provided by the CNES in order to study, characterize the performance and propose improvements to this tool. The first part of the thesis consisted in studying the reliability of SPRING. As we do not have access to the software code, this first part was based on configuring the software parameters to give the most reliable approximation of GNSS signals propagation in the environment under study.

The basic configuration parameters in SPRING simulation are associated with the constellation configuration, the propagation and 3D modeling configuration (for example materials configuration by modifying the electromagnetic characteristics of the materials selected, the configuration of number of rays per satellite, the configuration of the number of the GNSS signal reflections and the activation or not of multiple reflections and diffractions) and the signal acquisition configuration (configuration of the antenna model (gain, antenna diagram) depending on the polarization and the elevation angle, the configuration of the software module simulating the GNSS receiver channels, the configuration of the noise model, and the configuration of the receiver type and parameters). The goal of this part is to configure all

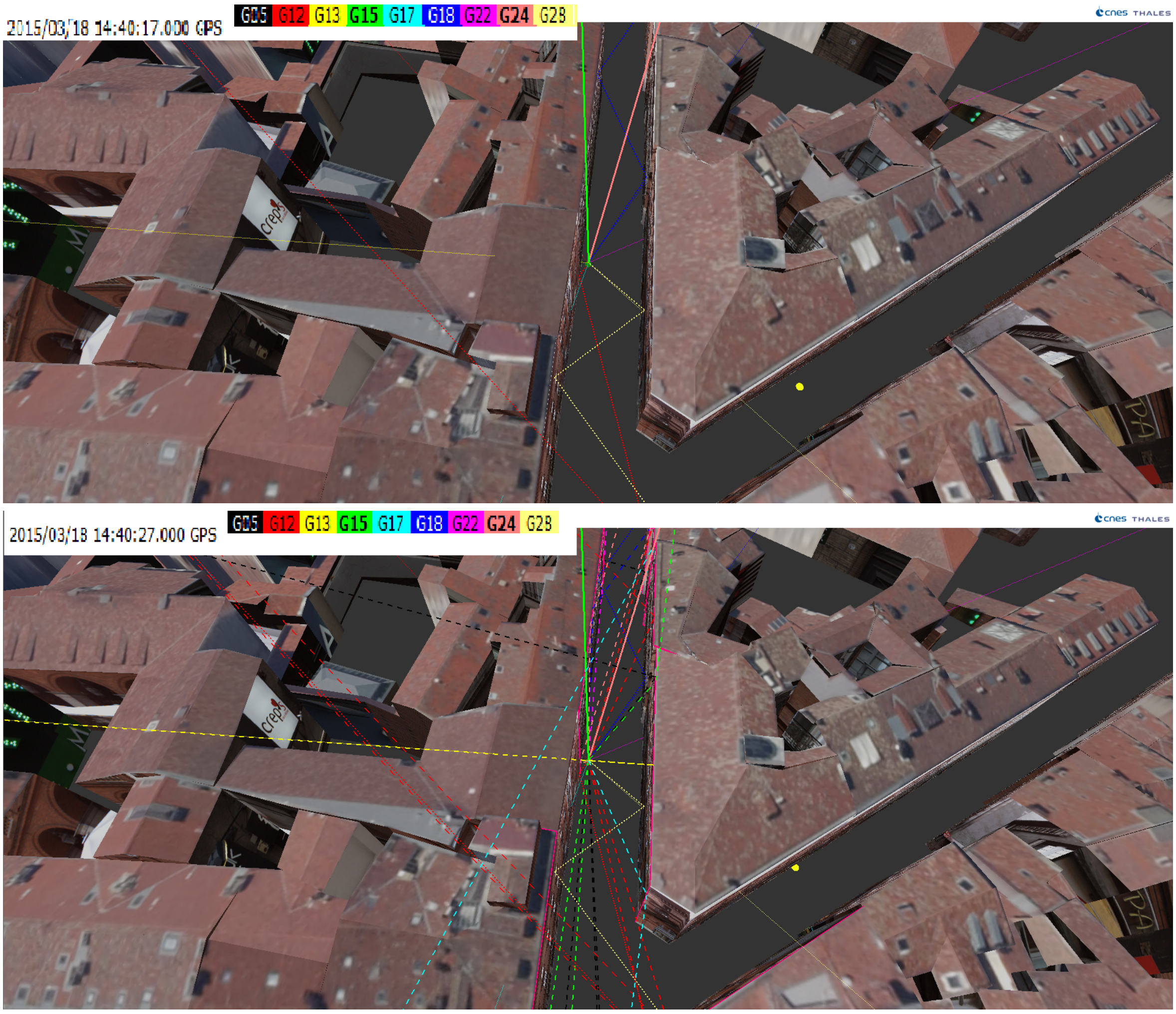

FIGURE 3.1 – 3D GNSS signal propagation simulation using SPRING. Top : Simulation by considering only multiple reflections. Bottom : Simulation by considering both diffractions and multiple reflections

these parameters to enhance the reliability of simulation. Ideally, SPRING receiver parameters should be set as equal as possible to the receiver parameters used during the data collection (that will be described in section 3.4.1).

As many of these configuration parameters are unknowns, the uncertainty in GNSS simulation using SPRING software is unavoidable. SPRING GNSS signal propagation is still a mere approximation and cannot be identical to the real-world signal propagation. However, we have configured the SPRING receiver model to give a good approximation of the receiver used during the data collection described in section 3.4.1 as it will be quantified in the following section. This configuration step is essential before any use of the software for PR bias constructive use.

3.1.3 SPRING : 3D GNSS signal propagation simulator Reliability

3.1.3.1 SPRING Reliability study

Many factors may greatly impact the reliability of 3D GNSS signal propagation simulation via SPRING. These factors encompass the reliability of the 3D models, the accuracy of electromagnetic field propagation and the adequateness of the implemented receiver model. In this subsection, we discuss the uncertainty of the bias estimation provided by the 3D GNSS signal propagation simulator SPRING in a dense urban environment in Toulouse. The considered urban area is the same environment shown in Fig. 3.1.

Fig. 3.2 shows the uncertainty of the bias prediction by 3D GNSS signal propagation simulation using SPRING compared to the "measured" PR bias. The "measured" PR bias or bias predicted using the true user position from the reference system) is predicted using the algorithm proposed in [3]. This pseudorange bias prediction technique relies on the use of position errors, based on a reference system, and the compensation of the receiver clock bias using PR measurement from a reference satellite. Other errors, such as ionosphere and troposphere propagation errors, satellite position and clock errors are reduced using some models and we neglect here the effect of PR measurements noise. In other words, it exploits the errors in computed positions to predict the errors in observations or pseudoranges.

The error in the computed position represents the difference between the estimated position using the least-squares (LS) algorithm and the reference position. This error can be simply estimated using the reference information of the vehicle position provided by a DGPS receiver tightly integrated with an IMU. As we compensate ionospheric, tropospheric and satellite clocks errors using some models and neglect the PR measurements noise $\mathbf{n}$ in the linearized PR measurements , the error in linearized PR measurements, i.e. PR bias, represents the additional path travelled by the signal received through indirect paths. This error is the difference between the signal received through reflections, with or without reception of direct signal, and the direct line-of-sight (LOS) signal from the satellite. Having a reference pseudorange, i.e. the value of direct line-of-sight (LOS) signal, is difficult to obtain. But as the error of LS estimation depends linearly on the pseudorange error as expressed in equation (A.10) of appendix A, true pseudorange error, i.e. PR bias, can be determined by simply inverting this equation (if the number of unknowns doesn't exceed the number of PR measurements).

The main problem is having a reference of the receiver clock bias to apply within this algorithm. The receiver clock bias is eliminated differencing all ranging measurements across satellites using a reference satellite. The selection of the reference satellite is quite important. This satellite must have a reliable and almost "clean" ranging measurement. Basic indicators for this selection process include elevation angle and C/N0 values. Generally, it is better to use both elevation and C/N0 as the highest-elevation signal can still be NLOS. However, in our data collect, we have received signals from a GNSS satellite having an elevation angle higher than 80° as shown in Fig. 3.2. So, in this section, we have used the elevation angle as indicator, i.e. we assume that the satellite with the highest elevation angle has no PR bias. In summary, this PR bias prediction technique, detailed in [3], relies on the use of position errors using a reference system and the compensation of the clock bias using a reference satellite.

Finally, these experiments have been carried out in Toulouse in the same urban section shown in Fig. 3.1. An AsteRx3 Septentrio receiver is used to record GPS L1 C/A code PR measurements. A Novatel SPAN system including a DGPS receiver tightly integrated with an FSAS-IMU (from iMAR), with decimetre level of positioning accuracy, is used as the reference system. Measurements from both receivers were sampled at 10 Hz. For this SPRING reliability test, we have selected a 3-min trajectory along the urban section shown in Fig. 3.1. With 10 Hz sampling, this mean that 1800 samples (test locations) are used in Fig. 3.2. Fig. 3.2 shows also the sky-plot of GPS satellites during this measurement campaign.

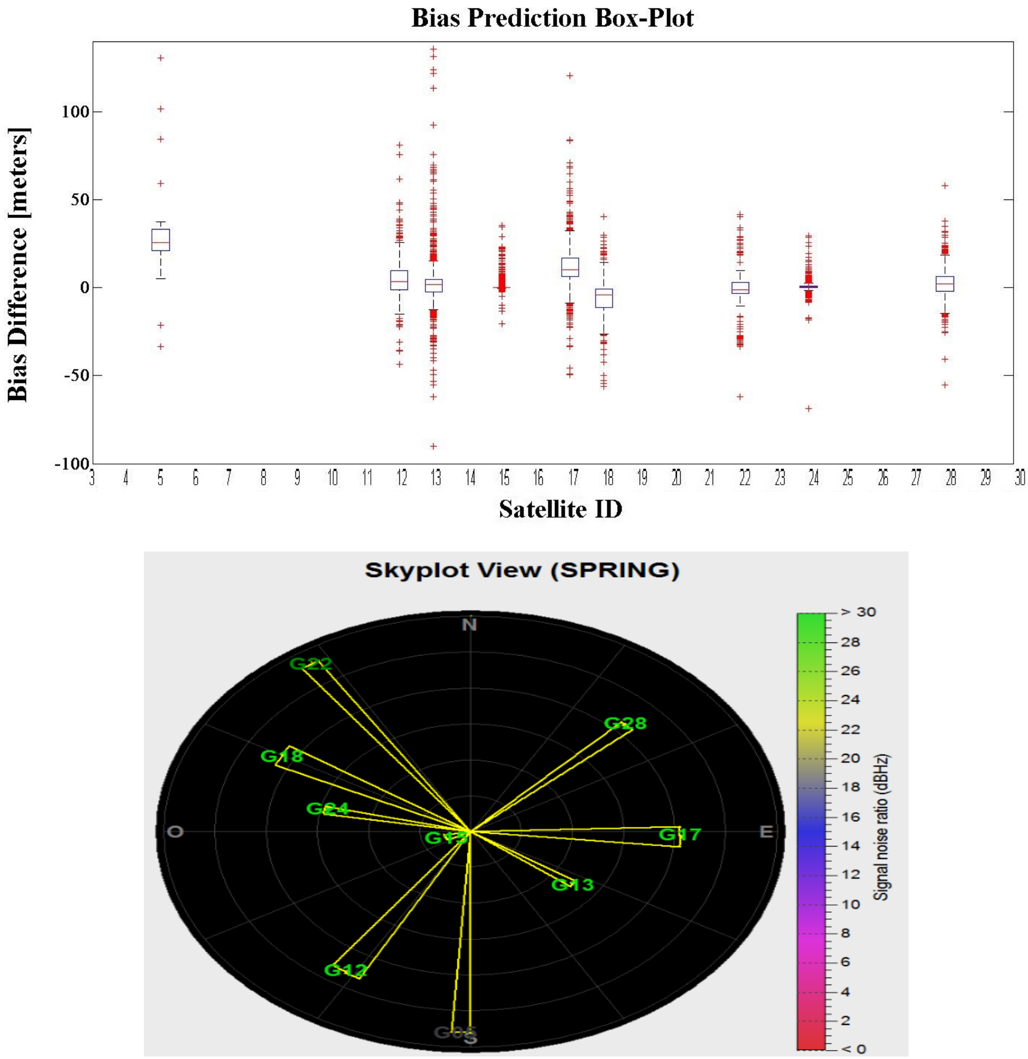

FIGURE 3.2 – SPRING reliability in an urban area described above. Top : PR bias prediction error using SPRING simulation in this environment. Bottom : Sky-Plot of GPS Satellites

The analysis of the PR bias values obtained by the signal simulation makes it possible to conclude that : for high-elevation satellites (such as satellite GPS 15), an accurate bias prediction is obtained by the SPRING simulation. For example, the difference between the "measured" true bias values and the SPRING predicted biases for satellite GPS 15 has a Gaussian distribution centred on 0 meters with low variance of 1 meter. For satellites with medium and low elevations, there are some differences between the "measured" true bias and 3D bias predicted by SPRING. For example, for the satellite GPS 13, the 3D bias prediction difference has a distribution centred on the value of 2 meters with a large variance of more than 10 meters, as shown in Fig. 3.3. For very low elevation satellites, this 3D bias prediction error is higher.

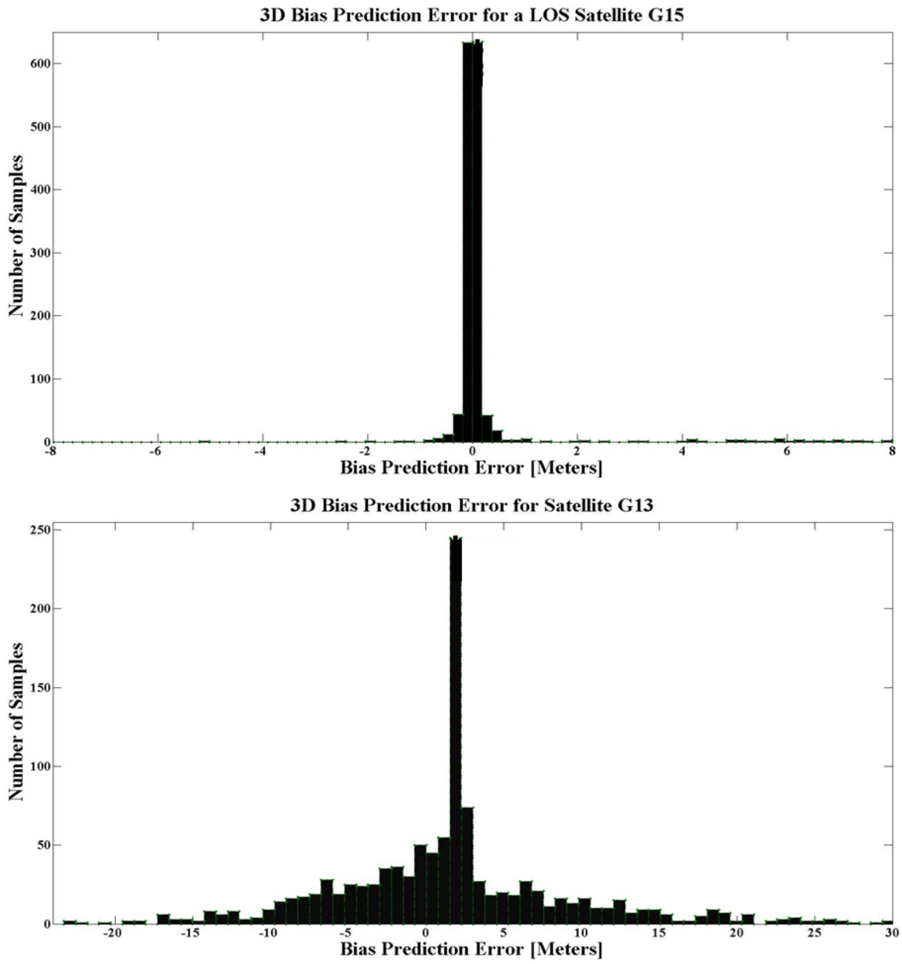

FIGURE 3.3 – 3D bias Prediction error using SPRING simulator for high and medium elevation satellites. The experiment is detailed above.

In summary, taking into account that some uncertainty in GNSS simulation is unavoidable, SPRING is a versatile tool to explore GNSS propagation phenomena. Unfortunately, we do not have a "quantitative" evaluation of the true level of accuracy of SPRING at the moment. This task requires an evaluation using extensive GNSS data in various environments. This is under ongoing study by the French Space Agency (SPRING provider) in different types of environments.

3.1.3.2 SPRING limitations

As SPRING simulations aim to approximate PR errors using GNSS signal propagation, we discuss here how multipath interference is generated within a GNSS receiver. The PR measurements are generated within the GNSS receiver using the code measurements. However, the reflected MP signals distort the code correlation peak within the receiver, which bias the PR measurements estimation. This PR error depends on the path delays of the reflected signals with respect to LOS signal, the magnitude of the these signals, the phase lag between LOS signal and different reflected signals and the receiver design. Therefore, prediction of multipath errors, using GNSS signal propagation simulations, requires the 3D mapping to be accurate to cm level and the position of the receiver to be known to cm accuracy in order to obtain the correct phase log. However, the 3D mapping used in SPRING is not accurate to cm level. Besides, the position truth reference used for the experiments are not precise to cm level under all scenarios. Therefore, the uncertainty on multipath interference prediction using SPRING GNSS simulation is unavoidable.

In addition, it is very complicated to reproduce the physical reality of GNSS signal propagation in the environment. To do so, it is necessary to know the phase change that occurs each time a signal is reflected. The 180° rule only applies to flat surfaces and angles of incidence less that Brewster's angle, which varies according to the surface material. Any surface irregularities will change the phase shift. PR errors also depend on the relative amplitude of the reflected signals within the receiver. This depends on the reflection coefficient of each surface that reflects the signal. However, even if it is possible to configure the materials in the SPRING 3D city model (by modifying the electromagnetic characteristics of these materials), it is quite complicated to reproduce the reflection coefficient of each surface and therefore the GNSS signal propagation will not be representative of reality.

Another problem is that GNSS signals are not rays. The Fresnel zone when a signal interacts with a building is of order a metre in diameter, so the surface characteristics in this whole area must be considered. The relative amplitude of the reflected and direct signals within the receiver will also depend on the antenna gain, which is different for right-hand circularly polarised (RHCP) and left-hand circularly polarised (LHCP) signals, as well as being elevation dependent. Directly received GNSS signals are RHCP, whereas reflected signals can be LHCP or mixed polarisation. Finally, the pseudo-range error also depends on which particular GNSS signal is used and on the receiver design, including correlator design, pre-correlation bandwidth and the use of any advanced discrimination techniques. Receiver manufacturers consider this information to be a trade secret, thus it is not possible to obtain the necessary design information for the receivers used in the experiments.

A consequence of these problems is that the pseudo-range errors due to multipath interference predicted by the SPRING simulator will have no correspondence to those experienced by the actual receiver. Only the standard deviation of the multipath error can be estimated, not the error itself. Applying SPRING-generated multipath corrections to the pseudo-range measurements will, on average, make them worse. These problems only apply to multipath interference and not to NLOS reception. For NLOS reception, the ranging error is simply equal to the additional path or the path delay.

To enhance the performance of the positioning algorithms that are based on SPRING PR bias prediction, multipath predictions using SPRING should be removed from the PR errors and only NLOS predictions should be kept. But, NLOS reception and multipath interference are merged in SPRING simulations. To discard SPRING-generated multipath corrections, the software code must be modified. As this code is owned by the CNES and should only be modified by them (as a partner, we have not access to the simulator code), discarding SPRING-multipath corrections was not possible. Then, in this chapter, we will present the positioning performance of our proposed algorithms with SPRING PR errors prediction that encompass both multipath and NLOS. Better positioning accuracy of these algorithms could potentially be obtained if SPRING multipath corrections was removed.

3.2 Measurements-Domain GNSS-3D GNSS signal propagation simulator Integration : Positioning by 3D PR Bias Bounding

In this section, we evaluate the added-value of deteriorated pseudorange correction, using complementary aiding information from the 3D GNSS signal propagation simulator SPRING, in term of localization performance along a deep urban path. It is worthy to note that some previous works tends to correct pseudorange measurements by subtracting estimated non-zero mean value from the received PR measurements when detecting as a non-zero jump in the mean values of measurement residuals using a chi-square based statistical test applied to residuals [69, 68, 200]. However, a reliable residual test assumes that the previous position used for residuals computation is accurate enough to be able to detect an error in the pseudorange measurements. Measurement residuals are not a reliable source of information to detect or correct PR measurements error as shown in Fig. 3.4. The experiment used to obtain this figure is the same used in the previous section and is detailed above in 3.1.3.1. In this figure, we compare residuals with "measured" true bias errors in an urban environment in Toulouse. The "measured" PR bias is predicted using the algorithm described in section 3.1.3.1 [3].

In this work, we are interested in the scenario where most or all pseudormanges are contaminated by MP or NLOS errors. In this case, measurement residuals are not reliable to infer about PR measurements errors. Hence, it is necessary to use external aiding information about the MP/NLOS bias. We have used the 3D GNSS signal propagation simulator SPRING to predict these PR biases and then correct them. Instead of using the deterministic bias value provided by the 3D GNSS signal propagation simulator, as it was classically done in previous studies [169], we use upper and lower bounds of these PR biases. Using the simulator SPRING, we predict the most appropriate bounds of the measurement bias. Predicted bias bounds are then integrated as additional inequality constraints in the position estimation problem for pseudorange correction and bounding. As GNSS simulation errors are unavoidable, correcting PR bias using a PR bias bounds is more realistic in reduced satellite visibility scenarios than relying on instantaneous predicted bias from the 3D GNSS signal propagation simulator.

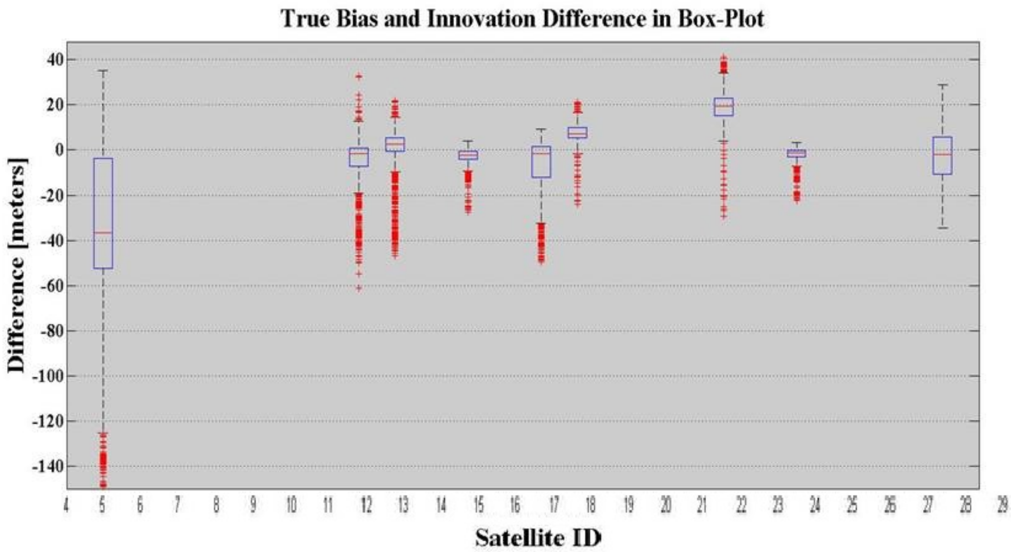

FIGURE 3.4 – Difference between measurement residuals and measured MP/NLOS bias in urban environment. The experiment is detailed in section 3.1.3.1.

Our proposed algorithm for positioning using 3D PR bias bounding follows these steps :

— **Step 1 : Candidate Positions Creation**
We start by defining a search area in the environment under study. Within this search area, we set up an array of candidate positions $\Gamma = \{\mathbf{x}_i = (x_i, y_i, z)^T\}$ with a defined spacing. The index i refers to the index of the candidate position. The used spacing will be defined in the experimental section. This array of candidate positions is an array of 2D points $\Gamma = \{\mathbf{x}_i = (x_i, y_i, z)^T\}$. The height z is computed using terrain height aiding via the 3D simulator. We use software Q-GIS v2.18. "Las Palmas" on the 3D model of the search area to define this square grid of regular equidistant points. The size of the grid and the number of points will be defined in the experimental section.

— **Step 2 : Exclusion of Indoor (Inside Building) Positions**
Using Q-GIS software, we find the square polygons of grid of positions that overlap with the polygons of buildings in the considered 3D model, in order to discard them. Once these points that are inside building are identified, we delete those unwanted points to end-up with a grid of outdoor candidate positions.

— **Step 3 : PR Bias Prediction by 3D SPRING Simulation**
For each of these candidate positions, we perform 3D simulation using the 3D GNSS signal propagation simulator SPRING. At each time step, the 3D simulation is applied to an input point that allows the calculation and the prediction of the PR bias error on each received signal at this point. Providing an input position and a GNSS time, the 3D simulator SPRING is used to predict the corresponding PR biases for each received ranging measurement, i.e. for this grid of outdoor candidate positions Γ, we estimate a bank (per satellite and candidate position) of PR bias vectors $\Omega = \{\mathbf{b}_{3D}(\mathbf{x}_i) = (\mathbf{b}_{3D}(\mathbf{x}_i)_1, \cdots, \mathbf{b}_{3D}(\mathbf{x}_i)_N)^T\}$. The index i refers to the index of the candidate position. N refers to the number of received PR measurements. The main steps used for 3D PR

bias estimation at each candidate position are summarized in the following algorithm 1. It must be emphasised that the receiver clock bias is omitted in 3D signal propagation simulation as the receiver is supposed to be synchronized with emitted satellites. This is used in SPRING simulation to avoid satellite/receiver synchronization and to simplify the prediction of PR bias, but it is not how GNSS positioning normally works.

Algorithm 1 3D GNSS signal propagation simulation

Inputs : GPS Time, Satellite ephemeris, 3D city Model and candidate position $\mathbf{x}_i$

Output : 3D bias $\mathbf{b}_{3D}(\mathbf{x}_i)$

1: **Compute satellite positions**

2: **Determine LOS distance between each satellite and the candidate position**
For each satellite Sat_j, compute $PR_i^{LOS} = \|\mathbf{x}_i - \mathbf{x}_i^{Sat_j}\|_2$. The index j refers to the index of the PR measurement and the index i refers to the index of the candidate position.

3: **Predict 3D received PR measurements**
For each satellite Sat_j, predict PR_j^{3D}, using the 3D model, ray-launching algorithm and the receiver model implemented in SPRING.

4: **Compute PR bias**
As the other ranging errors are not modelled, the PR bias is the difference between predicted PR measurements and LOS distance : $[\mathbf{b}_{3D}(\mathbf{x}_i)]_j = PR_j^{3D} - PR_j^{LOS}$.

— **Step 4 : Upper and Lower PR Bounds Computation**
Once the bank of MP/NLOS bias vectors is computed using the 3D GNSS signal propagation simulators SPRING, we consider only the upper and lower values of these 3D PR bias for each received satellite. In other words, for each received satellite, we predict the PR bias at different locations, i.e. different $\mathbf{x}_i$, using SPRING to get different 3D PR bias for that satellite depending on the considered location and we finally consider only the highest and the lowest 3D PR bias. We have chosen maximum and minimum PR biases here as metrics but other quantiles could be chosen.

$$\mathbf{l}_{3D} = \min_{\mathbf{x}_i \in \Gamma}(\mathbf{b}_{3D}(\mathbf{x}_i)), \quad \mathbf{u}_{3D} = \max_{\mathbf{x}_i \in \Gamma}(\mathbf{b}_{3D}(\mathbf{x}_i)) \tag{3.1}$$

Where $\mathbf{l}_{3D}$ refers to the lower bound of PR bias and $\mathbf{u}_{3D}$ is the upper bound of PR bias. They are vectors with one row per satellite.

— **Step 5 : PR Correction and Bounding**
Using equation 1.4,this PR bias bounding allows bounding the predicted measurement innovation vector $\mathbf{Hx}$:

$$\mathbf{c}_{inf} \leq \mathbf{Hx} \leq \mathbf{c}_{sup} \tag{3.2}$$

Where $\mathbf{c}_{inf} = \mathbf{y} - \mathbf{u}_{3D} - 3(\sigma)_{i=[1,\dots,N]}$ is the lower bound of the vector $\mathbf{Hx}$ and $\mathbf{c}_{sup} = \mathbf{y} - \mathbf{l}_{3D} + 3(\sigma)_{i=[1,\dots,N]}$ is the upper bound of the vector $\mathbf{Hx}$ and $\sigma_i^2 = \mathbf{R}_{i,i}, \forall i = [1, \dots, N]$. The other terms are defined in section 1.2.2. N refers to the number of received PR measurements and $\mathbf{R}$ is the covariance matrix of the measurements noise $\mathbf{n}$.

Assuming that the MP/NLOS bias is Gaussian between these upper and lower bounds and since the MP-NLOS bias $\mathbf{b}$ and the measurement noise $\mathbf{n}$ are independent, the total noise $\mathbf{n} + \mathbf{b}$ have a non-zero Gaussian distribution with a mean of $\dfrac{\mathbf{u}_{3D} + \mathbf{l}_{3D}}{2}$ and a covariance matrix equal to :

$$\mathbf{R_b} = \mathbf{R} + diag((\mathbf{u}_{3D} - \mathbf{l}_{3D}/6)^2_{j=1...N}) \tag{3.3}$$

The factor 6 is obtained based on simple mathematical derivations as we suppose that $\mathbf{b}^j \sim \mathcal{N}\left(\frac{\mathbf{u}^j_{3D}+\mathbf{l}^j_{3D}}{2}, [\frac{\mathbf{u}^j_{3D}-\mathbf{l}^j_{3D}}{6}]^2\mathbf{I}_N\right)$, for each satellite j. The mean value of the total noise distribution must be subtracted from the PR measurement vector when estimating the state vector. We hence get a new corrected PR measurement vector corrected with the mean value of 3D predicted MP/NLOS bias bounds (as we suppose that $\mathbf{b}^j \sim \mathcal{N}\left(\frac{\mathbf{u}^j_{3D}+\mathbf{l}^j_{3D}}{2}, [\frac{\mathbf{u}^j_{3D}-\mathbf{l}^j_{3D}}{6}]^2\mathbf{I}_N\right)$, for each satellite j) :

$$\mathbf{y}_{cor} = \mathbf{y} - (\mathbf{u}_{3D} + \mathbf{l}_{3D})/2 \tag{3.4}$$

— **Step 6 : Final Position Estimation**
We get finally a constrained state estimate with PR measurements correction using 3D predicted PR bias bounds (CLS for constrained LS) :

$$\begin{cases} \hat{\mathbf{x}}_{CLS} = \underset{\mathbf{x}}{\text{argmin}} \|\mathbf{y}_{cor} - \mathbf{Hx}\|_{\mathbf{R_b}} & = \underset{\mathbf{x}}{\text{argmin}} \|\mathbf{y} - (\mathbf{u}_{3D} + \mathbf{l}_{3D})/2 - \mathbf{Hx}\|_{\mathbf{R_b}} \\ & \mathbf{c}_{inf} \leq \mathbf{H}\hat{\mathbf{x}}_{CLS} \leq \mathbf{c}_{sup} \end{cases} \tag{3.5}$$

This constrained quadratic problem is resolved using the Matlab routine "quadprog" [201].

This obtained solution is termed the constrained solution and can be combined with a motion model to obtain a constrained EKF with bias bounding (CEKF). The proposed approach is summarized in the following algorithm 2. The main innovations in this algorithm are :

✔ PR measurements correction based on the mean of 3D PR bias bounds

✔ Augmented noise covariance matrix based on 3D PR bias bounds

✔ Constrained search area using equation 3.2

In summary, this proposed approach is illustrated in Fig. 3.5.

Algorithm 2 constrained EKF with bias bounding (CEKF)

Inputs : linearized PR measurement vector $\mathbf{y}$, Measurement matrix $\mathbf{H}$

Output : CEKF solution (position incrementation+Rx clock bias) $\hat{\mathbf{x}}_{CEKF}$

1: **Outdoor Candidate Positions :**
Define an array of 2D points $\Gamma = \{\mathbf{x}_i = (x_i, y_i, z)^T\}$, where the height z is obtained using terrain height aiding via the 3D simulator and exclude indoor positions using Q-GIS software.

2: **Bank of 3D PR bias measurements :**
Predict a bank (per satellite and candidate position) of PR bias $\Omega = \{\mathbf{b}_{3D}(\mathbf{x}_i) = (\mathbf{b}_{3D}(\mathbf{x}_i)_1, \cdots, \mathbf{b}_{3D}(\mathbf{x}_i)_N)^T\}$ using SPRING.

3: **Lower and upper PR bias bounds :**
Define lower and upper bias bounds as : $\mathbf{l}_{3D} = \min_{\mathbf{x}_i \in \Gamma} w(\mathbf{b}_{3D}(\mathbf{x}_i)), \quad \mathbf{u}_{3D} = \max_{\mathbf{x}_i \in \Gamma} (\mathbf{b}_{3D}(\mathbf{x}_i))$.

4: **Lower and upper bound of the vector Hx :**
Compute $\mathbf{c}_{inf} = \mathbf{y} - \mathbf{u}_{3D} - 3(\sigma)_{i=[1,\ldots,N]}$ the lower bound, $\mathbf{c}_{sup} = \mathbf{y} - \mathbf{l}_{3D} + 3(\sigma)_{i=[1,\ldots,N]}$ the upper bound and $\mathbf{R_b} = \mathbf{R} + diag([(\mathbf{u}_{3D} - \mathbf{l}_{3D})/6]^2)$.

5: **Final Estimate :** EKF applied to corrected PR with augmented covariance noise matrix and LOS PR bounding (Where $EKF[\mathbf{y}, \mathbf{R}]$ means applying the EKF algorithm to measurement vector $\mathbf{y}$ and noise covariance matrix $\mathbf{R}$) :

$$\begin{cases} \hat{\mathbf{x}}_{CEKF} & = EKF[\mathbf{y} - (\mathbf{u}_{3D} + \mathbf{l}_{3D})/2, \mathbf{R_b}] \\ & \mathbf{c}_{inf} \leq \mathbf{H}\hat{\mathbf{x}}_{CEKF} \leq \mathbf{c}_{sup} \end{cases}$$

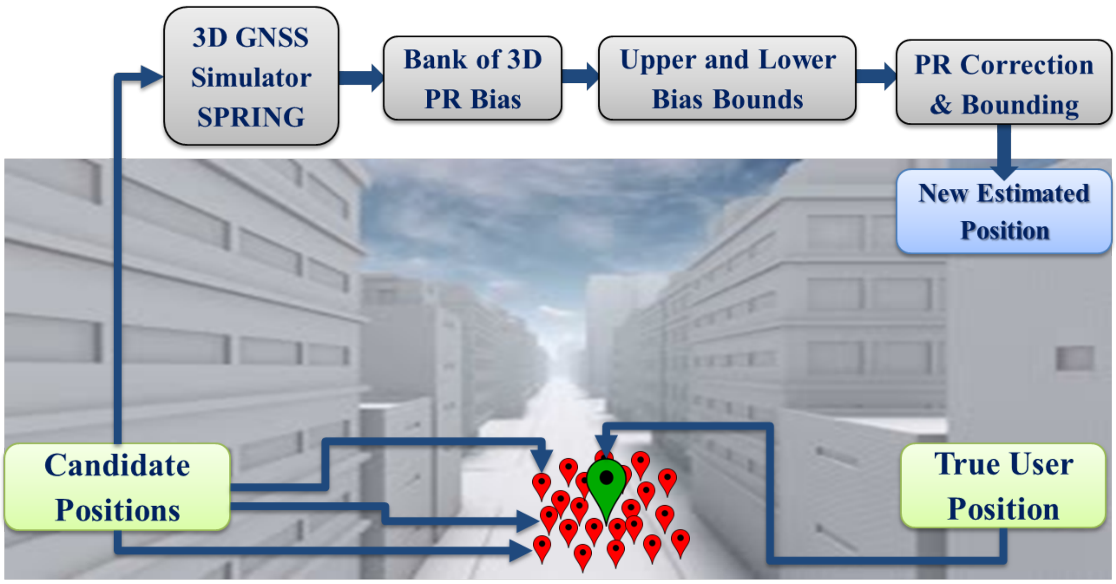

FIGURE 3.5 – PR Measurement correction with 3D bias Bounding using SPRING

3.3 Position-Domain GNSS-3D GNSS signal propagation simulator Integration : 3D Positioning over Candidate Positions

3.3.1 AML-3D : 3D Approximate Maximum Likelihood

3.3.1.1 Principle

Since the computation of the general likelihood cost function of the GNSS problem, presented in chapter 1, is potentially biased without any prior information on the PR bias, we propose in this section a new approximate cost function that approximates this theoretical maximum-likelihood cost function. To do that, we make use of the simulator SPRING.

In this method, we use the 3D GNSS signal propagation simulator SPRING to characterize ranging errors and define this approximate maximum-likelihood cost function. To do this, our proposed algorithm follows these following steps :

— **Step 1 : Outdoor Candidate Positions Definition**
As shown in the previous section, using the software Q-GIS and the 3D city model, we define an outdoor of candidate position in the search area of the environment under study. This 2D array of equidistant candidate positions will be termed as $\Gamma = \{\mathbf{x}_i = (x_i, y_i, z)^T\}$, where the height z is obtained using terrain height aiding via the 3D GNSS signal propagation simulator. The index i refers to the index of the candidate position. The used spacing will be defined in the experimental section. The size of the grid, the number of candidate position will be defined in the experimental section.

— **Step 2 : PR Bias Prediction by 3D SPRING Simulation**
As explained in algorithm 1, we perform 3D SPRING simulation for each of these candidate positions. 3D simulator SPRING allows predicting the corresponding PR biases for each received ranging measurement for this array of candidate positions : $\Omega = \{\mathbf{b}_{3D}(\mathbf{x}_i) = (\mathbf{b}_{3D}(\mathbf{x}_i)_1, \cdots, \mathbf{b}_{3D}(\mathbf{x}_i)_N)^T\}$. The index i refers to the index of the candidate position. N refers to the number of received PR measurements.

— **Step 3 : Approximate Maximum-likelihood Cost Function**
Based on predicted 3D PR bias, we define the approximate maximum-likelihood cost function as ($\rightarrow$ and $\mapsto$ are common functional declarations) :

$$\begin{aligned} P : \Gamma &\rightarrow \mathbb{R} \\ \mathbf{x}_i &\mapsto P(\mathbf{y}|\mathbf{x}_i, \mathbf{b}_{3D}(\mathbf{x}_i)) = \|\mathbf{y} - \mathbf{H}\mathbf{x}_i - \mathbf{b}_{3D}(\mathbf{x}_i)\|^2_{\mathbf{R}^{-1}} \end{aligned} \tag{3.6}$$

Where, as defined in section 1.2.2, $\mathbf{y}$ is the linearised pseudorange (PR) measurements vector. $\mathbf{H}$ contains the unit line-of-sight (LOS) vectors between satellites and reference point $\mathbf{x_0} = (x_0, y_0, z_0)^T$. $\mathbf{x}_i = (x_i - x_0, y_i - y_0, z_i - z_0, b_{Rx})^T$ is candidate state vector containing an incremental deviation from the known reference point $\mathbf{x_0}$, i.e. the three coordinates of the candidate position $(x_i, y_i, z_i)^T$ and the receiver clock bias b_{Rx}. $\mathbf{R} = E[\mathbf{n}\mathbf{n}^T]$ is the covariance matrix of the white Gaussian noise $\mathbf{n}$. This new cost function is based on predicted 3D PR bias and is approximating the maximum-likelihood cost function of the GNSS problem by substituting the unknown MP/NLOS bias $\mathbf{b}$ with the 3D predicted PR bias from SPRING $\mathbf{b}_{3D}(\mathbf{x}_i)$.

— **Step 4 : Final Estimate**
By evaluating the previous approximate maximum-likelihood cost function (score function) on the array of candidate positions, we define an approximate maximum likelihood (AML) estimator as :

$$\hat{\mathbf{x}}_{AML} = \underset{\mathbf{x}_i}{\operatorname{argmin}}\, P(\mathbf{y}|\mathbf{x}_i, \mathbf{b}_{3D}(\mathbf{x}_i)) \tag{3.7}$$

This AML estimator represents the candidate position that minimizes likelihood scores (approximate maximum-likelihood function) for the set of candidate positions. A weighted average is likely to give a better result and this is taken into account in 3.3.1.3. Likelihood surfaces of this cost function will be presented in the experimental validation section in 3.4.3.2.

3.3.1.2 Physical Interpretation

The approximate maximum-likelihood function in (3.6) can be seen as a scoring function applied to a candidate positions $\Gamma = \{\mathbf{x}_i\}$ by evaluating the similarity between true received PR measurements innovation $\mathbf{y}$ at the user unknown location and 3D predicted PR measurements, using SPRING simulation, at each candidate position $\mathbf{H}\mathbf{x}_i + \mathbf{b}_{3D}(\mathbf{x}_i)$. It can be seen also as PR bias similarity between 3D predicted PR bias, using 3D simulation at each candidate position $\mathbf{b}_{3D}(\mathbf{x}_i)$ and true PR bias at each candidate position $\mathbf{y} - \mathbf{H}\mathbf{x}_i$ (as, by using the notation of this dissertation provided in 1.2.2, $\mathbf{H}\mathbf{x}_i = \mathbf{h}(\mathbf{x}_i) - \mathbf{h}(\mathbf{x}_0) = \mathbf{h}(\mathbf{x}_i) - (\mathbf{z} - \mathbf{y} + c.\mathbf{dT}^i_{Sat} - \mathbf{I}_i - \mathbf{T}_i)$, which gives $\mathbf{y} - \mathbf{H}\mathbf{x}_i = \mathbf{z} - (\mathbf{h}(\mathbf{x}_i) - c.\mathbf{dT}^i_{Sat} + \mathbf{I}_i + \mathbf{T}_i)$, i.e. the difference between received PR and LOS PR at each candidate position). AML-3D positioning is then based on PR measurement similarity scoring or PR bias similarity scoring of an array of candidate positions. By way of illustration, a block diagram of our proposed algorithm is given in Fig. 3.7. The physical interpretation of the AML-3D algorithm is explained in Fig. 3.6.

3.3.1.3 Practical Implementation

Practical Computation of the Scoring Function
Even if it has been proven that the AML estimator converges to the most efficient ML estimator under the assumption of an accurate 3D simulation, the expression of such estimator is very computationally intensive since it requires a minimum search over a grid of candidate position containing four unknowns. These unknowns are the user position (x, y, z) and the clock bias b_{Rx} (common between all the received satellites).

To reduce the estimation complexity, a standard method [66] consists of using the 3D city model to avoid the estimation of the height information. Given the horizontal coordinates of each grid point, a height is associated to this point using the 3D city model which avoids the computational load over a 3D search area.

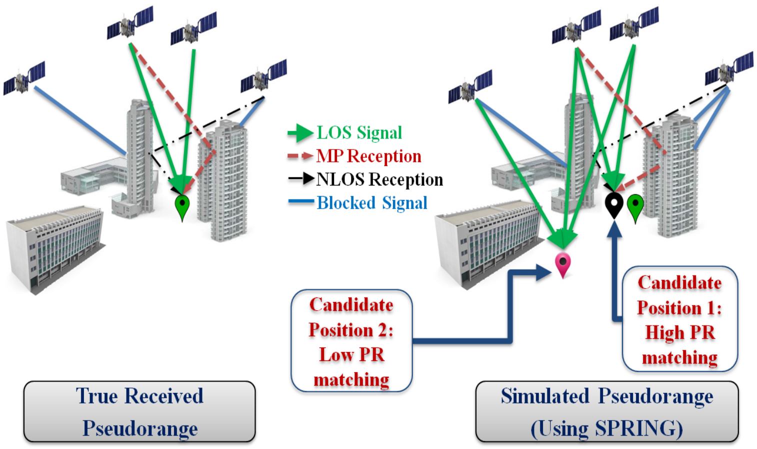

FIGURE 3.6 – AML-3D : Physical interpretation

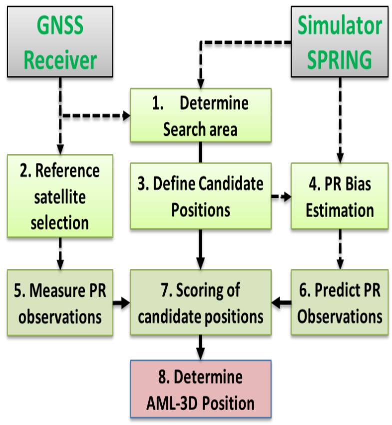

FIGURE 3.7 – AML-3D algorithm block diagram

For the sake of simplification, the receiver clock bias is eliminated by proceeding to a differencing of all ranging measurements across satellites using a reference satellite. The selection of reference satellite is quite important. This satellite must have a reliable and almost “clean” ranging measurement. Basic indicators for this selection process include elevation angle and C/N0 values. Ref. [3] proposes a reference satellite selection using LOS probability obtained via experimental data. This LOS probability is computed using signal power distributions with tuning parameters fixed using experimental data. It can be expressed as :

$$P_{LOS} = \ln \frac{p_{LOS}(C/N_0|\theta)}{p_{NLOS}(C/N_0|\theta)}$$

Where P_{LOS} is the LOS probability for a considered satellite, θ is the vector containing the satellite elevation angles, expressed in degrees. C/N_0 is the carrier-to-noise-density ratio vector, expressed in dB-Hz. $p_{LOS}(C/N_0|\theta)$ and $p_{NLOS}(C/N_0|\theta)$ are the signal power distributions of LOS and NLOS satellites, which depend on fixed tuning parameters. Further details about these tuning parameters may be obtained in [3].

Since the proposed approach is 3D-simulation-accuracy-dependent, we propose to estimate the uncertainty in the bias estimation provided by the 3D GNSS signal propagation simulator. As shown in the SPRING simulator reliability sub-section 3.1.3.1, PR biases of high elevation signals are usually correctly estimated by 3D GNSS signal propagation simulations, as the signal have less interactions with the environment surrounding the receiver contrary to low or medium elevation signals. Then, we propose the following formula as estimation for this uncertainty in the bias prediction. This formula is proposed to ensure a low inaccuracy for high elevation satellites.

$$(\tilde{\delta}_{3D})_j = \alpha_{Max-Inaccuracy} \exp(\theta_j/(\theta_j - 90°)) \tag{3.8}$$

where $\alpha_{Max-Inaccuracy}$ refers to the highest error on bias estimation, obtained using experimental data and θ are satellite elevation angles, expressed in degrees. In this dissertation, this uncertainty in the bias prediction $\tilde{\delta}_{3D}$ is not used to correct the 3D PR bias prediction using SPRING because we aim to present a general implementation of the algorithm. However, this aspect have been studied in the author's paper [202]. We have shown in [202] that this correction of the uncertainty of SPRING simulation improves the accuracy of our algorithm. The parameter $\alpha_{Max-Inaccuracy}$ is fixed to 5 meters in [202]. Finally, we remind that $\tilde{\delta}_{3D}$ is a vector with N components where N is the number of received satellites.

Once a reference satellite is selected, we modify the approximate maximum-likelihood cost function (3.6) as follows :

$$\tilde{P}(\mathbf{y}|\mathbf{x}_i) = \|\mathbf{y} - y_{ref}\mathbf{1}_N - (\mathbf{H} - \mathbf{1}_N\mathbf{H}(ref,:))\mathbf{x}_i - \mathbf{b}_{3D}(\mathbf{x}_i) - \tilde{\delta}_{3D}\|^2_{\mathbf{R}^{-1}} \tag{3.9}$$

Where y_{ref} is the ranging measurement of the reference satellite and $\mathbf{H}(ref,:)$ is the row of observation matrix $\mathbf{H}$ corresponding to the reference satellite. The observation matrix $\mathbf{H}$ is defined in the notation section in 1.2.2. $\mathbf{1}_N$ refers to the vector containing N elements with all components being equal to 1. N being the number of received satellites. $\tilde{P}$ is the approximate maximum-likelihood cost function defined in (3.6) and $\tilde{P}$ is the modified approximate maximum-likelihood cost function used for the practical implementation of the AML-3D algorithm, that take into account the receiver clock bias compensation, the height aiding and the correction of the uncertainty on 3D PR bias prediction.

Practical Estimation of the Final AML-3D Position

Considering the final position as the candidate position having the lowest score, i.e. minimizing the approximate maximum-likelihood cost function in (3.9), could gives a bad estimate. Therefore, we propose to estimate the final AML-3D solution as a weighted average of the candidate positions with the lowest scores, i.e. the highest PR measurements matching, as :

$$\hat{\mathbf{x}}_{AML} = \frac{\sum_{i=1}^{N_{Th}} (\tilde{P}(\mathbf{y}|\mathbf{x}_i^{\Omega}) < Th)\mathbf{x}_i^{\Omega}}{\sum_{i=1}^{N_{Th}} (\tilde{P}(\mathbf{y}|\mathbf{x}_i^{\Omega}) < Th)} \tag{3.10}$$

Where Th is the threshold used for selecting the lowest scores, N_{Th} corresponds to the number of grid points with a matching score lower than the threshold Th and the set $\Omega = \{\mathbf{x}_i^{\Omega}, i = 1, \cdots, N_{Th}\}$ refers to the subset of candidate positions with the lowest scores. Th is determined using experimental data. The used value of Th is detailed in the experimental section 3.4.3.2. Finally, the proposed approach is summarized in algorithm 3 below :

Algorithm 3 AML Estimation

Inputs : linearized PR $\mathbf{y}$, Measurement matrix $\mathbf{H}$ and maybe the uncertainty on 3D PR bias prediction by SPRING simulation $\tilde{\delta}_{3D}$

Output : incremental deviation in 2D $\hat{\mathbf{x}}_{AML}$

1: **Reference satellite selection using elevation criterion**

2: **Define search area and grid of outdoor candidate positions**
Define an array of 2D outdoor points $\Gamma = \{\mathbf{x}_i = (x_i, y_i, z)^T\}$ using Q-GIS software and the 3D city model

3: **Estimate a bank of PR biases over candidate positions**
Estimate PR biases, using 3D GNSS signal propagation simulation, for the considered array of candidate positions $\Omega = \{\mathbf{b}_{3D}(\mathbf{x}_i) = (\mathbf{b}_{3D}(\mathbf{x}_i)_1, \cdots, \mathbf{b}_{3D}(\mathbf{x}_i)_N)^T\}$

4: **Likelihood scoring for each candidate position**
Compute $\tilde{P}(\mathbf{y}|\mathbf{x}_i)$ using (3.9)

5: **AML-3D position estimation**
Estimate AML-3D solution $\hat{\mathbf{x}}_{AML}$ using (3.10)

3.3.1.4 Innovation compared to the state of the art

Much of the previous research described in section 2.6.2 has focused on using 3D model for position candidates scoring among an array of candidate positions using different scoring functions. The proposed method in this section is based on defining a likelihood function based on similarity between received PR measurements and predicted PR measurement at each candidate by use of 3D predicted PR biases from the 3D GNSS signal propagation simulator SPRING. In this work, we eliminate the receiver clock bias from the problem estimation by computing the difference between all ranging measurements across satellites and a reference satellite selected using different indicators such as elevation angles, C/N0 levels and LOS probability. This point represents the main difference compared to the work in [168], where the receiver clock bias is used (the clock bias is not estimated but instead the value of receiver clock bias estimated by the commercial receiver is directly used). Besides, in this work, we prove that this likelihood function is an approximation of the maximum likelihood function of the GNSS problem, which, to the best of our knowledge, have not been proven before. Another innovative aspect compared to the state of the art (in particular [168]) is the derivation of the theoretical performance of this method in case of accurate bias estimation by a 3D GNSS signal propagation simulator. This derivation is provided in the appendix B. A further innovative aspect is the new modelling of the uncertainty on the bias prediction by 3D signal propagation simulation that have been taken into account to improve the accuracy of the proposed approach.

3.3.2 PM-3D : 3D Position Matching

3.3.2.1 Principle

In this sub-section, we use the 3D GNSS signal propagation simulator SPRING to estimate PR errors and define another scoring function based on position matching (the reason for this denomination will be explained in section 3.3.2.2) and not measurement matching as in the previous method. This position matching metric evaluates the similarity between each point of a set of candidate positions $\Gamma = \{\mathbf{x}_i = (x_i, y_i, z)^T\}_i$ and each point of a set of calculated positions $\Gamma_1 = \{\mathbf{H}^+(\mathbf{y} - \mathbf{b}_{3D}(\mathbf{x}_i))\}_i$ obtained via LS-type projection (using $\mathbf{H}^+$) applied to corrected linearized PR measurements using 3D predicted PR biases from SPRING simulations. This proposed algorithm follows these following steps :

— **Step 1 : Outdoor Candidate Positions Definition and PR Bias Prediction**
As detailed in the AML-3D algorithm, we define a 2D array of equidistant outdoor candidate positions $\Gamma = \{\mathbf{x}_i = (x_i, y_i, z)^T\}$ in the environment under study, using the software Q-GIS and the 3D city model. The index i refers to the index of the candidate position. The used spacing, the size of the grid and the number of candidate position will be defined in the experimental section 3.4.3.2. For each candidate position, we predict the corresponding PR bias using SPRING to obtain a bank (per satellite and per candidate position) of 3D PR bias : $\Omega = \{\mathbf{b}_{3D}(\mathbf{x}_i) = (\mathbf{b}_{3D}(\mathbf{x}_i)_1, \cdots, \mathbf{b}_{3D}(\mathbf{x}_i)_N)^T\}$.

— **Step 2 : Define a Reference Satellite**
Based on C/N_0 ratios or elevation angles or LOS probabilities, we define a reference satellite : satellite having the most reliable and "healthy" PR measurements.

— **Step 3 : Estimate 3D PR bias prediction uncertainty**
Estimate the uncertainty on 3D PR bias prediction using SPRING simulation $\tilde{\delta}_{3D}$ based on the presented model in (3.8).

— **Step 4 : Position Matching Cost Function**
Based on predicted 3D PR bias, we define the following cost function Ψ as :

$$\begin{aligned} \Psi : \Gamma &\to \mathbb{R} \\ \mathbf{x}_i \mapsto \Psi(\mathbf{y}|\mathbf{x}_i, \mathbf{b}_{3D}(\mathbf{x}_i)) &= \|\mathbf{H}^+(\mathbf{y} - \mathbf{b}_{3D}(\mathbf{x}_i)) - \mathbf{x}_i\|_2^2 = \|\mathbf{H}^+[P(\mathbf{y}|\mathbf{x}_i, \mathbf{b}_{3D}(\mathbf{x}_i))]\|_2^2 \\ &= \|\mathbf{H}^+(\mathbf{H}\mathbf{x}_i + \mathbf{b}_{3D}(\mathbf{x}_i)) - \hat{\mathbf{x}}_{LS}\|_2^2 \end{aligned} \quad (3.11)$$

Where $\to$ and $\mapsto$ are common functional declarations, $\hat{\mathbf{x}}_{LS} = \mathbf{H}^+\mathbf{y} = (\mathbf{H}^T\mathbf{R}^{-1}\mathbf{H})^{-1}\mathbf{H}^T\mathbf{R}^{-1}\mathbf{y}$ is the LS solution of the GNSS problem and $\|\mathbf{z}\|_2^2 = \mathbf{z}^T\mathbf{z}$ is the norm 2 for any vector $\mathbf{z}$. $\mathbf{y}$ is the linearised pseudorange (PR) measurements vector. $\mathbf{H}$ contains the unit line-of-sight (LOS) vectors between satellites and reference point $\mathbf{x_0} = (x_0, y_0, z_0)^T$. $\mathbf{x}_i = (x_i - x_0, y_i - y_0, z_i - z_0, b_{Rx})^T$ is candidate state vector containing an incremental deviation from the known reference point $\mathbf{x_0}$, i.e. the three coordinates of the candidate position $(x_i, y_i, z_i)^T$ and the receiver clock bias b_{Rx}. This new cost function is based on predicted 3D PR bias. This metric represents a projection of the previous metric P (the approximate maximum-likelihood function of the AML-3D estimator) from the measurement level onto the position level using the operator $\mathbf{H}^+ = (\mathbf{H}^T\mathbf{R}^{-1}\mathbf{H})^{-1}\mathbf{H}^T\mathbf{R}^{-1}$.

As for the AML-3D cost function, the practical implementation of this metric will require the use of a reference satellite for receiver clock bias elimination. The modified position matching cost function is then the following :

$$\tilde{\Psi}(\mathbf{y}|\mathbf{x}_i, \mathbf{b}_{3D}(\mathbf{x}_i)) = \|(\mathbf{H}^{+} - \mathbf{1}_M \mathbf{H}^{+}(:, ref))(\mathbf{y} - y_{ref}\mathbf{1}_N - \mathbf{b}_{3D}(\mathbf{x}_i) - \tilde{\delta}_{3D}) - \mathbf{x}_i\|_2^2 \tag{3.12}$$

Where y_{ref} is the ranging measurement of the reference satellite and $\mathbf{H}^{+}(ref, :)$ is the row of matrix $\mathbf{H}^{+}$ corresponding to the reference satellite. $\mathbf{1}_N$ and $\mathbf{1}_M$ refer to vectors containing N and M elements with all components being equal to 1, respectively. N being the number of received satellites and M the number of unknowns to be estimated. As in the AML-3D estimator, $\tilde{\Psi}$ is an approximation of the cost function Ψ that takes into account the receiver clock bias compensation, the height aiding and the correction of the uncertainty on 3D PR bias prediction.

— **Step 5 : Final Estimate**
By evaluating the previous cost function on the array of candidate positions, we define the position matching (PM) estimator as :

$$\hat{\mathbf{x}}_{PM} = \frac{\sum_{i=1}^{N_{Th}} (\tilde{\Psi}(\mathbf{y}|\mathbf{x}_i^{\Omega}) < Th)\mathbf{x}_i^{\Omega}}{\sum_{i=1}^{N_{Th}} (\tilde{\Psi}(\mathbf{y}|\mathbf{x}_i^{\Omega}) < Th)} \tag{3.13}$$

Where Th is the threshold used for selecting the lowest scores, N_{Th} corresponds to the number of grid points with a matching score lower than the threshold Th and the set $\Omega = \{\mathbf{x}_i^{\Omega}, i = 1, \cdots, N_{Th}\}$ refers to the subset of candidate positions with the lowest scores. This PM estimator represents a weighted average of the candidate positions with the lowest scores, i.e. the highest matching. Th is determined using experimental data. The used value of Th is detailed in the experimental section 3.4.3.2.

3.3.2.2 Physical Interpretation

The position matching metric evaluates the similarly between candidate positions and position obtained by PR measurement correction, over an array of candidate positions.

If the 3D GNSS signal propagation simulator is sufficiently accurate, the projection of the "LS" type applied to simulated PR measurements (predicted by the SPRING-3D simulator) obtained by SPRING simulation at a candidate position $\mathbf{x}_i$ close to the true position $\mathbf{x}$, will give a solution close to the LS solution obtained by applying the LS algorithm to true PR measurements received at the true unknown position. The physical interpretation of PM-3D algorithm is explained in Fig. 3.8. By way of illustration, a block diagram of our proposed PM-3D algorithm is given in Fig. 3.9.

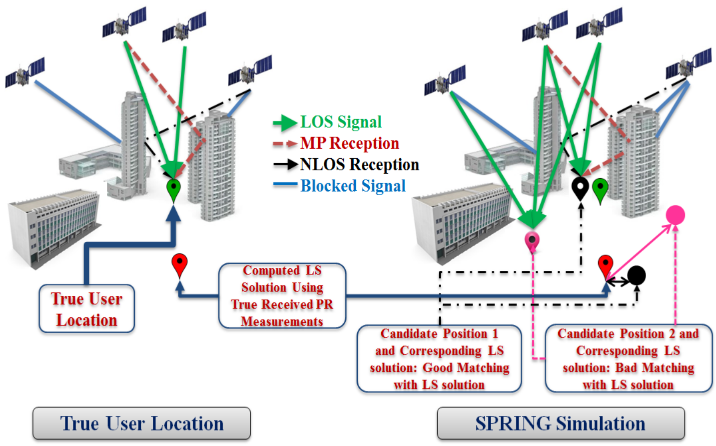

FIGURE 3.8 – PM-3D : Physical interpretation

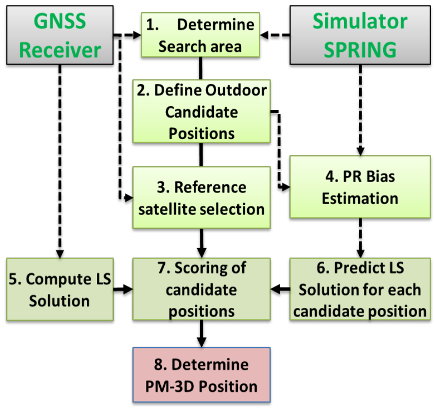

FIGURE 3.9 – PM-3D algorithm block diagram

3.3.2.3 Innovation and differences with AML-3D

The proposed method in this section is based on a likelihood function computing the similarity between a conventional Least-Squares (LS) solution, obtained by a LS-like projection of the true received PR measurements at the unknown user location, and a virtual LS solution obtained by a LS-like projection of predicted PR measurements, obtained by use of the 3D GNSS signal propagation simulator SPRING at a set of candidate points. This method belongs to the class of methods using 3D modelling to score an array of candidate positions.

In this work, we use PR bias prediction from a 3D GNSS signal propagation simulator to define a new scoring function. To compute this function, we eliminate the receiver clock bias by computing the difference between all ranging measurements across satellites and a reference satellite. A derivation of this function is also provided in the author paper [203]. The theoretical performance of this estimator is provided in the appendix B.

The defined scoring function in the section above represents a projection onto the position level of the AML-3D scoring function presented in the previous section. In fact, the AML-3D scoring function represents the similarity between true observations and predictions (from SPRING simulation) using the PR measurements information. By projecting this similarity onto the position level, we define it using the position information.

3.4 Experimental Validation

We have chosen in this section to evaluate separately the positioning performance of the proposed algorithm based on PR correction and the positioning performance of the proposed algorithms based on scoring over candidate positions.

3.4.1 Experimental Settings

Experiments have been carried out in Toulouse to assess the level of performance of the proposed positioning algorithms in this chapter. GPS L1 C/A code PR measurements were recorded along the "Capitole Square" in Toulouse using a Septentrio AsteRx3 receiver. A Novatel SPAN system including a DGPS receiver tightly integrated with an FSAS-IMU (from iMAR), with decimetre level of positioning accuracy is used as the reference system. Measurements from both receivers were sampled at 10 Hz. For this test, we used a 4-min trajectory along a deep urban environment characterized by narrow streets and buildings alongside the streets. Fig. 3.10 shows the number of GPS satellites obtained during this measurement campaign.

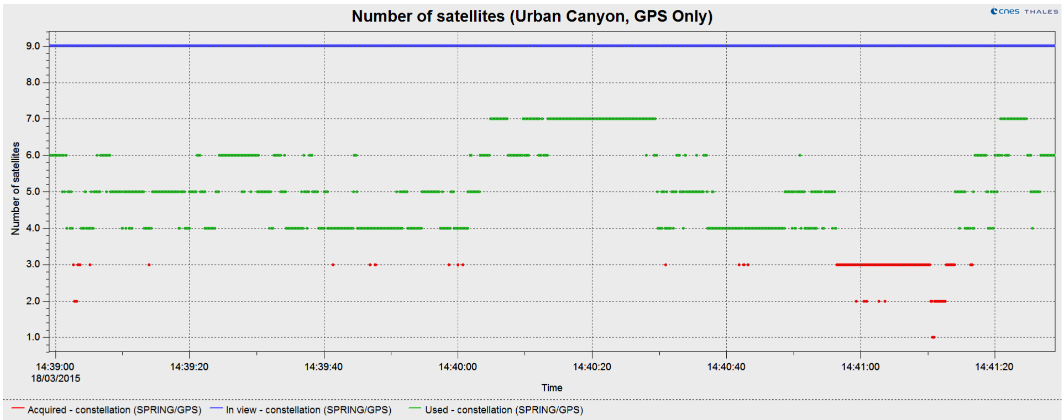

FIGURE 3.10 – Number of GPS Satellites across time (SPRING figure without possible modification of font-size)

An overview of the considered urban environment and the Sky-plot of the GPS received satellites in the deep urban section are shown in Fig. 3.11.

(a) Tested Urban Environment

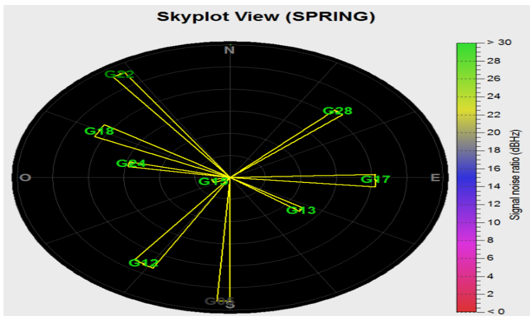

(b) Sky-Plot of GPS Satellites

FIGURE 3.11 – Tested Urban Environment and the obtained Sky-Plot

These recorded PR measurements collected using the AsteRx3 Septentrio receiver along this urban canyon environment show how poor the GNSS positioning performance is, using conventional LS estimation, in the presence of MP and NLOS bias. The obtained results are shown in Fig. 3.12. This figure presents also the cumulative distribution function (CDF) of the trajectory position error with respect to the reference trajectory in each ENU direction using a conventional least squares with GPS signal only.

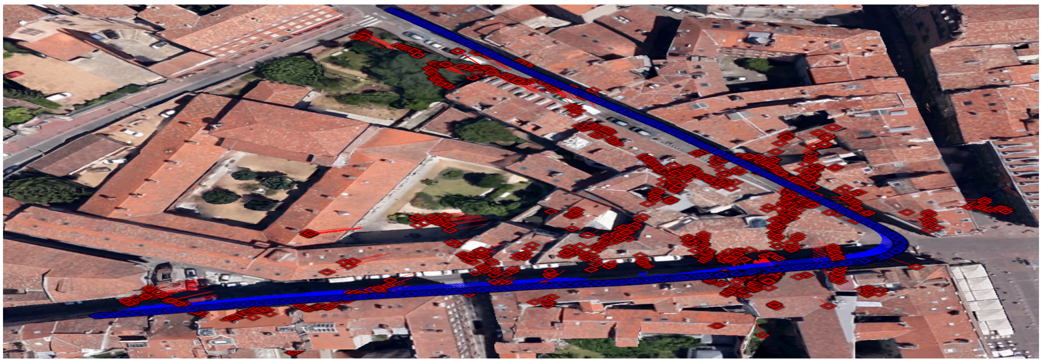

(a) Positioning using Least Squares solution : Blue dots refer to the reference trajectory ; red dots refer to the LS trajectory

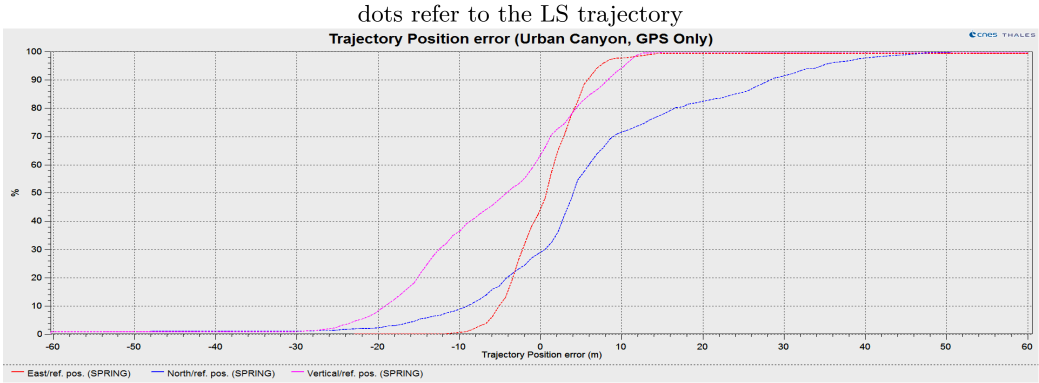

(b) Localization errors distribution of the Least Squares solution : North (Blue color), East (Red color) and Vertical (Pink color) positioning errors in urban environments (SPRING figure without possible modification of font-size)

FIGURE 3.12 – Example vehicular results in Toulouse

The performance of the PR Correction using Bias Bounds algorithm, termed as the CEKF algorithm for Constrained EKF, will be evaluated in the next sub-section using bias bounds predicted using the 3D GNSS signal propagation simulator SPRING (realistic case).

For the validation of the algorithms based on candidate positions scoring, we have selected a trajectory along an urban environment characterized by narrow streets and medium-height buildings. We have used the elevation angle as criterion for reference satellite selection for both AML-3D and PM-3D estimation, by considering the reference satellite, i.e. the satellite having no PR bias, at each candidate position as the satellite having the highest elevation angle. For the performance assessment of these two methods, we have used PR measurements collected using an Ublox 6T receiver and with the same Novatel SPAN reference system. The measurements from the Ublox receiver were sampled at 4 Hz and those of the Novatel SPAN system were sampled at 10 Hz and down-sampled to 4 Hz.

For illustration of the used grid of candidate positions, Fig. 3.13 shows the used array of positions. In this experimental evaluation of our algorithms, we have used 1600 outdoor candidate positions in a square area in the region of interest. These positions are uniformly distributed in this search area with a spacing of 1m. A pre-processing algorithm is implemented to exclude the indoor points based on the 3D model of the city and using the software Q-GIS. Hence, this grid of candidate positions contains only outdoor locations. The red cubes refer to the used reference trajectory, while white cubes represent the considered candidate positions. For the performance assessment of AML-3D and PM-3D algorithms, because of the excessive computational loads of SPRING simulations, we have selected a 20-seconds trajectory along this urban environment (red dots in Fig. 3.13) with a rate of 4 Hz. Hence, for the experimental analysis in 3.4.3.2, 80 epochs are considered.

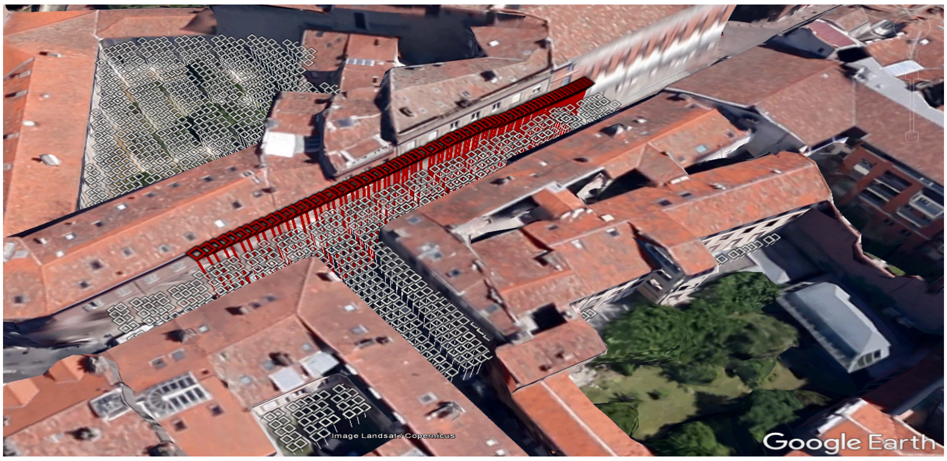

FIGURE 3.13 – Used Grid of candidate positions

3.4.2 GNSS Measurements correction by bias bounding using a 3D GNSS signal propagation simulator

In this sub-section, we use the 3D GNSS signal propagation simulator SPRING to define upper and lower bias bounds. We have used the same data recorded in the same urban canyon environment studied in the previous example above. For PR bias bounds prediction, we have used algorithm 1 with a grid of 3×3 points centred in the true position and spaced by approximately 1 meter in north and east directions. We have used a small grid of points because of the heavy computational loads of SPRING simulation in the case of a large grid with a 4-min trajectory.

After the PR bias bounds estimation using this grid, the CEKF position can be computed and compared to the conventional EKF position. Performances will depend on the quality of the PR bias bounds prediction using the 3D GNSS signal propagation simulators. By way of illustration, the variation of the bias bounds using the 3D simulator SPRING is drawn in Fig. 3.14(a) for PRN 28 for example. PRN 28 has been chosen by way of illustration and the other satellites give similar results. PRN 28 is a medium elevation satellite of approximately 35° of elevation angle as shown in Fig. 3.11. Fig. 3.14(b) provides the CDF of horizontal positioning errors of both solutions.

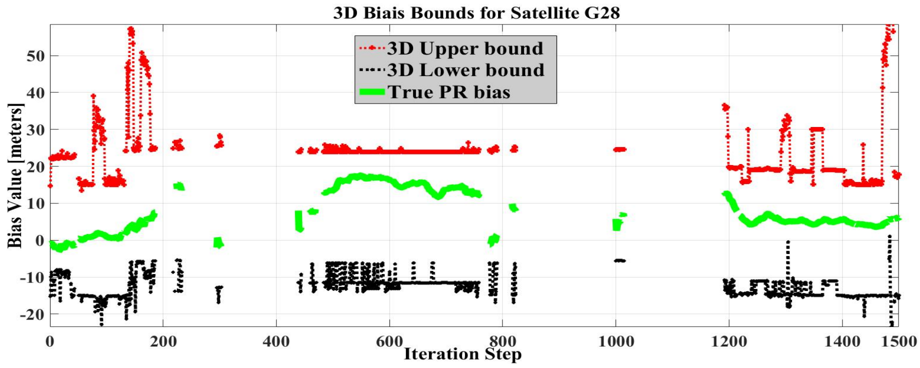

(a)

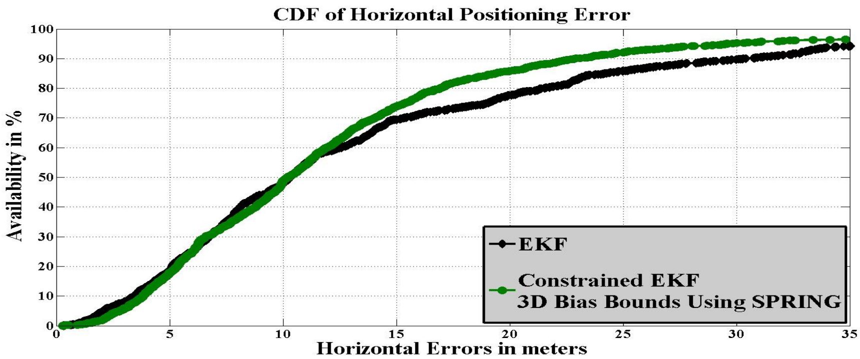

(b)

FIGURE 3.14 – Positioning performances using 3D bias bounds : 3.14(a) 3D Bias Bounds and "measured" true bias using [3] for satellite PRN 28 ; 3.14(b) CDF of horizontal errors along the considered trajectory using 3D bias bounds estimation. Experimental settings are described in section 3.4.1.

The gaps observed in Fig. 3.14(a) are caused by the non-reception of satellite PRN 28 during these epoch times. The predicted PR bias bounds have a different variation compared to the "measured" true PR bias which means that the 3D estimated mean bias bounds have a higher variation than the measured "true" unknown PR bias variation (estimated using the algorithm described in 3.1.3.1). The previous CDF figure shows that the CEKF estimator gives a performance improvement compared to EKF with bias bounds estimated using a 3D GNSS signal propagation simulators especially for high positioning errors.

The proposed method based on PR bias bounds is essentially sensitive to these PR bias correction by mean bias bounds (as CEKF algorithm is based on PR correction based on mean bias bounds as described in algorithm 2) and then to the bias bounds prediction as it will be studied and proven in section 3.5. We propose in this section 3.5 to study the acceptable level of PR bias estimation using a 3D simulator to obtain better positioning accuracy than a conventional algorithm such as LS. This admissible region of inaccuracy will be defined theoretically in section 3.5 and validated using real GNSS data.

3.4.3 Performance of Algorithms Based On Candidate Positions Scoring

3.4.3.1 Comparison Algorithm : Shadow-Matching (SM-3D)

Shadow Matching solution [157] uses 3D building models to improve cross-track positioning accuracy in harsh environments by predicting which satellites are visible from different candidate locations and comparing this information with the measured satellite visibility to determine the final user solution. This positioning approach is based on GNSS and 3D model fusion for satellite shadows scoring of candidate positions. By achieving metre-order cross-street positioning in urban canyons, it was implemented for smartphone applications [161, 162]. The basic Shadow-Matching approach can be summarized in algorithm 4.

Algorithm 4 Shadow-Matching Estimation

Inputs : C/N_0 Measurements (for satellite visibility)

Output : $\hat{\mathbf{x}}_{SM}$

1: **Define search area and grid of outdoor candidate positions**

2: **Building Boundaries (BB) computation [47]**
For each candidate position, predict building edges using the 3D city model

3: **Predict satellite visibility**
For each candidate position, predict satellite visibility using the Building Boundaries

4: **Measure satellite visibility**
Use C/N_0 ratios to determine the observed satellite visibility using the LOS probability model and the same parameters as presented in [158].

5: **Scoring of candidate positions**
Based on predicted and measured satellite visibility matching, score each candidate position. We have used the same scoring presented in [158].

6: **Final position estimation**
Estimate the final user position based on weighting of position having the highest scores as presented in [158] with the same parameters.

In this experiment, we have used our implementation of a Shadow Matching solution to compare and assess the performance of our proposed algorithm. The Shadow Matching algorithm has been implemented using GPS and GLONASS signals. Our proposed AML-3D and PM-3D algorithms have been implemented using GPS signals only since 3D GNSS signal propagation simulation using the GLONASS constellation is not yet developed by the CNES in the current version of the SPRING simulator.

3.4.3.2 Positioning Performance of AML-3D and PM-3D

For this validation test, we assess the positioning performance of the AML-3D and PM-3D solutions. We have set the uncertainty of the bias prediction using SPRING $\tilde{\delta}_{3D}$ to zero and we fixed the threshold Th to 15% of positions having the highest scores for both AML-3D and PM-3D estimators. As AML-3D, SM-3D and PM-3D are all epoch-by-epoch solutions, we have chosen to compare them with a conventional least-squares algorithm (an epoch-by epoch solution). Fig. 3.15 shows the cumulative distribution function of the horizontal position errors of the proposed AML-3D solution, the proposed PM-3D solution, Shadow-Matching solution (SM-3D) and the conventional solution in the considered scenario.

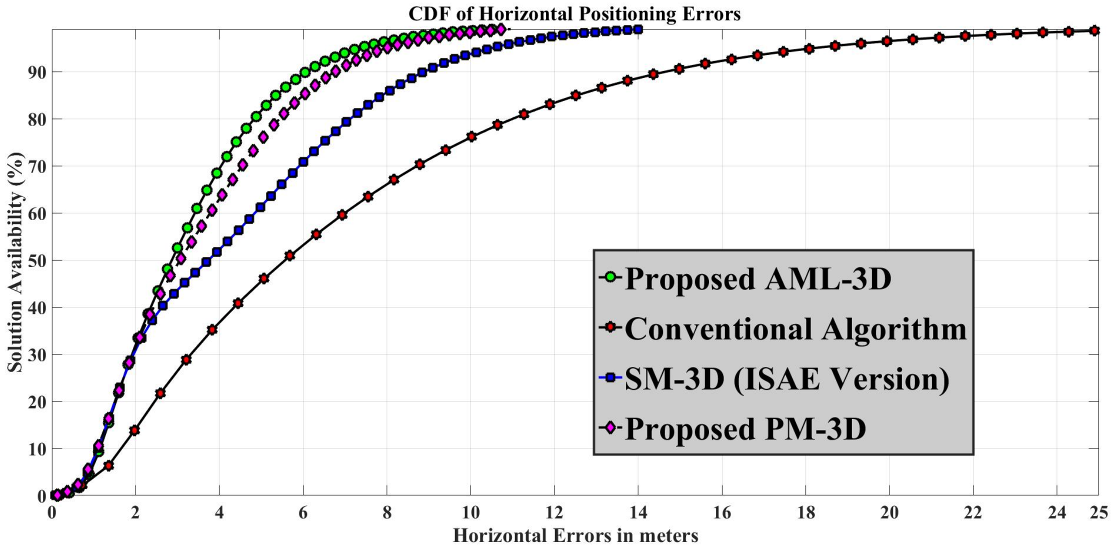

FIGURE 3.15 – CDF of Horizontal Positioning Errors

It is apparent from the CDF figure in Fig. 3.15 that our approach AML-3D gives the highest positioning performance in this scenario. Positioning performance of our proposed AML-3D and PM-3D algorithm are enhanced compared to the conventional GNSS solution. AML-3D and PM-3D solutions give almost the same horizontal positioning accuracy as the Shadow-Matching solution (SM-3D : ISAE Version) in this scenario.

We have compared the positioning performance using AML-3D and PM-3D solutions, Shadow-Matching solution (SM-3D), the Ublox receiver solution and a conventional Least-Squares solution. AML-3D, PM-3D, SM-3D and the Least-Squares solution are all epoch-by-epoch solutions. The Ublox solution is a filtered solution. We compare horizontal positioning errors (HPE) for these estimators in this scenario. Results are shown in Table 1.1. We notice that AML-3D outperforms, on average, all other solutions. However, PM-3D algorithm is more robust to large errors than the AML-3D algorithm.

The scoring map of the proposed AML-3D solution and the different solution for a fixed time epoch is shown in Fig. 3.16. Experimental settings are described in section 3.4.1. The selected epoch is at the end of the selected trajectory. We have chosen to add the position estimated by the Septentrio receiver used in these experiments jointly with the Ublox receiver. In this plot, scores of candidate positions are normalized between 0 and 100%.

Fig. 3.16 illustrates the effectiveness of the proposed AML-3D and PM-3D algorithms even in degraded conditions. Positioning performance of the solutions based on candidate positions scoring exceed that of the receiver solutions. Taking into account that the 3D simulator

Table 3.1 – Horizontal Positioning Performance of AML-3D and PM-3D

	AML-3D	**PM-3D**	**SM-3D**	**UBLOX**	**Conventional Algorithm (LS)**
Mean of HPE [m]	3.18	3.41	4.22	7.27	6.6
HPE at 95% [m]	5.86	6.36	7.95	11.65	14.66
HPE at 97% [m]	6.66	6.5	9.15	11.85	15.78
HPE at 99% [m]	9.18	8.64	9.56	12.41	18.32

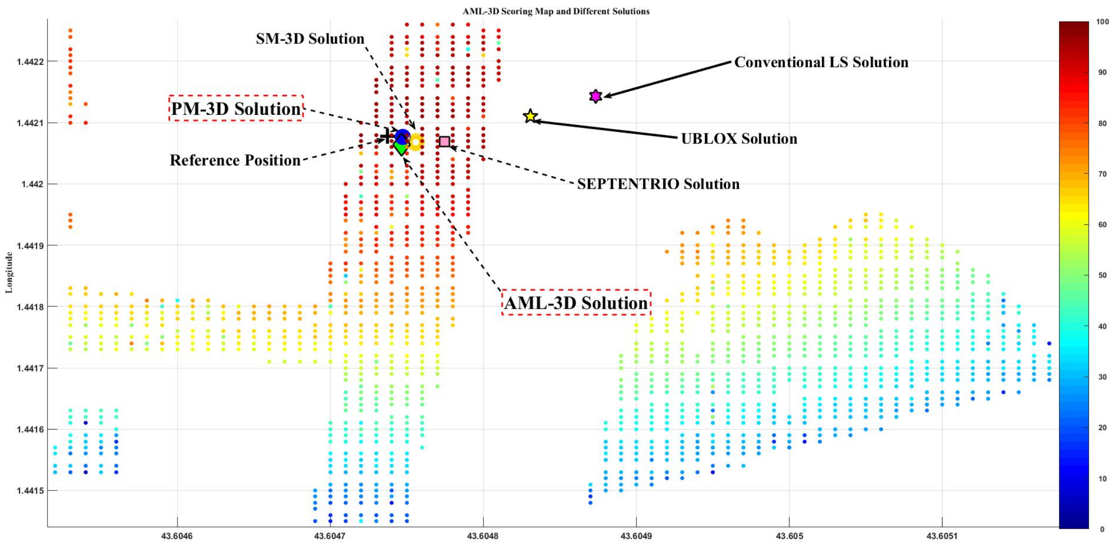

Figure 3.16 – AML-3D scoring map with different estimation solution

SPRING is continuously improved by CNES, these performance obtained by AML-3D and PM-3D might reach higher positioning accuracy. Finally, further analysis on the parameters used in these methods, and especially the enhancement obtained by applying a 3D bias uncertainty prediction, are provided in author's ION GNSS 2017 [202] and ITNST 2017 [203] papers. We have chosen to not add these analysis in the dissertation for the sake of clarity and ease of comprehension.

Despite this performance enhancement, the proposed approaches (AML-3D and PM-3D) are computationally intensive because of the bias estimation using the 3D GNSS signal propagation simulators. By way of comparison, Table 3.2 gives the computational loads of these algorithms compared to SM-3D for the same grid of positions. Nevertheless, with technological progress, this method may be implemented on a server and send the 3D biases to the mobile receiver to compute its position. It is worth recalling that Building Boundary (BB) computation in the SM-3D algorithm is performed using Matlab without the use of SPRING simulation. For the bias bounding algorithm (CEKF), the computational loads will be similar to those of the AML-3D and PM-3D solutions because these 3 algorithms use the same

SPRING simulations.

TABLE 3.2 – Computational loads for the whole trajectory (presented in Fig. 3.13) with 80 samples of AML-3D, PM-3D and SM-3D

	AML-3D (SPRING Simulation)	**PM-3D (SPRING Simulation)**	**SM-3D (Only BB computation - ISAE Implementation)**
Software	SPRING V4.1.0.7137	SPRING V4.1.0.7137	Matlab 2013a
CPU	i7-4770 3.4GHz	i7-4770 3.4GHz	i5-3470 3.2GHz
Time [s]	10640 ($2h57min$)	10640 ($2h57min$)	3981.65 ($1h6min$)

3.5 Minimum Acceptable Level of 3D Bias Prediction

It is obvious that the PR biases predicted by GNSS simulation can not be instantaneous and certainly accurate. The proposed method based on PR measurements correction based on PR bias bounds, presented in section 3.2, is very sensitive to these 3D PR bias predictions and correction as shown in the experimental section. This PR correction step is a sensitive task : poor PR biases prediction engenders an erroneous PR correction and then may sensitively reduce the position estimation accuracy instead of enhancing it. Consequently, we study in this section the influence of the inaccuracy on the prediction of PR bias, by GNSS simulation or other means, on positioning performance of algorithms based on PR measurements correction.

The fundamental question addressed in this sub-section is : how accurate the PR bias estimation, by a 3D simulator or others tools, should be to ensure that any algorithm based on PR correction, termed here as a CLS algorithm for Corrected Least-squares, gives better performance in term of positioning accuracy compared to conventional positioning algorithms such as the LS. This accuracy condition defines the acceptable/permissible level of imprecision on the estimation of PR bias that any 3D GNSS signal propagation simulators must not exceed in order to improve the positioning performance by correcting PR measurements. First, we formulate the general formulation of this accuracy condition on PR bias prediction. Then, this condition is tested on real measurements collected in the city of Toulouse. Finally, a detailed analysis of the maximum level of acceptable inaccuracy in PR bias prediction is carried out by type of environment (urban, suburban and rural) and by satellite elevation angles and CN0 levels. The performance condition for defining this maximum level of acceptable inaccuracy on PR bias prediction is defined by comparing the accuracy of the solution obtained by correcting PR measurements with a conventional LS. However, this methodology remains general and other estimators can be used. Also, the following analysis is valid for any other source of information allowing the prediction of PR bias, including multi-sensor navigation.

3.5.1 Theoretical condition on bias prediction for PR measurements correction

The maximum acceptable level of inaccuracy in PR bias prediction to achieve better performance by PR measurements correction compared to conventional LS can be defined based on the overall MSE of both the CLS and LS estimators as :

$$OMSE[\hat{\mathbf{x}}_{CLS}] = \mathrm{Tr}\{MSE(\hat{\mathbf{x}}_{CLS})\} \leq OMSE[\hat{\mathbf{x}}_{LS}] = \mathrm{Tr}\{MSE(\hat{\mathbf{x}}_{LS})\} \tag{3.14}$$

In the case of uncorrelated MP/NLOS bias $\mathbf{b}$ between satellites, this relation leads to :

$$\mathrm{Tr}\{\mathbf{H}_{\mathbf{b}}^{+} E\{\delta\mathbf{b}\delta\mathbf{b}^T\}\mathbf{H}_{\mathbf{b}}^{+}\} \leq \mathrm{Tr}\{\mathbf{H}^{+} E\{\mathbf{b}\mathbf{b}^T\}(\mathbf{H}^{+})^T\} - \beta_{\mathbf{b}} \tag{3.15}$$

Proof : See Appendix C.

Where $\delta\mathbf{b} = \mathbf{c} - \mathbf{b}$ the error in the PR bias prediction, $\mathbf{c}$ is the predicted PR bias (using 3D simulation or other tools), $\mathbf{H}^{+} = (\mathbf{H}^T\mathbf{R}^{-1}\mathbf{H})^{-1}\mathbf{H}^T\mathbf{R}^{-1}$ is the pseudo-inverse of matrix $\mathbf{H}$ weighted by the inverse of noise covariance matrix $\mathbf{R}$, $\mathbf{H}_{\mathbf{b}}^{+} = (\mathbf{H}^T\mathbf{R}_{\mathbf{b}}^{-1}\mathbf{H})^{-1}\mathbf{H}^T\mathbf{R}_{\mathbf{b}}^{-1}$ is the pseudo-inverse of $\mathbf{H}$ weighted by the noise covariance matrix of the CLS algorithm $\mathbf{R}_{\mathbf{b}}$ that might be different from the noise covariance matrix of the LS algorithm $\mathbf{R}$ and $\beta_{\mathbf{b}} = \mathrm{Tr}\{(\mathbf{H}^T\mathbf{R}_{\mathbf{b}}^{-1}\mathbf{H})^{-1}\} - \mathrm{Tr}\{(\mathbf{H}^T\mathbf{R}^{-1}\mathbf{H})^{-1}\}$.

In the theoretical case of only one faulty measurement in the ranging measurement from one satellite j, i.e. $\mathbf{b}$ contains only one non-zero value (if we compensate ionospheric, tropospheric, ephemeris and satellite clocks errors using some models and neglect the PR measurements noise), the condition (3.15) can be simplified as :

$$(E\{\delta\mathbf{b}\delta\mathbf{b}^T\})_j \leq \frac{\sum\limits_k [(\mathbf{H}^{+})_{k,j}]^2}{\sum\limits_k [(\mathbf{H}_{\mathbf{b}}^{+})_{k,j}]^2}(E\{\mathbf{b}\mathbf{b}^T\})_j - \frac{\beta_{\mathbf{b}}}{\sum\limits_k [(\mathbf{H}_{\mathbf{b}}^{+})_{k,j}]^2} \tag{3.16}$$

If we define the damping coefficient $\epsilon_j = \dfrac{\sum\limits_k [(\mathbf{H}^{+})_{k,j}]^2}{\sum\limits_k [(\mathbf{H}_{\mathbf{b}}^{+})_{k,j}]^2}$, then we have :

$$(E\{\delta\mathbf{b}\delta\mathbf{b}^T\})_j \leq \epsilon_j (E\{\mathbf{b}\mathbf{b}^T\})_j - (\beta_{\mathbf{b}} / \sum_k [(\mathbf{H}_{\mathbf{b}}^{+})_{k,j}]^2) \tag{3.17}$$

This damping coefficient appears because we have augmented the noise covariance matrix $\mathbf{R}_{\mathbf{b}}$ using the PR bias prediction $\mathbf{c}$, i.e. $\mathbf{R}_{\mathbf{b}}$ takes into account the prediction of PR bias $\mathbf{c}$ and may be different from $\mathbf{R}$. If we haven't use this augmentation, i.e. $\mathbf{R}_{\mathbf{b}} = \mathbf{R}$, then the damping coefficient ϵ_j will be equal to 1 and $\beta_{\mathbf{b}} = 0$. Thus, the condition (3.17) becomes :

$$(E\{\delta\mathbf{b}\delta\mathbf{b}^T\})_j \leq (E\{\mathbf{b}\mathbf{b}^T\})_j \tag{3.18}$$

This condition means that the bias bound prediction error must have a lower variation than the true unknown PR bias variation to obtain better performance by correcting the PR measurement. The damping coefficient allows widening the admissible region of bias estimation inaccuracy since it is higher than 1, in general.

Finally, the condition (3.15) is a general condition that any positioning algorithm based on PR measurements correction must verify to ensure lower estimation errors than conventional LS algorithm without PR measurement correction. This condition defines the maximum acceptable level of uncertainty on the PR bias prediction in term of positioning accuracy.

3.5.2 Experimental calculation of maximum acceptable imprecision on PR bias prediction

In this sub-section, we will experimentally evaluate and validate the previous found maximum acceptable level on PR bias prediction inaccuracy for different GNSS satellites. The procedure for the experimental validation (using the experimental settings introduced in subsection 3.4.1) is as follows :

— First, the PR measurements of all satellites are corrected using the measured "true" bias value, predicted using [3]. This method was explained in subsection 3.1.3.1.

— Then, we model the error on the prediction of PR bias of the satellite $(\delta \mathbf{b})_j$ under study by a Gaussian distribution with a variable mean and variance, i.e. $(\delta \mathbf{b})_j \sim \mathcal{N}(\mu, \sigma^2)$.

— Finally, the values of the mean μ and the variance σ^2 of this Gaussian distribution (of $(\delta \mathbf{b})_j$) are varied until reaching the condition of equality between the positioning errors of LS and CLS algorithms, i.e. LS algorithm and CLS algorithm based on PR of the satellite "j" correction using the correction value $(\delta \mathbf{b})_j$, i.e. $OMSE[\hat{\mathbf{x}}_{CLS}] = OMSE(\mu, \sigma) = OMSE[\hat{\mathbf{x}}_{LS}]$.

It is highlighted that in this particular case of a Gaussian error distribution of the estimate of the satellite bias "j", the mean square error of the CLS estimation is written as :

$$OMSE(\mu, \sigma) = \mathrm{Tr}\{(\mathbf{H}^T \mathbf{R}_{\mathbf{b}}^{-1} \mathbf{H})^{-1}\} + \sum_k [(\mathbf{H}_{\mathbf{b}}^{+})_{k,j}]^2 (\sigma^2 + \mu^2) \tag{3.19}$$

Proof : See Appendix C.

In this case, the condition on the mean μ and the variance σ^2 of this bias estimation error on satellite "j" $(\delta \mathbf{b})_j$ to obtain better positioning performance than the LS algorithm is obtained from equation (3.17) with $E\{\delta \mathbf{b} \delta \mathbf{b}^T\}_j = \sigma^2 + \mu^2$ as $(\delta \mathbf{b})_j \sim \mathcal{N}(\mu, \sigma^2)$. It is as follows :

$$(\sigma^2 + \mu^2) \leq \epsilon_j (E\{\mathbf{b}\mathbf{b}^T\})_j - (\beta_{\mathbf{b}} / \sum_k [(\mathbf{H}_{\mathbf{b}}^{+})_{k,j}]^2) \tag{3.20}$$

If no augmentation is present on the noise covariance matrix of the CLS estimator, ie. $\mathbf{R}_{\mathbf{b}} = \mathbf{R}$, the maximum acceptable level on the PR bias of the satellite "j" error estimation, termed in the following equation as $(E\{\delta \mathbf{b} \delta \mathbf{b}^T\})_j$, is equal to :

$$(E\{\delta \mathbf{b} \delta \mathbf{b}^T\})_j = (\sigma^2 + \mu^2) \quad \text{Where } \sigma \text{ and } \mu \text{ satisfy} \quad OMSE(\mu, \sigma) = OMSE[\hat{\mathbf{x}}_{LS}] \tag{3.21}$$

Fig. 3.17(a) illustrates the overall mean squares errors OMSE variation as a function of the mean and variance of the error on the prediction of the bias of a GPS satellite in an urban environment. The used GPS satellite is PRN 28. It have been chosen by way of illustration. PRN 28 is a medium elevation satellite of approximately 35° of elevation angle as shown in Fig. 3.11.PRN 28 have been chosen by way of illustration and the other satellites give similar results. PRN 28 is a medium elevation satellite of approximately 35° of elevation angle as shown in Fig. 3.11. The experimental settings are the same used in previous sections and are described in 3.4.1. The constant curve corresponds to the variation of the OMSE of the LS solution. It is normal that this OMSE is constant as a function of the mean and the variance of the error on the prediction of PR bias $(\delta \mathbf{b})_j$ since the LS algorithm is applied to uncorrected PR measurements. The other curve corresponds to the variation of OMSE obtained using the correction of PR measurement from the tested satellite. This figure shows that a poor prediction of the bias will lead to higher positioning errors by correcting the PR measurements with respect to the LS estimator. In Fig. 3.17(b), the top view of the OMSE curves is presented. This view illustrates an area of acceptable error on bias prediction of this satellite. This zone is defined as the region where the correction of PR bias, using predicted PR bias, allows performance enhancement compared to the conventional positioning algorithms such as the LS algorithm in this case. This figure shows a region of the maximum acceptable error on the prediction of the PR bias using a 3D GNSS signal propagation simulator, thus the minimum degree of realism of the 3D modelling necessary to make the PR measurement correction information useful for positioning.

The same experimental procedure described at the beginning of this subsection is carried out on several satellites and in various environments in order to estimate the experimental maximum acceptable level of error on the PR bias prediction for different satellites and in different environments. The results are analysed in the following subsections.

3.5.3 Minimum PR bias prediction error by environment and satellite

In this subsection, we will experimentally evaluate the levels of maximum acceptable uncertainty on PR bias prediction for different satellites in an urban environment. We analyse these levels of uncertainty according to the elevation angles of different satellites. In general, the higher the angle of elevation, the less the signal is blocked or reflected by a building. Therefore, the maximum acceptable uncertainty level should decrease as the elevation angle increases. For this part, all the data of the urban section presented in section 3.4.1 are used. The selected urban section consists of an approximately 4-min trajectory with a sampling rate of 10 Hz, which gives 2400 data samples. The presented result in Fig. 3.18(a) is the average of the required PR accuracy for each satellite using all data in this urban section.

Also, an analysis of the maximum acceptable levels on the prediction of the PR bias is

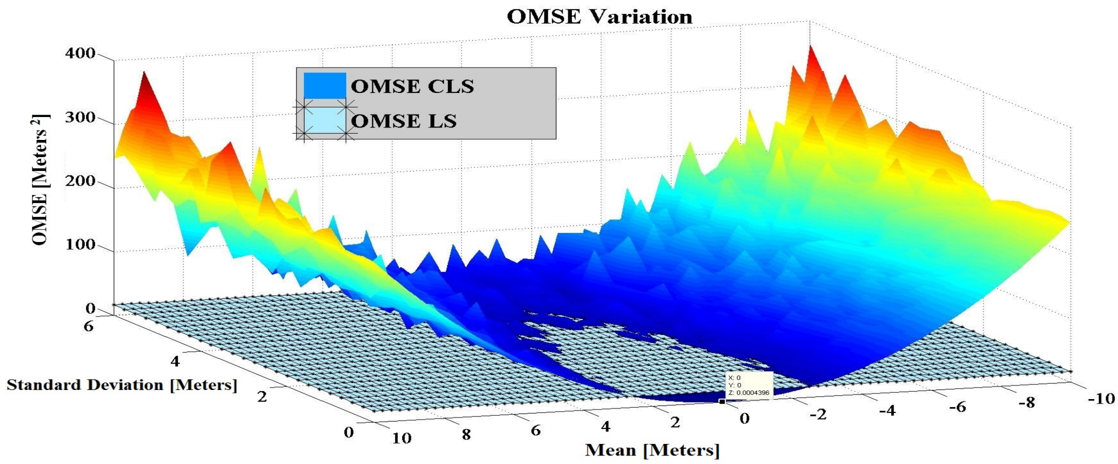

(a) RMS error variation as a function of PR bias estimation error for one satellite in an urban environment

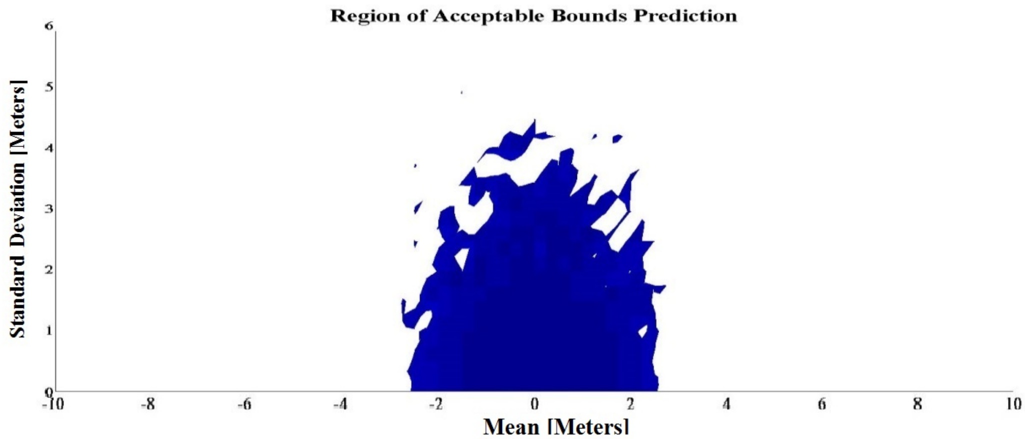

(b) Uncertainty bias prediction area in an urban environment

FIGURE 3.17 – Experimental minimum acceptable PR bias prediction error for a satellite (PRN 28) in an urban area. Experimental settings are described in section 3.4.1.

carried out. Three types of environments are considered : an urban environment, a suburban environment and an open environment. Since GNSS signals are generally of good quality in open environments, the maximum acceptable levels on PR prediction must be lower than those in urban environments. For this analysis, we have used the same equipment and data collection described in section 3.4.1, but we have selected three kinds of environments (urban, suburban and open environment). The selected suburban and open-sky sections consist of approximately 6-min and 10-min trajectory, respectively, with a sampling rate of 10 Hz, which gives 3600 data samples for the suburban section and 6000 data samples for the open-sky one.

The following figure shows the variation of these levels of maximum acceptable uncertainties as a function of the elevation angles in Fig. 3.18(a) and for two GPS satellites with different elevation angles in different environments Fig. 3.18(b). The used two satellites are

PRN 13, with an elevation angle of approximately 60°, and PRN 28, with an elevation angle of approximately 30° as it can be seen in Fig. 3.2.

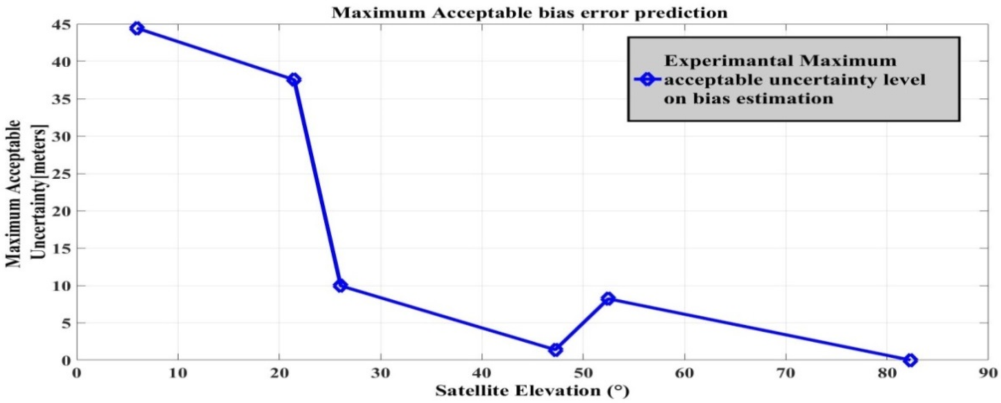

(a) Experimental maximum PR bias uncertainty as a function of satellite elevation in an urban environment

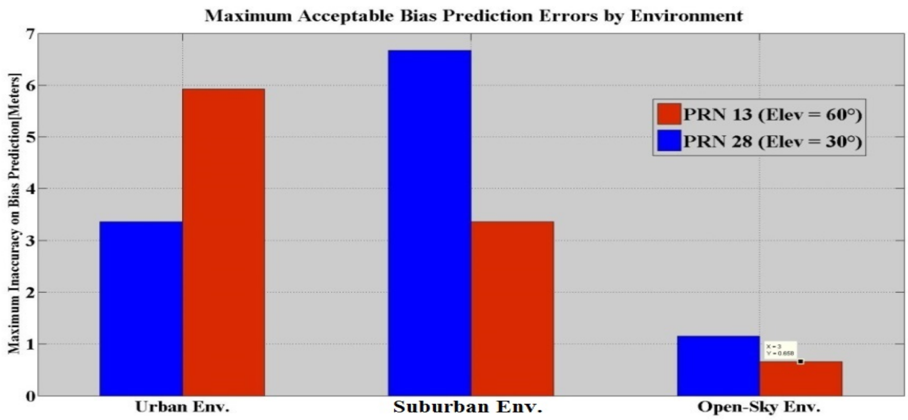

(b) Experimental maximum PR bias uncertainty in different environments for two GPS satellites

FIGURE 3.18 – Experimental minimum acceptable PR bias prediction error. Experimental settings are described above and in section 3.4.1.

This study makes it possible to identify PR measurements that are very difficult to correct on average, i.e. those of good quality and therefore should not be predicted using the 3D GNSS signal propagation simulator. However, this has not been tested in real-time. In this scenario, these signals are generally those of the high-elevation satellites. Also, the problem of GNSS signal degradation is much more prominent in urban and suburban setting as oppose to open-sky environments. This explains the difference between maximum acceptable PR bias uncertainties between urban and open-sky environments as shown in Fig. 3.18(b).

Then, it is useful to use the 3D GNSS signal propagation simulator to correct PR measurement in environments with high theoretical acceptable inaccuracy on bias estimation. However, 3D GNSS signal propagation simulation should not be performed in open sky environments with a small theoretical acceptable inaccuracy on bias estimation, since there is a great risk of deteriorating PR measurements by modifying them. Also, satellite elevation is not an absolute criterion to qualify the quality of the GNSS signal in urban environment. Indeed, the configuration of the urban environment means that high elevation signals can be reflected or received in NLOS situations, as is the case with the PRN 13 satellite at 53° elevation in this scenario.

3.5.4 Bias Estimation Using SPRING

In order to evaluate the PR bias prediction using SPRING and compare it with the maximum acceptable uncertainty level on bias prediction, Table 3.3 gives the variation of these two variables versus satellite elevation angles in an urban environment. This selected urban section consists of the same urban environment present in 3.4.1 with approximately 4-min trajectory at a sampling rate of 10 Hz (2400 data samples). Results consist of an average using all data in this urban section.

Table 3.3 – Experimental maximum acceptable bias estimation uncertainty and bias estimation error using SPRING. Experimental settings are described above and in section 3.4.1 with 2400 data samples

	Average Satellite Elevation (°)	**Average PR Bias Estimation Error using SPRING Simulation [Meters]**	**Average Experimental Maximum Acceptable Uncertainty Level on PR bias Estimation [Meters]**
GPS 22	5.93	0.83	44.45
GPS 12	21.47	26.30	37.53
GPS 28	26.35	4.53	9.94
GPS 24	47.23	0.39	1.38
GPS 13	52.47	7.22	8.2
GPS 15	82.29	0.25	0

This comparison leads to the conclusion that the PR bias prediction error using SPRING simulation (computed by comparing SPRING predictions with the measured "true" PR bias obtained using [3]) is lower than the maximum acceptable on PR bias prediction error in this particular environment presented in section 3.4.1. This result validates the use of the 3D GNSS signal propagation simulators SPRING for pseudorange bias correction in this environment, which enhances slightly the positioning performance compared to conventional algorithms as shown in section 3.4.2. It should be stressed that this study have been carried out in a particular scenario and environment. Other results, using the same methodology, should performed to validate PR bias prediction (on average) using SPRING. Unfortunately, this was not performed during the thesis, because of the excessive computational loads of SPRING simulations.

This original study makes it possible to identify environments where it is useful to use a 3D GNSS signal propagation simulator to predict PR biases in order to correct PR measurements. Therefore, it allows the production of a map representing the environments where it is useful to use a correction of PR measurements by prediction of PR biases via SPRING-3D simulation, or other tools. If the same methodology explained above is performed in other scenarios and environments, we can get these maps, that can be called "Bias Prediction Readiness Correction Availability Maps". This study allows also the production of a requirement metric on PR bias prediction by 3D GNSS signal propagation simulation. This metric express the average PR bias estimation error for each 3D GNSS signal propagation simulator. Having this metric allows to classify different 3D GNSS signal propagation simulators.

3.6 Summary and Conclusions

In the typical case of urban environments, the use of aiding information is generally mandatory. In this chapter, we propose the exploitation of the characteristics of the receiver environment using the CNES 3D GNSS signal propagation simulator SPRING to provide aided information to the GNSS receiver.

This simulator is hybridized with the GNSS receiver in different ways : hybridization in the measurements domain is based on the use of 3D predicted bounds on PR bias for PR measurements correction. Another hybridization scheme is proposed in the position domain which is based on scoring of an array of candidate positions using the 3D information from the 3D GNSS signal propagation simulator. The proposed positioning algorithms are based on the use of a grid of input positions introduced to the SPRING 3D GNSS signal propagation simulator to predict PR biases on these candidate points and retain the position with the best similarity between measurements and simulations based on two metrics : the metric of PR matching between measured pseudoranges and those predicted one via bias prediction by SPRING-3D, and the metric of position matching between candidate positions and position obtained by PR measurement correction using SPRING-3D, over an array of candidate positions. These proposed methods are summarized in Fig. 3.19.

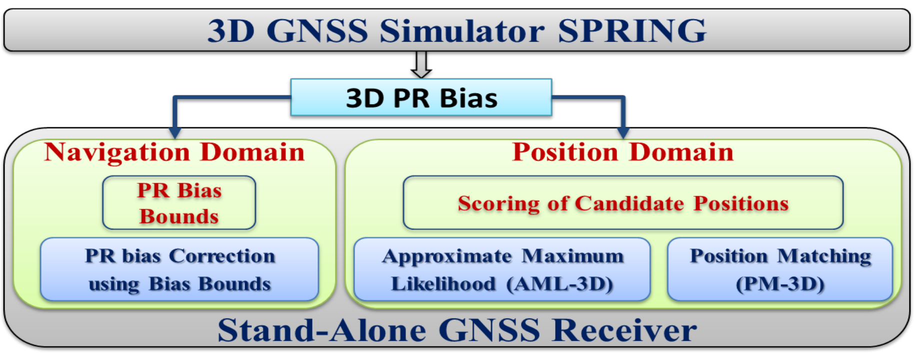

FIGURE 3.19 – Proposed 3D Simulator/GNSS Integration architecture

The proposed algorithms have been tested in an urban environment in Toulouse and allow a significant accuracy improvement of 52% compared to the conventional LS solution in deep urban environments. The disadvantage of these positioning algorithms, assisted by 3D information, is mainly the need for the availability of large computational resources because of SPRING simulations. However, other studies have used similar techniques with lighter GNSS signal propagation algorithms working in real-time [168].

Finally, we have addressed the question of the merit of integrating a 3D simulator with a GNSS receiver. This study enables the definition of the maximum level of inaccuracy on bias estimation that any 3D GNSS signal propagation simulators, or any other tools used for PR bias prediction, mustn't exceed. This first study gives a methodology that permit the identification of areas where on average a PR measurement correction is not useful or difficult to obtain ; i.e. when bias correction will probably engender more performance degradation than enhancement. This result would require applying the same methodology to different environments and using more data samples. This study has also justified the use of the SPRING simulator since 3D bias prediction using this tool is on average below the maximum acceptable level on PR bias prediction in the particular urban environment studied in this thesis. This result shows also the usefulness and the potential of these tools (3D models or 3D GNSS signal propagation simulator) for positioning enhancement in presence of PR biases.

Bornes inférieures de l'erreur d'estimation GNSS en conditions MP/NLOS

Introduction aux bornes inférieures

En estimation paramétrique, les performances d'un estimateur sont généralement caractérisées par son Erreur Quadratique Moyenne (EQM). Afin de quantifier les performances ultimes pour un problème donné, des bornes inférieures sur l'EQM, indépendantes de la technique d'estimation employée, ont été établies dans la littérature.

En effet, la distribution de probabilité des échantillons de données reçues permet de déduire certaines informations utiles sur les paramètres à estimer, ce qui permet d'estimer les bornes inférieures sur l'EQM d'estimation. Dans cette optique, il semble nécessaire de disposer d'une métrique quantifiant l'utilité de l'information fournie par la distribution de probabilité pour l'estimation de paramètres inconnus. Une telle mesure peut être utilisée pour trouver des limites inférieures (LB) sur les erreurs d'estimation de paramètres inconnus et ainsi donner un aperçu des limites inhérentes au problème.

Par conséquent, les bornes inférieures de l'EQM donnent les expressions des erreurs d'estimation minimales pouvant être obtenues de manière asymptotique (dans la limite d'un grand nombre d'observations indépendantes) lors de l'estimation des paramètres. Ces bornes inférieures sont généralement dérivées pour des classes données d'estimateurs biaisés ou non biaisés. Elles fournissent également des références auxquelles on peut comparer les performances des estimateurs afin d'évaluer la qualité de l'estimation. Par exemple, parmi toutes les bornes inférieures disponibles pour les estimateurs non biaisés, la plus utilisée est la borne de Cramer-Rao (BCR), qui fournit la précision maximale possible des estimateurs du maximum de vraisemblance (EMV). Dans ce chapitre, nous nous intéressons à la déduction de telles bornes inférieures (BI) dans le contexte GNSS en présence de dégradations sur les mesures de code, c'est-à-dire des échantillons de données reçues, provoqués par la réception de trajets multiples et de NLOS.

En effet, étant donné que de nombreux facteurs affectent la précision du positionnement final d'un récepteur GNSS en milieu urbain, il est judicieux de pouvoir analyser leur impact respectif sur la limite minimale de précision de l'estimation de la position, et en particulier pour les applications critiques qui englobent des exigences financières ou juridiques. C'est l'objectif de ce chapitre.

Non-Gaussianité de l'erreur GNSS

Comme indiqué dans les chapitres précédents, prévoir le niveau de dégradation de la précision du positionnement de l'utilisateur en milieu urbain à l'aide uniquement des mesures de pseudo-distances GNSS est une tâche très ardue. La prévision de ce niveau de précision maximal nécessite la modélisation de toutes les sources d'erreur de positionnement afin de définir la fonction de densité de probabilité (p.d.f.) des observations GNSS, une condition essentielle pour la dérivation des bornes inférieures de l'erreur quadratique moyenne. Les erreurs liées aux satellites (erreurs orbitales ou biais d'horloge satellite) et à la propagation (retards ionosphériques et troposphériques) sont généralement faciles à modéliser ou à réduire à partir d'observations à l'aide de modèles adéquats comme dans le SBAS (EGNOS, WAAS, ...). Cependant, dans les zones urbaines, les signaux GNSS directes deviennent rares. La plupart des signaux sont vulnérables aux réflexions et aux erreurs causées par la propagation du GNSS dans l'environnement, telles que la réception par trajets multiples. Ces erreurs sont donc très difficiles à modéliser avec précision. Généralement, dans ces zones urbaines, les erreurs GNSS sont non-gaussiennes.

Dans ces environnements sub-urbains et urbains, nous souhaitons évaluer la précision de positionnement asymptotique du GNSS, ce qui soulève les questions suivantes :

1. Les bornes inférieures et l'estimateur de maximum de vraisemblance standard peuvent-ils être calculés dans de tels environnements ?
2. Si les bornes inférieures standards ne peuvent pas être calculés, pouvons-nous dériver des bornes inférieures modifiées, qui sont calculables ?
3. Si l'estimateur de maximum de vraisemblance standard ne peut pas être calculé, pouvons-nous proposer un substitut, potentiellement sous-optimal mais calculable ?

Bornes inférieures modifiées

Malheureusement, comme déjà mentionné ci-dessus, dans le contexte GNSS en présence de erreurs non gaussiens, la d.d.p. marginale des observations GNSS n'a pas de forme analytique en raison de la présence de la contribution non gaussienne des MPs. En conséquence, aucune des méthodes de caractérisation de la performance d'estimation existantes telles que les bi ne peut être utilisée dans ce cas. En effet, pour cette classe de problèmes d'estimation paramétrique déterministe, la d.d.p. paramétrée par des paramètres déterministes inconnus résulte de la marginalisation d'une d.d.p. jointe qui dépend de variables aléatoires inconnuEs. Dans le cas général, cette marginalisation est mathématiquement intraitable, ce qui empêche d'utiliser les BI déterministes standard connues sur l'EQM.

On peut résoudre ce problème en plongeant l'espace d'observation initial dans un espace hybride plus grand où tout BI standard peut être transformé en une borne inférieure modifiée adaptée à une estimation déterministe non standard, au prix toutefois d'une éventuelle perte de proximité à l'EQM vraie des EMVs.

En effet, la forme modifiée d'une BI est plus optimiste (inférieure ou égale) que la forme standard de cette BI. Cela met en évidence le compromis associé aux BI modifiée dans une estimation non standard : une formulation aux dépens de la précision. Deuxièmement, en termes de BI relatives, c'est-à-dire destinées à caractériser l'estimateur (asymptotiquement sous-optimales) de maximum de vraisemblance non-standard, on montre que toute borne inférieure standard a une version non standard qui limite l'EQM de l'estimateur de maximum de vraisemblance non-standard.

Cependant, ces deux solutions n'ont pas été explicitement illustrées dans le contexte du GNSS en raison d'un manque de temps (toutefois, des exemples d'applications de BI modifiée et de BI non standard se trouvent en Radar et en Telecom). Une suite naturelle de ce travail consiste à quantifier ces BI modifiées et BI non standard dans le contexte du GNSS dans des environnements urbains non-gaussiens. Ce serait un axe fructueux pour des recherches ultérieures.

Chapitre 4

Lower Bounds on GNSS Positioning Performance in MP/NLOS Conditions

Contents

In parameter estimation problems, the probability distribution of samples of received data allows deduction of some useful information about the parameters to be estimated. With this in mind, it seems necessary to have a metric quantifying the usefulness of the information provided by the probability distribution on unknown parameters estimation. Such a measure can be used to find lower bounds (LBs) on the estimation errors of unknown parameters and hence give insight on the inherent limitations of the problem.

Hence, lower bounds on the mean squared error (MSE) give the expressions of the minimal estimation errors that can be obtained asymptotically (in the limit of large sample support) when estimating the parameters. These lower bounds are generally derived for given classes of biased or unbiased estimators and provide references to which performance of these estimators can be compared to evaluate the quality of estimation. For instance, among all the available lower bounds for unbiased estimators, the most used one is the Cramer-Rao bound (CRB) which is the lowest lower bound and provides the maximum achievable estimation accuracy of maximum likelihood estimators (MLEs), under reasonably general conditions on the observation model [204, 205]. In this chapter, we are interested in deriving such LBs in the GNSS context in presence of degradations on code measurements, i.e. received data samples, caused by reception of multipaths and NLOS. This chapter is divided into 6 sections :

- **Section 4.1 :** Introduction of the motivation and the objectives behind lower bounds derivation in the GNSS context.
- **Section 4.2 :** Description of the limitation of the classical standard deterministic lower bounds (LBs) on MSE in the case of non-Gaussian measurement errors.
- **Section 4.3 :** Derivation of the proposed alternative to circumvent the previous problem : modified lower bounds (MLBs).
- **Section 4.4 :** Derivation of sub-optimal non-standard MLEs (NSMLEs) as alternative to MLEs in non-standard deterministic estimation.
- **Section 4.5 :** A summary of the principal conclusions of this chapter.

4.1 Motivation and Objectives

Today, GNSS is used as a primary technology for positioning in a broad range of applications in urban areas, including critical applications with potential financial and legal impacts. For instance, ecological taxations, termed as EcoTax, are based on GNSS as a main technology in a road congestion pricing system depending on position solution. Road user charging is another illustration of successfully implemented road applications based on GNSS and involving financial aspects. Hence, it is necessary for constrained environments, where reliable GNSS positioning is difficult to achieve, to define the maximum positioning performance that GNSS can achieve to decide if the final applications requirement at the user level will be met or not in these harsh areas.

As many factors affect the final positioning accuracy of a GNSS receiver in urban environments, there is a pressing need to know the minimum bound of position estimation accuracy especially for critical applications which encompass financial, legal or safety-of-life stringent requirements. This is the objective of this chapter.

As shown in previous chapters, predicting the level of positioning degradation and the final user positioning accuracy in urban environment using only GNSS pseudorange measurements is a very challenging task. Predicting this maximum accuracy level requires modelling of all positioning error sources in order to define the probability density function (p.d.f.) of the GNSS observations, an essential requirement for lower bounds derivation. Satellite-related errors (orbital errors or satellite clock bias) and propagation-related errors (ionospheric and tropospheric delays) are generally easy to model, or to be reduced from observations using some adequate models as in SBAS (EGNOS, WAAS, ...). However, in urban areas where direct GNSS signals become too scarce and most signals are vulnerable to reflections, receiver-related errors caused by GNSS propagation in the environment, such as multipath reception, are very hard to be modelled accurately. However, in order to highlight the problem, two standard signal models are recalled in the next paragraph : 1) the case with only LOS signals, 2) the case with LOS and MP signals.

GNSS observation models including LOS and MP : Firstly, we recall a standard first order model of the GNSS observations in the case of a single reception antenna and without considering signal reflections [206]. We assume that K scaled, delayed and Doppler-shifted front waves, transmitted by each in-view satellite impinge on a GNSS receiver antenna. Under the narrowband assumption, the complex baseband model can be written as follows :

$$s(t) = \sum_{k=0}^{K-1} \alpha_k . c_k(t - \tau_k).e^{2i\pi f_k t} + n(t) \tag{4.1}$$

where

- α_k denotes each complex satellite signal amplitude, supposed to be deterministic and unknown,
- $c_k(t)$ stands for the transmitted complex baseband navigation signal spread by the pseudo-random code corresponding to the k-th satellite,
- $n(t)$ corresponds to an additive zero-mean white Gaussian noise with variance σ^2,
- and τ_k, f_k are respectively the delay and Doppler frequency shift of the k-th satellite signal, observed from the receiver.

We suppose that N snapshots are sampled at a $F_s = \frac{1}{T_s}$ rate from $s(t)$, so that we can write :

$$\mathbf{s} = \mathbf{s}(\boldsymbol{\theta}_d) = \mathbf{A}(\boldsymbol{\eta})\boldsymbol{\alpha} + \mathbf{n}, \qquad \boldsymbol{\theta}_d = (\boldsymbol{\eta}^T \boldsymbol{\alpha}^T)^T \tag{4.2}$$

where

- $\mathbf{x} = (x(0), ..., x((N-1)T_s))^T$,
- $\mathbf{A} = [\mathbf{a}_0, ..., \mathbf{a}_{K-1}]$ is the manifold corresponding to all in-view satellite signals, with $\mathbf{a}_k = (c_k(-\tau_k), ..., c_k((N-1)T_s - \tau_k).e^{2i\pi f_k (N-1)T_s})^T$,

— $\boldsymbol{\eta} = (\tau_1, ..., \tau_K, f_1, ..., f_K)^T$ is the vector of unknown deterministic parameters of primary interest (delays, Doppler-frequency shifts,...).

— $\boldsymbol{\alpha} = (\alpha_0, ..., \alpha_{K-1})^T$ and,

— $\mathbf{n} = (n(0), ..., n((N-1)T_s))^T$

Secondly, we consider now the case of a single reception antenna in the presence of N_{MP} signal reflections. Then, under the narrowband assumption, the complex baseband model (4.1) must be updated as follows :

$$s(t) = \sum_{k=0}^{K-1} \alpha_k.c_k(t-\tau_k).e^{2i\pi f_k t} + \sum_{i=1}^{N_{MP}} \alpha_{r,i}.c_k(t-\tau_{r,i}).e^{2i\pi f_{r,i} t} + n(t) \tag{4.3}$$

where

— $\alpha_{r,i}$ denotes each complex satellite signal amplitude after signal reflections, supposed to be random and unknown,

— and $\tau_{r,i}$, $f_{r,i}$ are respectively the delay and Doppler frequency shift after signal reflections, observed from the receiver, and supposed to be random and unknown.

We suppose that N snapshots are available as in (4.2), so (4.2) becomes :

$$\mathbf{s} = \mathbf{s}(\boldsymbol{\theta}_d, \boldsymbol{\theta}_r) = \mathbf{A}(\boldsymbol{\eta})\boldsymbol{\alpha} + \mathbf{m}(\boldsymbol{\eta}_r, \boldsymbol{\alpha}_r) + \mathbf{n}; \qquad \boldsymbol{\theta}_d = (\boldsymbol{\eta}^T \boldsymbol{\alpha}^T)^T, \quad \boldsymbol{\theta}_r = (\boldsymbol{\eta}_r^T \boldsymbol{\alpha}_r^T)^T \tag{4.4}$$

where, $\mathbf{m}(\boldsymbol{\eta}_r, \boldsymbol{\alpha}_r) = \sum_{i=1}^{N_{MP}} \mathbf{B}_i(\boldsymbol{\eta}_{r,i})\boldsymbol{\alpha}_{r,i}$ represents the contribution of all MP and :

— $\forall i \in [1, N_{MP}]$, $\mathbf{B}_i$ is the manifold corresponding to transmitted signal after signal reflections for the i-th multipath (may be different from MP to MP).

— $\boldsymbol{\eta}_r = (\eta_{r,1}, ..., \eta_{r,N_{MP}})^T$ is the vector of unknown nuisance parameters which may represent, in this case of GNSS in non-Gaussian environments, the delay and the Doppler frequency shift, of each MP after reflections.

— $\boldsymbol{\alpha}_r = (\alpha_{r,1}, ..., \alpha_{r,N_{MP}})^T$ refers to the vector of GNSS signal amplitudes of each MP after reflections.

Illustration of GNSS p.d.f errors in different environments : The signal model (4.2) without MPs have been extensively studied in the open literature where it is generally referred to as the conditional signal model (CSM) [207]. Asymptotically, i.e. at high signal-to-noise-ratio and/or large number of snapshots, the maximum-likelihood estimator of $\boldsymbol{\eta}$ is unbiased, Gaussian distributed, and its covariance matrix is equals to the deterministic Cramer-Rao bound.

In contrast, in the presence of MP and NLOS signals as in (4.4), the GNSS problem falls into the situation where the p.d.f. $p(\mathbf{s}; \boldsymbol{\theta}_d)$, where $\boldsymbol{\theta}_d = (\boldsymbol{\eta}^T, \boldsymbol{\alpha}^T)^T$, parametrized by unknown deterministic parameters $(\boldsymbol{\theta}_d)$ results from the marginalization of a joint p.d.f. depending on random variables as well (the delays, Doppler frequency shifts and amplitudes of MPs).

Indeed, in that case, this p.d.f. can be expressed as :

$$p\left(\mathbf{s};\boldsymbol{\theta}_d\right) = \int p\left(\mathbf{s}|\boldsymbol{\theta}_r;\boldsymbol{\theta}_d\right) p\left(\boldsymbol{\theta}_r;\boldsymbol{\theta}_d\right) d\boldsymbol{\theta}_r; \qquad \boldsymbol{\theta}_d = (\boldsymbol{\eta}^T, \boldsymbol{\alpha}^T)^T, \quad \boldsymbol{\theta}_r = (\boldsymbol{\eta}_r^T, \boldsymbol{\alpha}_r^T)^T \tag{4.5a}$$

$$p\left(\mathbf{s}|\boldsymbol{\theta}_r;\boldsymbol{\theta}_d\right) = p\left(\mathbf{s}|\boldsymbol{\eta}_r, \boldsymbol{\alpha}_r; \boldsymbol{\eta}, \boldsymbol{\alpha}\right) = \mathcal{CN}\left(\mathbf{A}(\boldsymbol{\eta})\boldsymbol{\alpha} + \mathbf{m}(\boldsymbol{\eta}_r, \boldsymbol{\alpha}_r), \sigma^2\mathbf{I}\right) \tag{4.5b}$$

Then, the resulting p.d.f $p\left(\mathbf{s};\boldsymbol{\theta}_d\right)$ is, in general, no longer Gaussian, which leads to a maximum-likelihood estimator of $\boldsymbol{\eta}$ which is no longer asymptotically Gaussian distributed, possibly biased and generally non efficient (its covariance matrix become greater than the Cramer-Rao bound). As an illustration, dynamic positioning experiments have been carried out in different types of environment in Toulouse using a low-cost GNSS receiver. The tested trajectory can be classified in three main kinds of environments : open-sky areas, suburban areas and urban areas. An overview of the considered environments is provided in Fig. 4.1.

FIGURE 4.1 – Classification of the tested trajectory in Toulouse by environmental category : Green : Open-sky, Yellow : Suburban, Red : Urban

These extensive recorded measurements are used to model GNSS pseudorange errors caused by multipath (MP) reflections by type of environment. True MP errors are predicted using the algorithm proposed in [3]. This algorithm is explained in section 3.1.3.1. Fig. 4.2 shows GNSS MP errors on PR measurements [1] in different environments and for a GNSS satellite with a medium to high elevation angles (more than 35°).

Fig. 4.2 illustrates the evolution of the PR Errors distribution in different environments, from Gaussian (open-sky areas) to non-Gaussian distribution (suburban and urban areas) as explained above. Hence, these environments are termed as non-Gaussian environment in this chapter.

1. The error of the maximum-likelihood estimate of the PR after ionospheric and tropospheric errors compensation using models.

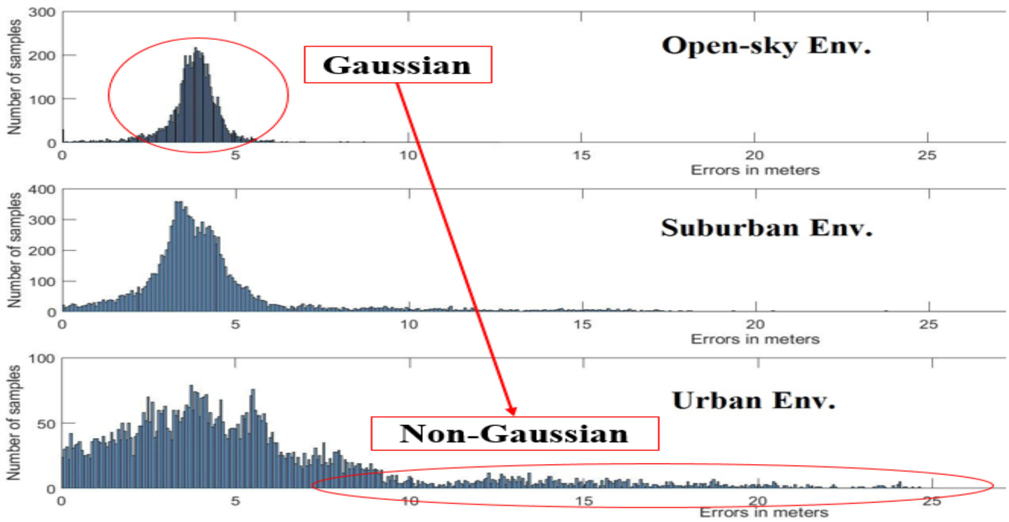

FIGURE 4.2 – PR Errors distribution in different environments. The used equipments, for data collection, are described in section 3.4.1.

In these suburban and urban environments, we want to assess GNSS asymptotic positioning accuracy, which raises the following questions :

1. *Can standard LBs and MLEs be computed in these environments ?*
2. *If standard LBs can not be computed, can we derive modified LBs that are computable ?*
3. *If standard MLEs can not be computed, can we derive a substitute, potentially suboptimal but computable ?*

Relation with a general framework : Actually, the problem under consideration belongs to the general deterministic estimation problem consisting of the following four components [2] :

1. a parameter space Θ_d,
2. an observation space $\mathcal{S}$,
3. a probabilistic mapping from parameter vector space Θ_d to observation space $\mathcal{S}$, that is the probability law that governs the effect of a parameter vector value $\boldsymbol{\theta}_d$ on the observation $\mathbf{s}$
4. an estimation rule, that is the mapping of the observation space $\mathcal{S}$ into vector parameter estimates $\widehat{\boldsymbol{\theta}_d}(\mathbf{s})$.

In the GNSS scenarios where MPs occur, as in many estimation problems [212, 213, 214, 215], the probabilistic mapping results from a two step probabilistic mechanism involving an additional random vector $\boldsymbol{\theta}_r$ (for instance, in the case of GNSS, $\boldsymbol{\theta}_r$ may represent the parameters of MPs (delays, Doppler frequency shifts,...)), $\boldsymbol{\theta}_r \in \Theta_r \subset \mathbb{R}^{P_r}$, that is i) $\boldsymbol{\theta}_d \rightarrow \boldsymbol{\theta}_r \sim$

2. In this paragraph, we adopt the notation proposed in several works involving both deterministic and random parameters [208, 209, 210, 211].

$p(\boldsymbol{\theta}_r;\boldsymbol{\theta}_d)$, ii) $(\boldsymbol{\theta}_d,\boldsymbol{\theta}_r) \to \mathbf{s} \sim p(\mathbf{s}|\boldsymbol{\theta}_r;\boldsymbol{\theta_d})$, and leading to a compound probability distribution :

$$p(\mathbf{s};\boldsymbol{\theta_d}) = \int_{\Theta_r} p(\mathbf{s},\boldsymbol{\theta}_r;\boldsymbol{\theta_d})\, d\boldsymbol{\theta}_r, \tag{4.6a}$$

$$p(\mathbf{s},\boldsymbol{\theta}_r;\boldsymbol{\theta_d}) = p(\mathbf{s}|\boldsymbol{\theta}_r;\boldsymbol{\theta}_d)\, p(\boldsymbol{\theta}_r;\boldsymbol{\theta_d}), \tag{4.6b}$$

where $p(\mathbf{s}|\boldsymbol{\theta}_r;\boldsymbol{\theta_d})$ is the conditional probability density function (p.d.f.) of $\mathbf{s}$ given $\boldsymbol{\theta}_r$, and $p(\boldsymbol{\theta}_r;\boldsymbol{\theta}_d)$ is the prior p.d.f. of $\boldsymbol{\theta}_r$, parameterized by $\boldsymbol{\theta}_d$.

For the sake of brevity, in the following $\boldsymbol{\theta}_d$ will be simply denoted $\boldsymbol{\theta}$, since this does not introduce any ambiguity with the random parameters notations which remains $\boldsymbol{\theta}_r$.

Throughout this chapter, we divide deterministic estimation problems into two subsets : the subset of "standard" deterministic estimation problems for which a closed-form expression of $p(\mathbf{s};\boldsymbol{\theta})$ is available, and the subset of "non-standard" deterministic estimation problems for which only an integral form of $p(\mathbf{s};\boldsymbol{\theta})$ (4.6a) (4.5a) is available.

In the next section, we provide an overview of a general method to derive the standard deterministic lower bounds on MSE when the marginal pdf $p(\mathbf{s};\boldsymbol{\theta})$ is available. In case of reception of non-Gaussian MP/NLOS signals, these bounds can not be computed. This motivates the derivation of modified lower bounds in section 4.3, to circumvent the limitation of non-computable standard LBs. In this chapter and for the sake of simplicity, unless otherwise stated, we will focus on the estimation of a single unknown real deterministic parameter θ (for instance the pseudo-range associated to a single non-moving satellite), although the results are easily extended to the estimation of multiple functions of multiple parameters.

4.2 An overview of lower bounds for standard estimation

4.2.1 Notations

In this chapter, we adopt the following notations :

• $\mathcal{S}_{\mathcal{X}}$, $\mathcal{S}_{\mathcal{X},\Theta_r}$, $\mathcal{S}_{\mathcal{X}|\boldsymbol{\theta}_r}$, $\mathcal{S}_{\Theta_r}$ and $\mathcal{S}_{\Theta_r|\mathbf{s}}$ denote, respectively, the support of $p(\mathbf{s};\theta)$, $p(\mathbf{s},\theta_r;\theta)$, $p(\mathbf{s}|\boldsymbol{\theta}_r;\theta)$, $p(\boldsymbol{\theta}_r;\theta)$ and $p(\boldsymbol{\theta}_r|\mathbf{s};\theta)$, i.e., $\mathcal{S}_{\mathcal{S}} = \left\{\mathbf{s} \in \mathbb{C}^M \mid p(\mathbf{s};\theta) > 0\right\}$, $\mathcal{S}_{\mathcal{S},\Theta_r} = \left\{(\mathbf{s},\theta_r) \in \mathbb{C}^M \times \mathbb{R}^{P_r} \mid p(\mathbf{s},\boldsymbol{\theta}_r;\theta) > 0\right\}$, $\mathcal{S}_{\mathcal{S}|\boldsymbol{\theta}_r} = \left\{\mathbf{s} \in \mathbb{C}^M \mid p(\mathbf{s}|\boldsymbol{\theta}_r;\theta) > 0\right\}$, $\mathcal{S}_{\Theta_r} = \left\{\boldsymbol{\theta}_r \in \mathbb{R}^{P_r} \mid p(\boldsymbol{\theta}_r;\theta) > 0\right\}$, and $\mathcal{S}_{\Theta_r|\mathbf{s}} = \left\{\boldsymbol{\theta}_r \in \mathbb{R}^{P_r} \mid p(\boldsymbol{\theta}_r|\mathbf{s};\theta) > 0\right\}$ [3].

• $E_{\mathbf{s};\theta}[\mathbf{g}(\mathbf{s})]$, $E_{\boldsymbol{\theta}_r;\theta}[\mathbf{g}(\boldsymbol{\theta}_r)]$ and $E_{\mathbf{s},\boldsymbol{\theta}_r;\theta}[\mathbf{g}(\mathbf{s},\boldsymbol{\theta}_r)]$ denote, respectively, the statistical expectation of the vector of functions $\mathbf{g}(\;)$ with respect to $\mathbf{s}$, to $\boldsymbol{\theta}_r$, to $\mathbf{s}$ and $\boldsymbol{\theta}_r$, parameterized by θ, and satisfy :

$$E_{\mathbf{s},\boldsymbol{\theta}_r;\theta}[\mathbf{g}(\mathbf{s},\boldsymbol{\theta}_r)] = E_{\mathbf{s};\theta}\left[E_{\boldsymbol{\theta}_r|\mathbf{s};\theta}[\mathbf{g}(\mathbf{s},\boldsymbol{\theta}_r)]\right] = E_{\boldsymbol{\theta}_r;\theta}\left[E_{\mathbf{s}|\boldsymbol{\theta}_r;\theta}[\mathbf{g}(\mathbf{s},\boldsymbol{\theta}_r)]\right].$$

3. The Barankin approach [216] (see Section 4.2) and its extensions to non-standard estimation (see Sections 4.3 and 4.4) require that all the supports be independent of θ.

• $\mathcal{L}_2(\mathcal{S}_\mathcal{S})$, $\mathcal{L}_2(\mathcal{S}_{\mathcal{S},\Theta_r})$ and $\mathcal{L}_2(\mathcal{S}_{\mathcal{S}|\boldsymbol{\theta}_r})$ denote, respectively, the real inner product space of square-integrable real-valued functions w.r.t. $p(\mathbf{s};\theta)$, $p(\mathbf{s},\boldsymbol{\theta}_r;\theta)$ and $p(\mathbf{s}|\boldsymbol{\theta}_r;\theta)$,
• $1_A(\boldsymbol{\theta}_r)$ denote the indicator function of subset A of $\mathbb{R}^{P_r}$.

4.2.2 On Lower Bounds and Norm Minimization

In the search for a LB on the MSE of unbiased estimators, two fundamental properties of the problem at hand, introduced by Barankin [216], must be noticed. The first property is that the MSE of a particular estimator $\widehat{\theta^0} \in \mathcal{L}_2(\mathcal{S}_\mathcal{S})$ of θ^0, i.e., $\widehat{\theta^0} \triangleq \widehat{\theta^0}(\mathbf{s})$, where θ^0 is a selected value of the parameter θ, is the square of a norm $\| \ \|_\theta^2$ associated the scalar product $\langle \ | \ \rangle_\theta$:

$$MSE_{\theta^0}\left[\widehat{\theta^0}\right] = \left\|\widehat{\theta^0}(\mathbf{s}) - \theta^0\right\|_{\theta^0}^2, \tag{4.7a}$$

$$\langle g(\mathbf{s}) \mid h(\mathbf{s})\rangle_\theta = E_{\mathbf{s};\theta}\left[g(\mathbf{s})\, h(\mathbf{s})\right]. \tag{4.7b}$$

This property allows the use of two equivalent fundamental results : the generalization of the Cauchy-Schwartz inequality to Gram matrices (generally referred to as the "covariance inequality" [217, 218]) and the minimization of a norm under linear constraints [219, 220, 221, 222]. Nevertheless, we shall prefer the "norm minimization" form as its use :
• provides a straightforward understanding of the hypotheses associated with the different LBs on the MSE expressed as a set of linear constraints,
• allows to resort to the same rationale for the derivation of LBs whatever the observation space considered,
• allows to easily reveal LBs inequalities and tightness conditions without the complex derivations (based on the use of the covariance inequality) introduced by previous works [223, 210, 224].
The second property is that an unbiased estimator $\widehat{\theta^0} \in \mathcal{L}_2(\mathcal{S}_\mathcal{S})$ of θ^0 should be uniformly unbiased :

$$\forall \theta \in \Theta_d : E_{\mathbf{s};\theta}\left[\widehat{\theta^0}(\mathbf{s})\right] = \int_{\mathcal{S}_\mathcal{S}} \widehat{\theta^0}(\mathbf{s})\, p(\mathbf{s};\theta)\, d\mathbf{s} = \theta. \tag{4.8a}$$

If $\mathcal{S}_\mathcal{S}$, i.e. the support of $p(\mathbf{s};\theta)$, does not depend on θ, then (4.8a) can be recasted as :

$$\forall \theta \in \Theta_d : E_{\mathbf{s};\theta^0}\left[\left(\widehat{\theta^0}(\mathbf{s}) - \theta^0\right)\upsilon_{\theta^0}(\mathbf{s};\theta)\right] = \theta - \theta^0, \tag{4.8b}$$

where $\upsilon_{\theta^0}(\mathbf{s};\theta) = p(\mathbf{s};\theta)/p(\mathbf{s};\theta^0)$ denotes the Likelihood Ratio (LR). As a consequence, the locally-best (at θ^0) unbiased estimator in $\mathcal{L}_2(\mathcal{S}_\mathcal{S})$ is the solution of a norm minimization under linear constraints :

$$\min_{\widehat{\theta^0} \in \mathcal{L}_2(\mathcal{S}_\mathcal{S})} \left\{\left\|\widehat{\theta^0}(\mathbf{s}) - \theta^0\right\|_{\theta^0}^2\right\} \text{ under } \left\langle \widehat{\theta^0}(\mathbf{s}) - \theta^0 \mid \upsilon_{\theta^0}(\mathbf{s};\theta)\right\rangle_{\theta^0} = \theta - \theta^0, \forall \theta \in \Theta_d. \tag{4.9}$$

Unfortunately, as recalled hereinafter, if Θ_d contains a non empty interval of $\mathbb{R}$, then the norm minimization problem (4.9) leads to an integral equation (4.13a) with no analytical solution in general. Therefore, since the seminal work of Barankin [216], many studies quoted in [218, 220, 225, 226] have been dedicated to the derivation of "computable" LBs approximating the MSE of the locally-best unbiased estimator, which defines the Barankin bound (BB). All these approximations derive from sets of discrete or integral linear transform of the "Barankin" constraint (4.8b) and can be easily obtained (see next Section) using the following well known norm minimization lemma [227]. Let $\mathbb{U}$ be an Euclidean vector space on the field of real numbers $\mathbb{R}$ which has a scalar product $\langle \mid \rangle$. Let $(\mathbf{c}_1, \ldots, \mathbf{c}_K)$ be a family of K linearly independent vectors of $\mathbb{U}$ and $\mathbf{v} \in \mathbb{R}^K$. The problem of the minimization of $\|\mathbf{u}\|^2$ under the K linear constraints $\langle \mathbf{u} \mid \mathbf{c}_k \rangle = v_k$, $k \in [1, K]$ then has the solution :

$$\min \left\{ \|\mathbf{u}\|^2 \right\} = \|\mathbf{u}_{opt}\|^2 = \mathbf{v}^T \mathbf{G}^{-1} \mathbf{v}, \tag{4.10}$$
$$\mathbf{u}_{opt} = \sum_{k=1}^{K} \alpha_k \mathbf{c}_k, \ \boldsymbol{\alpha} = \mathbf{G}^{-1}\mathbf{v}, \ \mathbf{G}_{k',k} = \langle \mathbf{c}_k \mid \mathbf{c}_{k'} \rangle .$$

4.2.3 Lower Bounds via linear transformations of the McAulay-Seidman bound

The McAulay-Seidman bound (MSB) is the BB approximation obtained from a discretization of the Barankin unbiasedness constraint (4.8b). Let $\boldsymbol{\theta}^N = \left(\theta^1, \ldots, \theta^N\right)^T \in \Theta_d^N$ be a vector of N selected values of the parameter θ (aka test points), $\boldsymbol{\upsilon}_{\theta^0}\left(\mathbf{s}; \boldsymbol{\theta}^N\right) = \left(\upsilon_{\theta^0}\left(\mathbf{s}; \theta^1\right), \ldots, \upsilon_{\theta^0}\left(\mathbf{s}; \theta^N\right)\right)^T$ be the vector of LRs associated to $\boldsymbol{\theta}^N$, $\xi(\theta) = \theta - \theta^0$ and $\boldsymbol{\xi}\left(\boldsymbol{\theta}^N\right) = \left(\xi\left(\theta^1\right), \ldots, \xi\left(\theta^N\right)\right)^T$. Then, any unbiased estimator $\widehat{\theta^0} \in \mathcal{L}_2\left(\mathcal{S}_{\mathcal{S}}\right)$ verifying (4.8b) must comply with the following subset of N linear constraints :

$$E_{\mathbf{s};\theta^0}\left[\left(\widehat{\theta^0}\left(\mathbf{s}\right) - \theta^0\right) \boldsymbol{\upsilon}_{\theta^0}\left(\mathbf{s}; \boldsymbol{\theta}^N\right)\right] = \boldsymbol{\xi}\left(\boldsymbol{\theta}^N\right), \tag{4.11a}$$

yielding, via the norm minimization lemma (4.10), the MSB [228] :

$$MSE_{\theta^0}\left[\widehat{\theta^0}\right] \geq \boldsymbol{\xi}\left(\boldsymbol{\theta}^N\right)^T \mathbf{R}_{\boldsymbol{\upsilon}_{\theta^0}}^{-1} \boldsymbol{\xi}\left(\boldsymbol{\theta}^N\right), \quad \left(\mathbf{R}_{\boldsymbol{\upsilon}_{\theta^0}}\right)_{n,m} = E_{\mathbf{s};\theta^0}\left[\upsilon_{\theta^0}\left(\mathbf{s}; \theta^m\right) \upsilon_{\theta^0}\left(\mathbf{s}; \theta^n\right)\right], \tag{4.11b}$$

which is a generalization of the Hammersley-Chapman-Robbins bound (HaCRB) previously introduced in [229] and [230] for 2 test points ($N = 2$). Obviously, any given set of K ($K \leq N$) linear transformations of (4.11a) :

$$E_{\mathbf{s};\theta^0}\left[\left(\widehat{\theta^0}\left(\mathbf{s}\right) - \theta^0\right) \mathbf{H}_K^T \boldsymbol{\upsilon}_{\theta^0}\left(\mathbf{s}; \boldsymbol{\theta}^N\right)\right] = \mathbf{H}_K^T \boldsymbol{\xi}\left(\boldsymbol{\theta}^N\right), \ \mathbf{H}_K = \left[\mathbf{h}_1, \ldots, \mathbf{h}_K\right], \ \mathbf{h}_k \in \mathbb{R}^N, \ 1 \leq k \leq K, \tag{4.12a}$$

where $\mathbf{H}_K$ has a full rank, provides, via the norm minimization lemma (4.10), another LB on the MSE :

$$MSE_{\theta^0}\left[\widehat{\theta^0}\right] \geq \boldsymbol{\xi}\left(\boldsymbol{\theta}^N\right)^T \mathbf{R}_{\mathbf{H}_K}^{\dagger} \boldsymbol{\xi}\left(\boldsymbol{\theta}^N\right), \quad \mathbf{R}_{\mathbf{H}_K}^{\dagger} = \mathbf{H}_K \left(\mathbf{H}_K^T \mathbf{R}_{\boldsymbol{\upsilon}_{\theta^0}} \mathbf{H}_K\right)^{-1} \mathbf{H}_K^T. \tag{4.12b}$$

It is worth noting that, for a given vector of test points $\boldsymbol{\theta}^N$, the LB (4.12b) reaches its maximum if, and only if, the matrix $\mathbf{H}_K$ is invertible ($K = N$) [228][231, Lemma 3], which represents a bijective transformation of the set of constraints associated with the MSB (4.11a).

Thus :

$$MSE_{\theta^0}\left[\widehat{\theta^0}\right] \geq \boldsymbol{\xi}\left(\boldsymbol{\theta}^N\right)^T \mathbf{R}_{\upsilon_{\theta^0}}^{-1}\boldsymbol{\xi}\left(\boldsymbol{\theta}^N\right) \geq \boldsymbol{\xi}\left(\boldsymbol{\theta}^N\right)^T \mathbf{R}_{\mathbf{H}_K}^{\dagger}\boldsymbol{\xi}\left(\boldsymbol{\theta}^N\right).$$

The BB [216, Theorem 4] is obtained by taking the supremum of (4.12b) over all the existing degrees of freedom $\left(N, \boldsymbol{\theta}^N, K, \mathbf{H}_K\right)$. All known LBs on the MSE deriving from the BB can be obtained with appropriate instantiations of (4.12b), that is with appropriate linear transformations of the MSB [4] (4.11b). For example, under mild regularity conditions on $p\left(\mathbf{s};\theta\right)$, the CRB is the limiting form of the HaCRB, that is the MSB where $N=2$, $\boldsymbol{\theta}^2 = \left(\theta^0, \theta^0 + d\theta\right)^T$ and $d\theta \to 0$ [216, 229, 230, 228, 231]. More generally, appropriate linear transformations of the MSB (4.12a-4.12b) for finite values of N and K lead to the Fraser-Gutman bound (FGB) [232], the Bhattacharyya bound (BaB) [233], the McAulay-Hofstetter bound (MHB), the Glave bound (GlB) [219], and the Abel bound (AbB) [218]. Furthermore, the class of LBs introduced lately in [225] can also be obtained as linear transformations of the MSB (4.12a-4.12b) in the limiting case where $N, K \to \infty$. It suffices to define each $\mathbf{h}_k$ as a vector of samples of a parametric function $h\left(\tau,\theta\right)$, $\tau \in \Lambda \subset \mathbb{R}$, integrable over Θ_d, $\forall \tau \in \Lambda$, i.e., $\mathbf{h}_k^T = \left(h\left(\tau_k,\theta^1\right), \ldots, h\left(\tau_k,\theta^N\right)\right)$, $1 \leq k \leq K$. In such a setting, one obtains the integral form of (4.12b) (see [221, Section 2] for details) released in [225, (34-36)] :

$$MSE_{\theta^0}\left[\widehat{\theta^0}\right] \geq TTB_{\theta^0}^h = \int\limits_{\Lambda} \Gamma_{\theta^0}^h\left(\tau\right)\beta_{\theta^0}^h\left(\tau\right)d\tau, \tag{4.13a}$$

where $\Gamma_{\theta^0}^h\left(\tau\right) = \int\limits_{\Theta_d} h\left(\tau,\theta\right)\left(\theta-\theta^0\right)d\theta$, and $\beta_{\theta^0}^h\left(\tau\right)$ is the solution of the following integral equation :

$$\Gamma_{\theta^0}^h\left(\tau'\right) = \int\limits_{\Lambda} K_{\theta^0}^h\left(\tau',\tau\right)\beta_{\theta^0}^h\left(\tau\right)d\tau, \tag{4.13b}$$

$$K_{\theta^0}^h\left(\tau,\tau'\right) = \int\limits_{\Theta_d^2} h\left(\tau,\theta\right)R_{\upsilon_{\theta^0}}\left(\theta,\theta'\right)h\left(\tau',\theta'\right)d\theta d\theta', \tag{4.13c}$$

$$R_{\upsilon_{\theta^0}}\left(\theta,\theta'\right) = E_{\mathbf{s};\theta^0}\left[\frac{p\left(\mathbf{s};\theta\right)}{p\left(\mathbf{s};\theta^0\right)}\frac{p\left(\mathbf{s};\theta'\right)}{p\left(\mathbf{s};\theta^0\right)}\right]. \tag{4.13d}$$

Note that if $h\left(\tau,\theta\right) = \delta\left(\tau-\theta\right)$ (limiting case of $\mathbf{H}_N = \mathbf{I}_N$ where $N=K\to\infty$) then $K_{\theta^0}^h\left(\tau,\tau'\right) = R_{\upsilon_{\theta^0}}\left(\tau,\tau'\right)$ and (4.13a) becomes the expression of the BB [220, (10)][222, (6-7)]. As mentioned above, in most practical cases, it is impossible to find an analytical solution of (4.13b) to obtain an explicit form of the $TTB_{\theta^0}^h$ (4.13a), which somewhat limits its interest. Nevertheless, as highlighted in [225], this formalism allows to use discrete or integral linear transforms of the LR, possibly non-invertible, possibly optimized for a set of p.d.f. (such as the Fourier transform) in order to get a tight approximation of the BB.

4. Since there is a one-to-one correspondence between a LB and a set of linear constraints, in the following, a linear transformation of a given LB actually refers to the LB obtained from a linear transformation of the corresponding set of linear constraints.

4.2.4 On the uncomputability of standard LBs in GNSS harsh environments

Unfortunately, as already mentioned above, in the GNSS context in presence of non-Gaussian MPs, the marginal p.d.f. of the GNSS observations has not an analytical form because of the presence of non-Gaussian MP fluctuation p.d.f.. As a consequence, none of the standard existing estimation performance characterization methods such as the previously presented LBs can be used in this case. This situation is known as deterministic parameter estimation, where the p.d.f. parametrized by unknown deterministic parameters results from the marginalization of a joint p.d.f. depending on random variables as well. In the general case, this marginalization is mathematically intractable, which prevents from using the known standard deterministic LBs on MSE. Actually, this case can be tackled by embedding the initial observation space in a hybrid one where any standard LB can be transformed into a modified one fitted to non-standard deterministic estimation, at a possible expense of tightness however. This derivation will be the objective of the next section.

4.3 Modified Lower Bounds for Non-Standard Estimation

Interestingly enough, in many estimation problems [212]–[215] $p(\mathbf{s}, \boldsymbol{\theta}_r; \theta)$ is known in the form of a compound probability distribution, i.e., $p(\mathbf{s}, \boldsymbol{\theta}_r; \theta) = p(\mathbf{s}|\boldsymbol{\theta}_r; \theta)\, p(\boldsymbol{\theta}_r; \theta)$, where both closed-forms of $p(\mathbf{s}|\boldsymbol{\theta}_r; \theta)$ and $p(\boldsymbol{\theta}_r; \theta)$ are known. Therefore, it just makes sense to look for LBs based on $p(\mathbf{s}, \boldsymbol{\theta}_r; \theta)$ instead of $p(\mathbf{s}; \theta)$. Moreover, in the previous Section 4.2.3, we have pointed out that in standard estimation, the computability of the MSB (4.11b) is the cornerstone to generate the class of LBs on the MSE of uniformly unbiased estimate deriving from Barankin's work [216]. Therefore it seems sensible to check whether or not the MSB is computable where only $p(\mathbf{s}, \boldsymbol{\theta}_r; \theta)$ is known.

4.3.1 A new look at modified lower bounds

If $\mathcal{S}_{\mathcal{S},\Theta_r}$, i.e. the support of $p(\mathbf{s}, \boldsymbol{\theta}_r; \theta)$, is independent of θ, then :

$$E_{\mathbf{s},\boldsymbol{\theta}_r;\theta}\left[g(\mathbf{s}, \boldsymbol{\theta}_r)\right] = E_{\mathbf{s},\boldsymbol{\theta}_r;\theta^0}\left[g(\mathbf{s}, \boldsymbol{\theta}_r)\, \upsilon_{\theta^0}(\mathbf{s}, \boldsymbol{\theta}_r; \theta)\right], \quad \upsilon_{\theta^0}(\mathbf{s}, \boldsymbol{\theta}_r; \theta) = \frac{p(\mathbf{s}, \boldsymbol{\theta}_r; \theta)}{p(\mathbf{s}, \boldsymbol{\theta}_r; \theta^0)}. \tag{4.14}$$

Therefore, for any unbiased estimator $\widehat{\theta^0} \in \mathcal{L}_2(\mathcal{S}_\mathcal{S})$, (4.11a) can be reformulated as, $\forall n \in [1, N]$:

$$\begin{aligned}
\theta^n - \theta^0 &= E_{\mathbf{s};\theta^0}\left[\left(\widehat{\theta^0}(\mathbf{s}) - \theta^0\right)\upsilon_{\theta^0}(\mathbf{s};\theta^n)\right] \\
&= E_{\mathbf{s};\theta^n}\left[\widehat{\theta^0}(\mathbf{s}) - \theta^0\right] \\
&= E_{\mathbf{s},\boldsymbol{\theta}_r;\theta^n}\left[\widehat{\theta^0}(\mathbf{s}) - \theta^0\right] \\
&= E_{\mathbf{s},\boldsymbol{\theta}_r;\theta^0}\left[\left(\widehat{\theta^0}(\mathbf{s}) - \theta^0\right)\upsilon_{\theta^0}(\mathbf{s},\boldsymbol{\theta}_r;\theta^n)\right],
\end{aligned}$$

that is in vector form :

$$\begin{aligned}
\boldsymbol{\xi}\left(\boldsymbol{\theta}^N\right) &= E_{\mathbf{s};\theta^0}\left[\left(\widehat{\theta^0}(\mathbf{s}) - \theta^0\right)\boldsymbol{\upsilon}_{\theta^0}\left(\mathbf{s};\boldsymbol{\theta}^N\right)\right] \\
&= E_{\mathbf{s},\boldsymbol{\theta}_r;\theta^0}\left[\left(\widehat{\theta^0}(\mathbf{s}) - \theta^0\right)\boldsymbol{\upsilon}_{\theta^0}\left(\mathbf{s},\boldsymbol{\theta}_r;\boldsymbol{\theta}^N\right)\right],
\end{aligned} \tag{4.15}$$

where $\left(\upsilon_{\theta^0}(\mathbf{s},\boldsymbol{\theta}_r;\theta^1),\ldots,\upsilon_{\theta^0}\left(\mathbf{s},\boldsymbol{\theta}_r;\theta^N\right)\right) = \boldsymbol{\upsilon}_{\theta^0}^T\left(\mathbf{s},\boldsymbol{\theta}_r;\boldsymbol{\theta}^N\right)$. Additionally, since $\widehat{\theta^0} \in \mathcal{L}_2(\mathcal{S}_\mathcal{S})$, then :

$$E_{\mathbf{s};\theta^0}\left[\left(\widehat{\theta^0}(\mathbf{s}) - \theta^0\right)^2\right] = E_{\mathbf{s},\boldsymbol{\theta}_r;\theta^0}\left[\left(\widehat{\theta^0}(\mathbf{s}) - \theta^0\right)^2\right]. \tag{4.16}$$

Therefore :

$$\min_{\widehat{\theta^0}\in\mathcal{L}_2(\mathcal{S}_\mathcal{S})}\left\{E_{\mathbf{s};\theta^0}\left[\left(\widehat{\theta^0}(\mathbf{s}) - \theta^0\right)^2\right]\right\} \text{ under } \boldsymbol{\xi}\left(\boldsymbol{\theta}^N\right) = E_{\mathbf{s};\theta^0}\left[\left(\widehat{\theta^0}(\mathbf{s}) - \theta^0\right)\boldsymbol{\upsilon}_{\theta^0}\left(\mathbf{s};\boldsymbol{\theta}^N\right)\right], \tag{4.17a}$$

is equivalent to :

$$\min_{\widehat{\theta^0}\in\mathcal{L}_2(\mathcal{S}_\mathcal{S})}\left\{E_{\mathbf{s},\boldsymbol{\theta}_r;\theta^0}\left[\left(\widehat{\theta^0}(\mathbf{s}) - \theta^0\right)^2\right]\right\} \text{ under } \boldsymbol{\xi}\left(\boldsymbol{\theta}^N\right) = E_{\mathbf{s},\boldsymbol{\theta}_r;\theta^0}\left[\left(\widehat{\theta^0}(\mathbf{s}) - \theta^0\right)\boldsymbol{\upsilon}_{\theta^0}\left(\mathbf{s},\boldsymbol{\theta}_r;\boldsymbol{\theta}^N\right)\right]. \tag{4.17b}$$

Note that the equivalence between (4.17a) and (4.17b) holds only if $\widehat{\theta^0} \in \mathcal{L}_2(\mathcal{S}_\mathcal{S})$. Unfortunately, since $\mathcal{L}_2(\mathcal{S}_\mathcal{S})$ is a subspace of $\mathcal{L}_2(\mathcal{S}_{\mathcal{S},\Theta_r})$, the solution of (4.17b) cannot be given by the minimum norm lemma (4.10) in general, since the lemma provides a solution in $\mathcal{L}_2(\mathcal{S}_{\mathcal{S},\Theta_r})$, that is the solution of :

$$\min_{\widehat{\theta^0}\in\mathcal{L}_2(\mathcal{S}_{\mathcal{S},\Theta_r})}\left\{E_{\mathbf{s},\boldsymbol{\theta}_r;\theta^0}\left[\left(\widehat{\theta^0}(\mathbf{s},\boldsymbol{\theta}_r) - \theta^0\right)^2\right]\right\} \text{ under } \boldsymbol{\xi}\left(\boldsymbol{\theta}^N\right) = E_{\mathbf{s},\boldsymbol{\theta}_r;\theta^0}\left[\left(\widehat{\theta^0}(\mathbf{s},\boldsymbol{\theta}_r) - \theta^0\right)\boldsymbol{\upsilon}_{\theta^0}\left(\mathbf{s},\boldsymbol{\theta}_r;\boldsymbol{\theta}^N\right)\right], \tag{4.17c}$$

yielding the following modified MSB :

$$MSE_{\theta^0}\left[\widehat{\theta^0}\right] \geq \boldsymbol{\xi}\left(\boldsymbol{\theta}^N\right)^T \mathbf{R}_{\boldsymbol{\upsilon}_{\theta^0}}^{-1}\boldsymbol{\xi}\left(\boldsymbol{\theta}^N\right), \quad \left(\mathbf{R}_{\boldsymbol{\upsilon}_{\theta^0}}\right)_{n,m} = E_{\mathbf{s},\boldsymbol{\theta}_r;\theta^0}\left[\upsilon_{\theta^0}(\mathbf{s},\boldsymbol{\theta}_r;\theta^m)\,\upsilon_{\theta^0}(\mathbf{s},\boldsymbol{\theta}_r;\theta^n)\right], \tag{4.18}$$

in the sense that it is a LB for unbiased estimates belonging to $\mathcal{L}_2(\mathcal{S}_{\mathcal{S},\Theta_r})$. One noteworthy point is that the modified MSB (4.18) is obtained from the MSB (4.11b) by substituting $E_{\mathbf{s},\boldsymbol{\theta}_r;\theta^0}[\,]$ for $E_{\mathbf{s};\theta^0}[\,]$ and $\boldsymbol{\upsilon}_{\theta^0}\left(\mathbf{s},\boldsymbol{\theta}_r;\boldsymbol{\theta}^N\right)$ for $\boldsymbol{\upsilon}_{\theta^0}\left(\mathbf{s};\boldsymbol{\theta}^N\right)$. More generally, since (4.17a) and (4.17c) share a similar formulation, reasoning by analogy, one can state that any approximation of the BB deriving from linear transformations of the set of constraints associated with the MSB (4.12a-4.12b), has an analog formulation in non-standard estimation obtained by substituting $E_{\mathbf{s},\boldsymbol{\theta}_r;\theta^0}[\ ]$ for $E_{\mathbf{s};\theta^0}[\ ]$ and $\boldsymbol{\upsilon}_{\theta^0}\left(\mathbf{s},\boldsymbol{\theta}_r;\boldsymbol{\theta}^N\right)$ for $\boldsymbol{\upsilon}_{\theta^0}\left(\mathbf{s};\boldsymbol{\theta}^N\right)$. Actually, this is obtained by substituting $p(\mathbf{s},\boldsymbol{\theta}_r;\theta)$ for $p(\mathbf{s};\theta)$ in any approximation of the BB. *This result holds whatever the prior p.d.f. depends or does not depend on the deterministic parameters.* In the end, we have simply embedded the search of the locally-best unbiased estimator initially performed in the vector space $\mathcal{L}_2(\mathcal{S}_{\mathcal{S}})$ (4.9) into a larger vector space containing $\mathcal{L}_2(\mathcal{S}_{\mathcal{S}})$, namely $\mathcal{L}_2(\mathcal{S}_{\mathcal{S},\Theta_r})$, where the search of the locally-best unbiased estimator is formulated as :

$$\min_{\widehat{\theta^0}\in\mathcal{L}_2\left(\mathcal{S}_{\mathcal{S},\Theta_r}\right)}\left\{E_{\mathbf{s},\boldsymbol{\theta}_r;\theta^0}\left[\left(\widehat{\theta^0}(\mathbf{s},\boldsymbol{\theta}_r)-\theta^0\right)^2\right]\right\} \text{ under } E_{\mathbf{s},\boldsymbol{\theta}_r;\theta}\left[\widehat{\theta^0}(\mathbf{s},\boldsymbol{\theta}_r)-\theta^0\right]=\theta-\theta^0,\forall\theta\in\Theta_d. \tag{4.19}$$

Indeed, if $\widehat{\theta^0}\in\mathcal{L}_2(\mathcal{S}_{\mathcal{S}})\subset\mathcal{L}_2(\mathcal{S}_{\mathcal{S},\Theta_r})$, then (4.19) reduces to (4.9). From this perspective, it seems appropriate to refer to these LBs for unbiased estimates belonging to $\mathcal{L}_2(\mathcal{S}_{\mathcal{S},\Theta_r})$ as modified LBs (MLBs) as it has been proposed initially in [215] and [223] for the modified CRB. Since (4.17a) and (4.17b) are equivalent and $\mathcal{L}_2(\mathcal{S}_{\mathcal{S}})\subset\mathcal{L}_2(\mathcal{S}_{\mathcal{S},\Theta_r})$, it follows naturally that the modified form of a LB is looser (lower or equal) than the standard form of the LB. This highlights the trade-off associated with MLBs in non-standard estimation : computability at the possible expense of tightness. However, it is possible to increase the tightness of MLBs by adding constraints to restrict the class of viable estimators $\widehat{\theta^0}\in\mathcal{L}_2(\mathcal{S}_{\mathcal{S},\Theta_r})$ and therefore to increase the minimum norm obtained from (4.17c) as shown hereinafter in section 4.3.2.

Old and new modified lower bounds :

In the light of the above, the MCRB is obtained directly from the CRB :

$$\mathbf{CRB}_\theta=E_{\mathbf{s};\theta}\left[\frac{\partial\ln p(\mathbf{s};\theta)}{\partial\theta}\frac{\partial\ln p(\mathbf{s};\theta)}{\partial\theta^T}\right]^{-1}\rightarrow\mathbf{MCRB}_\theta=E_{\mathbf{s},\boldsymbol{\theta}_r;\theta}\left[\frac{\partial\ln p(\mathbf{s},\boldsymbol{\theta}_r;\theta)}{\partial\theta}\frac{\partial\ln p(\mathbf{s},\boldsymbol{\theta}_r;\theta)}{\partial\theta^T}\right]^{-1}, \tag{4.20}$$

and one can assert that $\mathbf{CRB}_\theta\geq\mathbf{MCRB}_\theta$, without having to invoke neither the Jensen's inequality [215] nor to prove specific matrix inequality [223, (4)]. *Furthermore, the MCRB expression (4.20) is still valid if the prior depends on θ, which extends the historical results provided in [215] and [223] under the restrictive assumption of a prior independent of θ.* In the same way, the MBaB of order K is obtained from the BaB [233][222, (19)] :

$$\left|\begin{array}{l}BaB_\theta=\mathbf{e}_1^TE_{\mathbf{s};\theta}\left[\varrho(\mathbf{s};\theta)\,\varrho(\mathbf{s};\theta)^T\right]^{-1}\mathbf{e}_1,\\ \varrho(\mathbf{s};\theta)^T=\frac{1}{p(\mathbf{s};\theta)}\left(\frac{\partial p(\mathbf{s};\theta)}{\partial\theta},\ldots,\frac{\partial^K p(\mathbf{s};\theta)}{\partial^K\theta}\right)\end{array}\right.\rightarrow\left|\begin{array}{l}MBaB_\theta=\mathbf{e}_1^TE_{\mathbf{s},\boldsymbol{\theta}_r;\theta}\left[\varrho(\mathbf{s},\boldsymbol{\theta}_r;\theta)\,\varrho(\mathbf{s},\boldsymbol{\theta}_r;\theta)^T\right]^{-1}\mathbf{e}_1,\\ \varrho(\mathbf{s},\boldsymbol{\theta}_r;\theta)^T=\frac{1}{p(\mathbf{s},\boldsymbol{\theta}_r;\theta)}\left(\frac{\partial p(\mathbf{s},\boldsymbol{\theta}_r;\theta)}{\partial\theta},\ldots,\frac{\partial^K p(\mathbf{s},\boldsymbol{\theta}_r;\theta)}{\partial^K\theta}\right),\end{array}\right.$$

where $\mathbf{e}_1^T=(1,0,\ldots,0)$. Therefore, with the proposed approach, we not only extend the result introduced in [234, (4)] under the restrictive assumption of a prior independent of θ, but we can also assert that $BaB_\theta\geq MBaB_\theta$, which has not been proven in [234].

As with the CRB and the BaB, the modified form of all remaining BB approximations released in the open literature, namely the FGB [232], the MHB [235], the GlB [219], the AbB [218], and the CRFB [225, (101-102)], can be easily obtained with the proposed framework. For instance, the modified form of the general class of LBs (4.13a-4.13d) proposed in [225, (34-

36)] is obtained simply by updating the definition of $R_{\upsilon_{\theta^0}}(\theta,\theta')$ (4.13d) as follows :

$$R_{\upsilon_{\theta^0}}(\theta,\theta') = E_{\mathbf{s},\boldsymbol{\theta}_r;\theta^0}\left[\frac{p(\mathbf{s},\boldsymbol{\theta}_r;\theta)}{p(\mathbf{s},\boldsymbol{\theta}_r;\theta^0)}\frac{p(\mathbf{s},\boldsymbol{\theta}_r;\theta')}{p(\mathbf{s},\boldsymbol{\theta}_r;\theta^0)}\right], \tag{4.21}$$

and one can also assert that $TTB^h_{\theta^0} \geq MTTB^h_{\theta^0}$.

4.3.2 A general class of tighter modified lower bounds and its relationship with hybrid lower bounds (HLBs)

As mentioned above, it is possible to increase the tightness of MLBs by adding constraints in order to restrict the class of viable estimators $\widehat{\theta^0} \in \mathcal{L}_2(\mathcal{S}_{\mathcal{S},\Theta_r})$ and therefore to increase the minimum norm obtained from (4.17c). However, such additional constraints must keep on defining a subset of $\mathcal{L}_2(\mathcal{S}_{\mathcal{S},\Theta_r})$ including the set of unbiased estimates belonging to $\mathcal{L}_2(\mathcal{S}_{\mathcal{S}})$, as shown in appendix D with two general subsets of additional constraints. The first subset is related to historical works on hybrid LBs [214, 210] but addressed in a different way. The second subset is a generalization of [208, (8)] reformulated according to the proposed framework. The derivation of tighter MLBs with these two subsets of added constraints is provided in appendix D. Since these two tighter MLBs derive from two different subset of constraints, a comparison between these two forms is not possible.

Lastly, even more tighter MLBs can be derived based on the combination of the two above subset of constraints as shown in (D.10) in appendix D. This proposed unified framework allows to draw new interesting results regarding LBs derivation. Firstly, it provides a common framework for the formulation of MLBs for all known LBs on the MSE, without any regularity condition on the (nuisance) random vector estimates, since $\boldsymbol{\theta}_r$ is neither required nor expected to be estimated. Secondly, since any modified LB obtained from (D.10) is lower than or equal to its standard form (4.17a), one can assert that the deterministic part of any HLB [5] is looser (or equal) than the corresponding standard LB, which is a new general result. Thirdly, the deterministic part of any HLB is a valid MLBs whatever the prior depends on or does not depend on the deterministic parameter θ, which is another new general result. Tighter MLBs are exemplified in the case of the CRB in subsection D.1.4 of appendix D.

4.3.3 On closeness, tightness, regularity conditions and implementation of modified lower bounds

4.3.3.1 On the closeness of MLBs to LBs

Actually, a "closeness condition" required to obtain a modified LB equal to the standard LB

5. The deterministic part of a HLB denotes the HLB's submatrix which is a LB on the MSE of the determinisitic parameter vector.

is quite simple to express : it is necessary, and sufficient, that the estimator solution of the norm minimization under linear constraints (4.17c)(D.4)(D.9)(D.10) belongs to $\mathcal{L}_2(\mathcal{S}_\mathcal{X})$, that is according to (4.10) :

$$\widehat{\theta^0}(\mathbf{s}, \boldsymbol{\theta}_r)_{opt} - \theta^0 = \sum_{k=1}^{K} \alpha_k \left(\mathbf{c}_{\theta^0}(\mathbf{s}, \boldsymbol{\theta}_r)\right)_k \in \mathcal{L}_2(\mathcal{S}_\mathcal{S}), \tag{4.22}$$

a closeness condition fulfilled by a class of joint p.d.f. $p(\mathbf{s}, \boldsymbol{\theta}_r; \theta)$ which depends on the vector of constraint functions chosen. For example, if we consider the $\overline{MCRB}_{\theta^0}$ (D.12) then the tightness condition is :

$$\widehat{\theta}(\mathbf{s}, \boldsymbol{\theta}_r)_{opt} - \theta = \frac{\partial \ln p(\mathbf{s}, \boldsymbol{\theta}_r; \theta)}{\partial\left(\theta, \boldsymbol{\theta}_r^T\right)} \boldsymbol{\alpha}(\theta) = \widehat{\theta}(\mathbf{s})_{opt} - \theta. \tag{4.23}$$

Since $\mathbf{e}_1^T \mathbf{F}(\theta)^{-1} = \overline{MCRB}_\theta \left(1, -\mathbf{F}_{\boldsymbol{\theta}_r}^{-1} \mathbf{f}_{\boldsymbol{\theta}_r, \theta}(\theta)\right)$, therefore (4.23) is equivalent to :

$$\frac{\partial \ln p(\mathbf{s}, \boldsymbol{\theta}_r; \theta)}{\partial \theta} - \mathbf{f}_{\theta, \boldsymbol{\theta}_r}(\theta) \mathbf{F}_{\boldsymbol{\theta}_r}^{-1}(\theta) \frac{\partial \ln p(\mathbf{s}, \boldsymbol{\theta}_r; \theta)}{\partial \boldsymbol{\theta}_r} = \frac{\widehat{\theta}(\mathbf{s})_{opt} - \theta}{\overline{MCRB}_\theta},$$

leading to the necessary, and sufficient, condition :

$$\frac{\partial \ln p(\mathbf{s}, \boldsymbol{\theta}_r; \theta)}{\partial \theta \partial \boldsymbol{\theta}_r^T} = \mathbf{f}_{\theta, \boldsymbol{\theta}_r}(\theta) \mathbf{F}_{\boldsymbol{\theta}_r}^{-1}(\theta) \frac{\partial \ln p(\mathbf{s}, \boldsymbol{\theta}_r; \theta)}{\partial \boldsymbol{\theta}_r \partial \boldsymbol{\theta}_r^T}, \tag{4.24}$$

which has been introduced in [224, (34)] at the expense of a quite complex proof.

4.3.3.2 On tightness, regularity conditions and implementation of MLBs

As mentioned above, the trade-off associated with MLBs is computability at the possible expense of tightness. Indeed, a key feature of the simplest form of the MLBs deriving from the MMSB (4.18), is to be essentially free of regularity conditions both on the joint p.d.f. $p(\mathbf{s}, \boldsymbol{\theta}_r; \theta)$ w.r.t the random parameters $\boldsymbol{\theta}_r$, and on the support $\mathcal{S}_{\Theta_r|\mathbf{s}}$. This feature still holds for the tighter MLBs obtained with Bayesian LB-generating functions (D.9)(D.11a-D.11b). In contrast, none of the existing HLBs, which are all obtained via linear transformations on the CLR function [211], can be used if $\mathcal{S}_{\Theta_r|\mathbf{s}}$ does not satisfy (D.5), that is, for instance, if $\mathcal{S}_{\Theta_r|\mathbf{s}}$ is a connected set of $\mathbb{R}^{P_r}$ and in most cases, if $\mathcal{S}_{\Theta_r|\mathbf{s}}$ is a disconnected subset of $\mathbb{R}^{P_r}$. Off course, any time an existing HLB can be derived, its deterministic part provides a tighter LB than the corresponding MLB deriving from (4.18), however at the expense of an increased computational cost (see (D.12)). Thus, the proposed unified framework is a useful tool to look for the best possible trade-off between tightness, regularity conditions and computational cost, in the choice of a MLB for a given non-standard estimation problem. In that perspective, non-standard estimation can take advantage of the works on computable approximations of the BB in standard estimation [218, 220, 225], which have shown that the CRB and the BB can be regarded as key representatives of two general classes of bounds, respectively the Small-

Error bounds and the Large-Error bounds. Indeed, it is now well known that the Small-Error bounds, such as the CRB, are optimistic bounds in a non-linear estimation problem where the outliers effect generally appears [236, 237, 238]. This outliers effect leads to a characteristic threshold behaviour of estimators MSE which exhibits a "performance breakdown" highlighted by Large-Error bounds [228]. Furthermore, it has been underlined that under the norm minimization approach, the Small Error bounds derive from linear constraints expressed at the true value θ^0 only, whereas the Large-Error bounds derive from linear constraints expressed at vectors of test points $\boldsymbol{\theta}^{N+1}$ including the true value [228, 219, 218, 220, 225]. The tightness of a given Large Error bound is at the expense of some computational cost ; indeed as its tightness depends on the used vector of test points [225, 239], it generally incorporates the search of an optimum over a set of vectors of test points. As a consequence, the final practical form proposed by each author is an attempt to optimize the trade-off between tightness and computational cost. For example, in [228] the main goal was to reduce the complexity of use of the BB by substituting the simplified form (4.11b) for the initial form (4.12b). In [235] and generalized in [219] and [218], the rationale is to combine a Small Error bound (CRB [235, 219] or BaB [218]) with a Large Error bound (MSB [228]) in order to obtain a bound which accounts for both local and large errors and is able to handle the threshold phenomena. Indeed the use of derivatives is also helpful to decrease the computational burden since it allows to resort to smaller sets of tests point vectors to achieve similar tightness [218, 225], however at the expense of the existence of the derivatives (although this condition is mild and generally satisfied). Last, the norm minimization approach naturally incorporates possible tightness comparison between two MLBs. Indeed, if the subset of linear constraints associated with a MLB is included into the subset of linear constraints associated with another MLB, then the latter one is tighter. To wrap up, when looking at a MLB, the following questions should be answered : i) is the strong regularity condition (D.5) satisfied ?, e.g., is $\mathcal{S}_{\Theta_r|\mathbf{s}} \triangleq \mathbb{R}^{P_r}$?, ii) is the joint p.d.f. $p\left(\mathbf{s}, \boldsymbol{\theta}_r; \boldsymbol{\theta}\right)$ differentiable w.r.t the random parameters ? iii) which regions of operation of estimators, among the asymptotic region, the threshold region and the a priori region [237], are of interest ?, iv) are analytic forms of $E_{\mathbf{s},\boldsymbol{\theta}_r;\theta^0}\left[\boldsymbol{\psi}\left(\mathbf{s}, \boldsymbol{\theta}_r; \theta^0\right) \boldsymbol{\upsilon}_{\theta^0}^T\left(\mathbf{s}, \boldsymbol{\theta}_r; \boldsymbol{\theta}^N\right)\right]$ and $E_{\mathbf{s},\boldsymbol{\theta}_r;\theta^0}\left[\boldsymbol{\psi}\left(\mathbf{s}, \boldsymbol{\theta}_r; \theta^0\right) \psi\left(\mathbf{s}, \boldsymbol{\theta}_r; \theta^0\right)^T\right]$ available ? For instance, if the asymptotic and threshold regions are of interest, and if the answers to i), ii), iv) are positive, then at the expense of non negligible computational burden, the tightest MLBs will be probably obtained by deriving from (D.10) a combination of the tight version of the modified GlB (or of the modified CRFB) with Bayesian LB-generating functions (D.6), since the MLB obtained will incorporate most of the meaningful constraints available. If the asymptotic and threshold regions are of interest, and if the answers to i), ii), iv) are negative, then at the expense of a non negligible computational burden, the tightest MLBs is the MMSB (4.18).

4.4 Proposed Non-Standard Maximum Likelihood Estimator for Deterministic Estimation

Let us recall that the widespread use of MLEs in deterministic estimation originates from the fact that, under reasonably general conditions on the observation model [204, 205], the MLEs are asymptotically uniformly unbiased, Gaussian distributed and efficient when the number of independent observations tends to infinity. Additionally, if the observation model is Gaussian complex circular, some additional asymptotic regions of operation yielding uniformly unbiased Gaussian and efficient MLEs have also been identified at finite number of independent observations [207, 240, 241, 242, 243]. If a closed-form of $p(\mathbf{s};\theta)$ does not exist or if a closed-form of $p(\mathbf{s};\theta)$ does exist but the resulting expression is intractable to derive the standard MLE of θ :

$$\widehat{\theta}_{ML}(\mathbf{s}) = \arg\max_{\theta\in\Theta_d}\{p(\mathbf{s};\theta)\}, \tag{4.25a}$$

a sensible solution in the search of a realizable estimator based on the ML principle is to look for :

$$\left(\underline{\widehat{\boldsymbol{\theta}_r}}(\mathbf{s}), \underline{\widehat{\theta}}(\mathbf{s})\right) = \arg\max_{\theta\in\Theta_d, \boldsymbol{\theta}_r\in\mathcal{S}_{\Theta_r|\mathbf{s}}}\{p(\mathbf{s}|\boldsymbol{\theta}_r;\theta)\}. \tag{4.25b}$$

In the following $\underline{\widehat{\theta}}(\mathbf{s})$ and $\underline{\widehat{\boldsymbol{\theta}_r}}(\mathbf{s})$ (4.25b) are referred to as "non-standard" MLEs (NSMLEs). The underlying idea is that, since in many estimation problems [212, 213, 214, 215] $p(\mathbf{s},\boldsymbol{\theta}_r;\theta)$ is a compound probability distribution, i.e., $p(\mathbf{s},\boldsymbol{\theta}_r;\theta) = p(\mathbf{s}|\boldsymbol{\theta}_r;\theta)\,p(\boldsymbol{\theta}_r;\theta)$, the closed-form of $p(\mathbf{s}|\boldsymbol{\theta}_r;\theta)$ is known and the NSMLEs (4.25b) take advantage not only of the aforementioned properties, and in particular of the asymptotic uniform unbiasedeness w.r.t. $p(\mathbf{s}|\boldsymbol{\theta}_r;\theta)$, but also of the extensive open literature on MLE closed-form expressions or approximations [212]. These key features clearly make the "non-standard" maximum likelihood estimation more attractive than the two known following alternative approaches. The first alternative approach consists in deriving the joint maximum a posteriori-maximum likelihood estimate (JMAPMLE) of the hybrid parameter vector $\left(\boldsymbol{\theta}_r^T, \theta\right)$:

$$\left(\widehat{\boldsymbol{\theta}}_{rJ}(\mathbf{s}), \widehat{\theta}_J(\mathbf{s})\right) = \arg\max_{\theta\in\Theta_d, \boldsymbol{\theta}_r\in\mathcal{S}_{\Theta_r|\mathbf{s}}}\{p(\mathbf{s},\boldsymbol{\theta}_r;\theta)\}, \tag{4.26}$$

but suffers from a major drawback : the JMAPMLE is biased and inconsistent whatever the number of independent observations [244], except for a class of hybrid estimation problems yielding (4.25b) when the number of independent observations tends to infinity [245, p. 6, 12]. One point worthy of note is that the JMAPMLE may outperform the MLE (4.25a) in terms of MSE, especially with short data records, where MLE is indeed disarmed of its asymptotic optimality [244]. However the biasedness of the JMAPMLE prevents from the comparison of its MSE with deterministic LBs. Indeed, if any known bias can be taken into account in deterministic LBs formulation [216], the bias depends on the specific estimator and, furthermore, is hardly ever known in practice. The second alternative approach consists in resorting to the expectation-maximization (EM) algorithm [246]. In the general case the EM algorithm converges to a stationary point of $\ln p(\mathbf{s};\theta)$. The stationary point need not, however, be a local maximum. Indeed, if it is shown that, under suitable regularity conditions [247], it converges to the MLE (4.25a), it is also shown [248] that it is possible for the algorithm to converge to local minima or saddle points in unusual cases. Moreover, in non-standard estimation, the EM algorithm consists in the following iterative procedure :

$$\theta_{n+1} = \arg\max_{\theta\in\Theta_d}\left\{E_{\boldsymbol{\theta}_r|\mathbf{s};\theta_n}\left[\ln p(\mathbf{s},\boldsymbol{\theta}_r;\theta)\right]\right\}, \tag{4.27}$$

which is unlikely to be of practical use in many estimation problems of interest where $p(\boldsymbol{\theta}_r;\theta)$ is not a conjugate prior for the likelihood function $p(\mathbf{s}|\boldsymbol{\theta}_r;\theta)$ and $p(\boldsymbol{\theta}_r|\mathbf{s};\theta)$ is not computable. Last, in any case where the EM algorithm converge to the MLE (4.25a), its MSE is lower bounded by the MLBs.

4.4.1 Strict-sense and wide-sense unbiased estimators

Let us denote $\boldsymbol{\phi} = \left(\theta, \boldsymbol{\theta}_r^T\right)^T \in \Theta_d \times \mathbb{R}^{P_r}$, $p(\mathbf{s}|\boldsymbol{\phi}) \triangleq p(\mathbf{s}|\boldsymbol{\theta}_r;\theta)$ and $E_{\mathbf{s}|\boldsymbol{\phi}}[\,] \triangleq E_{\mathbf{s}|\boldsymbol{\theta}_r;\theta}[\,]$. Then any estimator $\widehat{\boldsymbol{\phi}}^T = \left(\widehat{\theta}, \widehat{\boldsymbol{\theta}}_r^T\right) \in \mathcal{L}_2(\mathcal{S}_{\mathcal{S},\Theta_r})$, i.e., $\widehat{\boldsymbol{\phi}} \triangleq \widehat{\boldsymbol{\phi}}(\mathbf{s},\boldsymbol{\theta}_r)$, of a selected vector value $\boldsymbol{\phi}$ [6] uniformly strict-sense unbiased [224], i.e., w.r.t. $p(\mathbf{s}|\boldsymbol{\phi})$, must comply with :

$$\forall \boldsymbol{\phi}' = \begin{pmatrix} \theta' \\ \boldsymbol{\theta}_r' \end{pmatrix} \in \Theta_d \times \mathbb{R}^{P_r} : E_{\mathbf{s}|\boldsymbol{\phi}'}\left[\widehat{\boldsymbol{\phi}}\right] = \boldsymbol{\phi}', \tag{4.28}$$

which implies that :

$$\forall \theta' \in \Theta_d : E_{\mathbf{s},\boldsymbol{\theta}_r';\theta'}\left[\widehat{\boldsymbol{\phi}}\right] = E_{\boldsymbol{\theta}_r';\theta'}\left[\boldsymbol{\phi}'\right] = \begin{pmatrix} \theta' \\ E_{\boldsymbol{\theta}_r';\theta'}\left[\boldsymbol{\theta}_r'\right] \end{pmatrix}, \tag{4.29}$$

that is $\widehat{\boldsymbol{\phi}} \in \mathcal{L}_2(\mathcal{S}_{\mathcal{S},\Theta_r})$ is a uniformly wide-sense unbiased [7] [224] estimate of $\mathbf{g}(\theta)^T = \left(\theta, E_{\boldsymbol{\theta}_r;\theta}\left[\boldsymbol{\theta}_r^T\right]\right)$, i.e., w.r.t. $p(\mathbf{s},\boldsymbol{\theta}_r;\theta)$. As the reciprocal is not true :

$$\forall \theta' \in \Theta_d : E_{\mathbf{s},\boldsymbol{\theta}_r';\theta'}\left[\widehat{\boldsymbol{\phi}} - \boldsymbol{\phi}'\right] = \mathbf{0} \;\not\Rightarrow\; \forall \boldsymbol{\phi}' \in \Theta_d \times \mathbb{R}^{P_r} : E_{\mathbf{s}|\boldsymbol{\phi}'}\left[\widehat{\boldsymbol{\phi}} - \boldsymbol{\phi}'\right] = \mathbf{0},$$

then $\mathcal{U}_S(\mathcal{S}_{\mathcal{S},\Theta_r}) = \left\{\widehat{\boldsymbol{\phi}} \in \mathcal{L}_2(\mathcal{S}_{\mathcal{S},\Theta_r}) \text{ verifying } (4.28)\right\} \subset \mathcal{U}_W(\mathcal{S}_{\mathcal{S},\Theta_r}) = \left\{\widehat{\boldsymbol{\phi}} \in \mathcal{L}_2(\mathcal{S}_{\mathcal{S},\Theta_r}) \text{ verifying } (4.29)\right\}$ [8]. Let $\mathcal{U}_S(\mathcal{S}_\mathcal{S})$ and $\mathcal{U}_W(\mathcal{S}_\mathcal{S})$ denote the restriction to $\mathcal{L}_2(\mathcal{S}_\mathcal{S})$ of $\mathcal{U}_S(\mathcal{S}_{\mathcal{S},\Theta_r})$ and $\mathcal{U}_W(\mathcal{S}_{\mathcal{S},\Theta_r})$.

4.4.2 Performance comparison

One can establish that the NSMLE of θ, which belongs to $\mathcal{U}_S(\mathcal{S}_\mathcal{S})$, is in general an asymptotically (when the number of independent observations tends to infinity) suboptimal estimator of θ (in the MSE sense) in comparison with the MLE of θ, which belongs to $\mathcal{U}_W(\mathcal{S}_\mathcal{S})$, within the set of unbiased estimates in the Barankin sense (4.8a)(see subsection D.2.1 of appendix D for details). Therefore, from a theoretical as well as a practical point of view, it is of interest to investigate on a possible quantification of the suboptimality of the NSMLE, which can be obtained in some extent by LBs derivation and comparison.

6. In this section, for sake of legibility, $\boldsymbol{\phi}$ denotes either the vector of unknown parameters or a selected vector value $\boldsymbol{\phi} \triangleq \boldsymbol{\phi}^0 = \left(\theta^0, \left(\boldsymbol{\theta}_r^0\right)^T\right)^T$.

7. Regarding the deterministic parameter θ, uniform wide-sense unbiasedeness is another name for unbiasedeness in the Barankin sense (4.8a).

8. In most cases, the inclusion is strict leading to strict inequalities (D.15a-**??**)

4.4.3 Non-standard lower bounds

For any $\widehat{\phi} \in \mathcal{U}_S(\mathcal{S}_{\mathcal{S},\Theta_r})$, let $\mathbf{C}_{\phi}\left(\widehat{\phi}\right) = E_{\mathbf{s}|\phi}\left[\left(\widehat{\phi}-\phi\right)\left(\widehat{\phi}-\phi\right)^T\right]$ denotes its covariance matrix w.r.t. $p(\mathbf{s}|\phi)$. Then by noticing that, $\forall \widehat{\phi} \in \mathcal{U}_S(\mathcal{S}_{\mathcal{S},\Theta_r})$:

$$E_{\mathbf{s},\boldsymbol{\theta}_r;\theta}\left[\left(\widehat{\phi}-\phi\right)\left(\widehat{\phi}-\phi\right)^T\right] = E_{\boldsymbol{\theta}_r;\theta}\left[\mathbf{C}_{\phi}\left(\widehat{\phi}\right)\right], \tag{4.30}$$

one can derive LBs on the MSE of NSMLEs as follows. Firstly, the rationale outlined in Sections 4.2.3 and 4.3.1 is generalizable to vector parameter [228, 220], that is any LB on $\mathbf{C}_{\phi}\left(\widehat{\phi}\right)$, $\widehat{\phi} \in \mathcal{U}_S(\mathcal{S}_{\mathcal{S}})$, can be expressed as linear transformations of the ad hoc form of the MSB, that is in the present case, w.r.t. to $p(\mathbf{s}|\phi)$ and for strict-sense unbiased estimates (4.28) satisfying :

$$E_{\mathbf{s}|\phi}\left[\left(\widehat{\phi}-\phi\right)\boldsymbol{\upsilon}_{\phi}^T\left(\phi^N\right)\right] = \boldsymbol{\Xi}\left(\phi^N\right), \tag{4.31a}$$

where $\phi^N = \left[\begin{array}{ccc}\phi^1 & \dots & \phi^N\end{array}\right]$, $\boldsymbol{\Xi}\left(\phi^N\right) = \left[\begin{array}{ccc}\phi^1-\phi & \dots & \phi^N-\phi\end{array}\right]$, $\boldsymbol{\upsilon}_{\phi}\left(\phi^N\right) \triangleq \boldsymbol{\upsilon}_{\phi}\left(\mathbf{s};\phi^N\right) = \left(\upsilon_{\phi}\left(\mathbf{s};\phi^1\right),\dots,\upsilon_{\phi}\left(\mathbf{s};\phi^N\right)\right)^T$ and $\upsilon_{\phi}(\mathbf{s};\phi') = p(\mathbf{s}|\phi')/p(\mathbf{s}|\phi)$. By resorting to the generalization of (4.10) to a vector of estimators [220, Lemma 1], the solution of :

$$\min_{\widehat{\phi}\in\mathcal{U}_S(\mathcal{S}_{\mathcal{S}})}\left\{\mathbf{C}_{\phi}\left(\widehat{\phi}\right)\right\} \text{ under } E_{\mathbf{s}|\phi}\left[\left(\widehat{\phi}-\phi\right)\boldsymbol{\upsilon}_{\phi}^T\left(\phi^N\right)\right] = \boldsymbol{\Xi}\left(\phi^N\right), \tag{4.31b}$$

is given by :

$$\mathbf{C}_{\phi}\left(\widehat{\phi}_{MSB}\right) = \boldsymbol{\Xi}\left(\phi^N\right)\mathbf{R}_{\boldsymbol{\upsilon}_{\phi}}^{-1}\left(\phi^N\right)\boldsymbol{\Xi}\left(\phi^N\right)^T, \quad \widehat{\phi}_{MSB}-\phi = \boldsymbol{\Xi}\left(\phi^N\right)\mathbf{R}_{\boldsymbol{\upsilon}_{\phi}}^{-1}\left(\phi^N\right)\boldsymbol{\upsilon}_{\phi}\left(\mathbf{s};\phi^N\right), \tag{4.31c}$$

where $\mathbf{R}_{\boldsymbol{\upsilon}_{\phi}}\left(\phi^N\right) = E_{\mathbf{s}|\phi}\left[\boldsymbol{\upsilon}_{\phi}\left(\phi^N\right)\boldsymbol{\upsilon}_{\phi}^T\left(\phi^N\right)\right]$. Therefore :

$$\mathbf{C}_{\phi}\left(\widehat{\phi}_{MSB}\right) \leq \min_{\widehat{\phi}\in\mathcal{U}_S(\mathcal{S}_{\mathcal{S}})}\left\{\mathbf{C}_{\phi}\left(\widehat{\phi}\right)\right\}, \tag{4.32a}$$

leading to (4.30) :

$$E_{\boldsymbol{\theta}_r;\theta}\left[\mathbf{C}_{\phi}\left(\widehat{\phi}_{MSB}\right)\right] \leq \min_{\widehat{\phi}\in\mathcal{U}_S(\mathcal{S}_{\mathcal{S}})}\left\{E_{\mathbf{s},\boldsymbol{\theta}_r;\theta}\left[\left(\widehat{\phi}-\phi\right)\left(\widehat{\phi}-\phi\right)^T\right]\right\}. \tag{4.32b}$$

In any asymptotic region of operation of NSMLEs, since NSMLEs belong to $\mathcal{U}_S(\mathcal{S}_{\mathcal{S}})$, then $E_{\boldsymbol{\theta}_r;\theta}\left[\mathbf{C}_{\phi}\left(\widehat{\phi}_{MSB}\right)\right]$ is a LB on the covariance matrix of NSMLEs. Therefore it seems sensible to refer to $E_{\boldsymbol{\theta}_r;\theta}\left[\mathbf{C}_{\phi}\left(\widehat{\phi}_{MSB}\right)\right]$ as a non-standard MSB (NSMSB) to make the difference with the modified MSB (4.18). Indeed, the NSMSB is a LB for $\widehat{\phi} \in \mathcal{U}_S(\mathcal{S}_{\mathcal{S}})$, i.e., strict-sense unbiased estimates, whereas the MMSB is a LB for $\widehat{\phi} \in \mathcal{U}_W(\mathcal{S}_{\mathcal{X},\Theta_r})$, i.e., wide-sense unbiased estimates (see Section 4.3.1). In the same vein, any Barankin bound approximation (BBA) on the MSE of MLEs resulting from a linear transformation of the MSB (4.11b), has a non-standard version, referred to as NSBBA or as NSLB hereinafter, and defined as :

$$\mathbf{NSBBA} = E_{\boldsymbol{\theta}_r;\theta}\left[\mathbf{C}_{\phi}\left(\widehat{\boldsymbol{\phi}}_{BBA}\right)\right], \tag{4.33}$$

where $\mathbf{C}_{\phi}\left(\widehat{\boldsymbol{\phi}}_{BBA}\right)$ is the LB resulting from the same linear transformation of (4.31c). As well as the NSMSB, any NSBBA is a lower bound on the MSE of NSMLEs in any asymptotic region of operation. Note that in general, the NSLBs cannot be arranged in closed form due to the presence of the statistical expectation. They however can be evaluated by numerical integration or Monte Carlo simulation [249].
Unfortunately, $\widehat{\boldsymbol{\phi}}_{BBA} \notin \mathcal{U}_S\left(\mathcal{S}_{\mathcal{S}}\right)$ and $\widehat{\boldsymbol{\phi}}_{BBA} \notin \mathcal{U}_W\left(\mathcal{S}_{\mathcal{S},\Theta_r}\right)$ in general, therefore no general result can be drawn on the ordering between **NSBBA** and $\min\limits_{\widehat{\boldsymbol{\phi}}\in\mathcal{U}_W(\mathcal{S}_{\mathcal{S}})}\left\{E_{\mathbf{s}|\theta}\left[\left(\widehat{\boldsymbol{\phi}}-\mathbf{g}\left(\theta\right)\right)\left(\widehat{\boldsymbol{\phi}}-\mathbf{g}\left(\theta\right)\right)^T\right]\right\}$, or any BBA computed on $\mathcal{U}_W\left(\mathcal{S}_{\mathcal{S}}\right)$.

4.4.4 Lower bounds comparison

If in general we cannot compare directly the performance of the NSMLEs and the MLEs, however it would be desirable to be able to compare their associated LBs. Actually, some comparisons are possible but for a restricted class of non-standard estimation problems, as shown in the following. Using the rationale outlined in Section 4.3.1, one can state that all MLBs on $\widehat{\boldsymbol{\phi}} \in \mathcal{U}_W\left(\mathcal{S}_{\mathcal{S},\Theta_r}\right)$ derive from sets of discrete or integral linear transform of :

$$\forall n \in [1, N],\ \mathbf{g}\left(\theta^n\right) - \mathbf{g}\left(\theta\right) = E_{\mathbf{s},\boldsymbol{\theta}_r;\theta}\left[\left(\widehat{\boldsymbol{\phi}}\left(\mathbf{s},\boldsymbol{\theta}_r\right) - \mathbf{g}\left(\theta\right)\right)\upsilon_\theta\left(\mathbf{s},\boldsymbol{\theta}_r;\theta^n\right)\right], \tag{4.34}$$

and yields the general form of the MMSB for unbiased estimates of functions of θ :

$$\mathbf{MMSB} = \boldsymbol{\Xi}\left(\boldsymbol{\theta}^N\right)\mathbf{R}_{\boldsymbol{\upsilon}_\theta}^{-1}\left(\boldsymbol{\theta}^N\right)\boldsymbol{\Xi}\left(\boldsymbol{\theta}^N\right)^T, \tag{4.35}$$

where $\boldsymbol{\Xi}\left(\boldsymbol{\theta}^N\right) = \begin{bmatrix} \mathbf{g}\left(\theta^1\right) - \mathbf{g}\left(\theta\right) & \ldots & \mathbf{g}\left(\theta^N\right) - \mathbf{g}\left(\theta\right) \end{bmatrix}$ and
$\mathbf{R}_{\boldsymbol{\upsilon}_\theta}\left(\boldsymbol{\theta}^N\right) = E_{\mathbf{s},\boldsymbol{\theta}_r;\theta}\left[\boldsymbol{\upsilon}_\theta\left(\mathbf{s},\boldsymbol{\theta}_r;\boldsymbol{\theta}^N\right)\boldsymbol{\upsilon}_\theta^T\left(\mathbf{s},\boldsymbol{\theta}_r;\boldsymbol{\theta}^N\right)\right]$.
If $p\left(\boldsymbol{\theta}_r;\theta\right)$ does not depend on θ, i.e. $p\left(\boldsymbol{\theta}_r;\theta\right) = p\left(\boldsymbol{\theta}_r\right)$, then :

$$\upsilon_\theta\left(\mathbf{s},\boldsymbol{\theta}_r;\theta'\right) = \frac{p\left(\mathbf{s},\boldsymbol{\theta}_r;\theta'\right)}{p\left(\mathbf{s},\boldsymbol{\theta}_r;\theta\right)} = \frac{p\left(\mathbf{s}|\boldsymbol{\theta}_r;\theta'\right)}{p\left(\mathbf{s}|\boldsymbol{\theta}_r;\theta\right)} = \frac{p\left(\mathbf{s}|\boldsymbol{\theta}_r;\theta'\right)}{p\left(\mathbf{s}|\boldsymbol{\theta}_r;\theta\right)} = \upsilon_{\boldsymbol{\phi}}\left(\mathbf{s};\boldsymbol{\phi}'\right).$$

Therefore, if $\boldsymbol{\phi}^N = \begin{bmatrix} \boldsymbol{\phi}^1 & \ldots & \boldsymbol{\phi}^N \end{bmatrix}$, $\boldsymbol{\phi}^n = \begin{pmatrix} \theta^n \\ \boldsymbol{\theta}_r \end{pmatrix}$, $1 \leq n \leq N$, then :

$$E_{\mathbf{s},\boldsymbol{\theta}_r;\theta^0}\left[\boldsymbol{\upsilon}_{(\boldsymbol{\theta}_r;\theta^0)}\left(\mathbf{s};\boldsymbol{\phi}^n\right)\boldsymbol{\upsilon}_{(\boldsymbol{\theta}_r;\theta^0)}^T\left(\mathbf{s};\boldsymbol{\phi}^{n'}\right)\right] = E_{\mathbf{s},\boldsymbol{\theta}_r;\theta^0}\left[\boldsymbol{\upsilon}_{\theta^0}\left(\mathbf{s},\boldsymbol{\theta}_r;\boldsymbol{\theta}^n\right)\boldsymbol{\upsilon}_{\theta^0}^T\left(\mathbf{s},\boldsymbol{\theta}_r;\boldsymbol{\theta}^{n'}\right)\right],$$

that is :

$$E_{\boldsymbol{\theta}_r;\theta^0}\left[\mathbf{R}_{\boldsymbol{\upsilon}_{(\boldsymbol{\theta}_r;\theta^0)}}\left(\boldsymbol{\phi}^N\right)\right] = \mathbf{R}_{\boldsymbol{\upsilon}_{(\boldsymbol{\theta}_r;\theta^0)}}\left(\boldsymbol{\phi}^N\right).$$

By the Jensen inequality :

$$E_{\boldsymbol{\theta}_r;\theta^0}\left[\mathbf{R}^{-1}_{\boldsymbol{\upsilon}_{(\boldsymbol{\theta}_r;\theta^0)}}\left(\boldsymbol{\phi}^N\right)\right] \geq E_{\boldsymbol{\theta}_r;\theta^0}\left[\mathbf{R}_{\boldsymbol{\upsilon}_{(\boldsymbol{\theta}_r;\theta^0)}}\left(\boldsymbol{\phi}^N\right)\right]^{-1} = \mathbf{R}^{-1}_{\boldsymbol{\upsilon}_{(\boldsymbol{\theta}_r;\theta^0)}}\left(\boldsymbol{\phi}^N\right),$$

leading to :

$$\boldsymbol{\Xi}\left(\boldsymbol{\theta}^N\right)\mathbf{R}^{-1}_{\boldsymbol{\upsilon}_\theta}\left(\boldsymbol{\theta}^N\right)\boldsymbol{\Xi}\left(\boldsymbol{\theta}^N\right)^T \leq \boldsymbol{\Xi}\left(\boldsymbol{\theta}^N\right)E_{\boldsymbol{\theta}_r;\theta^0}\left[\mathbf{R}^{-1}_{\boldsymbol{\upsilon}_{(\boldsymbol{\theta}_r;\theta^0)}}\left(\boldsymbol{\phi}^N\right)\right]\boldsymbol{\Xi}\left(\boldsymbol{\theta}^N\right)^T,$$

where $\boldsymbol{\Xi}\left(\boldsymbol{\theta}^N\right) = \begin{bmatrix} \boldsymbol{\xi}\left(\boldsymbol{\theta}^N\right)^T \\ \mathbf{0} \end{bmatrix} = \boldsymbol{\Xi}\left(\boldsymbol{\phi}^N\right)$. Finally, one obtains the following inequality :

$$\underbrace{\boldsymbol{\Xi}\left(\boldsymbol{\theta}^N\right)\mathbf{R}^{-1}_{\boldsymbol{\upsilon}_\theta}\left(\boldsymbol{\theta}^N\right)\boldsymbol{\Xi}\left(\boldsymbol{\theta}^N\right)^T}_{\textbf{MMSB}} \leq \underbrace{E_{\boldsymbol{\theta}_r;\theta}\left[\boldsymbol{\Xi}\left(\boldsymbol{\phi}^N\right)\mathbf{R}^{-1}_{\boldsymbol{\upsilon}_\phi}\left(\boldsymbol{\phi}^N\right)\boldsymbol{\Xi}\left(\boldsymbol{\phi}^N\right)^T\right]}_{\textbf{NSMSB}}. \tag{4.36a}$$

In particular, regarding the estimation of θ, since $\theta = \left(1, \mathbf{0}^T\right)\boldsymbol{\phi}$, one obtains :

$$\boldsymbol{\xi}\left(\boldsymbol{\theta}^N\right)^T\mathbf{R}^{-1}_{\boldsymbol{\upsilon}_\theta}\left(\boldsymbol{\theta}^N\right)\boldsymbol{\xi}\left(\boldsymbol{\theta}^N\right) \leq E_{\boldsymbol{\theta}_r;\theta}\left[\boldsymbol{\xi}\left(\boldsymbol{\theta}^N\right)^T\mathbf{R}^{-1}_{\boldsymbol{\upsilon}_\phi}\left(\boldsymbol{\phi}^N\right)\boldsymbol{\xi}\left(\boldsymbol{\theta}^N\right)\right]. \tag{4.36b}$$

Interestingly enough, it is straightforward to extend (4.36a-4.36b) by introducing tighter NSLBs. It suffices to note that the addition of any subset of K constraints :

$$\forall k \in [N+1, N+K], \boldsymbol{\phi}^k - \boldsymbol{\phi} = E_{\mathbf{s}|\boldsymbol{\phi}}\left[\left(\widehat{\boldsymbol{\phi}}\left(\mathbf{s}, \boldsymbol{\theta}_r\right) - \boldsymbol{\phi}\right)\upsilon_{\boldsymbol{\phi}}\left(\mathbf{s}; \boldsymbol{\phi}^k\right)\right], \boldsymbol{\phi}^k = \left(\theta^k, \left(\boldsymbol{\theta}_r^k\right)^T\right)^T,$$

to (4.34) restricts the class of viable estimators $\widehat{\boldsymbol{\phi}} \in \mathcal{U}_W\left(\mathcal{S}_{\mathcal{S},\Theta_r}\right)$ and therefore increases the associated NSBBA (4.31c), leading to :

$$\begin{aligned}\boldsymbol{\Xi}\left(\boldsymbol{\theta}^N\right)\mathbf{R}^{-1}_{\boldsymbol{\upsilon}_\theta}\left(\boldsymbol{\theta}^N\right)\boldsymbol{\Xi}\left(\boldsymbol{\theta}^N\right)^T &\leq E_{\boldsymbol{\theta}_r;\theta}\left[\boldsymbol{\Xi}\left(\boldsymbol{\phi}^N\right)\mathbf{R}^{-1}_{\boldsymbol{\upsilon}_\phi}\left(\boldsymbol{\phi}^N\right)\boldsymbol{\Xi}\left(\boldsymbol{\phi}^N\right)^T\right] \\ &\leq E_{\boldsymbol{\theta}_r;\theta}\left[\boldsymbol{\Xi}\left(\boldsymbol{\phi}^{N+K}\right)\mathbf{R}^{-1}_{\boldsymbol{\upsilon}_\phi}\left(\boldsymbol{\phi}^{N+K}\right)\boldsymbol{\Xi}\left(\boldsymbol{\phi}^{N+K}\right)^T\right],\end{aligned} \tag{4.37a}$$

and, regarding the estimation of θ, to :

$$\begin{aligned}\boldsymbol{\xi}\left(\boldsymbol{\theta}^N\right)^T\mathbf{R}^{-1}_{\boldsymbol{\upsilon}_\theta}\left(\boldsymbol{\theta}^N\right)\boldsymbol{\xi}\left(\boldsymbol{\theta}^N\right) &\leq E_{\boldsymbol{\theta}_r;\theta}\left[\boldsymbol{\xi}\left(\boldsymbol{\theta}^N\right)^T\mathbf{R}^{-1}_{\boldsymbol{\upsilon}_\phi}\left(\boldsymbol{\phi}^N\right)\boldsymbol{\xi}\left(\boldsymbol{\theta}^N\right)\right] \\ &\leq E_{\boldsymbol{\theta}_r;\theta}\left[\boldsymbol{\xi}\left(\boldsymbol{\theta}^{N+K}\right)^T\mathbf{R}^{-1}_{\boldsymbol{\upsilon}_\phi}\left(\boldsymbol{\phi}^{N+K}\right)\boldsymbol{\xi}\left(\boldsymbol{\theta}^{N+K}\right)\right],\end{aligned} \tag{4.37b}$$

where $\boldsymbol{\phi}^{N+K} = \left[\boldsymbol{\phi}^N, \begin{bmatrix} \theta^{N+1} & \cdots & \theta^{N+K} \\ \boldsymbol{\theta}_r^{N+1} & \cdots & \boldsymbol{\theta}_r^{N+K} \end{bmatrix}\right]$, $\boldsymbol{\Xi}\left(\boldsymbol{\phi}^{N+K}\right) = \left[\boldsymbol{\Xi}\left(\boldsymbol{\phi}^N\right), \begin{bmatrix} \xi\left(\theta^{N+1}\right) & \cdots & \xi\left(\theta^{N+K}\right) \\ \boldsymbol{\theta}_r^{N+1} - \boldsymbol{\theta}_r & \cdots & \boldsymbol{\theta}_r^{N+K} - \boldsymbol{\theta}_r \end{bmatrix}\right]$, and $\boldsymbol{\xi}\left(\boldsymbol{\theta}^{N+K}\right) = \left(\boldsymbol{\xi}\left(\boldsymbol{\theta}^N\right)^T, \xi\left(\theta^{N+1}\right), \ldots, \xi\left(\theta^{N+K}\right)\right)^T$. Then one can take advantage of the use of the numerous (standard) BBAs derived for parameter vector [220, 225], however, at a cost of numerical integration or Monte Carlo simulation to evaluate their statistical expectation.

Non-standard LBs are exemplified in the case of the CRB and the BaBs in subsection D.2.2 of appendix D. In particular, the non-standard CRB (NSCRB) example illustrates that the tightest form of any NSLB is obtained when the set of unbiasedness constraints are expressed for $\boldsymbol{\phi}$ as in (4.37b) and not only for θ as in (4.36b).

4.4.5 Non-standard lower bounds (continued)

Any of the NSLBs mentioned in the previous section can be derived in the general case where $p(\boldsymbol{\theta}_r; \theta)$ does depend on θ, except that no general inequalities between MBBA and NSBBA can any longer be exhibited. Interestingly enough, since any existing standard LB can be obtained from (4.31c) as $\mathbf{C}_{\boldsymbol{\phi}}\left(\widehat{\boldsymbol{\phi}}_{BBA}\right)$ (a multiple parameters version of (4.12b)), it has a non-standard counterpart $E_{\boldsymbol{\theta}_r;\theta}\left[\mathbf{C}_{\boldsymbol{\phi}}\left(\widehat{\boldsymbol{\phi}}_{BBA}\right)\right]$, which includes the FGB [232], the MHB [235], the GlB [219], the AbB [218], and the CRFB [225, (101-102)]. Last, let us recall that in general $\widehat{\boldsymbol{\phi}}_{BBA} \notin \mathcal{U}_W\left(\mathcal{S}_{\mathcal{S},\Theta_r}\right)$, therefore the associated NSLB cannot be compared a priori neither with the MSE of $\widehat{\theta}_{ML} \in \mathcal{U}_W\left(\mathcal{S}_{\mathcal{S}}\right)$ nor with any of its LBs (computed with $p(\mathbf{s};\theta)$). In particular, NSLBs are not in general neither upper bounds on the MSE of $\widehat{\theta}_{ML}$ nor on any of its LBs.

4.5 Conclusions

In the present chapter, we have addressed deterministic parameter estimation and the situation where a closed-form of the conditional p.d.f. does not exist or where a closed-form does exist but the resulting expression is intractable to derive either LBs or MLEs. To summarize, we have provided a unified framework allowing to extend the previous theoretical works released on that problem [213, 214, 215, 210, 223, 234, 250, 211, 208, 224]. First, in terms of intrinsic LBs by showing that any standard LB can be transformed into a modified one fitted to non-standard deterministic estimation, at the expense of tightness however. Second, in terms of relative LBs, i.e. dedicated to characterize the asymptotically suboptimal NSMLEs, by showing that any standard LB has a non-standard version lower bounding the MSE of NSMLEs.

In the practical GNSS problem in presence of non-Gaussian errors caused by signal reflections, a closed-form of the conditional p.d.f. does not exist. In this situation, the deterministic parameters of interest are the LOS delays and Doppler-frequency shifts and the nuisance random variables are the MPs delays, Doppler-frequency shifts and amplitude. In suburban and urban environments, MP p.d.f. are different from the Gaussian distribution which induces a marginal p.d.f of GNSS observations without any analytical form. In this case, none of the existing estimation performance characterization methods (for instance standard lower bounds) can be used as marginalization of joint p.d.f is mathematically intractable. Besides, standard MLEs can not be computed in this situation either. This motivates the derivation of the proposed MLBs and NSMLEs as alternatives to circumvent the previous problems. However, these two solutions have not been explicitly exemplified in the context of GNSS due to a lack of time (however application examples of MLBs and NSLBs can be found in Radar and Telecom (see [251, §V.A])). A natural sequel of this work is to quantify these MLBs and NSMLEs in the context of GNSS in real-life non-Gaussian environments. This would be a fruitful area for further researches.

Conclusions et Recommandations

Conclusions

Dans cette thèse, les conclusions suivantes peuvent être tirées :

1. Conclusions concernant le positionnement GNSS assisté par simulation 3D :
   Nous avons proposé une intégration du GNSS avec un simulateur de propagation de signaux GNSS 3D fournissant des informations utiles sur l'environnement géométrique de réception. Les conclusions finales de cette partie sont les suivantes :
   - Les résultats expérimentaux montrent que les méthodes basées sur la correspondance entre des positions candidates offrent une meilleure précision de positionnement par rapport à celles basées sur la correction des mesures PR. Cela s'explique par le fait que les corrections de MP générées par SPRING ne sont pas fiables et ne doivent pas être utilisées dans la correction des mesures PR.
   - Les algorithmes proposés basés sur la correspondance entre des positions candidates offrent une amélioration significative de précision de 52% par rapport à la solution conventionelle de LS dans des environnements urbains.
   - Les algorithmes proposés basés sur la correspondance entre des positions candidates utilisant les informations de propagation du signal GNSS ont été comparés à une méthode basée sur la correspondance entre des positions candidates utilisant la visibilité des satellites GNSS sans simulations de propagation du signal. Les résultats expérimentaux montrent que ces deux méthodes donnent approximativement les mêmes performances de positionnement. Mais les méthodes basées sur des simulations de propagation de signal nécessitent plus de charge de calcul que le second type de méthodes.
2. Conclusions concernant le niveau de précision de positionnement maximal dans des environnements non gaussiens :
   Premièrement, nous avons montré que, dans le cas où des bornes inférieures sur l'EQM standards ne peuvent pas être calculées, toute borne inférieure standard peut être transformée en une borne inférieure modifiée, aux dépens de la pertinence ("*tightness*") de cette borne. Deuxièmement, dans cette situation où les EMVs standard ne peuvent pas être calculés non plus, nous avons proposé un EMV non standard asymptotiquement sous-optimal comme alternative. Cependant, ces deux solutions n'ont pas été explicitement illustrées dans le contexte des GNSS par manque de temps.

Recommandations

Sur la base des résultats de cette thèse, plusieurs perspectives pour les travaux futurs peuvent être esquissées. Parmi celles-ci, les suivantes sont les plus intéressantes :

1. Evaluation des approches proposées dans d'autres contextes urbains :
   Les différents algorithmes proposés dans cette thèse de recherche devraient être vérifiés et validés à l'aide d'autres données GNSS d'autres villes.
2. Fusion d'un simulateur 3D / GNSS au niveau des blocs de réception :
   En ce qui concerne les boucles de poursuite, il serait intéressant d'étudier si les simulations GNSS peuvent permettre le suivi des signaux MP/NLOS dégradés à l'aide de boucles à verrouillage de délai vectoriel (VDLL).
3. Fusion simulateur 3D/GNSS en utilisant les mesures Doppler :
   Nos travaux se sont concentrés sur la fusion simulateur 3D/GNSS utilisant des mesures de codes. Il serait très intéressant d'étendre ce travail aux mesures Doppler, qui permettent d'estimer la vitesse du récepteur. La modélisation 3D peut également aider à bien estimer ces mesures car elle permet de simuler les effets Doppler subis par chacun des signaux parvenant au récepteur.

Chapitre 5

Conclusions and Recommendations

Contents

This chapter presents the conclusions of this research and draws some recommendations for future work. Potential applications of the proposed methods are also presented.

5.1 Brief summary and Conclusions

In this dissertation, the following conclusions can be drawn :

— **Conclusions regarding 3D mapping aided GNSS positioning :**
As signal processing based algorithms have generally limited positioning accuracy in urban areas, it is necessary to counteract the disadvantages of GNSS positioning in these areas using complementary information. In this research thesis, we have proposed an integration of the GNSS with a 3D GNSS signal propagation simulator providing aiding information about the geometric environment of reception. The following questions concerning this 3D GNSS simulator/GNSS fusion have been dealt with :

1. *What is the required level of realism of the information provided by 3D simulation to be constructively used for GNSS positioning ?*
2. *How could information from the 3D GNSS Simulator be used to enhance positioning performance ? At what level of processing this information should be used ?*

The final conclusions of this part are the following :

1. The integration of 3D GNSS signal propagation information has been made using either PR measurements correction or candidate positions scoring. Experimental results show that methods based on candidate positions scoring give better positioning accuracy compared to those based on PR measurements scoring. This is explained by the fact that SPRING-generated multipath corrections are not reliable and should not be used in the PR measurements correction.

2. The proposed algorithms based on candidate positions scoring give a significant accuracy improvement of 52% compared to the conventional LS solution in deep urban environments. These solutions have been compared to the LS solution because they are epoch-by-epoch solutions.
3. The proposed algorithms based on candidate positions scoring using 3D GNSS signal propagation information have been compared to a method based on candidate positions scoring using satellite visibility without signal propagation simulations. Experimental results shows that these two methods gives approximately the same positioning performance. But, methods based on signal propagation simulations need more computational load than the second kind of methods (i.e. without signal propagation simulations). However, other studies have used similar techniques based on GNSS signal propagation with lighter computational load [168].
4. When a GNSS signal propagation simulator is used to predict PR errors in urban areas with the aim of correcting these errors, we have presented a methodology to validate the prediction of these tools for a constructive use of PR errors. The conclusion of this part is that SPRING simulator is within the maximum acceptable level of uncertainty on PR errors predictions in the specific environment studied in this research thesis. However, other extensive analysis must be performed in various conditions to validate the SPRING simulator.

— **Conclusions regarding the maximum achievable positioning accuracy level reached in non-Gaussian environments**
In this research thesis, we study the lower bounds on position estimation accuracy in presence of non-Gaussian observations. First, we have shown that, in the case where standard LBs can not be computed, any standard LB can be transformed into a modified one fitted to non-standard deterministic estimation, at the expense of tightness however. Second, in this situation where standard MLEs can not be computed either, we have proposed a asymptotically suboptimal NSMLE as alternative. However, these two solutions have not been explicitly exemplified in the context of GNSS due to a lack of time.

5.2 Recommendations for Future Work

Based on the results of this thesis, several recommendations for future work are noticeable. Among them, the following ones are of greatest interest :

— **Evaluation of the proposed approaches in other urban settings :**
Different proposed algorithms in this research thesis should be verified and validated using more measurement samples obtained from various cities. With these intensive analysis, further assessment on the performance of positioning algorithms may be conducted. Other 3D city models are worth being investigated for this purpose. In fact, urban canyons characterized by very narrow streets but with low to medium buildings, such as those found in Toulouse, greatly reduce the visibility of satellites but do not give rise

to NLOS signals with a very high bias. It would be necessary to have a 3D map and a measurement campaign in an environment such as Manhattan in order to validate the performance of our 3D-mapping aided positioning approaches on real GNSS data.

— **3D Simulator/GNSS fusion at the receiver level :**
On the tracking aspects, it would be interesting in the future to study whether 3D GNSS simulations can allow the tracking of degraded MP/NLOS signals using Vector Delay Lock Loops (VDLL). This amounts to consider the 3D aided information provided by the 3D GNSS simulator at the signal level (inside the receiver). Indeed, in its traditional configuration, a VDLL predicts delays for the pseudorange observations as a function of the direct receiver/satellite path. This may disadvantage the tracking of reflected signals by ignoring their additional bias. However, because of the reflection undergone by the environment, reflected NLOS signals generally have very reduced power compared to LOS signals which make their tracking more difficult. 3D GNSS simulations of the receiver reception status can help to continue the tracking of these signals while estimating their additional bias using adaptation of the VDLL principle.

— **3D Simulator/GNSS fusion using Doppler measurements :**
Our work has concentrated on 3D simulator/GNSS fusion using pseudoranges measurements, and more specifically on ways to help the receiver to obtain, correct them or use them constructively through 3D simulations. It would be very interesting to extend this work to the Doppler measurements, which allow estimation of the speed of the receiver. 3D modeling can also help with these measurements because it can simulate the Doppler effects undergone by each of the signals reaching the receiver. This would be an additional aid to enhance the navigation solution in a constrained environments.

5.3 Potential Applications

The research in this thesis has led to a development of novel positioning methods that can be applied in commercial GNSS receiver following different configurations :

— **Proposed 3D mapping aided positioning methods :** Operating the proposed methods on a graphics processing unit (GPU) of a mobile device will surely increase the power consumption of the user devices. These problems apply to our proposed approaches and not to 3DMA GNSS in general. Besides, since these methods relies on information provided by 3D GNSS simulators and as computing these 3D data using these tools is generally computationally intensive, a possible adaptation of these methods can be performed in a server-based mode interacting with the user receiver or send as information like Assisted-GPS. In order to further reduce the computational loads of these methods, a binary data format should be used to minimize the capacity required.

— **Proposed MLBs and NSMLEs :** A natural sequel of the presented work on LBs in chapter 4 is to quantify the MLBs and NSMLEs in the context of GNSS in real-life non-Gaussian environments, involving for instance, Multivariate Elliptically Contoured Distributions, and in particular Generalized Gaussian Distribution used to characterize the clutter in radar [252].

Bibliographie

[1] GSA, “GNSS User Technology Report Issue 1,” GSA, Tech. Rep., Oct, 2016.

[2] IFSTTAR, “Better use of Global Navigation Satellite Systems for safer and greener transport,” Tech. Rep., September 2015.

[3] T. Iwase, N. Suzuki, and Y. Watanabe, “Estimation and exclusion of multipath range error for robust positioning,” *GPS solutions*, vol. 17, no. 1, pp. 53–62, 2013.

[4] D. Sobel, *Longitude : The true story of a lone genius who solved the greatest scientific problem of his time.* Bloomsbury Publishing USA, 2007.

[5] W. Guier and G. Weiffenbach, “A satellite Doppler navigation system,” *Proceedings of the IRE*, vol. 48, no. 4, pp. 507–516, 1960.

[6] R. J. Danchik, “An overview of transit development,” *Johns Hopkins APL technical digest*, vol. 19, no. 1, p. 19, 1998.

[7] H. Black, “Satellites for earth surveying and ocean navigating,” *Johns Hopkins APL Technical Digest*, vol. 2, pp. 3–13, 1981.

[8] T. A. Stansell, “The Navy navigation satellite system : Description and status,” *Navigation*, vol. 15, no. 3, pp. 229–243, 1968.

[9] C. Alexandrow, “The story of GPS,” *Defense Advanced Research Projects Agency (DARPA)(ed.) DARPA*, vol. 50, 2008.

[10] E. Kaplan and C. Hegarty, *Understanding GPS : Principles and Applications.* Artech House, 2005. [Online]. Available : https://books.google.fr/books?id=-sPXPuOW7ggC

[11] GSA, “GNSS Market Report Issue 5,” GSA, Tech. Rep., May, 2017.

[12] B. Hofmann-Wellenhof, H. Lichtenegger, and E. Wasle, *GNSS–Global Navigation Satellite Systems : GPS, GLONASS, Galileo, and more.* New York : Springer, Springer, 2008.

[13] P. Misra and P. Enge, *Global Positioning System : Signals, Measurements, and Performance*, 2nd ed. Ganga-Jamuna Press, Lincoln MA, 2006.

[14] B. W. Parkinson and J. J. Spilker, *Global Positioning System : Theory and Applications.* Progress in Astronautics and Aeronautics, 1996.

[15] U. S. Government, “Official US Government Information about the Global Positioning System (GPS),” http ://www.gps.gov, accessed : 2017-05-30.

[16] Russian Space Agency, “Official Russian Government Information about the GLObal Navigation Satellite System (GLONASS),” https ://www.glonass-iac.ru, accessed : 2017-05-30.

[17] C. J. Hegarty and E. Chatre, “Evolution of the Global Navigation Satellite System (GNSS),” *Proceedings of the IEEE*, vol. 96, no. 12, pp. 1902–1917, Dec 2008.

[18] Y. Urlichich, V. Subbotin, G. Stupak, V. Dvorkin, A. Povalyaev, S. Karutin, and R. Bakitko, “GLONASS Modernization,” *GPS World*, pp. 34–39, Novembre 2011.

[19] European GNSS Agency (GSA), "Official European GNSS Agency Information about the Galileo system," https ://www.gsa.europa.eu/, accessed : 2017-05-31.

[20] China Satellite Navigation Office, "BeiDou Navigation Satellite System Signal In Space Interface Control Document Open Service Signal (Version 2.1)," China Satellite Navigation Office, Tech. Rep., November 2016.

[21] J. Liu, "BEIDOU : China's Rapidly Emerging GNSS," *Inside GNSS*, pp. 30–31, May/June 2013.

[22] China Satellite Navigation Office, "Beidou Navigation Satellite System Open Service Performance Standard (Version 1.0)," China Satellite Navigation Office, Tech. Rep., December 2013.

[23] Government Of Japan, "Government Of Japan Quasi-Zenith Satellite System site," http ://qzss.go.jp/en/, accessed : 2017-05-31.

[24] Indian Space Research Organisation, Government Of INDIA, "Official Indian Space Research Organisation Information about IRNSS," http ://www.isro.gov.in/irnss-programme, accessed : 2017-05-31.

[25] M. S. Grewal, L. R. Weill, and A. P. Andrews, *Global Positioning Systems, Inertial Navigation, and Integration*. Wiley-Interscience, 2007.

[26] P. Groves, *Principles of GNSS, Inertial, and Multisensor Integrated Navigation Systems, Second Edition*, ser. GNSS/GPS. Artech House, 2013. [Online]. Available : https://books.google.fr/books?id=t94fAgAAQBAJ

[27] J. A. Klobuchar, "Ionospheric time-delay algorithm for single-frequency GPS users," *IEEE Transactions on Aerospace Electronic Systems*, vol. 23, pp. 325–331, May 1987.

[28] R. F. SC-159, *Minimum Operational Performance Standards for Global Positioning System/Wide Area Augmentation System Airborne Equipment*. RTCA, 2006. [Online]. Available : https://books.google.fr/books?id=nXCRQQAACAAJ

[29] U. S. Departement of Defense, "Global Positioning System Standard Positioning Service Performance Standard, 4th edition," Tech. Rep., September 2008.

[30] S. M. Kay, *Fundamentals of statistical signal processing, volume I : estimation theory*. Prentice Hall, 1993.

[31] S. Gleason and D. Gebre-Egziabher, *GNSS Applications and Methods*, ser. GNSS technology and applications series. Artech House, 2009. [Online]. Available : https://books.google.fr/books?id=juXAE3SHQroC

[32] R. E. Kalman, "A new approach to linear filtering and prediction problems," *ASME Journal of Basic Engineering*, 1960.

[33] M. Grewal and A. Andrews, *Kalman filtering : theory and practice using MATLAB*, ser. Wiley InterScience Online Books, Electronic and Electrical Engineering Collection. Wiley, 2001. [Online]. Available : https://books.google.fr/books?id=9UoZAQAAIAAJ

[34] T. Kailath, A. H. Sayed, and B. Hassibi, *Linear estimation*. Prentice Hall, 2000, no. EPFL-BOOK-233814.

[35] D. Simon, *Optimal state estimation : Kalman, H infinity, and nonlinear approaches*. John Wiley & Sons, 2006.

[36] Toll Collect, Germany, "Service on the road," https ://www.toll-collect.de/en, accessed : 2017-06-01.

[37] P. Groves, "Multipath vs. NLOS signals. How Does Non-Line-of-Sight Reception Differ from Multipath Interference," *Inside GNSS Magazine*, pp. 40–42, November/December 2013.

[38] Z. Jiang and P. D. Groves, "NLOS GPS signal detection using a dual-polarisation antenna," *GPS Solutions*, vol. 18, no. 1, pp. 15–26, 2014.

[39] K. Zhang, B. Li, X. Zhu, H. Chen, and G. Sun, "NLOS Signal Detection Based on Single Orthogonal Dual-Polarized GNSS Antenna," *International Journal of Antennas and Propagation*, 2017.

[40] M. H. Keshvadi, A. Broumandan, and G. Lachapelle, "Analysis of GNSS beamforming and Angle of Arrival Estimation in Multipath Environements," in *Proceedings of ION ITM 2011*.

[41] L. Wang, P. D. Groves, and M. K. Ziebart, "GNSS Shadow Matching : Improving Urban Positioning Accuracy Using a 3D City Model with Optimized Visibility Prediction Scoring," in *Proceedings of the 25th International Technical Meeting of The Satellite Division of the Institute of Navigation (ION GNSS 2012)*.

[42] M. Obst, S. Bauer, and G. Wanielik, "Urban Multipath Detection and mitigation with dynamic 3D Maps for reliable Land vehicle Localization," in *Proceedings of IEEE/ION PLANS 2012*.

[43] J. Bradbury, M. Ziebart, P. Cross, P. Boulton, and A. Read, "Code Multipath Modelling in the Urban Environment Using Large Virtual Reality City Models : Determining the Local Environment," *Journal of Navigation*, 2007.

[44] K. A. Bin Ahmad, M. Sahmoudi, C. Macabiau, A. Bourdeau, and G. Moura, "Reliable GNSS Positioning in Mixed LOS/NLOS Environments Using a 3D Model," in *ENC 2013, European Navigation Conference*, Vienne, Austria, Apr. 2013. [Online]. Available : https://hal-enac.archives-ouvertes.fr/hal-00943395

[45] D. Betaille, F. Peyret, M. Ortiz, S. Miquel, and L. Fontenay, "A New Modeling Based on Urban Trenches to Improve GNSS Positioning Quality of Service in Cities," *IEEE Intelligent Transportation Systems Magazine*, vol. 5, no. 3, pp. 59–70, Fall 2013.

[46] P. D. Groves, Z. Jiang, L. Wang, and M. K. Ziebart, "Intelligent Urban Positioning using Multi-Constellation GNSS with 3D Mapping and NLOS Signal Detection," in *Proceedings of the 25th International Technical Meeting of The Satellite Division of the Institute of Navigation (ION GNSS 2012)*, no. 458 - 472.

[47] L. Wang, P. D. Groves, and M. K. Ziebart, "Multi-Constellation GNSS Performance Evaluation for Urban Canyons Using Large Virtual Reality City Models," *JOURNAL OF NAVIGATION*, 2012.

[48] A. Soloviev and F. V. Graas, "Use of Deeply Integrated GPS/INS Architecture and Laser Scanners for the Identification of Multipath Reflections in Urban Environments," *IEEE Journal of Selected Topics in Signal Processing*, vol. 3, no. 5, pp. 786–797, Oct 2009.

[49] J. Marais, M. Berbineau, and M. Heddebaut, "Land mobile gnss availability and multipath evaluation tool," *IEEE Transactions on Vehicular Technology*, vol. 54, no. 5, pp. 1697–1704, Sept 2005.

[50] J. I. Meguro, T. Murata, J. I. Takiguchi, Y. Amano, and T. Hashizume, "GPS Multipath Mitigation for Urban Area Using Omnidirectional Infrared Camera," *IEEE Transactions on Intelligent Transportation Systems*, vol. 10, no. 1, pp. 22–30, March 2009.

[51] J. Moreau, S. Ambellouis, and Y. Ruichek, "Equisolid fisheye stereovision calibration and point cloud computation," in *ISPRS-SSG 2013, conference on Serving Society with Geoinformatics*, Turkey, Nov. 2013, p. 6p. [Online]. Available : https://hal.archives-ouvertes.fr/hal-00912647

[52] J. Marais, S. Tay, A. Flancquart, and C. Meurie, "Weighting with the pre-knowledge of GNSS signal state of reception in urban areas," in *Proceedings of ENC 2015*.

[53] J. Moreau, S. Ambellouis, and Y. Ruichek, "Fisheye-Based Method for GPS Localization Improvement in Unknown Semi-Obstructed Areas," *Sensors*, 2017.

[54] S. Peyraud, D. Bétaille, S. Renault, M. Ortiz, F. Mougel, D. Meizel, and F. Peyret, "About non-line-of-sight satellite detection and exclusion in a 3D map-aided localization algorithm," *Sensors*, vol. 13, no. 1, pp. 829–847, 2013.

[55] J. Khodjaev, Y. Park, and A. S. Malik, "Survey of NLOS identification and error mitigation problems in UWB-based positioning algorithms for dense environments." *Annales des Télécommunications*, vol. 65, no. 5-6, pp. 301–311, 2010.

[56] J. Schroeder, S. Galler, K. Kyamakya, and K. Jobmann, "NLOS detection algorithms for Ultra-Wideband localization," in *2007 4th Workshop on Positioning, Navigation and Communication*, March 2007, pp. 159–166.

[57] J. Borras, P. Hatrack, and N. B. Mandayam, "Decision theoretic framework for NLOS identification," in *Vehicular Technology Conference, 1998. VTC 98. 48th IEEE*, vol. 2, May 1998, pp. 1583–1587 vol.2.

[58] I. Güvenç, C.-C. Chong, F. Watanabe, and H. Inamura, "NLOS Identification and Weighted Least-squares Localization for UWB Systems Using Multipath Channel Statistics," *EURASIP J. Adv. Signal Process*, 2008.

[59] Z. Xiao, H. Wen, A. Markham, N. Trigoni, P. Blunsom, and J. Frolik, "Non-Line-of-Sight Identification and Mitigation Using Received Signal Strength," *IEEE Transactions on Wireless Communications*, vol. 14, no. 3, pp. 1689–1702, March 2015.

[60] I. Guvenc and C. Chong, "Line-of-sight (LOS) or non-LOS (NLOS) identification method using multipath channel statistics," Aug. 18 2009, uS Patent 7,577,445. [Online]. Available : http://www.google.ch/patents/US7577445

[61] L. Mucchi and P. Marcocci, "A new UWB indoor channel identification method," in *2007 2nd International Conference on Cognitive Radio Oriented Wireless Networks and Communications*, Aug 2007, pp. 58–62.

[62] R. Casas, A. Marco, J. J. Guerrero, and J. Falcó, "Robust Estimator for Non-line-of-sight Error Mitigation in Indoor Localization," *EURASIP J. Appl. Signal Process.*, pp. 156–156, 2006.

[63] A. Lakhzouri, E. S. Lohan, R. Hamila, and M. Renfors, “Extended Kalman Filter Channel Estimation for Line-of-Sight Detection in WCDMA Mobile Positioning,” *EURASIP J. Adv. Sig. Proc.*, vol. 2003, no. 13, pp. 1268–1278, 2003. [Online]. Available : https://doi.org/10.1155/S1110865703306018

[64] B. Denis, L. Ouvry, B. Uguen, and F. Tchoffo-Talom, “Advanced Bayesian filtering techniques for UWB tracking systems in indoor environments,” in *2005 IEEE International Conference on Ultra-Wideband*, Sept 2005, pp. 6 pp.–.

[65] P. D. Groves, Z. Jiang, M. Rudi, and P. Strode, “A Portfolio Approach to NLOS and Multipath Mitigation in Dense Urban Areas,” in *Proceedings of the 26th International Technical Meeting of The Satellite Division of the Institute of Navigation (ION GNSS 2013)*.

[66] P. D. Groves and Z. Jiang, “Height Aiding, C/N0 Weighting and Consistency Checking for GNSS NLOS and Multipath Mitigation in Urban Areas,” *Journal of Navigation*, pp. 653–659, 2013.

[67] P. R. Strode and P. D. Groves, “GNSS Multipath Detection Using Three-frequency Signal-to-noise Measurements,” *GPS Solution*, pp. 399–412, 2016.

[68] M. Spangenberg, J. Y. Tourneret, V. Calmettes, and G. Duchateau, “Detection of variance changes and mean value jumps in measurement noise for multipath mitigation in urban navigation,” in *2008 42nd Asilomar Conference on Signals, Systems and Computers*, Oct 2008, pp. 1193–1197.

[69] C. Cheng, J.-Y. Tourneret, Q. Pan, and V. Calmettes, “Detecting, estimating and correcting multipath biases affecting GNSS signals using a marginalized likelihood ratio-based method,” *Signal Processing*, vol. vol. 118, pp. pp. 221–234, Jan. 2016. [Online]. Available : https://hal.archives-ouvertes.fr/hal-01260529

[70] G. Audrey and G. Julie, “An Unscented Kalman filter based maximum likelihood ratio for NLOS bias detection in UMTS localization,” in *2008 16th European Signal Processing Conference*, Aug 2008, pp. 1–5.

[71] A. Giremus and J. Y. Tourneret, “Joint detection/estimation of multipath effects for the Global Positioning System,” in *Proceedings. (ICASSP ’05). IEEE International Conference on Acoustics, Speech, and Signal Processing, 2005.*, vol. 4, March 2005, pp. iv/17–iv/20 Vol. 4.

[72] N. Viandier, D. F. Nahimana, J. Marais, and E. Duflos, “GNSS performance enhancement in urban environment based on pseudo-range error model,” in *2008 IEEE/ION Position, Location and Navigation Symposium*, May 2008, pp. 377–382.

[73] Z. Jiang, P. Groves, W. Ochieng, S. Feng, C. Milner, and P. Mattos, “Multi-Constellation GNSS Multipath Mitigation Using Consistency Checking ,” in *Proceedings of the 24th International Technical Meeting of The Satellite Division of the Institute of Navigation (ION GNSS 2011)*, 2011, pp. 3889 – 3902.

[74] Z. Jiang and P. Groves, “GNSS NLOS and Multipath Error Mitigation using Advanced Multi-Constellation Consistency Checking with Height Aiding,” in *Proceedings of the 25th International Technical Meeting of The Satellite Division of the Institute of Navigation (ION GNSS 2012)*, pp. 79–88.

[75] O. M. Mubarak and A. G. Dempster, "Analysis of Early Late Phase in Single-and Dual-frequency GPS Receivers for Multipath Detection," *GPS Solut.*, vol. 14, no. 4, pp. 381–388, Sep. 2010.

[76] P. G. Mattos, "Multipath indicator to enhance RAIM and FDE in GPS/GNSS Systems," 2011, patent Application No. 11112819.5, Filed July 2011.

[77] L.-T. Hsu, S.-S. Jan, P. D. Groves, and N. Kubo, "Multipath Mitigation and NLOS Detection Using Vector Tracking in Urban Environments," *GPS Solution*, vol. 19, no. 2, pp. 249–262, April 2015.

[78] O. Leisten and V. Knobe, "Optimizing Small Antennas for Body-Loading Applications," *GPS World*, 2012.

[79] M. G. J. K. and D. Orban, "Innovation : GNSS Antennas : An Introduction to Bandwidth, Gain Pattern, Polarization and All That," *GPS World*, 2009.

[80] V. Filippov, D. Tatarnicov, J. Ashjaee, A. Astakhov, and I. Sutiagin, "The First Dual-Depth Dual-Frequency Choke Ring," in *Proceedings of the 11th International Technical Meeting of the Satellite Division of The Institute of Navigation (ION GPS 1998)*, pp. 1035 – 1040.

[81] H. Yang, X. Yang, B. Sun, and H. Su, "Global Navigation Satellite System Multipath Mitigation Using a Wave-Absorbing Shield," *Sensors*, 2016.

[82] A. Konovaltsev, F. Antreich, and A. Hornbostel, "Performance Assessment of Antenna Array Algorithms for Multipath and Interference Mitigation," in *2nd Workshop on GNSS Signals & Signal Processing - GNSS SIGNALS'2007*, 2007.

[83] M. Sahmoudi and M. G. Amin, "Optimal Robust Beamforming for Interference and Multipath Mitigation in GNSS Arrays," in *2007 IEEE International Conference on Acoustics, Speech and Signal Processing - ICASSP '07*, vol. 3, April 2007, pp. III–693–III–696.

[84] A. Brown and N. Gerein, "Test Results from a Digital P(Y) Code Beamsteering Receiver for Multipath Minimization ," in *Proceedings of ION 57th Annual Meeting, Albuquerque, NM, June 2001.*

[85] N. Vagle, A. Broumandan, A. Jafarnia-Jahromi, and G. Lachapelle, "Performance analysis of GNSS multipath mitigation using antenna arrays," *The Journal of Global Positioning Systems*, vol. 14, no. 1, p. 4, 2016.

[86] J. Ray and M. Cannon, "Mitigation of Static Carrier Phase Multipath Effects Using Multiple Closely-Spaced Antennas," in *Proceedings of ION GPS-98, Nashville, September 15-18, 1998.*

[87] S. Rougerie, G. Carrié, F. Vincent, L. Ries, and M. Monnerat, "A New Multipath Mitigation Method for GNSS Receivers Based on an Antenna Array," *International Journal of Navigation and Observation*, 2012.

[88] N. Kubo, R. Kikuchi, and M. Higuchi, "A Unique Approach to Strong Multipath Mitigation in Dense Urban Areas," in *Proceedings of the 28th International Technical Meeting of The Satellite Division of the Institute of Navigation (ION GNSS+ 2015)*, 2015.

[89] A. J. VAN DIERENDONCK, P. FENTON, and T. FORD, "Theory and Performance of Narrow Correlator Spacing in a GPS Receiver," *Navigation*, vol. 39, no. 3, pp. 265–283, 1992.

[90] M. S. Braasch, "Performance comparison of multipath mitigating receiver architectures," in *2001 IEEE Aerospace Conference Proceedings (Cat. No.01TH8542)*, vol. 3, 2001, pp. 3/1309–3/1315 vol.3.

[91] M. Bhuiyan, *Analysis of Multipath Mitigation Techniques for Satellite-based Positioning Applications*. Tampere University of Technology, 9 2011.

[92] M. Sahmoudi and R. J. Landry, "Multipath Mitigation Techniques using Maximum-Likelihood Principles," *Inside GNSS*, pp. 24–29, November/December 2008.

[93] L. Garin and J. Rousseau, "Enhanced Strobe Correlator Multipath Rejection for Code & Carrier ," in *Proceedings of the 10th International Technical Meeting of the Satellite Division of The Institute of Navigation (ION GPS 1997)*, Kansas City, MO, Sep. 1996, pp. 657–664.

[94] B. Townsend and P. Fenton, "A Practical Approach to the Reduction of Pseudorange Multipath Errors in a L1 GPS Receiver," in *Proceedings of the ION GPS*, Salt Lake City, UT, Sep. 1994, pp. 143–148.

[95] L. R. Weill, "Multipath mitigation using modernized GPS signals : How good can it get ?" in *Proceedings of the ION GPS/GNSS*, Portland, OR, Sep. 2002, pp. 24–27.

[96] I. Guvenc and C. C. Chong, "A Survey on TOA Based Wireless Localization and NLOS Mitigation Techniques," *IEEE Communications Surveys Tutorials*, vol. 11, no. 3, pp. 107–124, rd 2009.

[97] J. Riba and A. Urruela, "A non-line-of-sight mitigation technique based on ML-detection," in *2004 IEEE International Conference on Acoustics, Speech, and Signal Processing*, vol. 2, May 2004, pp. ii–153–6 vol.2.

[98] S. Gezici and Z. Sahinoglu, "UWB geolocation techniques for IEEE 802.15. 4a personal area networks," *MERL Technical report*, 2004.

[99] K. Yu and Y. J. Guo, "NLOS Error Mitigation for Mobile Location Estimation in Wireless Networks," in *2007 IEEE 65th Vehicular Technology Conference - VTC2007-Spring*, April 2007, pp. 1071–1075.

[100] L. Cong and W. Zhuang, "Non-line-of-sight error mitigation in mobile location," *IEEE Transactions on Wireless Communications*, vol. 4, no. 2, pp. 560–573, March 2005.

[101] X. Wang, Z. Wang, and B. O'Dea, "A TOA-based location algorithm reducing the errors due to non-line-of-sight (NLOS) propagation," in *IEEE 54th Vehicular Technology Conference. VTC Fall 2001. Proceedings (Cat. No.01CH37211)*, vol. 1, 2001, pp. 97–100 vol.1.

[102] S. Yousefi, X. W. Chang, and B. Champagne, "An Improved Extended Kalman Filter for Localization of a Mobile Node with NLOS Anchors," in *In Proceedings of the Ninth International Conference on Wireless and Mobile Communications (ICWMC)*, 2013, pp. 25–30.

[103] ——, “Mobile Localization in Non-Line-of-Sight Using Constrained Square-Root Unscented Kalman Filter,” *IEEE Transactions on Vehicular Technology*, vol. 64, no. 5, pp. 2071–2083, May 2015.

[104] S. Venkatesh and R. M. Buehrer, “NLOS Mitigation Using Linear Programming in Ultrawideband Location-Aware Networks,” *IEEE Transactions on Vehicular Technology*, vol. 56, no. 5, pp. 3182–3198, Sept 2007.

[105] Y.-T. Chan, W.-Y. Tsui, H.-C. So, and P. chung Ching, “Time-of-arrival based localization under NLOS conditions,” *IEEE Transactions on Vehicular Technology*, vol. 55, no. 1, pp. 17–24, Jan 2006.

[106] S. Mohiuddin, D. E. Gustafson, and Y. Rachlin, “Mitigating the Effects of GNSS Multipath with a Coded Filter,” in *n Proceedings of the 24th International Technical Meeting of The Satellite Division of the Institute of Navigation (ION GNSS 2011)*, 2011.

[107] C. Satirapod and C. Rizos, “Multipath Mitigation by Wavelet Analysis for GPS Base Station Applications,” *Survey Review*, vol. 38, no. 295, pp. 2–10, 2005.

[108] G. Wang, K. de Jong, Q. Zhao, Z. Hu, and J. Guo, “Multipath analysis of code measurements for beidou geostationary satellites,” *GPS Solutions*, vol. 19, no. 1, pp. 129–139, 2015.

[109] M. Wang, H. Chai, J. Liu, and A. Zeng, “BDS relative static positioning over long baseline improved by GEO multipath mitigation,” *Advances in Space Research*, vol. 57, pp. 782–793, Feb. 2016.

[110] R. Ercek, P. De Doncker, and F. Grenez, “Statistical determination of the PR error due to NLOS-Multipath in urban canyons,” in *Proc. of the ION GNSS 2006*, 2006, conference : (Sept. 2006 : Fort Worth, USA).

[111] ——, “Statistical study of NLOS-Multipath in Urban Canyons,” *European journal of navigation*, vol. 4, no. 3, pp. 41–48, 2006.

[112] A. Wieser, M. Gaggl, and H. Hartinger, “Improved Positioning Accuracy with High-Sensitivity GNSS Receivers and SNR Aided Integrity Monitoring of Pseudo-Range Observations ,” in *Proceedings of the 18th International Technical Meeting of the Satellite Division of The Institute of Navigation (ION GNSS 2005).*

[113] D. F. Nahimana, E. Duflos, and J. Marais, “Reception state estimation of GNSS satellites in urban environment using particle filtering,” in *2008 11th International Conference on Information Fusion*, June 2008, pp. 1–5.

[114] Q. Wang, I. Balasingham, M. Zhang, and X. Huang, “Improving RSS-Based Ranging in LOS-NLOS Scenario Using GMMs,” *IEEE Communications Letters*, vol. 15, no. 10, pp. 1065–1067, 2011.

[115] N. Viandier, J. Marais, A. Rabaoui, and D. Duflos, “GNSS pseudorange error density tracking using dirichlet process mixture,” in *13th Conference on Information Fusion, FUSION 2010, Edinburgh, UK, July 26-29, 2010*, 2010, pp. 1–7.

[116] A. Rabaoui, N. Viandier, E. Duflos, J. Marais, and P. Vanheeghe, “Dirichlet Process Mixtures for Density Estimation in Dynamic Nonlinear Modeling : Application to GPS Positioning in Urban Canyons,” *IEEE Transactions on Signal Processing*, vol. 60, no. 4, pp. 1638–1655, April 2012.

[117] T. Jia and R. M. Buehrer, "Collaborative position location with NLOS mitigation," in *2010 IEEE 21st International Symposium on Personal, Indoor and Mobile Radio Communications Workshops*, Sept 2010, pp. 267–271.

[118] I. Guvenc, C. C. Chong, and F. Watanabe, "NLOS Identification and Mitigation for UWB Localization Systems," in *2007 IEEE Wireless Communications and Networking Conference*, March 2007, pp. 1571–1576.

[119] K. A. Bin Ahmad, M. Sahmoudi, and C. Macabiau, "Characterization of GNSS Receiver Position Errors for User Integrity Monitoring in Urban Environments," in *ENC-GNSS 2014, European Navigation Conference*, Rotterdam, Netherlands, 2014.

[120] J. Rife, T. Walter, and J. Blanch, "Overbounding SBAS and GBAS error distributions with excess-mass functions," in *Proceedings of the International Symposium on GNSS/GPS*, Sydney, Australia, December 2004.

[121] C. Shively and R. Braff, "An overbound concept for pseudorange error from the LAAS ground facility," in *Proceedings of Institute of Navigation Annual Meeting*, June 2000.

[122] J. Rife, S. Pullen, B. Pervan, and P. Enge, "Core overbounding and its implications for LAAS integrity," in *Proceedings of ION GNSS*, September 2004.

[123] P. J. Huber, "Robust regression : asymptotics, conjectures and Monte Carlo," *The Annals of Statistics*, pp. 799–821, 1973.

[124] C.-S. Chen, "A non-line-of-sight error mitigation method for location estimation," *International Journal of Distributed Sensor Networks*, vol. 13, no. 1, p. 1550147716682739, 2017.

[125] X. Li, "An iterative nlos mitigation algorithm for location estimation in sensor networks," *Proceedings of the15 th IST Mobile and Wireless Communications Summit*, pp. 1–5, 2006.

[126] Y. Gao, "A new algorithm of Receiver Autonomous Integrity Monitoring (RAIM) for GPS navigation," *ION GPS-91*, 1991.

[127] A. H. Mohamed, "Robust and reliable Kalman filtering of GPS data," in *ION GPS-96*, 1996, pp. 1441–1450.

[128] P. Petrus, "Robust Huber adaptive filter," *IEEE Transactions on Signal Processing*, vol. 47, no. 4, pp. 1129–1133, 1999.

[129] K. D. Rao, M. Swamy, and E. Plotkin, "GPS navigation with increased immunity to modeling errors," *IEEE transactions on aerospace and electronic systems*, vol. 40, no. 1, pp. 2–11, 2004.

[130] G.-L. Sun and W. Guo, "Bootstrapping M-estimators for reducing errors due to non-line-of-sight (NLOS) propagation," *IEEE Communications Letters*, vol. 8, no. 8, pp. 509–510, 2004.

[131] T. Delaporte, R. J. Landry, M. Sahmoudi, and J. Guay, "A robust RTK software for high-precision GPS positioning," in *Proc. Eur. Navigation Conf., ENC-GNSS*, 2008.

[132] T. Perala, *Robust Kalman-type filtering in positioning applications.* INTECH Open Access Publisher, 2010.

[133] D. A. Medina, M. Romanovas, I. Herrera-Pinzón, and R. Ziebold, "Robust position and velocity estimation methods in integrated navigation systems for inland water applications," in *Position, Location and Navigation Symposium (PLANS), 2016 IEEE/ION*. IEEE, 2016, pp. 491–501.

[134] A. Wieser and F. K. Brunner, "An extended weight model for GPS phase observations," *Earth, planets and space*, vol. 52, no. 10, pp. 777–782, 2000.

[135] H. Hartinger and F. Brunner, "Variances of GPS phase observations : the SIGMA-ϵ model," *GPS solutions*, vol. 2, no. 4, pp. 35–43, 1999.

[136] H. Kuusniemi, G. Lachapelle, and J. Takala, "Reliability in personal positioning," in *CD-ROM Proceedings of GNSS 2004 Conference, Rotterdam (16-19 May)*, 2004.

[137] S. Tay and J. Marais, "Weighting models for GPS Pseudorange observations for land transportation in urban canyons," in *6th European Workshop on GNSS Signals and Signal Processing*, 2013, p. 4p.

[138] P. C. Fenton and J. Jones, "The theory and performance of NovAtel Inc.'s Vision Correlator," in *Proceedings of the ION GPS/GNSS 2005*, Palm Springs, CA, Sep. 2005.

[139] R. D. Van Nee, J. Siereveld, P. C. Fenton, and B. R. Townsend, "The multipath estimating delay lock loop : approaching theoretical accuracy limits," in *Position Location and Navigation Symposium, 1994., IEEE*, 1994, pp. 246–251.

[140] M. Lentmaier and B. Krach, "Maximum likelihood multipath estimation in comparison with conventional delay lock loops," in *The 19th International Technical Meeting of the Institute of Navigation Satellite Division, ION GNSS 2006*. The Institute of Navigation, USA, 2006.

[141] M. Z. H. Bhuiyan, E. S. Lohan, and M. Renfors, "Code tracking algorithms for mitigating multipath effects in fading channels for satellite-based positioning," *EURASIP Journal on Advances in Signal Processing*, vol. 2008, no. 1, p. 863629, 2007.

[142] B. Daniele, "A statistical theory for GNSS signal acquisition," Ph.D. dissertation, Dissertation : University of Calgary. Google Scholar, 2008.

[143] M. Lentmaier, B. Krach, P. Robertson, and T. Thiasiriphet, "Dynamic multipath estimation by sequential monte carlo methods," in *The 20th International Technical Meeting of the Institute of Navigation Satellite Division, ION GNSS 2007*. The Institute of Navigation, USA, 2007.

[144] M. Lentmaier, B. Krach, and P. Robertson, "Bayesian time delay estimation of gnss signals in dynamic multipath environments," *International Journal of Navigation and Observation*, vol. 2008, 2008.

[145] B. Krach, M. Lentmaier, and P. Robertson, "Joint Bayesian positioning and multipath mitigation in GNSS," in *Acoustics, Speech and Signal Processing, 2008. ICASSP 2008. IEEE International Conference on*. IEEE, 2008, pp. 3437–3440.

[146] H. Saarnisaari and V. Tapio, "A simple multipath delay estimator based on alternating projection algorithm," in *Position, Location, And Navigation Symposium, 2006 IEEE/ION*. IEEE, 2006, pp. 1086–1093.

[147] A. Giremus, J.-Y. Tourneret, and V. Calmettes, “A particle filtering approach for joint detection/estimation of multipath effects on gps measurements,” *IEEE Transactions on Signal Processing*, vol. 55, no. 4, pp. 1275–1285, 2007.

[148] M. Nájar, J. M. Huerta, J. Vidal, and J. A. Castro, “Mobile location with bias tracking in non-line-of-sight,” in *Acoustics, Speech, and Signal Processing, 2004. Proceedings.(ICASSP'04). IEEE International Conference on*, vol. 3. IEEE, 2004, pp. iii–956.

[149] J. Marais, D.-F. Nahimana, N. Viandier, and E. Duflos, “GNSS accuracy enhancement based on pseudo range error estimation in an urban propagation environment,” *Expert systems with applications*, vol. 40, no. 15, pp. 5956–5964, 2013.

[150] J. M. Huerta, J. Vidal, A. Giremus, and J.-Y. Tourneret, “Joint particle filter and ukf position tracking in severe non-line-of-sight situations,” *IEEE Journal of Selected Topics in Signal Processing*, vol. 3, no. 5, pp. 874–888, 2009.

[151] D. E. Gustafson, J. M. Elwell, and J. A. Soltz, “Innovative indoor geolocation using RF multipath diversity,” in *Proc. 2006 IEEE/ION Position Location and Navigation Symp.* Citeseer, 2006, pp. 904–912.

[152] A. Soloviev and F. van Graas, “Utilizing multipath reflections in deeply integrated GPS/INS architecture for navigation in urban environments,” in *Position, Location and Navigation Symposium, 2008 IEEE/ION.* IEEE, 2008, pp. 383–393.

[153] P. Delmas, C. Debain, R. Chapuis, and C. Tessier, “Reliable Localization Systems including GNSS Bias Correction,” in *Robot Localization and Map Building.* InTech, 2010.

[154] P. Delmas, C. Tessier, C. Debain, and R. Chapuis, “GNSS bias correction for localization systems,” in *Information Fusion, 2008 11th International Conference on.* IEEE, 2008, pp. 1–6.

[155] L. Wang, P. D. Groves, and M. K. Ziebart, “GNSS shadow matching : Improving urban positioning accuracy using a 3D city model with optimized visibility scoring scheme,” *Navigation*, vol. 60, no. 3, pp. 195–207, 2013.

[156] T. Chapuis, B. Bonhoure, F. Lacoste, C. Boulanger, D. Lapeyre, K. Urbanska, P. Noirat, and A. Marion, “SPRING simulator A powerful 3D computing engine toward urban canyons modelling,” in *Satellite Navigation Technologies and European Workshop on GNSS Signals and Signal Processing,(NAVITEC), 2012 6th ESA Workshop on.* IEEE, 2012, pp. 1–8.

[157] P. D. Groves, “Shadow Matching : A New GNSS Positioning Technique for Urban Canyons,” *Journal of Navigation*, vol. 64, no. 3, 2011.

[158] M. Adjrad and P. D. Groves, “Intelligent Urban Positioning using Shadow Matching and GNSS Ranging aided by 3D Mapping,” in *Proceedings of ION GNSS+ 2016*, Portland, September 2016.

[159] J. T. Isaacs, A. T. Irish, F. Quitin, U. Madhow, and J. P. Hespanha, “Bayesian localization and mapping using GNSS SNR measurements,” in *Position, Location and Navigation Symposium-PLANS 2014, 2014 IEEE/ION.* IEEE, 2014, pp. 445–451.

[160] E. Takeuchi, M. Yamazaki, K. Ohno, and S. Tadokoro, “GPS measurement model with satellite visibility using 3d map for particle filter,” in *Robotics and Biomimetics (ROBIO), 2011 IEEE International Conference on.* IEEE, 2011, pp. 590–595.

[161] A. Irish, J. Isaacs, D. Iland, J. Hespanha, E. Belding, and U. Madhow, "Demo : ShadowMaps, the urban phone tracking system," in *Proceedings of the 20th annual international conference on Mobile computing and networking.* ACM, 2014, pp. 283–286.

[162] L. Wang, P. D. Groves, and M. K. Ziebart, "Urban positioning on a smartphone : Real-time shadow matching using GNSS and 3D city models." The Institute of Navigation, 2013.

[163] S. Ramalingam, S. Bouaziz, P. Sturm, and M. Brand, "Skyline2gps : Localization in urban canyons using omni-skylines," in *International Conference on Intelligent Robots and Systems.* IEEE, 2010, pp. 3816–3823.

[164] T. Suzuki and N. Kubo, "GNSS Photo Matching : Positioning using GNSS and Camera in Urban Canyon," in *Proceedings of the 28th International Technical Meeting of The Satellite Division of the Institute of Navigation (ION GNSS+ 2015)*, Tampa, Florida, September 2015.

[165] R. Kumar and M. G. Petovello, "A novel GNSS positioning technique for improved accuracy in urban canyon scenarios using 3D city model," in *Proceedings of the 27th International Technical Meeting of the Satellite Division of the Institute of Navigation (ION GNSS+ 2014), Tampa, FL, USA*, vol. 812, 2014, p. 21392148.

[166] T. Suzuki and N. Kubo, "Correcting GNSS multipath errors using a 3D surface model and particle filter," *Proc. ION GNSS+ 2013*, 2013.

[167] S. Miura, S. Hisaka, and S. Kamijo, "GPS multipath detection and rectification using 3D maps," in *16th International IEEE Conference on Intelligent Transportation Systems-(ITSC), 2013.* IEEE, 2013, pp. 1528–1534.

[168] L.-T. Hsu, Y. Gu, and S. Kamijo, "3D building model-based pedestrian positioning method using GPS/GLONASS/QZSS and its reliability calculation," *GPS solutions*, vol. 20, no. 3, pp. 413–428, 2016.

[169] A. Bourdeau, M. Sahmoudi, and J.-Y. Tourneret, "Constructive use of GNSS NLOS-multipath : Augmenting the navigation Kalman filter with a 3D model of the environment," in *15th International Conference on Information Fusion (FUSION), 2012.* IEEE, 2012, pp. 2271–2276.

[170] D. Betaille, F. Peyret, M. Ortiz, S. Miquel, and L. Fontenay, "A new modeling based on urban trenches to improve GNSS positioning quality of service in cities," *IEEE Intelligent Transportation Systems Magazine*, vol. 5, no. 3, pp. 59–70, 2013.

[171] D. Bétaille, F. Peyret, M. Ortiz, S. Miquel, and F. Godan, "Improving accuracy and integrity with a probabilistic Urban Trench modeling," *Navigation*, vol. 63, no. 3, pp. 283–294, 2016.

[172] D. Bétaille, "Paving the way for future use of the Urban Trench model along with a lane level road map," in *Navigation Conference (ENC), 2017 European.* IEEE, 2017, pp. 143–149.

[173] Y. Ng and G. X. Gao, "Direct Position Estimation Utilizing Non-Line-of-Sight (NLOS) GPS Signals," in *Proceedings of the 29th International Technical Meeting of The Satellite Division of the Institute of Navigation (ION GNSS+ 2016).*

[174] P. D. Groves, L. Wang, M. Adjrad, and C. Ellul, “Gnss shadow matching : The challenges ahead.” The Institute of Navigation, 2015.

[175] H. Durrant-Whyte and T. Bailey, “Simultaneous localization and mapping : part I,” *IEEE robotics & automation magazine*, vol. 13, no. 2, pp. 99–110, 2006.

[176] C. Gentner, R. Pöhlmann, M. Ulmschneider, T. Jost, and A. Dammann, “Multipath assisted positioning for pedestrians,” 2015.

[177] C. Gentner, B. Ma, M. Ulmschneider, T. Jost, and A. Dammann, “Simultaneous localization and mapping in multipath environments,” in *Position, Location and Navigation Symposium (PLANS), 2016 IEEE/ION*. IEEE, 2016, pp. 807–815.

[178] B. Ben-Moshe, E. Elkin, H. Levi, and A. Weissman, “Improving Accuracy of GNSS Devices in Urban Canyons,” in *CCCG*, 2011, pp. 511–515.

[179] A. Weissman, B. Ben-Moshe, H. Levi, and R. Yozevitch, “2.5 D mapping using GNSS signal analysis,” in *Positioning Navigation and Communication (WPNC), 2013 10th Workshop on*. IEEE, 2013, pp. 1–6.

[180] Y. Gu, Y. Wada, L.-T. Hsu, and S. Kamijo, “SLAM with 3Dimensional-GNSS,” in *Position, Location and Navigation Symposium (PLANS), 2016 IEEE/ION*. IEEE, 2016, pp. 190–197.

[181] S. Zhu, M. Pressigout, M. Servieres, L. Morin, and G. Moreau, “Skyline Matching : A robust registration method between Video and GIS,” in *Usage, Usability, and Utility of 3D City Models–European COST Action TU0801*. EDP Sciences, 2012, p. 03007.

[182] L.-T. Hsu, Y. Wada, Y. Gu, and S. Kamijo, “A Study of City Building Model Based Positioning Method using Multi-GNSS in Deep Urban Canyon,” in *Proc. European Navigation Conference (ENC 2015), Bordeaux, France*, 2015.

[183] T. Suzuki, “Integration of GNSS Positioning and 3D Map using Particle Filter,” in *Proceedings of the 29th International Technical Meeting of The Satellite Division of the Institute of Navigation (ION GNSS+ 2016)*, September 2016.

[184] L.-T. Hsu, Y. Gu, and S. Kamijo, “Autonomous driving positioning using building model and DGNSS,” in *European Navigation Conference (ENC),*. IEEE, 2016, pp. 1–7.

[185] R. G. Brown, “Receiver autonomous integrity monitoring,” *Global Positioning System : Theory and applications.*, vol. 2, pp. 143–165, 1996.

[186] A. Martineau, C. Macabiau, I. Nikiforov, and B. Roturier, “Performance of receiver autonomous integrity monitoring (RAIM) for vertically guided approaches,” in *ENC-GNSS 2008, Europpean Navigation Conference*, 2008.

[187] N. Kbayer, M. Sahmoudi, and E. Chaumette, “Robust GNSS Navigation in Urban Environments by Bounding NLOS Bias of GNSS Pseudoranges Using a 3D City Model ,” in *Proceeding of ION GNSS 2015*, September 2015.

[188] J. Breßler, P. Reisdorf, M. Obst, and G. Wanielik, “GNSS positioning in non-line-of-sight context—A survey,” in *19th International Conference on Intelligent Transportation Systems (ITSC)*. IEEE, 2016, pp. 1147–1154.

[189] P. D. Groves, “The PNT boom : Future trends in integrated navigation,” *Inside GNSs*, vol. 8, no. 2, pp. 44–49, 2013.

[190] T. Chapuis, B. Bonhoure, , S. Rougerie, F. Lacoste, T. Grelier, D. Lapeyre, and P. Noirat, "SPRING : A Powerful 3D GNSS Simulator for Constraint Environment," in *Proceedings of the 27th International Technical Meeting of The Satellite Division of the Institute of Navigation (ION GNSS+ 2014)*, September 2014, pp. 454 – 465.

[191] G. Gröger, T. H. Kolbe, A. Czerwinski, and C. Nagel, "OpenGIS city geography markup language (CityGML) encoding standard," *Open Geospatial Consortium Inc*, pp. 1–234, 2008.

[192] B. Dalton and M. Parfitt, "Immersive visualization of building information models," *Design Innovation Research Center Working Paper*, vol. 6, no. 1.0, 2013.

[193] A. S. Glassner, *An introduction to ray tracing.* Elsevier, 1989.

[194] "Nvidia optix ray tracing engine," https://developer.nvidia.com/optix, accessed : 2017-11-25.

[195] "Nvidia scenix," http://www.nvidia.com/object/scenix.html, accessed : 2017-11-25.

[196] M. Ait-Ighil, "Enhanced Physical Statistical Simulator of the Land Mobile Satellite Channel for Multipath Modelling Applied to Satellite Navigation Systems," 2013.

[197] M. Ait-Ighil, J. Lemorton, F. Pérez-Fontán, F. Lacoste, G. Artaud, C. Bourga, and M. Bousquet, "Simplifying the propagation environment representation for LMS channel modelling," *EURASIP Journal on Wireless Communications and Networking*, vol. 2012, no. 1, p. 110, 2012.

[198] J. Bradbury, "Prediction of urban GNSS availability and signal degradation using virtual reality city models," in *Proceedings of the 20th International Technical Meeting of the Satellite Division of The Institute of Navigation (ION GNSS 2007)*, 2007, pp. 2696–2706.

[199] A. Bourdeau, M. Sahmoudi, and J.-Y. Tourneret, "Prediction of GNSS Signal Bias Using a 3D Model in Urban Environments," in *Proc. European Navigation Conference (ENC 2012)*, 2013.

[200] M. Spangenberg, "Safe navigation for vehicles." Thèse de doctorat, Institut National Polytechnique de Toulouse, Toulouse, France, juin 2009.

[201] "Matlab quadprog function," https://fr.mathworks.com/help/optim/ug/quadprog.html, accessed : 2017-11-25.

[202] N. Kbayer, M. Sahmoudi, H. Ortega, and C. Rouch, "Approximate Maximum Likelihood Estimation Using a 3D GNSS Simulator for Positioning in MP/NLOS Conditions," in *Proceeding of ION GNSS+ 2017*, September 2017.

[203] ——, "Position Matching Estimation Using 3D Simulator for GNSS Positioning in Multipath/Non-Line-Of-Sight Environments," in *Proceeding of ITNST 2017*, November 2017.

[204] H. Cramir, "Mathematical methods of statistics," *Princeton U. Press, Princeton*, 1946.

[205] E. L. Lehmann and G. Casella, *Theory of point estimation.* Springer Science & Business Media, 2006.

[206] F. Vincent, E. Chaumette, C. Charbonnieras, J. Israel, M. Aubault, and F. Barbiero, "Asymptotically efficient GNSS trilateration," *Signal Processing*, vol. 133, pp. 270–277, 2017.

[207] P. Stoica and A. Nehorai, “Performance study of conditional and unconditional direction-of-arrival estimation,” *IEEE Transactions on Acoustics, Speech, and Signal Processing*, vol. 38, no. 10, pp. 1783–1795, 1990.

[208] C. Ren, J. Galy, E. Chaumette, P. Larzabal, and A. Renaux, “Hybrid barankin–weiss–weinstein bounds,” *IEEE Signal Processing Letters*, vol. 22, no. 11, pp. 2064–2068, 2015.

[209] C. Ren, J. Le Kernec, J. Galy, E. Chaumette, P. Larzabal, and A. Renaux, “A constrained hybrid cramér-rao bound for parameter estimation,” in *Acoustics, Speech and Signal Processing (ICASSP), 2015 IEEE International Conference on*. IEEE, 2015, pp. 3472–3476.

[210] I. Reuven and H. Messer, “A barankin-type lower bound on the estimation error of a hybrid parameter vector,” *IEEE Transactions on Information Theory*, vol. 43, no. 3, pp. 1084–1093, 1997.

[211] K. Todros and J. Tabrikian, “Hybrid lower bound via compression of the sampled CLR function,” in *Statistical Signal Processing, 2009. SSP’09. IEEE/SP 15th Workshop on*. IEEE, 2009, pp. 602–605.

[212] H. L. Van Trees, “Detection, estimation and modulation theory,” 1968.

[213] R. Miller and C. Chang, “A modified Cramér-Rao bound and its applications (Corresp.),” *IEEE Transactions on Information theory*, vol. 24, no. 3, pp. 398–400, 1978.

[214] Y. Rockah and P. Schultheiss, “Array shape calibration using sources in unknown locations–Part I : Far-field sources,” *IEEE Transactions on Acoustics, Speech, and Signal Processing*, vol. 35, no. 3, pp. 286–299, 1987.

[215] A. N. D’Andrea, U. Mengali, and R. Reggiannini, “The modified Cramer-Rao bound and its application to synchronization problems,” *IEEE Transactions on Communications*, vol. 42, no. 234, pp. 1391–1399, 1994.

[216] E. Barankin, “Locally best unbiased estimates,” *The Annals of Mathematical Statistics*, pp. 477–501, 1949.

[217] C. R. Blyth, “Necessary and sufficient conditions for inequalities of cramér-rao type,” *The Annals of Statistics*, pp. 464–473, 1974.

[218] J. S. Abel, “A bound on mean-square-estimate error,” *IEEE Transactions on Information Theory*, vol. 39, no. 5, pp. 1675–1680, 1993.

[219] F. Glave, “A new look at the barankin lower bound,” *IEEE Transactions on Information Theory*, vol. 18, no. 3, pp. 349–356, 1972.

[220] E. Chaumette, J. Galy, A. Quinlan, and P. Larzabal, “A new barankin bound approximation for the prediction of the threshold region performance of maximum likelihood estimators,” *IEEE Transactions on Signal Processing*, vol. 56, no. 11, pp. 5319–5333, 2008.

[221] E. Chaumette, A. Renaux, and P. Larzabal, “Lower bounds on the mean square error derived from mixture of linear and non-linear transformations of the unbiasness definition,” in *Acoustics, Speech and Signal Processing, 2009. ICASSP 2009. IEEE International Conference on*. IEEE, 2009, pp. 3045–3048.

[222] P. Forster and P. Larzabal, “On lower bounds for deterministic parameter estimation,” in *Acoustics, Speech, and Signal Processing (ICASSP), 2002 IEEE International Conference on*, vol. 2. IEEE, 2002, pp. II–1137.

[223] F. Gini, R. Reggiannini, and U. Mengali, “The modified Cramer-Rao bound in vector parameter estimation,” *IEEE Transactions on Communications*, vol. 46, no. 1, pp. 52–60, 1998.

[224] Y. Noam and H. Messer, “Notes on the tightness of the hybrid cramér–rao lower bound,” *IEEE Transactions on Signal Processing*, vol. 57, no. 6, pp. 2074–2084, 2009.

[225] K. Todros and J. Tabrikian, “General classes of performance lower bounds for parameter estimation—Part I : Non-Bayesian bounds for unbiased estimators,” *IEEE Transactions on Information Theory*, vol. 56, no. 10, pp. 5045–5063, 2010.

[226] ——, “Uniformly best biased estimators in non-bayesian parameter estimation,” *IEEE Transactions on Information Theory*, vol. 57, no. 11, pp. 7635–7647, 2011.

[227] D. G. Luenberger, *Optimization by vector space methods.* John Wiley & Sons, 1969.

[228] R. McAulay and L. Seidman, “A useful form of the Barankin lower bound and its application to PPM threshold analysis,” *IEEE Transactions on Information Theory*, vol. 15, no. 2, pp. 273–279, 1969.

[229] J. Hammersley, “On estimating restricted parameters,” *Journal of the Royal Statistical Society. Series B (Methodological)*, vol. 12, no. 2, pp. 192–240, 1950.

[230] D. G. Chapman and H. Robbins, “Minimum variance estimation without regularity assumptions,” *The Annals of Mathematical Statistics*, pp. 581–586, 1951.

[231] T. Menni, E. Chaumette, P. Larzabal, and J. P. Barbot, “New results on deterministic cramér–rao bounds for real and complex parameters,” *IEEE Transactions on Signal Processing*, vol. 60, no. 3, pp. 1032–1049, 2012.

[232] D. Fraser and I. Guttman, “Bhattacharyya bounds without regularity assumptions,” *The Annals of Mathematical Statistics*, pp. 629–632, 1952.

[233] A. Bhattacharyya, “On some analogues of the amount of information and their use in statistical estimation,” *Sankhyā : The Indian Journal of Statistics*, pp. 1–14, 1946.

[234] F. Lu and J. V. Krogmeier, “Modified bhattacharyya bounds and their application to timing estimation,” in *Wireless Communications and Networking Conference, 2002. WCNC2002. 2002 IEEE*, vol. 1. IEEE, 2002, pp. 244–248.

[235] R. McAulay and E. Hofstetter, “Barankin bounds on parameter estimation,” *IEEE Transactions on Information Theory*, vol. 17, no. 6, pp. 669–676, 1971.

[236] D. Rife and R. Boorstyn, “Single tone parameter estimation from discrete-time observations,” *IEEE Transactions on information theory*, vol. 20, no. 5, pp. 591–598, 1974.

[237] F. Athley, “Threshold region performance of maximum likelihood direction of arrival estimators,” *IEEE Transactions on Signal Processing*, vol. 53, no. 4, pp. 1359–1373, 2005.

[238] C. D. Richmond, “Capon algorithm mean-squared error threshold snr prediction and probability of resolution,” *IEEE Transactions on Signal Processing*, vol. 53, no. 8, pp. 2748–2764, 2005.

[239] J. Tabrikian and J. L. Krolik, “Barankin bounds for source localization in an uncertain ocean environment,” *IEEE Transactions on Signal Processing*, vol. 47, no. 11, pp. 2917–2927, 1999.

[240] M. Viberg and B. Ottersten, “Sensor array processing based on subspace fitting,” *IEEE Transactions on signal processing*, vol. 39, no. 5, pp. 1110–1121, 1991.

[241] T. Ho, J. McWhirter, A. Nehorai, U. Nickel, B. Ottersten, B. Steinberg, P. Stoica, M. Viberg, and Z. Zhu, *Radar array processing.* Springer Science & Business Media, 2013, vol. 25.

[242] J. Li and R. Compton, “Maximum likelihood angle estimation for signals with known waveforms,” *IEEE Transactions on Signal Processing*, vol. 41, no. 9, pp. 2850–2862, 1993.

[243] A. Renaux, P. Forster, E. Chaumette, and P. Larzabal, “On the high-SNR conditional maximum-likelihood estimator full statistical characterization,” *IEEE Transactions on Signal Processing*, vol. 54, no. 12, pp. 4840–4843, 2006.

[244] A. Yeredor, “The joint MAP-ML criterion and its relation to ML and to extended least-squares,” *IEEE Transactions on Signal Processing*, vol. 48, no. 12, pp. 3484–3492, 2000.

[245] H. L. Van Trees and K. L. Bell, “Bayesian bounds for parameter estimation and nonlinear filtering/tracking,” *AMC*, vol. 10, p. 12, 2007.

[246] A. P. Dempster, N. M. Laird, and D. B. Rubin, “Maximum likelihood from incomplete data via the EM algorithm,” *Journal of the royal statistical society. Series B (methodological)*, pp. 1–38, 1977.

[247] C. J. Wu, “On the convergence properties of the EM algorithm,” *The Annals of statistics*, pp. 95–103, 1983.

[248] G. McLachlan and T. Krishnan, *The EM algorithm and extensions.* John Wiley & Sons, 2007, vol. 382.

[249] F. Gini and R. Reggiannini, “On the use of Cramer-Rao-like bounds in the presence of random nuisance parameters,” *IEEE Transactions on Communications*, vol. 48, no. 12, pp. 2120–2126, 2000.

[250] S. Bay, B. Geller, A. Renaux, J.-P. Barbot, and J.-M. Brossier, “On the hybrid cramer rao bound and its application to dynamical phase estimation,” *IEEE Signal Processing Letters*, vol. 15, pp. 453–456, 2008.

[251] N. Kbayer, J. Galy, E. Chaumette, F. Vincent, A. Renaux, and P. Larzabal, “On lower bounds for nonstandard deterministic estimation,” *IEEE Transactions on Signal Processing*, vol. 65, no. 6, pp. 1538–1553, 2017.

[252] R. Palama, M. Greco, P. Stinco, and F. Gini, “Statistical analysis of netrad high resolution sea clutter,” in *Signal Processing Conference (EUSIPCO), 2013 Proceedings of the 21st European.* IEEE, 2013, pp. 1–5.

[253] N. Kbayer and M. Sahmoudi, “Performances Analysis of GNSS NLOS Bias Correction in Urban Environment Using a 3D City Model and GNSS Simulator,” *IEEE Transactions on Aerospace and Electronic Systems, Accepted for publication*, vol. -, no. -, pp. –, 2018.

[254] E. Weinstein and A. J. Weiss, "A general class of lower bounds in parameter estimation," *IEEE Transactions on Information Theory*, vol. 34, no. 2, pp. 338–342, 1988.

[255] H. Messer and Y. Adar, "New lower bounds on frequency estimation of a multitone random signal in noise," *Signal processing*, vol. 18, no. 4, pp. 413–424, 1989.

Appendix : Multipath and NLOS Reception : Theoretical Consideration

In this paragraph, we will mathematically demonstrate the adverse effect of MP/NLOS phenomena on user position estimation using GNSS signals. First, for ease of notation, throughout this dissertation, the MP/NLOS bias will be denoted simply as $\mathbf{b} = \mathbf{b}_{MP-NLOS}$. Let us define the following scalar product related to the noise covariance matrix $\mathbf{R}$ and its corresponding norm as :

$$\forall \mathbf{a}, \mathbf{c} \in \mathbb{R}^N,\ \langle \mathbf{a}, \mathbf{c} \rangle_{\mathbf{R}^{-1}} = \mathbf{a}^T \mathbf{R}^{-1} \mathbf{c}; \qquad \forall \mathbf{a} \in \mathbb{R}^N,\ \|\mathbf{a}\|^2_{\mathbf{R}^{-1}} = \mathbf{a}^T \mathbf{R}^{-1} \mathbf{a} \tag{A.1}$$

Let $\mathbf{H}^\perp$ be the subspace orthogonal to $\mathbf{H}$ with regard to the scalar product (A.1). We can define the orthogonal projection on the observation matrix $\mathbf{H}$ and on the subspace orthogonal $\mathbf{H}^\perp$ with regard to this scalar product as :

$$\forall \mathbf{a} \in \mathbb{R}^N,\ \Pi^{\mathbf{H}}_{\mathbf{R}^{-1}} \mathbf{a} = \mathbf{H}(\mathbf{H}^T \mathbf{R}^{-1} \mathbf{H})^{-1} \mathbf{H}^T \mathbf{R}^{-1} \mathbf{a}; \qquad \forall \mathbf{a} \in \mathbb{R}^N,\ \Pi^{\mathbf{H}^\perp}_{\mathbf{R}^{-1}} \mathbf{a} = \mathbf{a} - \Pi^{\mathbf{H}}_{\mathbf{R}^{-1}} \mathbf{a} \tag{A.2}$$

The cost function of the navigation equation (1.4) is expressed as [30] :

$$J(\mathbf{y}|\mathbf{x}, \mathbf{b}) = \|\mathbf{y} - \mathbf{H}\mathbf{x} - \mathbf{b}\|^2_{\mathbf{R}^{-1}} \tag{A.3}$$

The likelihood function can be expressed as :

$$\begin{aligned} J(\mathbf{y}|\mathbf{x}, \mathbf{b}) &= \|\mathbf{y} - \mathbf{H}\mathbf{x} - \mathbf{b}\|^2_{\mathbf{R}^{-1}} \\ &= \|\Pi^{\mathbf{H}}_{\mathbf{R}^{-1}}(\mathbf{y} - \mathbf{H}\mathbf{x} - \mathbf{b})\|^2_{\mathbf{R}^{-1}} + \|\Pi^{\mathbf{H}^\perp}_{\mathbf{R}^{-1}}(\mathbf{y} - \mathbf{H}\mathbf{x} - \mathbf{b})\|^2_{\mathbf{R}^{-1}} \\ &= \|\Pi^{\mathbf{H}}_{\mathbf{R}^{-1}}(\mathbf{y} - \mathbf{b}) - \mathbf{H}\mathbf{x}\|^2_{\mathbf{R}^{-1}} + \|\Pi^{\mathbf{H}^\perp}_{\mathbf{R}^{-1}}(\mathbf{y} - \mathbf{b})\|^2_{\mathbf{R}^{-1}} \end{aligned}$$

The maximum likelihood (ML) estimate of equation (1.4) is the state vector minimizing the previous cost function. By definition, the maximum likelihood (ML) estimator is the estimator minimizing the likelihood function :

$$\hat{\mathbf{x}}_{ML} = \underset{\mathbf{x}}{\operatorname{argmin}}\, J(\mathbf{y}|\mathbf{x}, \mathbf{b})$$

This yields the following expression for the ML estimator :

$$\begin{aligned}
\hat{\mathbf{x}}_{ML} &= \underset{\mathbf{x}}{\operatorname{argmin}}(\|\Pi^{\mathbf{H}}_{\mathbf{R}^{-1}}(\mathbf{y}-\mathbf{b}) - \mathbf{H}\mathbf{x}\|^2_{\mathbf{R}^{-1}} + \|\Pi^{\mathbf{H}^{\perp}}_{\mathbf{R}^{-1}}(\mathbf{y}-\mathbf{b})\|^2_{\mathbf{R}^{-1}}) \\
&= \underset{\mathbf{x}}{\operatorname{argmin}} \|\Pi^{\mathbf{H}}_{\mathbf{R}^{-1}}(\mathbf{y}-\mathbf{b}) - \mathbf{H}\mathbf{x}\|^2_{\mathbf{R}^{-1}} \\
&= \underset{\mathbf{x}}{\operatorname{argmin}} \|\mathbf{H}(\mathbf{H}^{+}(\mathbf{y}-\mathbf{b}) - \mathbf{x})\|^2_{\mathbf{R}^{-1}}
\end{aligned}$$

where $\mathbf{H}^{+} = (\mathbf{H}^T\mathbf{R}^{-1}\mathbf{H})^{-1}\mathbf{H}^T\mathbf{R}^{-1}$ is the pseudo-inverse of $\mathbf{H}$ weighted by the inverse of the measurements covariance matrix $\mathbf{R}$. This last expression gives the final expression of the ML estimator :

$$\hat{\mathbf{x}}_{ML} = \mathbf{H}^{+}(\mathbf{y}-\mathbf{b}) = (\mathbf{H}^T\mathbf{R}^{-1}\mathbf{H})^{-1}\mathbf{H}^T\mathbf{R}^{-1}(\mathbf{y}-\mathbf{b}) \iff \mathbf{H}\hat{\mathbf{x}}_{ML} = \Pi^{\mathbf{H}}_{\mathbf{R}^{-1}}(\mathbf{y}-\mathbf{b}) \tag{A.4}$$

The maximum likelihood state estimation is equal to the least squares solution by considering the PR measurement corrected by the MP/NLOS bias. This state estimation can be seen as a sum of a bias free-estimate computed as if no MP and NLOS bias were present and a bias-correction term. Without knowing the MP/NLOS bias value, the ML estimation of the state vector will be inaccurate. Then, we aim to estimate this MP/NLOS bias and then use this estimation to correct pseudorange measurements as in equation (A.4). The MP/NLOS bias can be estimated by minimizing the cost function (A.3) regard to $\mathbf{b}$:

$$\hat{\mathbf{b}} = \underset{\mathbf{b}}{\operatorname{argmin}}\, J(\mathbf{y}|\hat{\mathbf{x}}_{ML}, \mathbf{b}) \tag{A.5}$$

As $\|\Pi^{\mathbf{H}}_{\mathbf{R}^{-1}}(\mathbf{y}-\mathbf{b}) - \mathbf{H}\hat{\mathbf{x}}_{ML}\|^2_{\mathbf{R}^{-1}} = 0$, then :

$$\hat{\mathbf{b}} = \underset{\mathbf{b}}{\operatorname{argmin}} \|\Pi^{\mathbf{H}^{\perp}}_{\mathbf{R}^{-1}}\mathbf{y} - \Pi^{\mathbf{H}^{\perp}}_{\mathbf{R}^{-1}}\mathbf{b}\|^2_{\mathbf{R}^{-1}} \tag{A.6}$$

Let us define $\mathbf{y}_b = \Pi^{\mathbf{H}^{\perp}}_{\mathbf{R}^{-1}}\mathbf{y}$. Then, we express the MP/NLOS bias $\mathbf{b}$ projection on subspace orthogonal to the observation matrix $\mathbf{H}^{\perp}$ as :

$$\Pi^{\mathbf{H}^{\perp}}_{\mathbf{R}^{-1}}\mathbf{b} = \mathbf{H}_b\mathbf{b} \tag{A.7}$$

Where $\mathbf{H}_b = \mathbf{I}_N - \mathbf{H}\mathbf{H}^{+}$ and $\mathbf{H}^{+}$ is the pseudo-inverse matrix of matrix $\mathbf{H}$. The solution of the equation (A.6) is then given by :

$$\hat{\mathbf{b}} = (\mathbf{H}_b^T\mathbf{R}^{-1}\mathbf{H}_b)^{-1}\mathbf{H}_b^T\mathbf{R}^{-1}(\mathbf{y}_b) \tag{A.8}$$

Noting that $\mathbf{b} = \Pi^{\mathbf{H}^{\perp}}_{\mathbf{R}^{-1}}\mathbf{b} + \Pi^{\mathbf{H}}_{\mathbf{R}^{-1}}\mathbf{b}$, we conclude that what we have estimated in (A.8), in fact, the orthogonal projection of the MP/NLOS bias $\mathbf{b}$ on the subspace $\mathbf{H}^{\perp}$ since $\mathbf{y}_b$ is the orthogonal projection of $\mathbf{y}$ on this subspace. Then, we have $\hat{\mathbf{b}} = \Pi^{\mathbf{H}^{\perp}}_{\mathbf{R}^{-1}}\mathbf{b}$. Then, we can only estimate $(N-M)$ components of the MP/NLOS bias vector which is equals to the dimension of the subspace $\mathbf{H}^{\perp}$ where M denotes the size of the state vector and N is the number of PR measurements. To correctly estimate the MP/NLOS bias, we have to estimate the other components of the MP/NLOS bias $\mathbf{b}$ on the observation space $\mathbf{H}$. The error estimation in state vector ML estimate in (A.4) is equal to :

$$\delta\mathbf{x}_{ML} = \hat{\mathbf{x}}_{ML} - \mathbf{x} = \mathbf{H}^{+}\mathbf{n} \tag{A.9}$$

Where $\mathbf{n}$ is the receiver measurements noise defined in (1.4). The Mean Square Error (MSE) of this ML estimation can be expressed as :

$$\begin{aligned}\mathbf{MSE}[\hat{\mathbf{x}}_{ML}] &= E[\delta\mathbf{x}_{ML}\delta\mathbf{x}_{ML}^{T}] = E[(\mathbf{H}^{+}\mathbf{n})(\mathbf{H}^{+}\mathbf{n})^{T}] \\ &= E[\mathbf{H}^{+}\mathbf{n}\mathbf{n}^{T}(\mathbf{H}^{+})^{T}] = \mathbf{H}^{+}E[\mathbf{n}\mathbf{n}^{T}](\mathbf{H}^{+})^{T}\end{aligned}$$

As $E\{\mathbf{n}\mathbf{n}^{T}\} = \mathbf{R}$, then this yields :

$$\begin{aligned}\mathbf{MSE}[\hat{\mathbf{x}}_{ML}] &= \mathbf{H}^{+}\mathbf{R}(\mathbf{H}^{+})^{T} \\ &= (\mathbf{H}^{T}\mathbf{R}^{-1}\mathbf{H})^{-1}\mathbf{H}^{T}\mathbf{R}^{-1}\mathbf{R}\mathbf{R}^{-1}\mathbf{H}(\mathbf{H}^{T}\mathbf{R}^{-1}\mathbf{H})^{-1} \\ &= (\mathbf{H}^{T}\mathbf{R}^{-1}\mathbf{H})^{-1}\end{aligned}$$

Without estimating the MP/NLOS bias, a possible estimation of the state vector is given by the Least Squares (LS) solution in (1.5). The error of this LS estimation is given by the following :

$$\delta\mathbf{x}_{LS} = \hat{\mathbf{x}}_{LS} - \mathbf{x} = \mathbf{H}^{+}(\mathbf{n} + \mathbf{b}) \tag{A.10}$$

Using the same derivation as the MSE of the ML estimator, we can prove the MSE derivation of the LS estimator :

$$\begin{aligned}\mathbf{MSE}[\hat{\mathbf{x}}_{LS}] &= E[\delta\mathbf{x}_{LS}\delta\mathbf{x}_{LS}^{T}] \\ &= E[(\mathbf{H}^{+}(\mathbf{n}+\mathbf{b}))(\mathbf{H}^{+}(\mathbf{n}+\mathbf{b}))^{T}] \\ &= E[\mathbf{H}^{+}\mathbf{n}\mathbf{n}^{T}(\mathbf{H}^{+})^{T}] + E[\mathbf{H}^{+}\mathbf{b}\mathbf{b}^{T}(\mathbf{H}^{+})^{T}] \\ &= (\mathbf{H}^{T}\mathbf{R}^{-1}\mathbf{H})^{-1} + \mathbf{H}^{+}E[\mathbf{b}\mathbf{b}^{T}](\mathbf{H}^{+})^{T}\end{aligned}$$

The overall MSE (OMSE), defined as the trace of MSE matrix, of this LS estimator can be expressed and compared to the OMSE of the ML estimation as :

$$(OMSE[\hat{\mathbf{x}}_{LS}] = \mathrm{Tr}\{(\mathbf{H}^{T}\mathbf{R}^{-1}\mathbf{H})^{-1}\} + \mathrm{Tr}\{\mathbf{H}^{+}E[\mathbf{b}\mathbf{b}^{T}](\mathbf{H}^{+})^{T}\}) \geq (\mathrm{Tr}\{(\mathbf{H}^{T}\mathbf{R}^{-1}\mathbf{H})^{-1}\} = OMSE[\hat{\mathbf{x}}_{ML}]) \tag{A.11}$$

This previous equation illustrates the effect of MP/NLOS biases on the final positioning error. Indeed, without knowing these biases, we have the previous inequality and then the LS estimation, under MP/NLOS conditions, will be degraded.

Annexe B

Appendix : AML-3D and PM-3D efficiency

B.1 AML-3D efficiency

In this following sub-section, we will derive some properties on AML estimator $\hat{\mathbf{x}}_{AML}$ and cost function that demonstrate the convergence of this estimator to the ML estimator in some conditions.

It is evident that the predicted bias and errors from the 3D simulation cannot be instantaneous and accurate. The quality and reliability of the PR bias estimation depends on many factors such as the accuracy of signal propagation modeling, the precision of 3D city modeling, receiver setting, etc... We want here to quantify the loss in AML-3D estimation compared to ML estimation by substituting the unknown MP/NLOS bias $\mathbf{b}$ with 3D predicted MP/NLOS bias $\mathbf{b}_{3D}(\mathbf{x}_i)$. Since the bias estimation by 3D simulations cannot be accurate, we define the uncertainty on the bias estimation as :

$$\delta_{3D} = \|\mathbf{b} - \mathbf{b}_{3D}(\mathbf{x})\|^2_{\mathbf{R}^{-1}} \tag{B.1}$$

We can prove the following lemmas :

B.1.1 Lemma 1 : Convergence of cost function to maximum-likelihood cost function :

If we consider $\eta \ll 1$ and the maximum-likelihood cost function J expressed in chapter 1, then :

$$|\min_{\mathbf{x}_i} P(\mathbf{y}|\mathbf{x}_i, \mathbf{b}_{3D}(\mathbf{x}_i)) - \min_{\mathbf{x}_i} J(\mathbf{y}|\mathbf{x}_i, \mathbf{b})| \leq (1+\eta)\delta_{3D} \tag{B.2}$$

Proof : If we consider $\eta \ll 1$, then :

$$\left|\min_{\mathbf{x}_i} P(\mathbf{y}|\mathbf{x}_i, \mathbf{b}_{3D}(\mathbf{x}_i)) - \min_{\mathbf{x}_i} J(\mathbf{y}|\mathbf{x}_i, \mathbf{b})\right| \leq (1+\eta)\delta_{3D} \tag{B.3}$$

Proof : Using the reverse triangle inequality, the difference between the two cost functions can be increased by :

$$|P(\mathbf{y}|\mathbf{x}_i, \mathbf{b}_{3D}(\mathbf{x}_i)) - J(\mathbf{y}|\mathbf{x}_i, \mathbf{b})| \leq \|[\mathbf{y} - \mathbf{H}\mathbf{x}_i - \mathbf{b}_{3D}(\mathbf{x}_i)] - [\mathbf{y} - \mathbf{H}\mathbf{x}_i - \mathbf{b}]\|^2_{\mathbf{R}^{-1}}$$

It follows :

$$|P(\mathbf{y}|\mathbf{x}_i, \mathbf{b}_{3D}(\mathbf{x}_i)) - J(\mathbf{y}|\mathbf{x}_i, \mathbf{b})| \leq \|[\mathbf{b} - \mathbf{b}_{3D}(\mathbf{x}_i])\|^2_{\mathbf{R}^{-1}}$$

Using the following inequality :

$$\|\mathbf{b} - \mathbf{b}_{3D}(\mathbf{x}_i)\|^2_{\mathbf{R}^{-1}} \leq \|\mathbf{b} - \mathbf{b}_{3D}(\mathbf{x})\|^2_{\mathbf{R}^{-1}} + \|\mathbf{b}_{3D}(\mathbf{x}) - \mathbf{b}_{3D}(\mathbf{x}_i)\|^2_{\mathbf{R}^{-1}}$$

We can conclude that :

$$\left|\min_{\mathbf{x}_i} P(\mathbf{y}|\mathbf{x}_i, \mathbf{b}_{3D}(\mathbf{x}_i)) - \min_{\mathbf{x}_i} J(\mathbf{y}|\mathbf{x}_i, \mathbf{b})\right| \leq \delta_{3D} + \min_{\mathbf{x}_i} \|\mathbf{b}_{3D}(\mathbf{x}) - \mathbf{b}_{3D}(\mathbf{x}_i)\|^2_{\mathbf{R}^{-1}}$$

If the array of candidate positions is wisely chosen, the true position will be close or among the considered grid of candidate positions and hence we will get :

$$\min_{\mathbf{x}_i} \|\mathbf{b}_{3D}(\mathbf{x}) - \mathbf{b}_{3D}(\mathbf{x}_i)\|^2_{\mathbf{R}^{-1}} \leq \eta\delta_{3D}$$

This proves lemma 1.

B.1.2 Lemma 2 : Convergence of AML estimator to true position :

$$\mathrm{Tr}\{MSE(\hat{\mathbf{x}}_{AML})\} \underset{\delta_{3D}\to 0}{\longrightarrow} \mathrm{Tr}\{MSE(\hat{\mathbf{x}}_{ML})\} \tag{B.4}$$

Proof : We start by computing the expression of $\hat{\mathbf{x}}_{AML}$:

$$\hat{\mathbf{x}}_{AML} = \underset{\mathbf{x}_i}{\mathrm{argmin}}\{\frac{\partial}{\partial \mathbf{x}_i}(P(\mathbf{y}|\mathbf{x}_i, \mathbf{b}_{3D}(\mathbf{x}_i)) = 0)\}$$

We compute the derivative of the cost function :

$$\frac{\partial}{\partial \mathbf{x}_i}(P(\mathbf{y}|\mathbf{x}_i, \mathbf{b}_{3D}(\mathbf{x}_i))) = -2(\mathbf{H}^T + \frac{\partial}{\partial \mathbf{x}_i}\mathbf{b}_{3D}(\mathbf{x}_i))\mathbf{R}^{-1}\mathbf{G}(\mathbf{x}_i)$$

Where $\mathbf{G}(\mathbf{x}_i) = \mathbf{y} - \mathbf{H}\mathbf{x}_i - \mathbf{b}_{3D}(\mathbf{x}_i)$. Then, we get the following expression for the approximate maximum likelihood :

$$\mathbf{y} - \mathbf{H}\hat{\mathbf{x}}_{AML} - \mathbf{b}_{3D}(\hat{\mathbf{x}}_{AML}) = 0$$

Since the MSE matrix is diagonal, the overall mean square error of the AML estimation is expressed as :

$$\begin{aligned}\text{Tr}\{MSE[\hat{\mathbf{x}}_{AML}]\} &= \text{Tr}\{E[(\hat{\mathbf{x}}_{AML} - \mathbf{x})(\hat{\mathbf{x}}_{AML} - \mathbf{x})^T]\} \\ &= E[\|\hat{\mathbf{x}}_{AML} - \mathbf{x}\|_2^2]\end{aligned}$$

The AML estimation error can be expressed as :

$$\|\hat{\mathbf{x}}_{AML} - \mathbf{x}\|_2^2 = \|\mathbf{H}^+(\mathbf{H}\hat{\mathbf{x}}_{AML} - \mathbf{H}\mathbf{x})\|_2^2 = \|\mathbf{H}^+(\mathbf{b} - \mathbf{b}_{3D}(\hat{\mathbf{x}}_{AML}) + \mathbf{n})\|_2^2$$

The previous expression gives :

$$\text{Tr}\{MSE[\hat{\mathbf{x}}_{AML}]\} \leq E\{\|\mathbf{H}^+(\mathbf{b} - \mathbf{b}_{3D}(\hat{\mathbf{x}}_{AML}))\|_2^2\} + E\{\|\mathbf{H}^+\mathbf{n}\|_2^2\}$$

By developing the two parts of this inequality, we show that :

$$E[\|\mathbf{H}^+\mathbf{n}\|_2^2] = \text{Tr}\{(\mathbf{H}^T\mathbf{R}^{-1}\mathbf{H})^{-1}\} = \text{Tr}\{MSE[\hat{\mathbf{x}}_{ML}]\}$$

$$E[\|\mathbf{H}^+(\mathbf{b} - \mathbf{b}_{3D}(\hat{\mathbf{x}}_{AML}))\|_2^2] = \text{Tr}\{(\mathbf{H}^+E[\delta_{3D}^{AML}(\delta_{3D}^{AML})^T](\mathbf{H}^+)^T)\}$$

Where $\delta_{3D}^{AML} = \mathbf{b} - \mathbf{b}_{3D}(\hat{\mathbf{x}}_{AML})$. Besides, we have the following inequality for all candidate positions :

$$\|\mathbf{b} - \mathbf{b}_{3D}(\mathbf{x}_i)\|_{\mathbf{R}^{-1}}^2 \leq \|\mathbf{b} - \mathbf{b}_{3D}(\mathbf{x})\|_{\mathbf{R}^{-1}}^2 + \|\mathbf{b}_{3D}(\mathbf{x}_i) - \mathbf{b}_{3D}(\mathbf{x})\|_{\mathbf{R}^{-1}}^2$$

And then, we deduce that :

$$\|\delta_{3D}^{AML}\|_{\mathbf{R}^{-1}}^2 = \min_{\mathbf{x}_i} \|\mathbf{b} - \mathbf{b}_{3D}(\mathbf{x}_i)\|_{\mathbf{R}^{-1}}^2 \leq \delta_{3D} + \min_{\mathbf{x}_i} \|\mathbf{b}_{3D}(\mathbf{x}_i) - \mathbf{b}_{3D}(\mathbf{x})\|_{\mathbf{R}^{-1}}^2 \leq (1+\eta)\delta_{3D}$$

where $\eta \ll 1$ and then lemma 2 is proven.

B.1.3 Lemma 3 : Convergence of AML estimator to ML estimator :

If we suppose that all the diagonal values of the covariance matrix are equals, i.e $\mathbf{R} = \sigma\mathbf{I}$, then we have :

$$\|\hat{\mathbf{x}}_{AML} - \hat{\mathbf{x}}_{ML}\|_2^2 \leq \frac{N \times GDOP}{\sigma^2}(1+\eta)\delta_{3D} \tag{B.5}$$

where $GDOP$ is the Geometric Dilution Of Precision, N is the number of received GNSS signals and $\eta \ll 1$.

Proof : We start from the following relation for the AML solution :

$$\mathbf{y} - \mathbf{H}\hat{\mathbf{x}}_{AML} - \mathbf{b}_{3D}(\hat{\mathbf{x}}_{AML}) = 0$$

Let us compute the AML and ML solutions difference, which can be expressed as :

$$\|\hat{\mathbf{x}}_{AML} - \hat{\mathbf{x}}_{ML}\|_2^2 = \|\mathbf{H}^+(\mathbf{H}\hat{\mathbf{x}}_{AML} - \mathbf{y} + \mathbf{b})\|_2^2 = \|\mathbf{H}^+(\mathbf{b} - \mathbf{b}_{3D}(\hat{\mathbf{x}}_{AML}))\|_2^2$$

By definition of the operator norm of matrix $\mathbf{H}^+$:

$$\|\hat{\mathbf{x}}_{AML} - \hat{\mathbf{x}}_{ML}\|_2^2 \leq \|\mathbf{R}^{-1/2}\mathbf{H}^+\|_F^2 \|\mathbf{b} - \mathbf{b}_{3D}(\hat{\mathbf{x}}_{AML})\|_2^2$$

Where, we define the Frobenius matrix norm as :

$$\|\mathbf{R}^{-1/2}\mathbf{H}^+\|_F = \text{Tr}\{(\mathbf{H}^+)^T\mathbf{R}^{-1}\mathbf{H}^+\} = \text{Tr}\{\mathbf{R}^{-1/2}\mathbf{H}^+(\mathbf{H}^+)^T\mathbf{R}^{-1/2}\}$$

Since matrix $\mathbf{R}$ is diagonal with equal diagonal elements :

$$\|\mathbf{R}^{-1/2}\mathbf{H}^+\|_F = \text{Tr}\{\mathbf{R}^{-2}(\mathbf{H}^T\mathbf{R}^{-1}\mathbf{H})^{-1}\}$$

Matrices in the trace operator are matrices with positive diagonal elements. Then, we get the following inequality :

$$\text{Tr}\{\mathbf{R}^{-2}(\mathbf{H}^T\mathbf{R}^{-1}\mathbf{H})^{-1}\} \leq \text{Tr}\{\mathbf{R}^{-2}\}\text{Tr}\{(\mathbf{H}^T\mathbf{R}^{-1}\mathbf{H})^{-1}\}$$

The second term can be expressed as :

$$\text{Tr}\{\mathbf{R}^{-2}\}\text{Tr}\{(\mathbf{H}^T\mathbf{R}^{-1}\mathbf{H})^{-1}\} = \frac{N \times \text{Tr}\{\mathbf{DOP}\}}{\sigma^2} = \frac{N \times GDOP}{\sigma^2}$$

Where $\mathbf{DOP} = (\mathbf{H}^T\mathbf{H})^{-1}$ is the Dilution of Precision (DOP) matrix, $GDOP$ is the Geometric Dilution Of Precision, N is the number of received GNSS signals and σ are the diagonal values of the noise covariance matrix, i.e $\mathbf{R} = \sigma\mathbf{I}$. Finally, using the previous proof, we have shown that :

$$\|\mathbf{b} - \mathbf{b}_{3D}(\hat{\mathbf{x}}_{AML})\|_{\mathbf{R}^{-1}}^2 \leq (1+\eta)\delta_{3D}$$

This proves lemma 3.

Lemma 1 shows that, conditioned by 3D P3D GNSS signal propagation simulators accuracy, the minimum of the approximate maximum-likelihood cost function P converges to the minimum of the maximum-likelihood cost function J. Lemma 2 demonstrates that, conditioned by 3D P3D GNSS signal propagation simulators accuracy, the overall mean square error (trace of the MSE matrix) of the AML estimator converges to the minimum overall mean square error of the ML solution of the GNSS problem (most efficient estimator). Lemma 3 proves that, conditioned by 3D P3D GNSS signal propagation simulators accuracy, the AML estimator converges to the ML estimator, i.e. if the 3D P3D GNSS signal propagation simulators is so accurate, the AML will converge to the ML estimator which is the Minimum Variance Unbiased Estimator (MVUE) of the GNSS problem. Other key factors are the number of satellites, the geometric configuration (GDOP) and the PR quality given by the noise variance σ^2.

B.2 PM-3D efficiency

B.2.1 Lemma 1 : Convergence of PM estimator to true position :

$$\mathrm{Tr}\{MSE(\hat{\mathbf{x}}_{PM})\}\underset{\delta_{3D}\to 0}{\longrightarrow}\mathrm{Tr}\{MSE(\hat{\mathbf{x}}_{ML})\} \tag{B.6}$$

Proof : We start by computing the expression of $\hat{\mathbf{x}}_{PM}$:

$$\hat{\mathbf{x}}_{PM} = \underset{\mathbf{x}_i}{\mathrm{argmin}}\{\frac{\partial}{\partial \mathbf{x}_i}(\Psi(\mathbf{y}|\mathbf{x}_i, \mathbf{b}_{3D}(\mathbf{x}_i)) = 0)\}$$

We compute the derivative of the cost function :

$$\frac{\partial}{\partial \mathbf{x}_i}(\Psi(\mathbf{y}|\mathbf{x}_i, \mathbf{b}_{3D}(\mathbf{x}_i))) = -2\mathbf{H}^{+}(\mathbf{H} + \frac{\partial}{\partial \mathbf{x}_i}\mathbf{b}_{3D}(\mathbf{x}_i))\mathbf{R}^{-1}\mathbf{K}(\mathbf{x}_i)$$

Where $\mathbf{K}(\mathbf{x}_i) = \mathbf{H}^{+}(\mathbf{y} - \mathbf{b}_{3D}(\mathbf{x}_i)) - \mathbf{x}_i$. Then, we get the following expression for the position matching estimate :

$$\mathbf{K}(\hat{\mathbf{x}}_{PM}) = 0 \iff \hat{\mathbf{x}}_{PM} = \mathbf{H}^{+}(\mathbf{y} - \mathbf{b}_{3D}(\hat{\mathbf{x}}_{PM}))$$

Since the MSE matrix is diagonal, the overall mean square error of the PM estimation is expressed as :

$$\mathrm{Tr}\{MSE[\hat{\mathbf{x}}_{PM}]\} = \mathrm{Tr}\{E[(\hat{\mathbf{x}}_{PM} - \mathbf{x})(\hat{\mathbf{x}}_{PM} - \mathbf{x})^T]\} = E[\|\hat{\mathbf{x}}_{PM} - \mathbf{x}\|_2^2]$$

The PM estimation error can be expressed as :

$$\|\hat{\mathbf{x}}_{PM} - \mathbf{x}\|_2^2 = \|\hat{\mathbf{x}}_{PM} - \mathbf{H}^{+}\mathbf{H}\mathbf{x}\|_2^2 = \|\mathbf{H}^{+}(\mathbf{b} - \mathbf{b}_{3D}(\hat{\mathbf{x}}_{PM}) + \mathbf{n})\|_2^2$$

The previous expression gives :

$$\mathrm{Tr}\{MSE[\hat{\mathbf{x}}_{PM}]\} \leq E\{\|\mathbf{H}^{+}(\mathbf{b} - \mathbf{b}_{3D}(\hat{\mathbf{x}}_{PM}))\|_2^2\} + E\{\|\mathbf{H}^{+}\mathbf{n}\|_2^2\}$$

By developing the two parts of this inequality, we show that :

$$\begin{cases} E\{\|\mathbf{H}^{+}\mathbf{n}\|_2^2\} & = \mathrm{Tr}\{(\mathbf{H}^T\mathbf{R}^{-1}\mathbf{H})^{-1}\} = \mathrm{Tr}\{MSE[\hat{\mathbf{x}}_{ML}]\} \\ E\{\|\mathbf{H}^{+}(\mathbf{b} - \mathbf{b}_{3D}(\hat{\mathbf{x}}_{PM}))\|_2^2\} & = \mathrm{Tr}\{(\mathbf{H}^{+}E[\delta_{3D}^{PM}(\delta_{3D}^{PM})^T](\mathbf{H}^{+})^T)\} \end{cases}$$

Where $\delta_{3D}^{PM} = \mathbf{b} - \mathbf{b}_{3D}(\hat{\mathbf{x}}_{PM})$. Besides, we have the following inequality for all candidate positions :

$$\|\mathbf{b} - \mathbf{b}_{3D}(\mathbf{x}_i)\|_{\mathbf{R}^{-1}}^2 \leq \|\mathbf{b} - \mathbf{b}_{3D}(\mathbf{x})\|_{\mathbf{R}^{-1}}^2 + \|\mathbf{b}_{3D}(\mathbf{x}_i) - \mathbf{b}_{3D}(\mathbf{x})\|_{\mathbf{R}^{-1}}^2$$

And then, we deduce that :

$$\|\delta_{3D}^{PM}\|^2_{\mathbf{R}^{-1}} = \min_{\mathbf{x}_i} \|\mathbf{b} - \mathbf{b}_{3D}(\mathbf{x}_i)\|^2_{\mathbf{R}^{-1}} \leq \delta_{3D} + \min_{\mathbf{x}_i} \|\mathbf{b}_{3D}(\mathbf{x}_i) - \mathbf{b}_{3D}(\mathbf{x})\|^2_{\mathbf{R}^{-1}} \leq (1+\eta)\delta_{3D}$$

where $\eta \ll 1$ and then lemma 1 is proven.

B.2.2 Lemma 2 : Comparison between PM estimator and AML estimator :

$$\mathrm{Tr}\{MSE(\hat{\mathbf{x}}_{AML})\} \leq \mathrm{Tr}\{MSE(\hat{\mathbf{x}}_{PM})\} \tag{B.7}$$

Proof : We start the demonstration by expressing a relation between the $\mathbf{K}$ and $\mathbf{G}$ functions defined in previous lemmas :

$$\mathbf{K}(\mathbf{x}_i) = \mathbf{H}^+(\mathbf{y} - \mathbf{b}_{3D}(\mathbf{x}_i)) - \mathbf{x}_i = \mathbf{H}^+\mathbf{G}(\mathbf{x}_i)$$

We note $\lambda_{min}(\mathbf{H}^+)$ the smallest singular value of matrix $\mathbf{H}^+$ that can be proven to be higher than 1. As $\|\mathbf{v}\|^2_{\mathbf{R}^{-1}} \leq \lambda_{min}(\mathbf{H}^+)\|\mathbf{v}\|^2_{\mathbf{R}^{-1}} \leq \|\mathbf{H}^+\mathbf{v}\|^2_2, \forall \mathbf{v} \in \mathbb{R}^N$, then this gives :

$$\Psi(\mathbf{y}|\mathbf{x}_i, \mathbf{b}_{3D}(\mathbf{x}_i)) = \|\mathbf{K}(\mathbf{x}_i)\|^2_2 = \|\mathbf{H}^+\mathbf{G}(\mathbf{x}_i)\|^2_2 \geq \|\mathbf{G}(\mathbf{x}_i)\|^2_{\mathbf{R}^{-1}} = P(\mathbf{y}|\mathbf{x}_i, \mathbf{b}_{3D}(\mathbf{x}_i))$$

In particular :

$$\Psi(\mathbf{y}|\hat{\mathbf{x}}_{PM}, \mathbf{b}_{3D}(\hat{\mathbf{x}}_{PM})) = \min_{\mathbf{x}_i} \Psi(\mathbf{y}|\mathbf{x}_i, \mathbf{b}_{3D}(\mathbf{x}_i)) \geq P(\mathbf{y}|\hat{\mathbf{x}}_{AML}, \mathbf{b}_{3D}(\hat{\mathbf{x}}_{AML})) = \min_{\mathbf{x}_i} P(\mathbf{y}|\mathbf{x}_i, \mathbf{b}_{3D}(\mathbf{x}_i))$$

Similarly, it can be shown that :

$$\|\mathbf{H}^+(\mathbf{b} + \mathbf{n} - \mathbf{b}_{3D}(\hat{\mathbf{x}}_{PM}))\|^2_2 \geq \|(\mathbf{b} + \mathbf{n} - \mathbf{b}_{3D}(\hat{\mathbf{x}}_{AML}))\|^2_{\mathbf{R}^{-1}}$$

By writing the expression of estimation errors for both AML and PM estimators as :

$$\begin{cases} \|\hat{\mathbf{x}}_{PM} - \mathbf{x}\|^2_2 & = \|\mathbf{H}^+\mathbf{G}(\hat{\mathbf{x}}_{PM}) - \mathbf{H}^+(\mathbf{b} + \mathbf{n} - \mathbf{b}_{3D}(\hat{\mathbf{x}}_{PM}))\|^2_2 \\ \|\hat{\mathbf{x}}_{AML} - \mathbf{x}\|^2_2 & = \|\mathbf{G}(\hat{\mathbf{x}}_{AML}) - (\mathbf{b} + \mathbf{n} - \mathbf{b}_{3D}(\hat{\mathbf{x}}_{AML}))\|^2_{\mathbf{R}^{-1}} \end{cases}$$

it yields :

$$\|\hat{\mathbf{x}}_{AML} - \mathbf{x}\|^2_2 \leq \|\hat{\mathbf{x}}_{PM} - \mathbf{x}\|^2_2$$

And, as :

$$\begin{cases} \mathrm{Tr}\{MSE[\hat{\mathbf{x}}_{PM}]\} & = E\{\|\hat{\mathbf{x}}_{PM} - \mathbf{x}\|^2_2]\} \\ \mathrm{Tr}\{MSE[\hat{\mathbf{x}}_{AML}]\} & = E\{\|\hat{\mathbf{x}}_{AML} - \mathbf{x}\|^2_2]\} \end{cases}$$

then, lemma 2 is proven.

Annexe C

Appendix : PR Bias Prediction Uncertainty

Proof of Relation (3.15)

We start from the accuracy requirement from (3.14) :

$$OMSE[\hat{\mathbf{x}}_{CLS}] \leq OMSE[\hat{\mathbf{x}}_{LS}]$$

The expressions of the OMSE of CLS and LS estimators are given in (A.11) and in equation (18) in [253]. They are recalled below :

$$\begin{cases} OMSE[\hat{\mathbf{x}}_{LS}] & = \mathrm{Tr}\{(\mathbf{H}^T\mathbf{R}^{-1}\mathbf{H})^{-1}\} + \mathrm{Tr}\{\mathbf{H}^+ E\{\mathbf{b}\mathbf{b}^T\}(\mathbf{H}^+)^T\} \\ OMSE[\hat{\mathbf{x}}_{CLS}] & = \mathrm{Tr}\{(\mathbf{H}^T\mathbf{R}_b^{-1}\mathbf{H})^{-1}\} + \mathrm{Tr}\{\mathbf{H}_b^+ E\{\delta\mathbf{b}\delta\mathbf{b}^T\}(\mathbf{H}_b^+)^T\} \end{cases}$$

If we define the following term $\beta_{\mathbf{b}} = \mathrm{Tr}\{(\mathbf{H}^T\mathbf{R}_{\mathbf{b}}^{-1}\mathbf{H})^{-1}\} - \mathrm{Tr}\{(\mathbf{H}^T\mathbf{R}^{-1}\mathbf{H})^{-1}\}$, the accuracy requirement expressed at the beginning of this appendix can be written as :

$$\mathrm{Tr}\{\mathbf{H}_b^+ E\{\delta\mathbf{b}\delta\mathbf{b}^T\}\mathbf{H}_b^+\} \leq \mathrm{Tr}\{\mathbf{H}^+ E\{\mathbf{b}\mathbf{b}^T\}(\mathbf{H}^+)^T\} - \beta_{\mathbf{b}}$$

Now, the OMSE of both LS and CLS estimators, can be expressed using the trace operator proprieties as :

$$\begin{cases} OMSE[\hat{\mathbf{x}}_{LS}] & = \sum_{k,i}[(\mathbf{H}^+)_{k,i}]^2(E\{\mathbf{b}\mathbf{b}^T\})_{i,i}] + \mathrm{Tr}\{(\mathbf{H}^T\mathbf{R}^{-1}\mathbf{H})^{-1}\} \\ OMSE[\hat{\mathbf{x}}_{CLS}] & = \sum_{k,i}[(\mathbf{H}_{\mathbf{b}}^+)_{k,i}]^2(E\{\delta\mathbf{b}\delta\mathbf{b}^T\})_{i,i}] + \mathrm{Tr}\{(\mathbf{H}^T\mathbf{R}_b^{-1}\mathbf{H})^{-1}\} \end{cases}$$

Proof of Relation (3.19)

The OMSE of the CLS estimator is given by (details are in equation (18) in [253]) :

$$OMSE[\hat{\mathbf{x}}_{CLS}] = \sum_{k,i}[(\mathbf{H}_{\mathbf{b}}^{+})_{k,i}]^2(E\{\delta\mathbf{b}\delta\mathbf{b}^T\})_{i,i}] + \mathrm{Tr}\{(\mathbf{H}^T\mathbf{R}_b^{-1}\mathbf{H})^{-1}\}$$

In case of only one ranging measurement error from satellite j and when correcting the ranging errors from all received satellites except satellite j, i.e. $(\delta\mathbf{b})_j \neq 0$ and $(\delta\mathbf{b})_{i\neq j} = 0$, the sum present in the previous expression can be simplified :

$$\sum_{k,i}[(\mathbf{H}_{\mathbf{b}}^{+})_{k,i}]^2(E\{\delta\mathbf{b}\delta\mathbf{b}^T\})_{i,i}] = \sum_{k}[(\mathbf{H}_{\mathbf{b}}^{+})_{k,j}]^2 E\{\delta\mathbf{b}\delta\mathbf{b}^T\}_{j,j}$$

As $(\delta\mathbf{b})_j \sim \mathcal{N}(\mu, \sigma^2)$, then $E\{\delta\mathbf{b}\delta\mathbf{b}^T\}_{j,j} = \sigma^2 + \mu^2$ (because $(\delta\mathbf{b})_{i\neq j} = 0$), which proves relation (3.19).

Annexe D

Appendix : Properties of Modified Lower Bounds

D.1 A general class of tighter modified lower bounds and its relationship with hybrid lower bounds

In this section, the tightness of the modified lower bounds (MLBs) proposed in chapter 5 is increased by adding different subset of constraints.

D.1.1 A first class of tighter modified lower bounds

Since :

$$\begin{aligned} p(\mathbf{z};\theta) &= \int_{\mathcal{S}_{\Theta_r|\mathbf{z}}} p(\mathbf{z},\boldsymbol{\theta}_r;\theta)\, d\theta_r \\ &= \int_{\mathbb{R}^{P_r}} p(\mathbf{z},\boldsymbol{\theta}_r;\theta)\, 1_{\mathcal{S}_{\Theta_r|\mathbf{z}}}(\boldsymbol{\theta}_r)\, d\theta_r, \end{aligned}$$

then, after change of variables $\boldsymbol{\theta}_r = \boldsymbol{\theta}'_r + \mathbf{h}_r$ and renaming $\boldsymbol{\theta}'_r$ as $\boldsymbol{\theta}_r$:

$$p(\mathbf{z};\theta) = \int_{\mathbb{R}^{P_r}} p(\mathbf{z},\boldsymbol{\theta}_r+\mathbf{h}_r;\theta)\, 1_{\mathcal{S}_{\Theta_r|\mathbf{z}}}(\boldsymbol{\theta}_r+\mathbf{h}_r)\, d\boldsymbol{\theta}_r.$$

Therefore for any $\mathbf{h}_r$ such that :

$$1_{\mathcal{S}_{\Theta_r|\mathbf{z}}}(\boldsymbol{\theta}_r+\mathbf{h}_r) = 1_{\mathcal{S}_{\Theta_r|\mathbf{z}}}(\boldsymbol{\theta}_r),\ \forall \boldsymbol{\theta}_r \in \mathbb{R}^{P_r}, \tag{D.1a}$$

then :

$$p(\mathbf{z};\theta) = \int_{\mathcal{S}_{\Theta_r|\mathbf{z}}} p(\mathbf{z},\boldsymbol{\theta}_r+\mathbf{h}_r;\theta)\, d\boldsymbol{\theta}_r, \tag{D.1b}$$

and for any unbiased estimator $\widehat{\theta^0} \in \mathcal{L}_2(\mathcal{S}_{\mathcal{Z}})$, (4.11a) can be reformulated as, $\forall n \in [1, N]$

$$\begin{aligned}
\theta^n - \theta^0 &= E_{\mathbf{z};\theta^0}\left[\left(\widehat{\theta^0}(\mathbf{z}) - \theta^0\right)\upsilon_{\theta^0}(\mathbf{z};\theta^n)\right] \\
&= \int\limits_{\mathcal{S}_{\mathcal{Z}}} \left(\widehat{\theta^0}(\mathbf{z}) - \theta^0\right) p(\mathbf{z};\theta^n)\, d\mathbf{z} \\
&= \int\limits_{\mathcal{S}_{\mathcal{Z}}} \left(\widehat{\theta^0}(\mathbf{z}) - \theta^0\right) \int\limits_{\mathcal{S}_{\Theta_r|\mathbf{z}}} p(\mathbf{z}, \boldsymbol{\theta}_r + \mathbf{h}_r;\theta^n)\, d\boldsymbol{\theta}_r d\mathbf{z} \\
&= E_{\mathbf{z},\boldsymbol{\theta}_r;\theta^0}\left[\left(\widehat{\theta^0}(\mathbf{z}) - \theta^0\right)\upsilon_{\theta^0}(\mathbf{z}, \boldsymbol{\theta}_r + \mathbf{h}_r;\theta^n)\right],
\end{aligned}$$

that is in vector form :

$$\begin{aligned}
\xi\left(\boldsymbol{\theta}^N\right) &= E_{\mathbf{z};\theta^0}\left[\left(\widehat{\theta^0}(\mathbf{z}) - \theta^0\right)\upsilon_{\theta^0}\left(\mathbf{z};\boldsymbol{\theta}^N\right)\right] \\
&= E_{\mathbf{z},\boldsymbol{\theta}_r;\theta^0}\left[\left(\widehat{\theta^0}(\mathbf{z}) - \theta^0\right)\upsilon_{\theta^0}\left(\mathbf{z}, \boldsymbol{\theta}_r + \mathbf{h}_r;\boldsymbol{\theta}^N\right)\right].
\end{aligned} \tag{D.2}$$

The identity (D.2) means that for any $\widehat{\theta^0} \in \mathcal{L}_2(\mathcal{S}_{\mathcal{Z}})$, the two subsets of N constraints are equivalent system of linear equations yielding the same vector subspace of $\mathcal{L}_2(\mathcal{S}_{\mathcal{Z}})$: $span\left(\upsilon_{\theta^0}(\mathbf{z};\theta^1), \ldots, \upsilon_{\theta^0}\left(\mathbf{z};\theta^N\right)\right)$. Therefore, for any $\widehat{\theta^0} \in \mathcal{L}_2(\mathcal{S}_{\mathcal{Z}})$, any set of $N \times K$ constraints of the form :

$$\xi\left(\boldsymbol{\theta}^N\right) = E_{\mathbf{z},\theta_r;\theta^0}\left[\left(\widehat{\theta^0}(\mathbf{z}) - \theta^0\right)\upsilon_{\theta^0}\left(\mathbf{z}, \boldsymbol{\theta}_r + \mathbf{h}_r^k;\boldsymbol{\theta}^N\right)\right], \tag{D.3}$$

where $\left\{\mathbf{h}_r^1, \ldots, \mathbf{h}_r^K\right\}$ satisfy (D.1a), is equivalent to the set of N constraints (4.15). Fortunately this result does not hold a priori for all $\widehat{\theta^0} \in \mathcal{L}_2(\mathcal{S}_{\mathcal{Z},\Theta_r})$ where the $N \times K$ constraints (D.3) are expected to be linearly independent (not necessarily true in the general case). As mentioned above, the main effect of adding constraints is to restrict the class of viable estimators $\widehat{\theta^0} \in \mathcal{L}_2(\mathcal{S}_{\mathcal{Z},\Theta_r})$ and therefore to increase the minimum norm obtained from (4.10) :

$$\min_{\widehat{\theta^0} \in \mathcal{L}_2(\mathcal{S}_{\mathcal{Z},\Theta_r})} \left\{E_{\mathbf{z},\boldsymbol{\theta}_r;\theta^0}\left[\left(\widehat{\theta^0}(\mathbf{z},\boldsymbol{\theta}_r) - \theta^0\right)^2\right]\right\} \text{ under } \xi\left(\boldsymbol{\theta}^N\right) = E_{\mathbf{z},\boldsymbol{\theta}_r;\theta^0}\left[\left(\widehat{\theta^0}(\mathbf{z},\boldsymbol{\theta}_r) - \theta^0\right)\upsilon_{\theta^0}\left(\mathbf{z}, \boldsymbol{\theta}_r + \mathbf{h}_r^k;\boldsymbol{\theta}^N\right)\right], \tag{D.4}$$

$1 \leq k \leq K$, which remains smaller (or equal) than the minimum norm obtained for $\widehat{\theta^0} \in \mathcal{L}_2(\mathcal{S}_{\mathcal{Z}})$ given by (4.17a). This LB ordering was previously introduced in [210, (29)], but only in the restricted case where the prior does not depend on the deterministic parameter and $\mathcal{S}_{\Theta_r|\mathbf{z}} = \mathbb{R}^{P_r}$, at the expense of a not straightforward derivation (see Subsections III.C and III.D in [210]). Note that the regularity condition (D.1a) only imposes on $1_{\mathcal{S}_{\Theta_r|\mathbf{z}}}(\boldsymbol{\theta}_r)$, $\mathbf{z} \in \mathcal{S}_{\mathcal{Z}}$, to be of the following form :

$$1_{\mathcal{S}_{\Theta_r|\mathbf{z}}}(\boldsymbol{\theta}_r) = \left| \begin{array}{l} 0 \text{ if } \sum\limits_{\mathbf{h}_r \in \mathcal{F}_{\mathbf{z}}} \left(\sum\limits_{l \in \mathbb{Z}} 1_{\mathcal{S}^0_{\Theta_r|\mathbf{z}}}(\boldsymbol{\theta}_r + l\mathbf{h}_r)\right) = 0, \\ 1, \text{ otherwise,} \end{array} \right. \tag{D.5}$$

where $\mathcal{F}_{\mathbf{z}}$ and $\mathcal{S}^0_{\Theta_r|\mathbf{z}}$ are subsets of $\mathbb{R}^{P_r}$, what means that the complementary of $\mathcal{S}_{\Theta_r|\mathbf{z}}$ is the union (possibly uncountable) of periodic subsets of $\mathbb{R}^{P_r}$.

D.1.2 A second class of tighter modified lower bounds

Let us recall that any real-valued function $\psi(\mathbf{z}, \boldsymbol{\theta}_r; \theta)$ defined on $\mathcal{S}_{\mathcal{Z},\Theta_r}$ satisfying

$$\int\limits_{\mathcal{S}_{\Theta_r|\mathbf{z}}} \psi(\mathbf{z}, \boldsymbol{\theta}_r; \theta)\, p(\mathbf{z}, \boldsymbol{\theta}_r; \theta)\, d\boldsymbol{\theta}_r = 0, \tag{D.6}$$

is a Bayesian LB-generating functions [254]. A well known example is, for $\gamma \in]0,1[$:

$$\psi_\gamma^{\mathbf{h}_r}(\mathbf{z}, \boldsymbol{\theta}_r; \theta) = \left(p(\mathbf{z}, \boldsymbol{\theta}_r + \mathbf{h}_r; \theta)/p(\mathbf{z}, \boldsymbol{\theta}_r; \theta)\right)^{\gamma} - \left(p(\mathbf{z}, \boldsymbol{\theta}_r - \mathbf{h}_r; \theta)/p(\mathbf{z}, \boldsymbol{\theta}_r; \theta)\right)^{1-\gamma}, \tag{D.7}$$

if $(\mathbf{z}, \boldsymbol{\theta}_r) \in \mathcal{S}_{\mathcal{X},\Theta_r}$, and $\psi_\gamma^{\mathbf{h}_r}(\mathbf{z}, \boldsymbol{\theta}_r; \theta) = 0$ otherwise, yielding the Bayesian Weiss-Weinstein bound (BWWB). Let $\boldsymbol{\psi}(\mathbf{z}, \boldsymbol{\theta}_r; \theta)$ be a vector of L linearly independent functions satisfying (D.6). Then $\forall g(.) \in \mathcal{L}_2(\mathcal{S}_{\mathcal{Z}})$:

$$E_{\mathbf{z},\boldsymbol{\theta}_r;\theta^0}\left[g(\mathbf{z})\, \boldsymbol{\psi}\left(\mathbf{z}, \boldsymbol{\theta}_r; \theta^0\right)\right] = \mathbf{0}, \tag{D.8a}$$

which means that the subspace $\mathcal{L}_2(\mathcal{S}_{\mathcal{Z}})$ is orthogonal to *span* $\{\psi_1(\mathbf{z}, \theta_r; \theta^0), \ldots, \psi_L(\mathbf{z}, \theta_r; \theta^0)\}$ in $\mathcal{L}_2(\mathcal{S}_{\mathcal{Z},\Theta_r})$. Therefore, since (4.17a) can be reformulated as (4.17b), it is straightforward that (4.17a) is equivalent to :

$$\min_{\widehat{\theta^0} \in \mathcal{L}_2(\mathcal{S}_{\mathcal{Z}})} \left\{ E_{\mathbf{z},\boldsymbol{\theta}_r;\theta^0}\left[\left(\widehat{\theta^0}(\mathbf{z}) - \theta^0\right)^2\right]\right\} \text{ under } \left| \begin{array}{r} \xi\left(\boldsymbol{\theta}^N\right) = E_{\mathbf{z},\boldsymbol{\theta}_r;\theta^0}\left[\left(\widehat{\theta^0}(\mathbf{z}) - \theta^0\right) \upsilon_{\theta^0}\left(\mathbf{z}; \boldsymbol{\theta}^N\right)\right] \\ \mathbf{0} = E_{\mathbf{z},\boldsymbol{\theta}_r;\theta^0}\left[\left(\widehat{\theta^0}(\mathbf{z}) - \theta^0\right) \boldsymbol{\psi}(\mathbf{z}, \boldsymbol{\theta}_r; \theta^0)\right] \end{array} \right. . \tag{D.8b}$$

In other words, the addition of the set of L constraints $E_{\mathbf{z},\boldsymbol{\theta}_r;\theta^0}\left[\left(\widehat{\theta^0}(\mathbf{z}) - \theta^0\right) \boldsymbol{\psi}(\mathbf{z}, \boldsymbol{\theta}_r; \theta^0)\right] = \mathbf{0}$ to any linear transformation of (4.11a) does not change the associated LB (4.12b) computed for $\widehat{\theta^0} \in \mathcal{L}_2(\mathcal{S}_{\mathcal{Z}})$. Fortunately, once again, this result does not hold a priori for all $\widehat{\theta^0} \in \mathcal{L}_2(\mathcal{S}_{\mathcal{Z},\Theta_r})$. Indeed, provided that $\psi(\mathbf{x}, \boldsymbol{\theta}_r; \theta)$ is chosen such that $E_{\mathbf{z},\boldsymbol{\theta}_r;\theta^0}\left[\boldsymbol{\upsilon}_{\theta^0}\left(\mathbf{z}, \boldsymbol{\theta}_r; \boldsymbol{\theta}^N\right) \boldsymbol{\psi}(\mathbf{z}, \boldsymbol{\theta}_r; \theta^0)^T\right] \neq \mathbf{0}$ [231, Lemma 2], one can increase the minimum norm obtained from (4.17c) by computing :

$$\min_{\widehat{\theta^0} \in \mathcal{L}_2(\mathcal{S}_{\mathcal{Z},\Theta_r})} \left\{ E_{\mathbf{z},\boldsymbol{\theta}_r;\theta^0}\left[\left(\widehat{\theta^0}(\mathbf{z}, \boldsymbol{\theta}_r) - \theta^0\right)^2\right]\right\} \text{ under } \left| \begin{array}{r} \xi\left(\boldsymbol{\theta}^N\right) = E_{\mathbf{z},\boldsymbol{\theta}_r;\theta^0}\left[\left(\widehat{\theta^0}(\mathbf{z}, \boldsymbol{\theta}_r) - \theta^0\right) \boldsymbol{\upsilon}_{\theta^0}\left(\mathbf{z}, \boldsymbol{\theta}_r; \boldsymbol{\theta}^N\right)\right] \\ \mathbf{0} = E_{\mathbf{z},\boldsymbol{\theta}_r;\theta^0}\left[\left(\widehat{\theta^0}(\mathbf{z}, \boldsymbol{\theta}_r) - \theta^0\right) \boldsymbol{\psi}(\mathbf{z}, \boldsymbol{\theta}_r; \theta^0)\right] \end{array} \right. , \tag{D.9}$$

which remains smaller (or equal) than the minimum norm obtained for $\widehat{\theta^0} \in \mathcal{L}_2(\mathcal{S}_{\mathcal{Z}})$ given by (4.17a). First note that it is in general not possible to compare (D.4) with (D.9) since they derive from different subset of constraints. Second, (D.9) can be used with joint p.d.f. $p(\mathbf{z}, \boldsymbol{\theta}_r; \theta)$ which does not satisfy the regularity condition (D.5) since functions (D.7) are essentially free of regularity conditions [254].

D.1.3 A general class of tighter modified lower bounds and its relationship with hybrid lower bounds

The tightest modified LBs are obtained by combination of constraints (D.4) and (D.9) as the solution of :

$$\min_{\widehat{\theta^0}\in\mathcal{L}_2(\mathcal{S}_{\mathcal{Z},\Theta_r})}\left\{E_{\mathbf{z},\boldsymbol{\theta}_r;\theta^0}\left[\left(\widehat{\theta^0}(\mathbf{z},\boldsymbol{\theta}_r)-\theta^0\right)^2\right]\right\} \text{ under } \left|\begin{array}{l}\xi\left(\boldsymbol{\theta}^N\right)=E_{\mathbf{z},\boldsymbol{\theta}_r;\theta^0}\left[\left(\widehat{\theta^0}(\mathbf{z},\boldsymbol{\theta}_r)-\theta^0\right)\boldsymbol{\upsilon}_{\theta^0}\left(\mathbf{z},\boldsymbol{\theta}_r+\mathbf{h}_r^k;\theta^N\right)\right]\\ \mathbf{0}=E_{\mathbf{z},\boldsymbol{\theta}_r;\theta^0}\left[\left(\widehat{\theta^0}(\mathbf{z},\boldsymbol{\theta}_r)-\theta^0\right)\boldsymbol{\psi}\left(\mathbf{z},\boldsymbol{\theta}_r;\theta^0\right)\right],\end{array}\right. \tag{D.10}$$

$1\leq k\leq K$, where $\boldsymbol{\psi}\left(\mathbf{z},\boldsymbol{\theta}_r;\theta^0\right)$ satisfies (D.6).

Firstly, if we restrict (D.10) to (D.4), that is no function $\boldsymbol{\psi}\left(\mathbf{z},\boldsymbol{\theta}_r;\theta^0\right)$ (D.6) is involved, then the solution of (D.4)(D.10) given by the minimum norm lemma (4.10) yields the deterministic part of the HLBs obtained as discrete forms [211, (30)] of linear transformations on the CLR function introduced in [211]. Following from similar argument given in Section 4.2.3 or in [208, Section III], one obtains the deterministic part of the HLB integral form proposed in [211], as linear transformations of (D.4) in the limiting case where $N,K\rightarrow\infty$. Note that in [211] two restrictive regularity conditions are assumed : i) $\mathcal{S}_{\Theta_r|\mathbf{z}}=\mathbb{R}^{P_r}$, ii) the prior does not depend on θ, which are relaxed with the proposed framework : HLBs obtained via linear transformations on the CLR function are still valid if the prior depends on θ as long as $\mathcal{S}_{\Theta_r|\mathbf{z}}$ satisfies (D.5), which includes $\mathbb{R}^{P_r}$. In contrast, according to (D.5) such bounds do not exist if $\mathcal{S}_{\Theta_r|\mathbf{z}}$ is a connected set of $\mathbb{R}^{P_r}$ and in most cases, if $\mathcal{S}_{\Theta_r|\mathbf{z}}$ is a disconnected subset of $\mathbb{R}^{P_r}$ (not stated in [211]). Last, since the modified LB obtained from (D.4) is lower than or equal to the standard LB from (4.17a), one can assert that the deterministic part of any HLB obtained via the linear transformation on the CLR is looser (or equal) than the corresponding standard LB (not proven in [211]).

Secondly, if $\mathcal{S}_{\Theta_r|\mathbf{z}}$ does not satisfy (D.5), e.g., if $\mathcal{S}_{\Theta_r|\mathbf{z}}$ is an interval, then (D.4) can no longer be used to increase the minimum norm obtained from (4.17c). One solution is therefore to restrict (D.10) to (D.9) and, following from similar argument given in Section 4.2.3, to resort to some of its possible integral forms obtained as the limiting cases where $N,K\rightarrow\infty$, where L has a finite value :

$$\min_{\widehat{\theta^0}\in\mathcal{L}_2(\mathcal{S}_{\mathcal{Z},\Theta_r})}\left\{E_{\mathbf{z},\boldsymbol{\theta}_r;\theta^0}\left[\left(\widehat{\theta^0}(\mathbf{z},\boldsymbol{\theta}_r)-\theta^0\right)^2\right]\right\} \text{ under } \left|\begin{array}{l}\Gamma_{\theta^0}^h(\tau)=E_{\mathbf{z},\boldsymbol{\theta}_r;\theta^0}\left[\left(\widehat{\theta^0}(\mathbf{z},\boldsymbol{\theta}_r)-\theta^0\right)\eta_{\theta^0}^h(\mathbf{z},\boldsymbol{\theta}_r;\tau)\right]\\ \mathbf{0}=E_{\mathbf{z},\boldsymbol{\theta}_r;\theta^0}\left[\left(\widehat{\theta^0}(\mathbf{z},\boldsymbol{\theta}_r)-\theta^0\right)\boldsymbol{\psi}\left(\mathbf{z},\boldsymbol{\theta}_r;\theta^0\right)\right],\end{array}\right. \tag{D.11a}$$

where $\eta_{\theta^0}^h(\mathbf{z},\boldsymbol{\theta}_r;\tau)=\int\limits_{\Theta_d}h(\tau,\theta)\,\upsilon_{\theta^0}(\mathbf{z},\boldsymbol{\theta}_r;\theta)\,d\theta$ and $\Gamma_{\theta^0}^h(\tau)=\int\limits_{\Theta_d}h(\tau,\theta)\left(\theta-\theta^0\right)d\theta$, or where $L\rightarrow\infty$, if we choose (D.7) :

$$\min_{\widehat{\theta^0}\in\mathcal{L}_2(\mathcal{S}_{\mathcal{Z},\Theta_r})}\left\{E_{\mathbf{z},\boldsymbol{\theta}_r;\theta^0}\left[\left(\widehat{\theta^0}(\mathbf{z},\boldsymbol{\theta}_r)-\theta^0\right)^2\right]\right\} \text{ under } \left|\begin{array}{l}\Gamma_{\theta^0}^h(\tau)=E_{\mathbf{z},\boldsymbol{\theta}_r;\theta^0}\left[\left(\widehat{\theta^0}(\mathbf{z},\boldsymbol{\theta}_r)-\theta^0\right)\eta_{\theta^0}^h(\mathbf{z},\boldsymbol{\theta}_r;\tau)\right]\\ \mathbf{0}=E_{\mathbf{z},\boldsymbol{\theta}_r;\theta^0}\left[\left(\widehat{\theta^0}(\mathbf{z},\boldsymbol{\theta}_r)-\theta^0\right)\kappa\left(\mathbf{z},\boldsymbol{\theta}_r;\theta^0\right)\right],\end{array}\right. \tag{D.11b}$$

where $\kappa\left(\mathbf{z},\boldsymbol{\theta}_r;\theta^0\right)=\int\limits_{\gamma,\mathbf{h}_r}\psi_\gamma^{\mathbf{h}_r}\left(\mathbf{z},\boldsymbol{\theta}_r;\theta^0\right)d\mathbf{h}_r d\gamma$. To the best of our knowledge, (D.11b) defines a new class of MLBs, whereas (D.11a) is a particular case of the deterministic part of HLBs introduced in [208].

Thirdly, if we restrict ourselves to the case where $\mathcal{S}_{\Theta_r|\mathbf{z}} = \mathbb{R}^{P_r}$, then (D.10) and its possible integral forms provide an extended class of MLBs which can be regarded as the deterministic part of an extended class of HLBs which includes all known HLBs introduced so far as shown in [211] and [208].

D.1.4 Old and new tighter modified lower bounds

A typical example is the case of the CRB. A tighter MCRB obtained from (D.4) for $N = 2$, $K = P_r$, where $\boldsymbol{\theta}^2 = (\theta^0 + d\theta, \theta^0)$ and $\mathbf{h}_r^k = \mathbf{u}_k h_r^k$, $1 \leq k \leq P_r$, leading to the following subset of constraints :

$$\mathbf{v} = d\theta \begin{pmatrix} 0 \\ \mathbf{e}_1 \end{pmatrix} = E_{\mathbf{z},\boldsymbol{\theta}_r;\theta^0}\left[\left(\widehat{\theta^0}\left(\mathbf{z},\boldsymbol{\theta}_r\right) - \theta^0\right)\mathbf{c}_{\theta^0}\left(\mathbf{z},\boldsymbol{\theta}_r\right)\right],$$
$$\mathbf{c}_{\theta^0}^T\left(\mathbf{z},\boldsymbol{\theta}_r\right) = \left(\upsilon_{\theta^0}\left(\mathbf{z},\boldsymbol{\theta}_r;\theta^0\right), \upsilon_{\theta^0}\left(\mathbf{z},\boldsymbol{\theta}_r;\theta^0 + d\theta\right), \upsilon_{\theta^0}\left(\mathbf{z},\boldsymbol{\theta}_r + \mathbf{u}_1 h_r^1;\theta^0\right), \ldots, \upsilon_{\theta^0}\left(\mathbf{z},\boldsymbol{\theta}_r + \mathbf{u}_{P_r} h_r^{P_r};\theta^0\right)\right)$$

where $\mathbf{e}_1 = (1, 0, \ldots, 0)^T$ and $\mathbf{u}_k$ is the kth column of the identity matrix $\mathbf{I}_{P_r}$. By letting $\left(d\theta, h_r^1, \ldots, h_r^{P_r}\right)$ be infinitesimally small, which imposes that (D.5) reduces to : $\forall \mathbf{z} \in \mathcal{S}_{\mathcal{Z}}$, $\mathcal{S}_{\Theta_r|\mathbf{z}} = \mathbb{R}^{P_r}$, the LB obtained from (4.10) is :

$$\overline{MCRB}_{\theta^0} = \mathbf{e}_1^T \mathbf{F}\left(\theta^0\right)^{-1}\mathbf{e}_1, \quad \mathbf{F}\left(\theta\right) = E_{\mathbf{z},\boldsymbol{\theta}_r;\theta}\left[\frac{\partial \ln p\left(\mathbf{z},\boldsymbol{\theta}_r;\theta\right)}{\partial\left(\theta,\boldsymbol{\theta}_r^T\right)^T}\frac{\partial \ln p\left(\mathbf{z},\boldsymbol{\theta}_r;\theta\right)}{\partial\left(\theta,\boldsymbol{\theta}_r^T\right)}\right]. \tag{D.12}$$

Since $\mathbf{F}\left(\theta\right) = \begin{bmatrix} f_\theta\left(\theta\right) & \mathbf{f}_{\boldsymbol{\theta}_r,\theta}^T\left(\theta\right) \\ \mathbf{f}_{\boldsymbol{\theta}_r,\theta}\left(\theta\right) & \mathbf{F}_{\boldsymbol{\theta}_r}\left(\theta\right) \end{bmatrix}$, therefore :

$$\overline{MCRB}_{\theta^0} = \frac{1}{f_\theta\left(\theta^0\right) - \mathbf{f}_{\boldsymbol{\theta}_r,\theta}^T\left(\theta^0\right)\mathbf{F}_{\boldsymbol{\theta}_r}^{-1}\left(\theta^0\right)\mathbf{f}_{\theta,\boldsymbol{\theta}_r}\left(\theta^0\right)} \geq \frac{1}{f_\theta\left(\theta^0\right)} = MCRB_{\theta^0}. \tag{D.13}$$

Actually, (D.12) is also the deterministic part of the HCRB [214] and a similar derivation was proposed in [210], but under the unnecessary restrictive assumption of a prior independent of θ, as in [214] which introduced the HCRB as an extension of the Bayesian CRB proposed in [212]. This condition was relaxed in [255, (20)] with sufficient conditions [255, (21)] unnecessary restrictive and which have been an impediment to the dissemination of their result. However if $\mathcal{S}_{\Theta_r|\mathbf{z}}$ is an interval of $\mathbb{R}^{P_r}$, then the tighter MCRB (D.12) cannot be derived any longer. Fortunately, as shown with the proposed rationale, an alternative tighter MCRB can be derived from (D.9). Indeed, for $N = 2$, where $\boldsymbol{\theta}^2 = (\theta^0 + d\theta, \theta^0)$, the following subset of constraints :

$$\mathbf{v} = d\theta \begin{pmatrix} 0 \\ \mathbf{e}_1 \end{pmatrix} = E_{\mathbf{z},\boldsymbol{\theta}_r;\theta^0}\left[\left(\widehat{\theta^0}\left(\mathbf{z},\boldsymbol{\theta}_r\right)-\theta^0\right)\mathbf{c}_{\theta^0}\left(\mathbf{z},\boldsymbol{\theta}_r\right)\right],$$

$$\mathbf{c}_{\theta^0}^T\left(\mathbf{z},\boldsymbol{\theta}_r\right) = \left(\upsilon_{\theta^0}\left(\mathbf{z},\boldsymbol{\theta}_r;\theta^0\right),\upsilon_{\theta^0}\left(\mathbf{z},\boldsymbol{\theta}_r;\theta^0+d\theta\right),\boldsymbol{\psi}\left(\mathbf{z},\boldsymbol{\theta}_r;\theta^0\right)^T\right)$$

yields, as a limiting form where $d\theta \to 0$, via Lemma (4.10) :

$$\overline{MCRB}_{\theta^0}^a = \mathbf{e}_1^T E_{\mathbf{z},\boldsymbol{\theta}_r;\theta^0}\left[\begin{pmatrix} \frac{\partial \ln p(\mathbf{z},\boldsymbol{\theta}_r;\theta)}{\partial\theta} \\ \boldsymbol{\psi}\left(\mathbf{z},\boldsymbol{\theta}_r;\theta\right) \end{pmatrix}\begin{pmatrix} \frac{\partial \ln p(\mathbf{z},\boldsymbol{\theta}_r;\theta)}{\partial\theta} \\ \boldsymbol{\psi}\left(\mathbf{z},\boldsymbol{\theta}_r;\theta\right) \end{pmatrix}^T\right]^{-1}\mathbf{e}_1,$$

that is :

$$\overline{MCRB}_{\theta^0}^a = \frac{1}{f_\theta\left(\theta^0\right)-\mathbf{f}\left(\theta^0\right)\mathbf{F}\left(\theta^0\right)^{-1}\mathbf{f}\left(\theta^0\right)} \geq \frac{1}{f_\theta\left(\theta^0\right)} = MCRB_{\theta^0},$$

where $\mathbf{F}\left(\theta\right) = E_{\mathbf{z},\boldsymbol{\theta}_r;\theta}\left[\boldsymbol{\psi}\left(\mathbf{z},\boldsymbol{\theta}_r;\theta\right)\boldsymbol{\psi}\left(\mathbf{z},\boldsymbol{\theta}_r;\theta\right)^T\right]$, $\mathbf{f}\left(\theta\right) = E_{\mathbf{z},\boldsymbol{\theta}_r;\theta}\left[\boldsymbol{\psi}\left(\mathbf{z},\boldsymbol{\theta}_r;\theta\right)\frac{\partial \ln p(\mathbf{z},\boldsymbol{\theta}_r;\theta)}{\partial\theta}\right]$ and $f_\theta\left(\theta\right) = E_{\mathbf{z},\boldsymbol{\theta}_r;\theta}\left[\left(\frac{\partial \ln p(\mathbf{z},\boldsymbol{\theta}_r;\theta)}{\partial\theta}\right)^2\right]$. In the same way, one could easily proposed an alternative to the tighter MBaB of order K deriving from (D.4), suitable to estimation problems for which $\mathcal{S}_{\Theta_r|\mathbf{z}}$ does not satisfy (D.5). Or for the modified form of any known standard LB.

D.2 Non-standard maximum likelihood estimator performance

D.2.1 Performance comparison with the standard MLE

First, $\forall\widehat{\boldsymbol{\phi}} \in \mathcal{L}_2\left(\mathcal{S}_{\mathcal{Z},\Theta_r}\right)$:

$$\begin{aligned} E_{\mathbf{z},\boldsymbol{\theta}_r;\theta}\left[\left(\widehat{\boldsymbol{\phi}}-\mathbf{g}\left(\theta\right)\right)\left(\widehat{\boldsymbol{\phi}}-\mathbf{g}\left(\theta\right)\right)^T\right] &= E_{\mathbf{z},\boldsymbol{\theta}_r;\theta}\left[\left(\widehat{\boldsymbol{\phi}}-E_{\mathbf{z}|\boldsymbol{\phi}}\left[\widehat{\boldsymbol{\phi}}\right]\right)\left(\widehat{\boldsymbol{\phi}}-E_{\mathbf{z}|\boldsymbol{\phi}}\left[\widehat{\boldsymbol{\phi}}\right]\right)^T\right]+ \\ & E_{\boldsymbol{\theta}_r;\theta}\left[\left(E_{\mathbf{z}|\phi}\left[\widehat{\phi}\right]-\mathbf{g}\left(\theta\right)\right)\left(E_{\mathbf{z}|\phi}\left[\widehat{\phi}\right]-\mathbf{g}\left(\theta\right)\right)^T\right]. \end{aligned} \quad \text{(D.14a)}$$

Therefore, if $\widehat{\boldsymbol{\phi}} \in \mathcal{U}_S\left(\mathcal{S}_{\mathcal{Z},\Theta_r}\right)$:

$$E_{\mathbf{z},\boldsymbol{\theta}_r;\theta}\left[\left(\widehat{\boldsymbol{\phi}}-\mathbf{g}\left(\theta\right)\right)\left(\widehat{\boldsymbol{\phi}}-\mathbf{g}\left(\theta\right)\right)^T\right] = E_{\mathbf{z},\boldsymbol{\theta}_r;\theta}\left[\left(\widehat{\boldsymbol{\phi}}-\boldsymbol{\phi}\right)\left(\widehat{\boldsymbol{\phi}}-\boldsymbol{\phi}\right)^T\right]+\mathbf{C}_\theta\left(\boldsymbol{\phi}\right), \quad \text{(D.14b)}$$

where :

$$\mathbf{C}_\theta\left(\boldsymbol{\phi}\right) = E_{\boldsymbol{\theta}_r;\theta}\left[\left(\boldsymbol{\phi}-E_{\boldsymbol{\theta}_r;\theta}\left[\boldsymbol{\phi}\right]\right)\left(\boldsymbol{\phi}-E_{\boldsymbol{\theta}_r;\theta}\left[\boldsymbol{\phi}\right]\right)^T\right] = \begin{bmatrix} 0 & \mathbf{0}^T \\ \mathbf{0} & \mathbf{C}_\theta\left(\boldsymbol{\theta}_r\right) \end{bmatrix}.$$

Second, as $\mathcal{U}_S(\mathcal{S}_{\mathcal{Z}}) \subset \mathcal{U}_W(\mathcal{S}_{\mathcal{Z}})$ and $\mathcal{U}_S(\mathcal{S}_{\mathcal{Z}}) \subset \mathcal{U}_S(\mathcal{S}_{\mathcal{Z},\Theta_r})$ and, finally :

$$\min_{\widehat{\phi} \in \mathcal{U}_W(\mathcal{S}_{\mathcal{Z}})} \left\{ E_{\mathbf{z}|\theta} \left[\left(\widehat{\phi} - \mathbf{g}(\theta) \right) \left(\widehat{\phi} - \mathbf{g}(\theta) \right)^T \right] \right\} \leq \min_{\widehat{\phi} \in \mathcal{U}_S(\mathcal{S}_{\mathcal{Z}})} \left\{ E_{\mathbf{z},\theta_r;\theta} \left[\left(\widehat{\phi} - \phi \right) \left(\widehat{\phi} - \phi \right)^T \right] \right\} + \mathbf{C}_\theta(\phi), \tag{D.15a}$$

and, in particular :

$$\min_{\widehat{\theta} \in \mathcal{U}_W(\mathcal{S}_{\mathcal{Z}})} \left\{ E_{\mathbf{z}|\theta} \left[\left(\widehat{\theta} - \theta \right)^2 \right] \right\} \leq \min_{\widehat{\theta} \in \mathcal{U}_S(\mathcal{S}_{\mathcal{Z}})} \left\{ E_{\mathbf{z}|\theta} \left[\left(\widehat{\theta} - \theta \right)^2 \right] \right\}. \tag{D.15b}$$

If we consider an asymptotic region of operation [204, 205, 207, 240, 241, 242, 243] for both $\widehat{\theta}_{ML}(\mathbf{z})$ and $\underline{\widehat{\theta}}(\mathbf{z})$, then $\widehat{\theta}_{ML}(\mathbf{z})$ is wide-sense unbiased, i.e., $\widehat{\theta}_{ML} \in \mathcal{U}_W(\mathcal{S}_{\mathcal{Z}})$, $\underline{\widehat{\theta}}(\mathbf{z})$ is strict-sense unbiased, i.e., $\underline{\widehat{\theta}} \in \mathcal{U}_S(\mathcal{S}_{\mathcal{Z}})$, and (D.15b) holds for $\widehat{\theta}_{ML}$ and $\underline{\widehat{\theta}}$.

D.2.2 Non-standard lower bounds performance

A typical example is the NSCRB obtained for $N = 2$, where $\boldsymbol{\theta}^2 = (\theta, \theta + d\theta)$ leading to the following subset of constraints :

$$\begin{pmatrix} 0 \\ d\theta \end{pmatrix} = E_{\mathbf{z},\boldsymbol{\theta}_r;\theta} \left[\left(\widehat{\theta}(\mathbf{z}, \boldsymbol{\theta}_r) - \theta \right) \begin{pmatrix} 1_{\mathcal{S}_{\mathcal{Z},\Theta_r}}(\mathbf{z}, \boldsymbol{\theta}_r) \\ \upsilon_\theta(\mathbf{z}, \boldsymbol{\theta}_r; \theta + d\theta) \end{pmatrix} \right], \tag{D.16a}$$

which is equivalent to [231, Lemma 3] :

$$\begin{pmatrix} 0 \\ 1 \end{pmatrix} = E_{\mathbf{z},\boldsymbol{\theta}_r;\theta} \left[\left(\widehat{\theta}(\mathbf{z}, \boldsymbol{\theta}_r) - \theta \right) \begin{pmatrix} 1_{\mathcal{S}_{\mathcal{Z},\Theta_r}}(\mathbf{z}, \boldsymbol{\theta}_r) \\ \frac{\upsilon_\theta(\mathbf{z}, \boldsymbol{\theta}_r; \theta + d\theta) - 1}{d\theta} \end{pmatrix} \right], \tag{D.16b}$$

and can be reduced to [231, Lemma 2] :

$$1 = E_{\mathbf{z},\boldsymbol{\theta}_r;\theta} \left[\left(\widehat{\theta}(\mathbf{z}, \boldsymbol{\theta}_r) - \theta \right) \frac{p(\mathbf{z}, \boldsymbol{\theta}_r; \theta + d\theta) - p(\mathbf{z}, \boldsymbol{\theta}_r; \theta)}{d\theta\, p(\mathbf{z}, \boldsymbol{\theta}_r; \theta)} \right], \tag{D.16c}$$

since $E_{\mathbf{z},\boldsymbol{\theta}_r;\theta} \left[1_{\mathcal{S}_{\mathcal{Z},\Theta_r}}(\mathbf{z}, \boldsymbol{\theta}_r) \left(\upsilon_\theta(\mathbf{z}, \boldsymbol{\theta}_r; \theta + d\theta) - 1 \right) \right] = 0$. Then by letting $d\theta$ be infinitesimally small, (4.36b) becomes [215, (5)] :

$$MCRB_\theta \triangleq E_{\mathbf{z},\boldsymbol{\theta}_r;\theta} \left[\left(\frac{\partial \ln p(\mathbf{z}, \boldsymbol{\theta}_r; \theta)}{\partial \theta} \right)^2 \right]^{-1} \leq NSCRB_\theta \triangleq E_{\boldsymbol{\theta}_r;\theta} \left[E_{\mathbf{z}|\phi} \left[\left(\frac{\partial \ln p(\mathbf{z}|\phi)}{\partial \theta} \right)^2 \right]^{-1} \right], \tag{D.17}$$

where the $NSCRB_\theta$ is the MCB [213, (7)]. Following the rationale introduced in [232], a straightforward extension of (D.17) is obtained for $\boldsymbol{\theta}^N = \left(\theta^1, \ldots, \theta^N \right)^T$, $\theta^n = \theta + (n-1)\, d\theta$, $1 \leq n \leq N$. Indeed the set of N associated constraints :

$$d\theta \mathbf{w}_N = E_{\mathbf{z},\boldsymbol{\theta}_r;\theta} \left[\left(\widehat{\theta}(\mathbf{z}, \boldsymbol{\theta}_r) - \theta \right) \upsilon_\theta \left(\mathbf{z}, \boldsymbol{\theta}_r; \boldsymbol{\theta}^N \right) \right], \tag{D.18a}$$

where $\mathbf{w}_N^T = (0, \ldots, N-1)$, by letting $d\theta$ be infinitesimally small, becomes equivalent to [232][231, Lemma 3] :

$$\mathbf{v}' = E_{\mathbf{z},\boldsymbol{\theta}_r;\theta}\left[\left(\widehat{\theta}\left(\mathbf{z},\boldsymbol{\theta}_r\right)-\theta\right)\mathbf{b}'_\theta\left(\mathbf{z},\theta_r\right)\right], \tag{D.18b}$$

where $\mathbf{v}' = (0,1,0,\ldots,0)^T$ and $\mathbf{b}'_\theta\left(\mathbf{z},\boldsymbol{\theta}_r\right) = \frac{1}{p(\mathbf{z},\boldsymbol{\theta}_r;\theta)}\left(p\left(\mathbf{z},\boldsymbol{\theta}_r;\theta\right), \frac{\partial p(\mathbf{z},\boldsymbol{\theta}_r;\theta)}{\partial\theta}, \ldots, \frac{\partial^{N-1}p(\mathbf{z},\boldsymbol{\theta}_r;\theta)}{\partial^{N-1}\theta}\right)^T$. Since $v'_1 = 0$ and $E_{\mathbf{z},\boldsymbol{\theta}_r;\theta}\left[\left(\mathbf{b}'_\theta\right)_1\left(\mathbf{z},\boldsymbol{\theta}_r\right)\left(\mathbf{b}'_\theta\right)_n\left(\mathbf{z},\boldsymbol{\theta}_r\right)\right] = E_{\mathbf{z},\boldsymbol{\theta}_r;\theta}\left[\frac{\partial^n p(\mathbf{z},\boldsymbol{\theta}_r;\theta)}{\partial^n\theta}\right] = 0$, $2 \leq n \leq N-1$, (D.18b) is actually equivalent to [231, Lemma 2] :

$$\mathbf{e}_1 = E_{\mathbf{z},\boldsymbol{\theta}_r;\theta}\left[\left(\widehat{\theta}\left(\mathbf{z},\boldsymbol{\theta}_r\right)-\theta\right)\mathbf{b}_\theta\left(\mathbf{z},\boldsymbol{\theta}_r\right)\right], \tag{D.18c}$$

where $\mathbf{b}_\theta\left(\mathbf{z},\boldsymbol{\theta}_r\right) = \frac{1}{p(\mathbf{z},\boldsymbol{\theta}_r;\theta)}\left(\frac{\partial p(\mathbf{z},\boldsymbol{\theta}_r;\theta)}{\partial\theta}, \ldots, \frac{\partial^{N-1}p(\mathbf{z},\boldsymbol{\theta}_r;\theta)}{\partial^{N-1}\theta}\right)^T$, and (4.36b) becomes an inequality between the Battacharayya bounds (BaBs) [233] of order $N-1$:

$$MBaB_\theta \triangleq \mathbf{e}_1^T E_{\mathbf{z},\boldsymbol{\theta}_r;\theta}\left[\mathbf{b}_\theta\left(\mathbf{z},\boldsymbol{\theta}_r\right)\mathbf{b}_\theta^T\left(\mathbf{z},\boldsymbol{\theta}_r\right)\right]^{-1}\mathbf{e}_1 \leq NSBaB_\theta \triangleq E_{\boldsymbol{\theta}_r;\theta}\left[\mathbf{e}_1^T E_{\mathbf{z}|\boldsymbol{\phi}}\left[\boldsymbol{\beta}\left(\mathbf{z};\boldsymbol{\phi}\right)\boldsymbol{\beta}^T\left(\mathbf{z};\boldsymbol{\phi}\right)\right]^{-1}\mathbf{e}_1\right], \tag{D.18d}$$

where $\boldsymbol{\beta}\left(\mathbf{z};\boldsymbol{\phi}\right) = \frac{1}{p(\mathbf{z}|\boldsymbol{\phi})}\left(\frac{\partial p(\mathbf{z}|\boldsymbol{\phi})}{\partial\theta}, \ldots, \frac{\partial^{N-1}p(\mathbf{z}|\boldsymbol{\phi})}{\partial^{N-1}\theta}\right)^T = \mathbf{b}_\theta\left(\mathbf{z},\boldsymbol{\theta}_r\right)$. Therefore, with the proposed approach, we not only extend the result introduced in [234, (11)] under the restrictive assumption of a prior independent of θ, but we can also assert that $MBaB_\theta \leq NSBaB_\theta$ if the prior does not depend on θ, which has not been proven in [234].
As with the CRB and the BaB, (4.36b) also allows to derive inequalities between modified and non-standard forms of all remaining BB approximations released in the open literature, namely the FGB [232], the MHB [235], the GlB [219], the AbB [218], and the CRFB [225, (101-102)].
Furthermore, an example of a tighter NSLB can be easily derived from the usual NSCRB (D.17). Indeed by adding to (D.16a) the following $K = P_r$ constraints :

$$\mathbf{0} = E_{\mathbf{z}|\boldsymbol{\phi}}\left[\left(\widehat{\theta}\left(\mathbf{z},\boldsymbol{\theta}_r\right)-\theta\right)\upsilon_{\boldsymbol{\phi}}\left(\mathbf{z};\boldsymbol{\Phi}^K\right)\right],$$

where $\boldsymbol{\phi}^k = \binom{\theta}{\boldsymbol{\theta}_r+\mathbf{u}_k h_r^k}$ and $\mathbf{u}_k$ is the kth column of the identity matrix $\mathbf{I}_{P_r}$, one obtains the following equivalent set of constraints [231, Lemma 3+Lemma 2] :

$$\mathbf{e}_1 = E_{\mathbf{z}|\boldsymbol{\phi}}\left[\left(\widehat{\theta}\left(\mathbf{z},\boldsymbol{\theta}_r\right)-\theta\right)\mathbf{c}\left(\mathbf{z};\boldsymbol{\Phi}^{K+1}\right)\right],$$
$$\mathbf{c}^T\left(\mathbf{z};\boldsymbol{\Phi}^{K+1}\right) = \left(\frac{p(\mathbf{z}|\boldsymbol{\theta}_r;\theta+d\theta)}{p(\mathbf{z}|\boldsymbol{\theta}_r;\theta)d\theta} - \frac{1}{d\theta}, \frac{p\left(\mathbf{z}|\boldsymbol{\theta}_r+\mathbf{u}_1 h_r^1,\theta\right)}{p(\mathbf{z}|\boldsymbol{\theta}_r;\theta)h_r^1} - \frac{1}{h_r^1}, \ldots, \frac{p\left(\mathbf{z}|\boldsymbol{\theta}_r+\mathbf{u}_K h_r^K,\theta\right)}{p(\mathbf{z}|\boldsymbol{\theta}_r;\theta)h_r^K} - \frac{1}{h_r^K}\right).$$

By letting $\left(d\theta, h_r^1, \ldots, h_r^{P_r}\right)$ be infinitesimally small, then $\mathbf{c}\left(\mathbf{z}; \mathbf{\Phi}^{K+1}\right) \to \frac{\partial \ln p(\mathbf{z}|\boldsymbol{\phi})}{\partial \boldsymbol{\phi}}$ and (4.37b) becomes [249, (24)] :

$$MCRB_\theta \triangleq E_{\mathbf{z},\boldsymbol{\theta}_r;\theta}\left[\left(\frac{\partial \ln p\left(\mathbf{z}, \boldsymbol{\theta}_r; \theta\right)}{\partial \theta}\right)^2\right]^{-1} \leq NSCRB_\theta \triangleq E_{\boldsymbol{\theta}_r;\theta}\left[E_{\mathbf{z}|\boldsymbol{\phi}}\left[\left(\frac{\partial \ln p\left(\mathbf{z}|\boldsymbol{\phi}\right)}{\partial \theta}\right)^2\right]^{-1}\right]$$
$$\leq \overline{NSCRB}_\theta = E_{\boldsymbol{\theta}_r;\theta}\left[\mathbf{e}_1^T E_{\mathbf{z}|\boldsymbol{\phi}}\left[\frac{\partial \ln p\left(\mathbf{z}|\boldsymbol{\phi}\right)}{\partial \boldsymbol{\phi}} \frac{\partial \ln p\left(\mathbf{z}|\boldsymbol{\phi}\right)}{\partial \boldsymbol{\phi}^T}\right]^{-1} \mathbf{e}_1\right]. \quad \text{(D.19)}$$

In [249], $\overline{NSCRB}_\theta$ was introduced under the restrictive assumption of a prior independent of θ, which can be relaxed as shown with the proposed framework.

Résumé — Les avancées récentes dans le domaine de navigation par satellites (GNSS) ont conduit à une prolifération des applications de géolocalisation dans les milieux urbains. Pour de tels environnements, les applications GNSS souffrent d'une grande dégradation liée à la réception des signaux satellitaires en lignes indirectes (NLOS) et en multitrajets (MP). Ce travail de thèse propose une méthodologie originale pour l'utilisation constructive des signaux dégradés MP/NLOS, en appliquant des techniques avancées de traitement du signal ou à l'aide d'une assistance d'un simulateur 3D de propagation des signaux GNSS. D'abord, nous avons établi le niveau maximal réalisable sur la précision de positionnement par un système GNSS "Stand-Alone" en présence de conditions MP/NLOS, en étudiant les bornes inférieures sur l'estimation en présence des signaux MP/NLOS. Pour mieux améliorer ce niveau de précision, nous avons proposé de compenser les erreurs NLOS en utilisant un simulateur 3D des signaux GNSS afin de prédire les biais MP/NLOS et de les intégrer comme des observations dans l'estimation de la position, soit par correction des mesures dégradées ou par sélection d'une position parmi une grille de positions candidates. L'application des approches proposées dans un environnement urbain profond montre une bonne amélioration des performances de positionnement dans ces conditions.
Mots clés : GNSS, Reception Multi-trajets ou NLOS, Positionnement en urbain, Méthodes de traitement du signal avancées, Simulateur GNSS, Bornes inférieures.

Abstract — Recent trends in Global Navigation Satellite System (GNSS) applications in urban environments have led to a proliferation of studies in this field that seek to mitigate the adverse effect of non-line-of-sight (NLOS). For such harsh urban settings, this dissertation proposes an original methodology for constructive use of degraded MP/NLOS signals, instead of their elimination, by applying advanced signal processing techniques or by using additional information from a 3D GNSS simulator. First, we studied different signal processing frameworks, namely robust estimation and regularized estimation, to tackle this GNSS problem without using an external information. Then, we have established the maximum achievable level (lower bounds) of GNSS Stand-Alone positioning accuracy in presence of MP/NLOS conditions. To better enhance this accuracy level, we have proposed to compensate for the MP/NLOS errors using a 3D GNSS signal propagation simulator to predict the biases and integrate them as observations in the estimation method. This could be either by correcting degraded measurements or by scoring an array of candidate positions. Besides, new metrics on the maximum acceptable errors on MP/NLOS errors predictions, using GNSS simulations, have been established. Experiment results using real GNSS data in a deep urban environment show that using these additional information provides good positioning performance enhancement, despite the intensive computational load of 3D GNSS simulation.
Keywords : GNSS, Multipath and NLOS reception, Positioning in urban areas, Advanced signal processing, 3D GNSS simulator, Lower bounds, Non-Standard Estimation.